Finite amplitude propagation in acoustic beams

Bacon, David R.

Award date:
1986

Awarding institution:
University of Bath

FINITE AMPLITUDE PROPAGATION

IN ACOUSTIC BEAMS

submitted by David R Bacon
for the degree of PhD

of the University of Bath

1986

ProQuest LLC
789 East Eisenhower Parkway
P.O. Box 1346
Ann Arbor, MI 48106-1346

CONTENTS

SUMMARY

The nonlinear propagation of an initially sinusoidal acoustic wave is described by modelling the field with a Gaussian beam. The theoretical model takes account of the effects of nonlinear distortion, absorption, dispersion and diffraction, although the application is mainly limited to the field on the acoustic axis of a transducer. The field of a circular disc radiator is explicitly considered, for both the unfocused and the focused case, and the numerical solution of the basic equations is described. The application of previously derived, approximate solutions is demonstrated and these solutions are assessed for their accuracy, particularly when used to predict the amplitudes of the harmonic components.

Experimental verification of the theoretical predictions has been obtained for propagation in water in the frequency range 1 to 100 MHz and also for propagation in a tissue-mimmicking gel. A particular feature of the measurement system, which uses a broad-band hydrophone, is the ability to record many harmonic components. It is demonstrated that nonlinear distortion occurs in media with acoustic properties similar to those of tissue and that the characteristic behaviour of the field is significantly different to the behaviour of the corresponding field in water. Consequently it is difficult to predict the behaviour of the field in tissue from measurements made in water, but nevertheless a procedure has been developed to make such predictions.

As an application of the work described here, a new method for the absolute calibration of hydrophones over a wide range of frequencies has been developed as well as a technique for intercomparing the sensitivities of hydrophones at a number of frequencies simultaneously.

1 INTRODUCTION

This thesis is a study of the nonlinear propagation of initially sinusoidal waves in a diffractive field. The emphasis is on predicting accurately the frequency content of the wave on the acoustic axis, for distances close to or beyond the Rayleigh distance. Chapter 2 contains the theory, whereas the experimental procedure is described in Chapter 3. The theoretical predictions are compared with experiment in Chapter 4, and the principal conclusions are given in Chapter 5. This chapter begins by outlining the motivation behind the work and then a simple review of the subject is given for the benefit of those who are not specialists in this field. Finally, relevant previous contributions in this area of research are discussed in sections 3 and 4.

1.1 Project aims

1.1.1 Measurement of the ultrasonic fields used in medicine

Acoustic waves in the frequency range of 0.5 to 15 MHz have a number of applications in medicine and biology. Diagnostic equipment, for example, is used extensively in obstetrics and cardiology, and ultrasound is an accepted form of therapy for the treatment of damaged muscle tissue. More recent developments are the treatment of cancer cells by ultrasonically induced hyperthermia and the destruction of kidney stones using shock wave lithotripsy. All of these developments bring with them a need for the characterisation of ultrasonic fields to allow performance

specifications to be established and to provide information on patient exposure levels. To meet this need on a national basis, the National Physical Laboratory (NPL) has a section which establishes standards of measurement, provides a calibration service and supports research and development projects to improve the accuracy and availability of relevant measurement techniques. Part of the programme of this section involves the study and application of the nonlinear propagation of ultrasound. The motivation behind this project is threefold.

Firstly, the most common form of medical diagnostic equipment is the scanning type, which produces images from the echoes received after the injection of an acoustic pulse. The pulses produced by such equipment are frequently of very high amplitude (up to about 10 MPa peak pressure), and to be able to calibrate them accurately it is necessary to understand the processes which govern their propagation in the test medium. Secondly, since the equipment is actually used with the sound propagating in tissue rather than in water, it is of considerable interest to know how the calibration measurements relate to the field that actually occurs within the patient and to be able to predict the field for a variety of exposure conditions. The third motivation is the possible exploitation of the propagation process in the calibration of ultrasonic instruments. The frequency range of 0.5 to 15 MHz is particularly useful for such applications, since it is not difficult to produce the required fields in practice.

The physical basis of nonlinear propagation lies in the fact that the velocity of sound depends on the density of the medium in which it is travelling. The denser portions of the acoustic

waveform, therefore, travel more quickly than the less dense ones and thus the shape of the waveform alters during propagation. As a consequence, the frequency spectrum of the wave becomes distorted and the changed frequency content results in a different attenuation coefficient because the higher frequency components are absorbed more rapidly than the lower frequency components. It is important to correct for this and other effects when calibrating some medical ultrasonic equipment. The loss in amplitude caused by absorption and scattering tends to oppose the distortion process, so that the significance of nonlinear propagation in tissue is a topic of current debate. Nevertheless, the characterisation of medical equipment is currently performed in water where there is no doubt as to the nature of the effect, and this thesis treats the propagation of ultrasound in water as well as in tissue-like media.

1.1.2 Scope of this project

The initial part of the work has been to demonstrate the relevance of nonlinear effects to medical ultrasound. Although such processes have been known in physics for a long time (see, for example, [1]), there has been considerable lack of belief in their relevance amongst those involved with ultrasound in medicine. One explanation for this may be the relative complexity of the theory involved and another may be the absence until recently of measuring devices which can readily demonstrate the effects. Thus the development of hydrophones with a wideband frequency response such as those used for this thesis [2-6] has contributed significantly to the recognition of nonlinear distortion in the

field of biomedical ultrasound. Several recent presentations in the literature [7-10] have also served to draw attention to these effects, and to explain the theoretical and experimental background in simple terms.

The main aims of this project have been defined as follows:

1) To establish a measurement system capable of giving reproducible and accurate results with a known dependence on the state of the water.

2) To develop theoretical models capable of predicting the harmonic amplitudes for a wide range of experimental conditions.

3) Following on from items (1) and (2): to establish methods of using nonlinear effects in calibration.

4) To gain a general understanding of finite amplitude effects as they apply to medical ultrasound.

The first three of these topics are dealt with in chapters 3, 2 and 4 of this report respectively while the fourth aim may be said to be covered by the report as a whole.

The project as stated above is potentially very wide ranging and it has been necessary to restrict the field of investigation in order to achieve a reasonable level of progress. Consequently the study to date has dealt exclusively with the acoustic field along the axis of symmetry of the radiating transducer. Although a number of interesting effects are thereby neglected, this approach can be justified in a number of ways. Firstly in the

characterisation of medical equipment, most of the important acoustical parameters are measured in this region of the field. Secondly, the amplitudes are generally greatest along the axis of symmetry and consequently any nonlinear effects are likely to be most significant there. Thirdly, as axisymmetrical transducers are most frequently used, this axis is a well-defined region of the field and easy to locate experimentally. Finally, this choice can give rise to certain theoretical simplifications, which are highly desirable in view of the very complex nature of the problem.

1.2 Nonlinear propagation

This section introduces a number of concepts which are relevant to the understanding of this report; the reader who is familiar with the elements of nonlinear acoustics may omit this material and proceed to section 1.3.

1.2.1 Second order equation of motion for one dimensional flow

The equation for conservation of mass, for a plane wave propagating in the z direction is given in Lagrangian co-ordinates as [11]:

$$\rho = \rho_o/(1 + x_z) \qquad 1.1$$

where ρ is the density, ρ_o the density when the medium is at rest, x the particle displacement at the position z, and the subscript z denotes partial differention with respect to z. Neglecting absorption, the equation of motion is given by [11]:

$$-p_z = \rho_o x_{tt} \qquad 1.2$$

where p is the acoustic pressure and the subscript t represents partial differention with respect to time. The two equations can be combined by putting $p_z = \rho_z \, dp/d\rho$ to obtain:

$$\frac{dp}{d\rho} x_{zz}/(1 + x_z)^2 = x_{tt} \qquad 1.3$$

The function $dp/d\rho$ may be evaluated by expanding the equation of state under the appropriate conditions in a Taylor series:

$$p = p_o + A(\rho-\rho_o)/\rho_o + B[(\rho-\rho_o)/\rho_o]^2/2 + \ldots$$

where A and B are constants representing properties of the medium.
Hence $dp/d\rho \simeq A/\rho_o + B(\rho-\rho_o)/\rho_o^2$

From Equation 1.1 above,

$$(\rho-\rho_o)/\rho_o = -x_z/(1 + x_z)$$

and hence $dp/d\rho \simeq [A/\rho_o][1 - Bx_z/A(1 + x_z)]$

and $dp/d\rho \simeq (A/\rho_o)/(1 + x_z)^{B/A}$ to first order in x_z.

Substituting into Equation 1.3 we obtain

$$c^2 x_{zz}/(1 + x_z)^{(2 + B/A)} = x_{tt} \qquad 1.4$$

where terms up to second order in x and its derivatives have been

included, and A/ρ_o has been set equal to c^2. If the amplitude of the wave is small, then $x_z << 1$ and it can be seen that c is the velocity of wave propagation. If the term in x_z is not neglected, then the wave velocity is not constant, and can be seen to be approximately equal to $c/[1+ (1 + B/2A)x_z]$. Inspection of Equation 1.1 shows that the velocity is greatest where the density of the medium is largest, provided that $B/2A > -1$. For a periodic waveform this means that the peaks will travel more quickly than the troughs and so the wave will distort as it travels. It is also evident from Equations 1.3 and 1.4 that this distortion arises from two causes. The first reason is that there is a nonlinear relationship between the density and x_z in the continuity equation (Equation 1.1). The physical meaning of this is that the wave velocity is the sum of the velocity at low amplitudes (c) plus the velocity of the medium, which is the particle velocity, and for this reason the effect is often called convection. The second reason for wave distortion is that the equation of state is nonlinear - in other words, if the medium is compressed or expanded adiabatically, then the velocity of sound is different from its initial value. This second reason means that different media give rise to different amounts of distortion. Consequently, it is convenient to define a parameter for a given medium, which depends on its adiabatic equation of state:

$$\beta = 1 + B/2A.$$

This parameter can be determined by a variety of methods (see section 3.7) and for water at room temperature and pressure is approximately 3.52.

Equation 1.4 may be written in terms of the particle velocity $u = x_t$, and rearranged to obtain, to second order, for waves travelling in the +z direction:

$$u_t + c\,u_z - \beta u u_t/c = 0$$

$$\text{or} \quad u_t \simeq -u_z(c + \beta u).$$

From this it is clear that the local propagation velocity is $c + \beta u$, and hence the above statements about the wave distortion are justified. Making the change of variables $t' = t - z/c$ and $z' = z$ gives

$$u_{z'} - (\beta/c^2)u u_{t'} = 0.$$

This is the lossless Burgers' equation, in the form suitable for boundary value problems. If the attenuation term is included, then

$$u_{z'} = (\beta/c^2)u u_{t'} + (b/2c^3)u_{t't'} \qquad 1.5$$

where the coefficient b is known as the "diffusivity of sound" [12]; this is related to the amplitude attenuation coefficient, α, and the angular frequency ω by

$$\alpha = b\omega^2/2c^3.$$

Equation 1.5 is the full Burgers' equation, and has been used to model many problems in nonlinear acoustics since it is the simplest equation which describes the relevant physical processes.

Another reason for the usefulness of this equation is the fact that it has an analytical solution [13]. It is evident that the second and third terms of Equation 1.5 describe the effects of wave distortion and absorption respectively. Since any practical situation will be characterised by the magnitude of these effects, it would be very convenient to derive parameters which describe them. To this end, the following change of variables is made, which relates to an initially harmonic wave:

$$\tau = \omega t', \qquad \sigma = (\beta u_o \omega / c^2) z \quad \text{and} \quad U = u/u_o$$

where u_o is a reference amplitude, such as the initial amplitude of the wave. In terms of these variables:

$$U_\sigma = UU_\tau + (1/\Gamma)U_{\tau\tau}, \qquad 1.6$$

where $\Gamma = \beta u_o \omega / \alpha c^2$.

This equation clearly indicates that the parameter Γ represents the relative importance of absorption and wave distortion ie if $\Gamma >> 1$ then distortion dominates, and if $\Gamma << 1$ then absorption is most important. It is also apparent from Equation 1.6 that (if $\Gamma > 1$) the variable σ describes the extent to which distortion has occurred, and so this parameter indicates the importance of nonlinearity.

The effect of σ on the waveform shape (for $\Gamma >> 1$) is illustrated in Figure 1 for an initially harmonic wave. Nonlinearity causes the crest to advance upon the trough until, at $\sigma = 1$, a small

vertical discontinuity or shock front forms. The amplitude of this discontinuity increases, until at $\sigma = \pi/2$ it extends to the entire wave amplitude. As σ increases, energy is dissipated at the shock front, so that the wave amplitude decreases and a sawtooth waveform occurs. As the wave amplitude decreases, so does the effect of nonlinearity, until eventually the absorption term becomes important, the shock front becomes smoothed out, and finally the waveform becomes sinusoidal again. This occurs at a distance given by $\sigma \simeq \Gamma$ which, for plane waves, is equivalent to $z \simeq 1/\alpha$, where α is the attenuation coefficient at the fundamental frequency of the wave.

The propagation can therefore be divided into three main domains, which are commonly known as the pre-shock region ($\sigma<1$), the sawtooth region ($3 <\sigma<\Gamma$) and the old-age region ($\sigma>\Gamma$). It shold be noted that Γ determines the extent of the sawtooth region, so that if Γ is large, then this region also is large. If however Γ is approximately 3 or less, then absorption is too great for a shock to be formed, and the sawtooth region no longer exists.

1.2.2 Main features of one-dimensional propagation

The discussion so far has concentrated on the distortion of the acoustic waveform in the time domain. It is obviously possible to make equivalent statements about the behaviour of the wave in the frequency domain and a few features of such an approach will be noted here. The three regimes of propagation which were identified when considering motion in the time domain are also found to be useful in the frequency domain description. If it is assumed that

Γ is large, then absorption is not important for $\sigma<1$ and can be neglected. This approximation results in an exact solution of Equation 1.6 (cf [14]):

$$U = f(\tau + \sigma U). \qquad 1.7$$

For an initially sinusoidal wave the solution may be written as

$$U = \sin \theta, \qquad 1.8$$

where $\tau = \theta - \sigma \sin \theta$

and the Fourier coefficients are

$$B_n = (2/\pi) \int_0^{\pi} \sin \theta \sin(ny)\, dy.$$

This may be rewritten as

$$B_n = (2/n\pi\sigma) \int_0^{\pi} \cos n(\theta - \sigma \sin\theta) d\theta$$

and hence

$$B_n = (2/n\sigma) J_n(n\sigma) \qquad 1.9$$

where J_n is the n^{th} order Bessel function of the first kind [15]. If σ is small ($\sigma \ll 1$) then:

$$B_n \simeq (1/n!)\ (n\sigma/2)^{n-1} \qquad \text{for } \sigma \ll 1 \qquad 1.10$$

so that initially the amplitude of the n^{th} harmonic varies with distance z, as z^{n-1}, and with initial amplitude u_o, as $u_o{}^n$. Equations 1.7-1.9 cease to be valid after the formation of a shock ($\sigma > 1$) since Equations 1.7 and 1.8 become multiple-valued. For all values of σ, a modified solution due to Blackstock [16] holds:

$$B_n = (2/n\pi)V_b + (2/n\pi\sigma)\int_{\sin^{-1}V_b}^{\pi} \cos n(\theta - \sigma\sin\theta)d\theta \qquad 1.11$$

where $V_b = 0$ for $\sigma \leq 1$

and V_b is the first non-zero solution of $V_b = \sin(\sigma V_b)$ for $\sigma > 1$.

The second term in Equation 1.11 is obviously a simple extension of Equation 1.9, whereas the first term has the harmonic content of a sawtooth wave and becomes more important as the shock front develops. For $\sigma \geq 3$, the second term is very small, and the approximate form of Equation 1.11 is:

$$B_n = 2/n(1 + \sigma). \qquad 1.12$$

Now σ is directly proportional to the initial amplitude, so that as the source amplitude is increased, the loss due to finite amplitude effects also increases. This phenomenon is known as saturation, and it places a limit on the maximum wave amplitude that can be obtained at a particular distance from the source. For plane waves in the sawtooth region, Equation 1.12 gives this limit for the maximum velocity amplitude u_n (max) as:-

$$u_n \text{ (max)} = 2c^2/n\beta\omega z. \qquad 1.13$$

An improved form of Equation 1.12 which accounts for absorption was obtained by Fay [17] and is in fact an asymptotic form of the exact solution to Equation 1.6 [13]:

$$B_n = 2/\Gamma \sinh[n(1+\sigma)/\Gamma]. \qquad 1.14$$

Whereas Equations 1.11-1.12 break down when the old age region is approached ($\sigma \simeq \Gamma$ or $z \simeq 1/\alpha$), Equation 1.14 is still valid in this region and can be used to obtain the saturation amplitude:

$$u_n \text{ (max)} = 2\,\alpha c^2/\beta\omega \sinh(n\alpha z). \qquad 1.15$$

As would be expected, Equation 1.15 agrees with Equation 1.13 when $\alpha z \ll 1$ but for $\alpha z \gg 1$ it becomes:

$$u_n \text{ (max)} = (2\,\alpha c^2/\beta\omega)e^{-n\alpha z}. \qquad 1.16$$

Thus the saturation amplitude is inversely proportional to distance in the sawtooth region, and varies exponentially with distance in the old-age region. Since $\alpha z \gg 1$ in the old-age region, it is also evident from Equation 1.15 that the waveform is then essentially sinusoidal.

1.2.3 Special characteristics of non-plane waves

For spherical and cylindrical waves, equations which are equivalent to Equations 1.5 and 1.6 can be obtained if effects due

to the finite size of the source are neglected (ie if $kr_o >> 1$ where r_o is the source radius). For spherical waves Equation 1.6 becomes [18, 19]:

$$U_\sigma = UU_\tau + (1/\Gamma_o)\exp(\sigma/\sigma_o)\, U_{\tau\tau} \qquad 1.17$$

where $U = (u/u_o)(z/r_o)$

$\sigma = \sigma_o \ln(z/r_o)$

$\Gamma_o = \beta u_o k/\alpha c$

$\sigma_o = \beta u_o k r_o/c.$

This equation is very similar to Equation 1.6, except that the coefficient of the absorption term increases as the propagation parameter increases. Consequently, all of the solutions which applied previously when absorption could be neglected (Equations 1.7 to 1.13) may be carried over to the spherical wave case, using the new definitions for U and σ [16]. If absorption must be accounted for, then Equations 1.14 to 1.16 may also be applied, but in this case their accuracy is considerably reduced. Instead of being asymptotic forms of the true solution, they are approximate forms, only being valid in the sawtooth region - ie for $\sigma < \Gamma$. In this case the parameter Γ varies with distance, and is defined, for spherical waves, by:

$$\Gamma = \Gamma_o \exp(-\sigma/\sigma_o) \qquad 1.18$$
$$= \Gamma_o r_o/z.$$

For propagation in horns of varying cross-section it is again possible to develop analogous equations to those above [20, cf 21]. In this case σ is given (see section 2.1.2) by:-

$$\sigma = (\beta u_o k/c) \int f(z')\, dz' \qquad 1.19$$

where f(z) describes the variation of velocity with distance in the absence of absorption and finite amplitude effects. When the analogous equation to Equation 1.6 is derived in these cases, the coefficient of the absorption term is again found to depend on σ. Nevertheless, the possibility of deriving equations similar to Equation 1.6 for many types of propagation is very significant, since it allows a number of approximate solutions to be used, and also gives the parameter σ a reinforced status as an indication of the amount of distortion that has occurred.

It is more difficult to describe acoustic fields where the low amplitude distribution is determined by diffraction rather than the geometry of the situation. This is because the principle of superposition no longer holds, and secondary diffraction occurs due to wave interaction during propagation. This situation is clearly much more complicated than those considered above, and the equations presented previously do not in general apply. Nevertheless, all acoustic sources of finite size have a Fraunhofer diffraction region, where the local effect of diffraction is weak and where spherical spreading usually occurs. In this case it is possible to develop Equation 1.17 to describe the motion [22-24]. This is achieved by noting that for each direction of propagation the initial amplitude, u_o, is determined by the directivity response of the transducer. Equation 1.17 may thus be used to describe the situation by substituting $u_o D(\theta)$ for u_o, where $D(\theta)$ is the directivity function of the transducer as a function of the off-axis angle [22]. The only quantity which is

difficult to define in Equation 1.17 is r_o, which is the assumed source radius where the waveform is taken to be sinusoidal with amplitude $u_o D(\theta)$. In practice, values of r_o which are between half and two thirds of the Rayleigh distance for the transducer have been found to give good agreement with experiment [23, 22, 25]. This is taken up later in this report (section 2.1.3).

When σ is small ($\sigma \ll 1$) and if absorption can be neglected, the directivity response for the harmonic components can be derived quite easily. It was noted above (after Equation 1.10) that the variation of harmonic amplitude with initial amplitude is u_o^n in this region, and consequently [22]:

$$D_n(\theta) = [D(\theta)]^n \qquad 1.20$$

for $\sigma(0) \ll 1$, ($\sigma(0)$ is for $\theta = 0$),

where $D_n(\theta)$ is the directivity response for the n^{th} harmonic. It is thus evident that the higher harmonics have a narrower directivity than the fundamental. If the source amplitude is increased so that $\sigma(0) \gtrsim 1$ then the beamshape for the fundamental and other harmonics becomes broader, because the higher amplitude parts are attenuated more severely. Thus the wave takes on an increasingly spherical shape as the amplitude increases. A similar feature, where the effects of diffraction are somewhat neutralised as the amplitude is increased, is noted later in this report (section 4.1.1).

Diffraction introduces phase variations into the acoustic field as well as variations in amplitude, and there are few simple theories

that can account for this (but see references 26 and 27). These phase changes in the near field of a transducer give rise to diffractive structure for the higher harmonics which is significantly different from that of the fundamental [28-31].

1.3 Previous Theoretical Work

As the literature of nonlinear acoustics is extensive, only the most relevant previous studies are outlined below. Thus, earlier work on one-dimensional waves is in general excluded, although some of this has been covered in section 1.2. Some of the work reported in this thesis has already been published and will therefore be included in the following review.

1.3.1 Low amplitude field of a transducer

Ingenito and Williams [29] were the first to take account of diffraction in the field of a transducer. They used a perturbation solution to derive the second harmonic amplitude for $\sigma \ll 1$. They neglected absorption and any possible backscattering and assumed that ka (a is the transducer radius) is large. They obtained solutions for the second harmonic - both the axial value and that averaged over a large area receiver. Their results were valid for propagation distances greater than 2.5 transducer diameters and could be evaluated using tabulated functions or by quite straightforward numerical integration. Under a certain approximation they found that the second harmonic amplitude depended on the integral of the square of the fundamental amplitude over a line parallel to the acoustic axis. Their result, which predicted significant structure for the axial value of the

second harmonic was found to agree with experiment.

More recently Cobb [30] extended the analysis for the average value of the second harmonic to account for absorption. He obtained good agreement with experiment and used the solution to calculate values of β for several different media. Kunitsyn and Rudenko [31] used the parabolic wave equation to calculate the second harmonic amplitude. This equation (see section 2.1.1) assumes that the pressure amplitude does not vary signficantly over a distance equal to the wavelength and is generally valid for z (propagation distance) > a $(ka)^{1/3}$. They showed that the second harmonic amplitude depends on the integral of the square of the fundamental component. They also obtained an analytical expression for the axial second harmonic which was valid for $z \lesssim a^2/\lambda$ and which had a similar form to the result of Ingenito and Williams.

In a later paper, Lapidus and Rudenko [32] introduced a co-ordinate transformation to the parabolic wave equation before obtaining a perturbation solution. The transformation describes the nonlinear distortion of a plane wave and so overcomes some of the limitations of the perturbation approach, permitting the prediction of asymmetric waveforms close to the point of shock formation. The limitation of the method lies in its separation of the description of distortion and diffraction, but nevertheless reasonable agreement was obtained with numerical calculations for the case of a source with a Gaussian shading function. Recently Burvingt [33] has also obtained a solution for a Gaussian source, apparently without recognition of earlier work (eg [34,35]) by writing the velocity potential as a sum of two terms. The particular choice of variables employed enabled the leading term

to be expressed as the Fubini solution, with the remaining term (representing the losses to higher harmonics) being small for the conditions considered of small near field distortion and no shock formation. The solution is essentially a far field one and does not to first order predict phase shifts between the harmonic components.

An alternative perturbation approach was used by Ginsberg [36] to obtain an integral expression for the second harmonic component in terms of the Hankel transform of the shading function of the axially symmetric source. This theoretical approach has similar limitations to that of Ingenito and Williams [29] in that it cannot describe accurately rapid radial fluctuations in the beam profile and is limited to the case where the nonlinear distortion is small. These limitations were addressed in a second paper [37] where the integral was corrected in an ad hoc fashion to account for rapid radial fluctuations of the beam and a co-ordinate straining transformation was used to derive a solution for significant amounts of distortion. The method can predict the waveform anywhere in the field, provided that a shock is not formed, and thus represents a significant advance on previous work; however to evaluate the result implicit equations must be solved for the co-ordinate transformations and an oscillatory integral must be evaluated, all of which depend on a number of special functions and so the method is costly in terms both of effort and computing time.

For the case of a focusing piston source Lucas and Muir [38] have also recently applied the parabolic wave equation to calculate the second harmonic field. They obtained an integral solution which

could be solved numerically, and verified the predictions of both amplitude and phase by experiment. Rugar [39] obtained a perturbation solution for the second harmonic amplitude in a focused Gaussian beam, using a Green's function approach. Because the assumption of a Gaussian profile introduces a great simplification into the calculations, the solution is expressed in terms of elementary functions and can be evaluated easily for both axial and off-axis locations.

The work described in this section demonstrates that progress can be made in the analytical description of diffractive fields, using a perturbation method. However it is necessary to make a number of approximations, and the final result is usually quite complicated and must be evaluated numerically.

1.3.2 Lossless field of a transducer - including shock formation

Several different approaches to this problem have been developed in the last ten years or so and are outlined in this section.

The easiest way to treat this problem is to attempt to separate out the two effects and treat the problem in two stages. In the far field of a transducer, the local effect of diffraction is weak, so that a geometrical acoustics approximation can be made. Lockwood et al [22] achieved this by assuming that the situation could be treated as a spherical wave whose amplitude varied with the polar angle θ according to the directivity function of the transducer. They then analysed the effect of nonlinear distortion by treating each propagation direction separately, using the theory of Blackstock [16]. They determined the radius of the

equivalent sphere empirically to be two thirds of the Rayleigh distance for the transducer and obtained agreement with experiment for the first three harmonics. Later, Shooter et al [23] used a similar approach to study the saturation of the fundamental component as a function of source amplitude. They used an equivalent source radius of half the Rayleigh distance and again gave experimental confirmation of their predictions. Concurrently, Ostrovskii and Fridman [24] used a similar approach to describe both an initially sinusoidal wave and a unipolar pulse. Although the approach described above is quite successful, it is only reliable when little or no distortion occurs in the near field region, and so has a limited usefulness. In an attempt to overcome this limitation, Ginsberg [40] has used a perturbation model to calculate the distortion in the near field and matched this to a spherical propagation model to determine the far field behaviour. Few details of the results of this method are available so it is difficult to assess its usefulness, but the fact that the influence of near field effects extends well into the far field [41] must limit the improvement in accuracy that is achieved.

In 1969 Zabolotskaya and Khokhlov [42] derived a second order lossless parabolic wave equation which has already been discussed in section 1.3.1. When this equation is expressed in non-dimensional form, the coefficient of the diffraction term is $1/\sigma_0$ where σ_0 is a parameter describing the distortion occurring within the near field. It is thus possible to obtain asymptotic solutions of this equation, valid for either small or large σ_0.

Several authors [42-46] have obtained asymptotic solutions to this equation, and have been able to predict several characteristics of

nonlinear sound beams. The formulation of these solutions, as with that of other exact solutions [47-48] makes them difficult to apply to a piston source and so only qualitative results can usually be obtained.

More useful results have been obtained by Rudenko et al [49-50] who considered a source with a Gaussian shading function. For the case when σ_o is small, they obtained [49] an analytical perturbation solution for the second harmonic, predicting both its amplitude and phase. In the opposite limit, for large σ_o, they obtained an expression for the distribution of energy across the beam. In [50] the full equation was reduced by assuming a quadratic dependence of the amplitude on the radial co-ordinate. It was thus possible to obtain a time domain solution, analogous to Equation 1.7 which was valid for distances well within the near field. The waveforms derived from this solution possessed the familiar asymmetric shape, with the amplitude for the positive half-cycle being greater than that for the negative. An extension of this method has recently been described [51] where extra terms have been included to account for the shading function of the source in more detail and to permit the description of focused sources. Unfortunately, the useful range of validity of the solution is again limited to propagation distances much less than either the Rayleigh length or the focal distance.

The work described above has only limited usefulness since it can only be applied in a few cases. To obtain solutions which have more general application, several authors have made various ad hoc approximations. Ostrovskii and Sutin [26-27] treated the case of focusing beams by separating out the effects of nonlinear

distortion and diffraction. In the pre-focal region they neglected diffraction and calculated the distortion of a spherically converging wave. Close to the focal point they assumed that the extra distortion is negligible and that diffraction dominates. If a shock occurs then the method has to be modified to account for distortion in the focal region. The results predict that, as the source amplitude is increased, the focusing gain initially increases before decreasing due to saturation. This prediction is in accord with experiment (see Section 4.4), although the quantitative predictions have not been verified. The same authors have used a similar approach to described the field of a plane piston source [52] but with much less justification.

Muir and Carstensen [8] have modelled the field close to the last axial maximum of a transducer as a spherically converging wave. They obtained the required equivalent radius for the source by considering the gain in amplitude which occurred at low levels and obtained reasonable agreement with experiment [9]. In the case of a focusing source, early work again used the low amplitude field to determine the geometry of an equivalent spherical wave [53-54]. However, this method cannot account for diffraction in the focal region in sufficient detail, and poor agreement with experiment was obtained [53-54]. An improved method of accounting for diffraction was given in [55], which describes some of the work reported in this thesis. This study derived a form of Burgers' equation for a focused beam, by modelling the beam profile with a Gaussian function and neglecting phase variations in the near field.The lossless form of this equation was solved using Blackstock's weak shock solution [16]. Agreement with experiment

was obtained for the amplitudes of the harmonic components, but the theory did not predict the asymmetry in the waveform that is observed in such fields.

For one-dimensional waves, it was shown in section 1.2.2 that an analytical implicit time domain solution can be obtained if absorption is neglected. Inspection of the result (Equation 1.8) shows that the solution is expressed in terms of a co-ordinate transformation. This transformation (often called co-ordinate straining) again has an implicit definition, and depends upon the local, time varying amplitude as well as on the shock parameter σ. It is possible to extend the concept of this method when diffraction is accounted for, and several of the papers referred to above utilise this approach. The method can also be developed in a more rigorous manner as is demonstrated in a review of the topic [56-57]. There are several possible approaches, but only one is mentioned below.

Initially, a perturbation solution to the wave equation is found for the dependent variables (velocity potential, velocity and pressure). The second order terms in such solutions will increase with distance and thus the solutions will not be uniformly accurate. To overcome this problem, the co-ordinates are strained in a manner analogous to Equation 1.8 so that the resulting expressions are uniformly accurate. If the solutions are used beyond the shock formation distance, then the equal area rule [58] is applied. Ginsberg [59] has applied the method in describing the interaction of a nonlinear wave with a plate, and more recently has considered the field of a infinitely long strip radiator [60]. He has also treated the field of a piston source [36-37,61], as

discussed in the previous section.

Kelly and Nayfeh [62] have used the method to describe the field of general directional spherical waves. This work has the advantage over earlier work [22-24] that the description is complete and accounts for the near field. In the far field the solution reduces to the form derived previously [22-24]. Unfortunately it is difficult to apply the solution to a piston transducer, because it is expressed in modes characterised by Legendre functions. To evaluate the waveform, the field would have to be expressed in these terms, and the appropriate series evaluated for each point in space and for each instant in time. Despite this difficulty, this method may prove to be viable if only a few waveforms are to be evaluated.

A final approach to the problem is to solve the equation directly by numerical methods. The parabolic wave equation [42] has been solved by this means for several cases of practical interest [63-67]. Unfortunately only scanty details of the method have been reported [63,68], but the procedure involves using a grid of field points and evaluating the amplitudes in a stepwise manner. The main limitations of the method are the difficulty of describing the field from sources with a discontinuous shading function and presumably the computing time which is required. Plane transducers with polynomial and Gaussian shading functions have been described [63,65] as well as focused transducers [64]. The propagation of pulses from a Gaussian source has also been studied [67]. Finally, the field from a plane piston source has been modelled approximately, and an harmonic analysis of the waveform performed [66].

To sum up, several methods have been used to analyse the given problem, each with their own limitations and advantages. In certain cases, accurate predictions can be obtained with a reasonable degree of effort, but there is still a need for improved techniques.

1.3.3 Diffractive fields with absorption

A number of papers treat the far field of a diffractive source as a spherical wave [69-71], in a similar way to that described in the previous sections. As they do not account for near field effects, they have little relevance to the present aim.

Merklinger et al [72] obtained a method for evaluating the loss incurred by the fundamental for an arbitrary axial beam profile. They neglected the effects of harmonics higher than the second and calculated the loss by evaluating the source term of the distorting wave. The final equation was Bernoulli's equation which has an exact solution. They approximated the axial profile of a transducer as $[2 + (1 + 2R)^{-1/2}]/[2R + (1 + 2R)^{1/2}]$ where R is the propagation distance normalised to the Rayleigh length. In general, agreement with experiment was obtained for short ranges, with differences of 1.5 dB (in 8 dB) occurring at larger ranges.

Kuznetsov [73] derived a parabolic wave equation similar to that of Zabolotskaya and Khokhlov [42] but accounting for absorption. Fenlon and Kesner [34,74] used this equation to obtain a form of Burgers' equation for the axial field of a piston source. They obtained this by approximating the field profile by a Gaussian function and neglecting a term related to phase variations. The

equation is discussed in more detail in Chapter 2 of this report. From this equation it was possible to deduce an expression for the variation of the fundamental amplitude and, for low levels, for the second harmonic [75]. Another numerical solution for the case of a Gaussian beam was obtained by Swindell [76] by considering a focused beam as a spherical wave with changing radius of curvature. In this work, the variation of attenuation with frequency could be varied so as to correspond to the physical situation being described, but phase shifts due to diffraction were neglected. In a later paper [77] the effect of phase shifts was accounted for in an ad hoc manner, although in the light of the work of this thesis it is not clear that the correct assumptions about the behaviour of the harmonic components were made. The method described in section 2.1.4 of this thesis was used to describe the field of a focusing source, including the effects of phase variations in the near field [78]. The asymmetric waveforms predicted by the theory were in agreement with previous measurements [55], but no detailed evidence to verify the model was presented.

Berntsen et al [79] performed a perturbation analysis to obtain the second harmonic field at low amplitudes, using a Green's function method. In general a triple integral must be evaluated and thus the method requires considerable computing effort, but an asymptotic far field solution was also obtained for the case when the absorption is small. This solution only requires the evaluation of a double integral and takes the form of the sum of contributions from the near field and from the far field distortion.

Numerical solution of Kuznetsov's equation has been achieved on a similar basis to that used for the lossless equation. The transducer shading functions described were a fourth degree polynomial and a Gaussian. Regions of existence of a shock wave were derived, and the effect of absorption on the temporal profile examined [80]. A second study described the behaviour of several harmonic components, which were obtained by Fourier analysis of the calculated waveform [81]. Several characteristics of the field structure were studied, such as amplitude and phase variations in the axial and radial directions.

McKendree [82] has also used a numerical finite-difference method to solve Kuznetsov's equation. He treated separately the three principal effects. Starting with the time domain waveform he allowed for nonlinear distortion using an incremental solution of the equation for plane waves. The Fourier transform was then obtained, and absorption accounted for in the frequency domain. Finally, diffractive effects were included, again with the frequency domain description. Results obtained with this algorithm were compared qualitatively with those of Bakhvalov et al and a certain amount of agreement shown. McKendree's waveforms were not very smooth, due to the coarse sampling used, and the characteristic asymmetric distortion was not as pronounced as in the waveforms of Bakhvalov et al. This latter feature could possibly be due to the manner in which nonlinear distortion was accounted for, as the possibility of self-refraction apparently was not fully considered.

A third finite-difference method of solving Kuznetsov's equation involves calculations entirely in the frequency domain [41,83-85],

avoiding the need to perform time-consuming Fourier transforms. Extensive results have been presented for the beam patterns of the first three harmonics in the field of a plane piston and a Gaussian source [83] and comparisons were made with the theoretical results of previous authors. Waveforms were also presented, but these demonstrated unsatisfactory Gibbs oscillations when a shock has been formed, due to the relatively small number of frequency components that it was possible to use for such time-consuming calculations (which can take several hours on a large computer). The numerical method was adapted for the prediction of far field beam patterns by rewriting the equations in terms of new parameters for the spatial and temporal co-ordinates [41,85] and the results were compared with experimental measurements of far field beam patterns. A feature of these results is the prediction of extra side-lobes called 'fingers' in the beam pattern, situated between the side-lobes of the fundamental component and which were not predicted by previous theories [66]. In addition there was an extensive discussion of the use of approximate models to describe the far field behaviour, and the limits of validity were demonstrated in general terms.

Although finite-difference techniques would currently appear to be the only way of obtaining a complete solution for the case of diffractive waves, they cannot attain high accuracies for the higher harmonic components using computers that are currently available. This is the main reason why the approach has not been used in the work described here.

1.3.4 Numerical Methods - for the one-dimensional case

Later in this thesis, a one-dimensional equation describing propagation in a diffractive field is solved numerically. Consequently, previous numerical methods for this case, all of which use a finite-difference approach, are briefly reviewed here.

Cook [86] allowed for wave distortion using the time domain waveform by approximating an equation similar to Equation 1.7. He then obtained the Fourier transform, and allowed for absorption in the frequency domain. To do this, he did not treat the two effects completely separately, but made approximate allowance for the variation in amplitude over the incremental distance. Cary [87] performed both operations in the time domain, using a Taylor series which included terms up to the tenth derivative with respect to time. The rapid fluctuations which occur close to the shock front make this method somewhat difficult to use.

Fenlon [88] and later Hennion and La Greve [89] used the frequency domain description to account for both processes. This approach avoids the need to calculate high order derivatives close to the shock front, and does not require repeated Fourier transformations as Cook's method does. The main difficulty with the method is associated with having to truncate the Fourier series, and this again arises because of shock formation. The consequent growth in the higher harmonics was overcome by applying a correction factor at each iteration.

A further development was made by Trivett and Van Buren [90], who allowed for absorption and geometrical attenuation by including them explicitly in the definition of the Fourier components.

Treating absorption in this way makes the procedure more accurate and stable when absorption is high, although it makes the harmonic amplitudes during computation very large. The implicit compensation for geometrical attenuation makes the algorithm efficient, since the amount of nonlinear distortion accounted for in each step is roughly constant. This description results in a series of linked differential equations, which are solved using the Runge-Kutta method. Recently, Haran and Cook [91-92] have used a similar method to predict the propagation of ultrasound in tissue and in biological fluids.

1.3.5 Propagation in dispersive media

In chapter 2 the propagation of ultrasound in tissue is described and it is therefore of interest to review previous work in this area. Before the present work there has been very little study of nonlinear propagation in tissue that has taken account of dispersion, but the effects of dispersion in relaxing media have been studied. Polyakova et al [93] derived the basic equations for a single relaxation process and demonstrated the effect on the profile of the shock front. Later work [94-95] described the shape of the shocked waveform for frequencies below and above the relaxation frequency and showed that in certain cases the profile was asymmetrical, with the amplitude of the peak-negative pressure being greater than that of the peak-positive. Similar dispersive effects occur for propagation in waveguides, and Webster and Blackstock [96] have validated theoretical predictions of asymmetric waveforms by comparison with experiment. Dispersion, whether it can be described in terms of a single relaxation

process or whether it is only known empirically has usually been accounted for in one-dimensional propagation by including an appropriate term to Burgers' equation in place of the original attenuation term, and this is the approach used by Blackstock [97], who used a perturbation solution to determine the effect of dispersion on the growth of the second harmonic. Frequency domain solutions have been obtained [98-99] corresponding to those of Fubini and Fay, which show that for plane wave propagation the phase relationships between the harmonic components are independent of the amount of distortion. Predictions of waveforms in biological media have recently been made [78] using the numerical method of section 2.1.5, and these indicate that dispersion leads to a reduction in asymmetry for tissue relative to that for water. In this work, dispersion and attenuation were taken account of in a similar manner to that of Blackstock [97], but a full numerical solution was used and the effect of diffraction was included.

1.4 Previous experimental work

For the purpose of this report, it is necessary to make accurate measurements of the harmonic content at a particular point in a diffractive field. The literature review presented here is confined to work relevant to this objective. Thus previous work which dealt with some averaged parameter of the field, or involving acoustic waveguides, for example, is generally excluded. Of prime interest is the extent and accuracy of experimental measurements which have been reported.

1.4.1 Early work and measurements of the fundamental component

Some of the earliest measurements were made in a tube or horn, so that an approximately plane wave could be obtained. In this way, the behaviour of the second harmonic at low amplitudes was verified [100], although the absolute levels of the predictions disagreed somewhat with experiment. Other early papers [101-103] used a shadowgraphic method to verify the general shape of the waveform obtained at finite amplitudes. By Fourier analysis of the waveform, it was possible to examine the growth of the second and third harmonics [103].

In common with other work which assumed plane wave propagation [104-106], these early studies used receivers with a large area, so that much of the diffractive structure was not detected. Naugol'nykh and Romanenko, however, used a miniature hydrophone to measure the variation of the positive peak pressure with distance from the source [107]. Several workers later measured the variation of the fundamental frequency component with distance along the acoustic axis [23,72,108] and also for off-axis points in the far field [23,109]. These measurements were used to verify a far field application of the theory for lossless spherical waves [23] and also to test an approximate model which could be used in the near and far field regions [72]. Recently [9] the variation of the total intensity in a transducer field has been compared in the near field region with an approximate application of the solution for lossless spherical waves.

A number of measurements of the fundamental amplitude or related parameters have therefore been made in a nonlinear acoustic field.

Nevertheless, several areas have still to be covered, such as measurements when absorption is significant, and the detailed confirmation of any model to predict the fundamental amplitude in the near field region. As both of these areas can be important for the sources and frequencies used in medical ultrasound, there is a need for such measurements to be made.

1.4.2 Measurements of more than one harmonic

Waveforms which demonstrate the progressive distortion due to nonlinear propagation were obtained with a small hydrophone by Browning and Mellen [110]. They confirmed the existence of the phase distortion which had been observed in earlier experiments [105,107] but did not compare their results with any quantitative theory. This phase distortion is always seen to exist in diffractive fields, and can usually be detected as asymmetry in the waveform, with the positive peak pressure being greater than the negative. Attempts have been made to confirm theoretical predictions of this asymmetry [111] but the measurements were not sufficiently reliable to give a conclusive result. Similar asymmetric waveforms have been observed for propagation in tubes, where dispersion is caused by the tube wall boundary layer. In this case, good agreement with predictions has been obtained [112]. Recently measurements of waveforms have been made in the field of a 1 MHz disc transducer [113], but the hydrophone used was large (1 cm diameter) and was made from quartz with a resonant frequency of 15 MHz, so that only qualitative comparisons with theoretical predictions could be made. Another recent paper has examined a related effect, that of the varying duration and beam

width of a pulse, in a highly nonlinear medium [114] but again only qualitative conclusions could be drawn from the results.

For diffractive fields at low amplitudes, rough agreement has been obtained [38] for the phase variation of the second harmonic in the focal region of a curved source. It can thus be seen that very little experimental study has been made of phase variations in finite amplitude diffractive fields. This aspect of the propagation is important for medical ultrasound because the asymmetric distortion is frequently quite marked in practice, and can significantly affect the observed peak acoustic pressures. Measurements made for this thesis have included the phase properties of the wave, but they have only been compared with theory for the case of a focused field.

Spherical wave

Although there has been little study of phase variations in nonlinear propagation, several workers have described the behaviour of the harmonic amplitudes. Romanenko [115] determined the variation of the second and third harmonics in a spherical wave field and confirmed theoretical predictions for $\sigma < 1$. He used a value for β which was 16% higher than the currently accepted value, but his results are nevertheless convincing. The radiator used was a hollow sphere, and the experimental symmetry was thus truly spherical.

Near Field

Measurements of the first three harmonics have been made for the near field of a transducer [28] and the variation of the second

harmonic used to confirm theoretical predictions [29]. Both the theory and measurements were confined to the case of small σ, where little energy has been lost by the fundamental component. The hydrophones used were calibrated for the first and second harmonics with an accuracy of $\pm$ 30%. A similar technique was used to measure the variation of the first four harmonics in a focused field [54]. Unfortunately only a very simple theory was available for comparison, so poor agreement was obtained with predictions. More recently, measurements of the second harmonic on the axis of a focused source have been used to confirm a theoretical model, valid for low amplitudes, which accounts for diffraction [38]. The variation of beamwidth for the first two harmonics has also been determined for a focused source [116], but no comparison with theory was made. The predictions of a simple model based on geometrical acoustics for the variation of intensity, total power and beam shape have been compared with experiment in the megahertz frequency range [9]. McClennan et al have reported measurements in the near field of a radiator with a 'near-Gaussian' shading function [117], describing the first three harmonics, but the results are of little use because no absolute levels were given. Recently, an unfocused transducer with Gaussian shading function has been used to verify predictions of the second harmonic field at low amplitudes [118].

To sum up, near field measurements have been used to confirm predictions of the second harmonic level on the acoustic axis, and for relatively low amplitudes ($\sigma<1$). Although several other cases have been studied, there have been no definitive measurements of the off-axis field, of the higher harmonics, or of the field when

$\sigma > 1$. Measurements made during the early stages of the present study have covered these cases to some extent (see also [119,120]) but as no theoretical model is currently available, they have yet to be analysed in detail.

Far Field

Marsh [121] measured the first three harmonics on the axis of a directional source, and verified predictions based on a numerical solution of the governing equation. This equation accounted for geometrical spreading and absorption, the latter apparently being significant for large ranges. Lockwood et al [22] studied the variation of the angular beamwidth and axial levels of the first three harmonics. The theoretical model used the lossless solution for spherical waves up to a certain distance, and thereafter calculated the levels on the basis of small-signal absorption. Despite the ad hoc nature of the model, agreement was obtained within a few dB.

Moffett [71] made far field measurements of the fundamental and second harmonic to examine the variation of the latter when absorption is significant. Lockwood et al [22] had assumed a normalised variation of $\exp(-4\alpha z)$ for the second harmonic, where α is the absorption coefficient of the fundamental, whereas the correct asymptotic dependence is $\exp(-2\alpha z)$. Moffett obtained reasonable agreement with his ad hoc theory and concluded that an absorption coefficient of 2α only applied at extremely long ranges. For most practical applications, a coefficient of 3α was found to be reliable.

Some of the most comprehensive experimental studies of harmonic

propagation have been carried out in air, the first of these being by Allen [119]. He measured the first six harmonics in both the near and the far field. Acoustic saturation was observed, and the dependence of harmonic amplitude on source pressure that is predicted by lossless theory was confirmed. At the time, few theoretical solutions were available, so Allen explained his results in terms of empirical relationships. Campanella [120] extended the measurements to cover different source frequencies, and obtained curves of the variation with propagation distance for different source amplitudes. It was observed that the 1/n dependence of amplitude on harmonic number could be exceeded within the near field. Again, no accurate theory was available for interpreting the results in detail, but nevertheless the broad dependence of the field on the experimental parameters was derived.

Further data have been obtained for propagation in air, describing the far field directional response and the response along the axis [122] for the first four harmonics. The amplitude response for the fundamental component and the propagation data for the first and second harmonic were compared with an ad hoc application of the theory for lossless spherical waves. The results were affected by streaming to some extent, but nevertheless the predictions were confirmed to within 3 dB.

The hydrophone calibration method described in section 4.2 relies on predicting the harmonic content of the far field of a transducer, and some of the results were presented in [35]. The success of this calibration method constituted a verification of the theoretical treatment used, which relied on modelling the

field of a piston source with that of a transducer with a Gaussian shading function. Recently, this theoretical method has also been validated by comparison with measurements in the field of a source having a Gaussian beam profile [78]. Measured and predicted waveforms were compared at distances of one and five Rayleigh lengths, but no results for the spectral content of the field were presented.

Focused Fields

In addition to the measurements that have already been discussed for this case there have recently been a number of investigations of the focused fields that occur in diagnostic ultrasound (including earlier reports of the work presented here [55,78]).

Although it is possible to detect the existence of sawtooth waves in measurements of the output of diagnostic ultrasound equipment made some years ago [123] it is only recently with the availability of broadband hydrophones that the effects have been recognised and become the subject of specific investigation. Duck and Starritt [124] demonstrated that asymmetric sawtooth waveforms are produced from commercially available equipment when the propagation is in water, and pointed out that this caused difficulties in the calibration of such devices as well as potentially affecting their performance and biological interaction. They also demonstrated the changing spectral character of the wave and calculated the shock parameter [55] according to the procedure described in this report, verifying that severe shock formation did indeed occur. In later work [125] nearly all of the 25 scanners tested gave rise to a shock

parameter greater than one at the focus and additional effects due to nonlinear propagation were noted such as the variation with amplitude of the beam profiles and the locations of maximum positive and negative acoustic pressure. It was also observed that the peak-positive acoustic pressure had a much narrower beam than the peak-negative, and the implications of this effect for calibration procedures have been discussed in [126]. These effects have recently been studied in more detail [127] with the distance to the location of peak-positive pressure being shown to initially increase and then to decrease with increasing source amplitude, whereas the distance for the peak-negative pressure decreases monotonically. These observations were predicted in general terms theoretically [64] but no quantitative comparison with theory has yet been undertaken.

In response to the assertion [128] that the observations of distorted waveforms were due to hydrophone nonlinearities, evidence has been obtained from measurements at different propagation distances [129] and (by the present author) from interferometric measurements [130-131] to show that the distortion is indeed the result of acoustical effects.

An investigation of the effect of nonlinear propagation on the performance of a B-scan instrument which uses a water path for acoustic coupling to the patient has shown that relatively small amounts of distortion ($\sigma = 1$) have no significant effect on image quality [132] but to date there has been no systematic investigation of this potential problem. Recently Humphrey et al [133] have performed measurements which confirmed the theory of Lucas and Muir [38] in the focal region, although discrepancies

were observed particularly in the phase of the second harmonic beyond the focus. Although the focusing gain of their source (12.5) was somewhat larger than is normally encountered in diagnostic ultrasound, their results are of interest because they showed marked changes in the waveform in the post-focal region, and also they demonstrated that the phase of the n^{th} harmonic was proportional to (n-1). This latter observation is confirmed by measurements reported in this thesis, but as yet no simple physical explanation of it has been advanced.

Propagation in tissue

Several studies have been undertaken to determine the effect of nonlinear distortion on the apparent absorption coefficient in tissue, usually determined by the temperature rise of the medium [134-136]. A water path was used so that nonlinear distortion occurred before the wave entered the sample, and the effects observed were generally explained by linear propagation within the tissue. Nevertheless, Carstensen et al [136] showed that at high amplitudes distortion occurred in the sample medium, giving rise to a further increase in absorption. The effect of nonlinear propagation on the measurement of attenuation of biological tissues has also been demonstrated by the use of a through-transmission technique [137]. Again, the measurement system included a water path and a plane-wave propagation model was used to explain the anomalous experimental results.

Recently there have been two demonstrations of wave distortion in tissue, where the transducer has been directly coupled to the sample. Starritt et al [138] obtained their results with

physiotherapy and imaging equipment for propagation through human calf muscle. The distortion of the waveform was evident, although relatively slight and second harmonic levels of about 10% were observed. Measurements in ox liver for shorter propagation lengths [139] have shown significantly greater amounts of distortion, including the formation of a sawtooth waveform. The magnitudes and phases of the second and third harmonics were reported, although no comparison was made with theoretical predictions.

Summing up, several harmonic components have been measured in the far field of a transducer, but comparisons with theory have only been made for the first three. The sophisticated theoretical developments discussed in section 1.3 have not yet been verified, instead only very simple theories have been tested against experiment. Furthermore there has been little study of the situation when attenuation is significant and for propagation in dispersive (ie biological) media there has been no comparison of experiment with theory. This thesis describes the verification of models which account for diffraction as well as nonlinear distortion, dispersion and attenuation. The measurements cover many harmonic components, as well as the characteristic parameters of the waveform, for several different source frequencies. The results presented in Chapter 4 thus represent a significant contribution to the current understanding of the subject.

2. THEORY

2.1 Derivation of the basic wave equations

2.1.1 The nonlinear parabolic wave equation

The detailed derivation of the propagation equations used in this study is quite a lengthy procedure. The major steps are given here along with a discussion of their validity.

A second-order nonlinear wave equation for irrotational flow was derived by Kuznetsov in 1971 [73]. He started with the equations of fluid dynamics: continuity, momentum, heat conduction and the equation of state for the fluid. He assumed that the maximum frequency in the wave was considerably less than the relaxation frequency, and only included terms up to second order in the perturbations of the state variables. The equation for the velocity potential ϕ, where $\underline{u} = \underline{\nabla}\phi$ is:

$$\nabla^2\phi - \frac{1}{c^2}\frac{\partial^2\phi}{\partial t^2} = \frac{1}{c^2}\frac{\partial}{\partial t}\left[- b\nabla^2\phi + (\underline{\nabla}\phi)^2 + \frac{(\beta-1)}{c^2}\left(\frac{\partial\phi}{\partial t}\right)^2\right] \qquad 2.1$$

The three second-order terms on the right represent the effects of absorption, convection and the nonlinear equation of state. The equation may be simplified if it is assumed that the change in the waveform over a propagation distance of one wavelength is small. This in turn implies that convection and diffraction are small - ie that $\beta u/c \ll 1$, $ka \gg 1$ (for a radiator with dimensions a) and $a^2/z^2 \ll 1$. The first two conditions certainly apply to the

measurements considered in this report (with minimum factors of 100 and 50 respectively). The third condition requires that no measurements be made close to the transducer, and that little nonlinear distortion occurs in this region. Making the change of variables $z = z$ and $t' = t - z/c$, Equation 2.1 becomes

$$\nabla_\perp^2 \phi - \frac{2}{c} \frac{\partial^2 \phi}{\partial t' \partial z} = \frac{1}{c^4} \frac{\partial}{\partial t'} \left\{ - b \frac{\partial^2 \phi}{\partial t'^2} + \beta \left(\frac{\partial \phi}{\partial t'} \right)^2 \right\} \qquad 2.2$$

where $\nabla_\perp^2 \equiv \frac{\partial^2}{\partial y^2} + \frac{\partial^2}{\partial x^2}$ and it has been assumed that

$c \frac{\partial^2 \phi}{\partial z^2} << \frac{\partial^2 \phi}{\partial t' \partial z}$. Hence

$$\frac{\partial p}{\partial z} - \frac{c}{2} \nabla_\perp^2 \int p \, dt' = \frac{b}{2c^3} \frac{\partial^2 p}{\partial t'^2} + \frac{\beta}{2\rho c^3} \frac{\partial}{\partial t'} (p^2) \qquad 2.3$$

Equation 2.3 is the second-order nonlinear parabolic wave equation [75] and forms the basis of the work in this thesis. It is valid for moderate nonlinearity and in the Fresnel approximation. Its plane wave form is the Burgers' equation [13] and for spherical waves it becomes

$$\frac{\partial p}{\partial r} + \frac{p}{r} = \frac{\beta}{\rho c^3} p \frac{\partial p}{\partial t'} + \frac{b}{2c^3} \frac{\partial^2 p}{\partial t'^2}$$

For propagation in tissue, the assumptions made above do not hold, and the equations require modification to take account of the different characteristics of the medium. Equation 2.3 predicts an attenuation coefficient that is proportional to the square of the frequency and assumes that the dispersion is negligible, whereas tissue demonstrates significant dispersion and has an attenuation

coefficient that typically varies linearly with frequency [140]. The variation in tissue of attenuation and dispersion with frequency cannot be accounted for by a simple theory of relaxation [140] but it is shown in Appendix 1 that these characteristics can be accounted for by assuming that the following equation of state applies to the medium:

$$p = c_o^2 \rho \left[1 + \frac{B}{2A}\frac{\rho}{\rho_o}\right] - mc_o^2 \left[\int_{t-\tau_2}^{t-\tau_1} \frac{\rho(t')}{t-t'}\,dt' - \rho\,\mathrm{Ln}\left(\frac{\tau_2}{\tau_1}\right)\right] \qquad 2.4$$

The first part of Equation 2.4 is the usual form that is used in nonlinear acoustics, while the second term describes a medium that is not in equilibrium, but demonstrates hysteresis in responding to past as well as present perturbations. In this equation, τ_1 and τ_2 are arbitrary parameters that satisfy the inequalities $\omega\tau_2 >> 1$ and $\omega\tau_1 << 1$, for all angular frequencies ω in the wave. If Equation 2.4 is used as the equation of state, then the following equation of motion can be derived (see Appendix 1):

$$\frac{\partial p}{\partial z} - \frac{c_o}{2}\nabla_\perp^2 \int p\,dt'' = -\frac{m}{2c_o}\left[\int_{-\infty}^{t'-\tau_1} \frac{\partial p}{\partial t''}\frac{dt''}{t'-t''} + \frac{\partial p}{\partial t'}\,\mathrm{Ln}(C_L\omega_o\tau_1)\right]$$

$$+ \frac{\beta}{2\rho c_o^3}\frac{\partial}{\partial t'}(p^2). \qquad 2.5$$

Here τ_1 is again an arbitrary parameter with $\omega\tau_1 << 1$, ω_o is a reference parameter, corresponding to the lowest angular frequency present in the wave and $C_L = \exp(C_E) \simeq 1.781$, where C_E is Euler's constant.

2.1.2 Application to the field on the axis of a diffracting beam

For one-dimensional waves, the solution of Equation 2.3 is relatively straightforward because, if the equation is expressed in the natural co-ordinates of the system, then there is no dependence on the off-axis (ie radial) co-ordinate. This arises because in these cases the nonlinear term does not alter the beam profile and consequently the operation of the diffraction term is unaffected by the propagation of the wave. This fact may be expressed by stating that the pressure field is always an eigenfunction of the diffraction operator of Equation 2.3 in the following sense:-

$$Lp = g(z)p$$

$$\text{where} \quad L = -(c/2)\,\nabla_{\perp}^{2} \int dt'$$

Reversing the argument, it is possible to say in general that for any type of radiation, a one-dimensional form of Equation 2.3 can be used if p is an eigenfunction of L. This condition will not usually be satisfied, because p will become distorted by the nonlinear term of Equation 2.3. This term will change the beam profile, and because of the need to evaluate $\nabla_{\perp}^{2}\, p$, it will not be possible to predict even the field along the axis without obtaining a complete solution of the equation. Nevertheless, there may be some circumstances in real diffracting fields where this effect may be small and, because of their relative ease of solution, such cases are of particular interest. An example of such a situation is the axial field of a symmetrical transducer if the distortion occuring within the near field is small. In this

case the beam profile will only be modified in the far field region, and there will be little error introduced by the assumption of an unmodified profile, because the effect of diffraction in this region is small. This approach will be considered in more detail in section 2.2.1, for the case of a piston with a Gaussian shading function.

The assumption that the effects of diffraction and nonlinear distortion can be treated separately has been applied previously to describe the far field behaviour of a beam [22], but no explicit account was taken of near field effects, the distortion occurring within the near field being assumed to be negligible. A general form of Equation 2.3 under the one-dimensional approximation will now be derived.

Let the axial variation of pressure with distance at low amplitudes and neglecting absorption be given by f(z), where f(0)=1 so that the pressure is

$$p_{lin} = p_o f(z),$$

where p_o is the initial pressure amplitude, and a factor of $e^{i\omega t'}$ has been omitted for clarity. Then p_{lin} satisfies

$$\frac{\partial p_{lin}}{\partial z} - p_{lin} f'(z)/f(z) = 0$$

so that the operator $L \equiv - f'(z)/f(z)$.

If it is assumed that p remains an eigenfunction of this operator in the nonlinear case, then Equation 2.3 becomes:

$$\frac{\partial p}{\partial z} - \frac{f'(z)}{f(z)} p - \frac{\beta}{\rho c^3} p \frac{\partial p}{\partial t'} - \frac{\alpha(\omega_o)}{\omega_o^2} \frac{\partial^2 p}{\partial t'^2} = 0 \qquad 2.6$$

here $\alpha(\omega_o)/\omega_o^2 \equiv b/2c^3$ and $\alpha(\omega)$ is the absorption coefficient at a given frequency. The following substitution and changes of variable are made:

$$P = p/p_o f(z)$$

$$\sigma = (\beta p_o k/\rho c^2)\int_o^z f(z')dz' \qquad 2.7$$

$\tau = \omega_o t'$ where $\omega_o = c\,k$ and ω_o is a reference angular frequency.

Then Equation 2.6 becomes:-

$$P_\sigma - PP_\tau - P_{\tau\tau}/\Gamma_o f(z) = 0.$$

where $\Gamma_o = \beta p_o k/\rho c^2 \alpha(\omega_o)$

Γ_o represents the relative importance of nonlinear distortion and absorption at the origin (see section 1.2.3). If it is assumed that $f(z)$ can be rewritten in terms of σ, so that $f(z) = f_1[\sigma(z)]$, then it is possible to use the parameter $\Gamma(\sigma)$ which represents the relative importance of absorption at the field point σ,

where $\Gamma(\sigma) = \Gamma_o f_1(\sigma)$.

The final generalised equation can be written:-

$$P_\sigma - PP_\tau - P_{\tau\tau}/\Gamma(\sigma) = 0 \qquad 2.8$$

Equation 2.8 is useful for two reasons: firstly it shows that a one-dimensional model can be used for the axial field in a number of cases and secondly it allows the use of the same computer

algorithm for different physical situations.

2.1.3 The field of a piston source

A particular case of Equation 2.8 can be obtained if a source with Gaussian shading function is assumed. Solution of the linear equation for this case gives $f(z)=1/(1-iz/r_o)$ where $r_o = ka^2/2$ and a is the waist radius of the source function. f(z) is thus a complex function, the phase angle of which changes with z. The changing phase angle represents the acoustic phase variations which occur mainly within the near field. Initially this effect is ignored, and f(z) is represented by its modulus ie $f(z) \simeq 1/\sqrt{1+z^2/r_o^2}$. Inspection of the full equation for this case (Equation 2.17) indicates that this approximation is strictly valid for R>>1. Applying Equations 2.7 to this case gives:

$$\sigma = \sigma_o \mathrm{Ln}(R + \sqrt{1 + R^2}) \quad \text{and} \quad \Gamma = \Gamma_o/\cosh(\sigma/\sigma_o)$$

$$\text{where} \quad R = z/r_o \quad \text{and} \quad \sigma_o = \beta p_o k r_o/\rho c^2 \ . \qquad 2.9$$

Equation 2.8 is then identical to that derived by Fenlon and Kesner [34] for the same situation. The advantage of the derivation presented here is that the stages of approximation are made clearer, allowing the physical basis of the assumptions to be seen.

If the phase variation of the primary wave is not neglected, then Equation 2.8 could still be applied but it has not been used in this study for two reasons. First, $\Gamma(\sigma)$ cannot be obtained explicitly, and second σ becomes complex. The physical basis of a complex value for σ has not been explored and so solutions

obtained for this case are not presented here. Nevertheless, such an approach has potential for further investigation since it can in some circumstances offer a simple explanation of various experimental observations, such as the variation of the phase of the frequency components of the wave with harmonic number. If phase variations must be accounted for Equation 2.6 can still be used, either as given, or by making the substitution $P = p/p_o f(z)$ as shown in section 2.2.1.

For preliminary work, use was made of Equations 2.8 and 2.9 as described above. The transducers used as sources were circular discs and had a piston-like shading function. Beyond the Rayleigh distance, the variation of axial pressure is similar to that of a Gaussian transducer. In the near field, however, a piston source has a broad axial peak in pressure whereas the Gaussian source has a more constant response. The peak of the piston field will have little effect on the distortion of waves in the far field because the distortion depends on the integral of the pressure amplitude. Nevertheless, within the near field, the peak must be accounted for. The following adjustment to the p_o used in calculating σ_o and Γ_o was therefore used:-

$$p_o = p_o' \sqrt{1 + R_m^2} \; 2 \sin(1/2R_m) \qquad 2.10$$

Here p_o' is the true initial pressure extrapolated to the face of the transducer, R_m is the value of R at the measurement point and p_o is used to calculate σ_o and Γ_o.

Equation 2.10 has the desired properties in that p_o approaches p_o' for large R_m and the correct pressure amplitude is obtained at R_m

for low amplitudes. Equation 2.10 is probably useful for $R_m \gtrsim 0.7$. In the remainder of this thesis, the theory based on Equations 2.8-2.10 will be referred to as the matched Gaussian model.

An alternative approach that has been used in modelling axial transducer beams [23], is to use the spherical wave form of Burgers' equation, and assume a source radius of $r_o/2$ and a source amplitude of $2p_o'$. The values of σ obtained by this approach, by assuming an unmatched Gaussian beam and by using Equation 2.10 are as follows:-

$$\sigma = \sigma_o' \, \mathrm{Ln}(2R_m)$$

$$\sigma = \sigma_o' \, \mathrm{Ln}(R_m + \sqrt{1 + R_m^2})$$

$$\sigma = \sigma_o' \, \mathrm{Ln}(R_m + \sqrt{1 + R_m^2}) \quad \sqrt{1 + R_m^2}\, 2\sin(1/2R_m)$$

$$(\sigma_o' \equiv \beta p_o' k r_o/\rho c^2)$$

All three values of σ become equal as R_m approaches infinity, whilst that of the spherical wave approximation is relatively small for small R_m. This is to be expected, as the spherical wave approximation neglects any distortion that occurs between R = 0 and R = 0.5.

From the above considerations it therefore seems reasonable to use Equation 2.10 with Equations 2.8 and 2.9 as a first attempt to describe the axial field of a piston beam, although the final justification must come from experimental measurements.

2.1.4 The field of a pulsed focused source

In the previous paragraphs an equation (Equation 2.8 with 2.9 and 2.10) was derived to describe the axial field from a transducer, which is valid for small near field distortion. Its principal advantage is that no explicit solution for the off-axis field is necessary, thus reducing considerably the amount of numerical computation required. The equation is strictly justified for the field from a transducer with a Gaussian shading function, but it was possible to apply it to a plane piston transducer by making an appropriate adjustment to the parameters. For the same reason, it would be very convenient to apply a similar equation to a focused piston source. If the nonlinear term is neglected, then the transformation from a plane Gaussian transducer to a focused Gaussian transducer is straightforward - the modes that are assumed to be present are still eigenfunctions of the wave equation, and the boundary conditions are satisfied simply by a change of origin. Two aspects require more detailed consideration, however, namely the question of whether Equation 2.8 is valid for this new situation and the method of relating the parameters for a Gaussian transducer to those of a focused piston. One application of this section is the prediction of the degree of nonlinear distortion present in the field of a pulsed focused piston source. Such fields are used very frequently in diagnostic ultrasound, and measurements of the peak pressures may be in error if nonlinear distortion occurs. It is therefore highly desirable to obtain a simple formula for predicting the probable maximum error in the measurement of peak-to-peak pressure. Of particular interest is the field at the focus, and this will be emphasised in the

discussion below. A second application of this work is the use of measurements of the acoustic field radiated by diagnostic equipment into water to predict the corresponding field when the equipment radiates into tissue. This requires a more sophisticated model of the propagation, which is able both to predict the shape of the waveforms that are produced and to take account of dispersion.

When discussing the field of a plane transducer, the region where diffraction was greatest (ie the near field) was not of crucial importance because the distortion there was assumed to be small, and because measurements were not made there. For the present case, however, diffraction is most significant at the focus, which is also the point of greatest interest. This means that the results obtained will probably be less accurate than those of the previous section. Nevertheless, for the practical situations considered, the extra attenuation of the beam is usually small, so that the beam shape is not severely distorted by the nonlinear processes and therefore the shortcomings of the model will not be fully evident.

The first stage of the theoretical treatment is to determine the field at low amplitudes. At low amplitudes the solution to Equation 2.3, neglecting the terms on the right hand side, for a Gaussian beam with focus at $z' = 0$ is

$$p = \left[p_o/(1 - iR)\right] \exp\left[- r^2/W_o^2(1 - iR)\right] \exp\left[i\tau\right]$$

where $R = 2z'/ kW_o^2$.

This relationship describes the field of a focused transducer situated at a distance -D from the origin, provided that the

radius of curvature, D_t, and the 1/e beam radius, W_t, are given by

$$D_t = D\ (1 + 1/R_o^2)$$

and $$W_t = W_o\ (1 + R_o^2)^{1/2},$$

where $R_o = 2D/\ kW_o^2$.

If a new coordinate, z, is defined with the origin at the transducer face then R may be re-expressed as

$$R = 2\ (z - D)/\ kW_o^2.$$

Having determined the field at low amplitudes, it is possible to deduce the modes that describe the beam shape of the harmonic components at finite amplitudes. This is achieved by assuming that these modes firstly satisfy the linear wave equation and secondly have the same axial profile as the fundamental component, as discussed in section 2.1.2. The mode for the harmonic number k is thus given by:

$$\Psi_k = \left[1/(1 - iR)\right] \exp\left[- r^2k/W_o^2\,(1 - iR)\right] \exp\left[i\,k\,\tau\right] \qquad 2.11$$

where k = 1, 2, 3 ....

Although the harmonic modes are now uniquely defined, it is still necessary to consider whether or not they are physically reasonable as approximate solutions of Equation 2.3. It is well known [16] that, for small amounts of distortion, the amplitude of the k^{th} harmonic is proportional to the fundamental amplitude raised to the power k. Consequently, if the radial profile of the fundamental retains a constant shape (ie if the distortion is small), the profile of the k^{th} harmonic will be given by:

$$\Psi_k(r) = \left[\Psi_1(r)\right]^k$$

This condition is satisfied by Equation 2.11. If the distortion of the wave is not small, then this simple behaviour will break down, and the relationship will not be valid. Because this equation is

meant to describe the near field of the transducer (in contrast to the results of section 2.1.3), this breakdown is significant and will limit its strict range of applicability to relatively small amounts of distortion ($\sigma < \pi/2$). Nevertheless the results will be useful, in view of the requirement for only approximate predictions and because of the way in which the results will be applied (see section 2.2.2).

Equation 2.11 predicts that the beam width at the focus will be proportional to $1/\sqrt{k}$. The measurements of Lucas [38] and Bjorno and Lewin [116] indicate that the second harmonic radius is approximately $1/\sqrt{2}$ times that of the fundamental, providing experimental confirmation of Equation 2.11. The physical basis for this $1/\sqrt{k}$ dependence is as follows. If the beamwidth of a higher harmonic was equal to that of the fundamental, at distances significantly away from the focus, then the dependence would be 1/k, because of the variation in wavelength. However, the beamwidth of a harmonic away from the focus is less than that of the fundamental, for reasons that have already been given, thus moderating the variation of focal width to $1/\sqrt{k}$.

Equation 2.3 may be solved for the focused field case by expressing the acoustic pressure as the sum of modes of the type given by Equation 2.11, with the addition of an extra term to account for the attenuation of the wave:

$$P = \left[p_o/2(1+R^2)^{\frac{1}{2}}\right] \sum_{n=1}^{\infty} \exp\left[-n^2 \alpha r_o (R+R_o)\right] \left\{\phi_n(R) \exp\left[in\tau - r^2 n/a^2(1-iR)\right]\right.$$

$$\left. + \phi_n^*(R) \exp\left[-in\tau - r^2 n/a^2(1+iR)\right]\right\}$$

If this relationship is substituted into Equation 2.3 then a set of coupled equations is obtained which can then be solved numerically (see section 2.2.1). Using this approach it is possible to predict the asymmetric waveforms that are observed experimentally (see Section 4.4). An alternative approach is to apply Equations 2.7 to the beam profile described by Equation 2.11 and so permit the use of Equation 2.8 for the focused field case. This procedure gives the following values for the parameters of Equation 2.8:

$$\sigma = \sigma_o \left\{ \mathrm{Ln}\left[R_o + \sqrt{1 + R_o^2}\right] + \mathrm{Ln}\left[R + \sqrt{1 + R^2}\right] \right\}$$

$$\Gamma = \Gamma_o/\sqrt{1 + R^2} = \Gamma_o/\cosh\left\{\left[\sigma(0) - \sigma\right]/\sigma_o\right\} \qquad 2.12$$

$$\sigma_o = \beta p_o k D/\rho c^2 R_o$$

$$\Gamma_o = \beta p_o k/\rho c^2 \alpha_o$$

Here, $-R_o$ is the value of R at z=0, $\sigma(0)$ is the value of σ at R=0 and p_o is the pressure amplitude at the focus that would be expected for linear propagation. If the linear gain in amplitude is denoted by G, then the value of σ at the focus (R=0) is:

$$\sigma_f = \beta p_o k D \,\mathrm{Ln}\left(G + \sqrt{G^2 - 1}\right) / \rho c^2 \sqrt{G^2 - 1} \qquad 2.13$$

This value of σ_f will be used in a later section to derive the peak pressure at the focus of a pulsed transducer. Another study has used a perturbation approach to obtain a corresponding value for σ_f [38], denoted here as σ_L, for the continuous wave (CW)

field from a focused piston transducer:

$$\sigma_L = 2\beta p_o kD\, F(G') / \rho c^2 G' \qquad 2.14$$

here F(G') is a function of G' which must be evaluated by numerical integration and G' is the theoretically predicted gain in amplitude at the focus. For values of G' greater than 10, F(G') may be approximated by Ln(G'). As G' is not defined in quite the same way as G, it is difficult to compare the predictions of the two models. However, for the measurements described in section 4.4 the two models give similar results, although the theory of Lucas and Muir [38] applies only for low amplitudes.

Having obtained a model of the field of a focused transducer, based on the use of Gaussian modes, the relationship between the parameters of the model and the characteristics of the real acoustic field has to be determined. The interpretation of most of the parameters in Equation 2.13 is self-evident, but it is not clear how the gain G should be determined. When characterising diagnostic ultrasound equipment, it is not always possible to make measurements of the field close to the transducer, so it is desirable to specify a method for determining G that relies only on measurements made in the focal region. Even given this limitation, however, there are several possible approaches that could be adopted. Two such possibilities are to equate the measured focal beam width to the width of the corresponding Gaussian beam, or to determine G from the ratio of the area of the active element of the transducer to the measured beam area. Having decided to use one of these two possible approaches, another

decision has to be made regarding the level to use in the definition of beam area or beam width (eg -6 dB or 1/e etc). Two tests were used in finding the best option, namely comparison of the predicted harmonic levels with experiment and comparison of the predicted second harmonic amplitude with other theoretical predictions [38]. In the first test (see [55] and section 4.4) agreement was obtained with experiment if G was determined from the ratio of the active area of the transducer to the focal beam area, the focal area being determined at a level of 1/e times the maximum amplitude in the focal plane. Comparison with the second harmonic levels predicted by another model [38] for values of the gain in the range 5 to 20 indicates that the above method underestimates the second harmonic amplitude by 20%. Agreement is obtained in this case if G is obtained by equating the -6 dB focal beam width of the field to the -6 dB width of the beam in the model. The conclusions drawn from the two tests are different because the measured focal beam width of the transducer is significantly greater than the theoretical value, due partly to the limited spatial resolution of the hydrophone used to characterise the field. Consequently, the method used in the first test to determine G is the better one in practice, because it gave agreement with experiment, and because it is less sensitive to errors in the measurement of beam width.

An important consideration in judging the applicability of the model developed in this section to the fields used in diagnostic ultrasound is its sensitivity to the precise geometry and shading function of the transducer. This consideration arises because a great variety of transducer types are used in diagnostic

ultrasound, and if the result were sensitive to such factors then a model of the nonlinear effects would be extremely difficult to apply. The extent to which the model satisfies this criterion can be judged by comparison of the results with the theoretical predictions for a focused piston source [38], which has a field profile containing large fluctuations in both amplitude and phase, in marked contrast to the smooth Gaussian profile. As stated above, the accuracy of the model is typically 20% in this case, for low amplitudes and continuous waves. Since the fields encountered in practice will have smoother beam profiles (due to the smoother shading function of the transducers and the limited coherence length of the pulses), the accuracy of the model is expected to be usually better than 20%. Equations 2.8, 2.12 and 2.13 have now been derived and justified to some extent; their solution will be obtained in section 2.2.2.

2.1.5 The field of a focused source in tissue

The relationship used in modelling the nonlinear propagation of ultrasound in tissue is Equation 2.5. At low amplitudes, this predicts a dispersion that depends logarithmically on frequency and an attenuation that is proportional to frequency (see Appendix 1); consequently the acoustic pressure for this case is expressed as follows:

$$p = (p_o/2) \sum_{n=1}^{\infty} \left\{ \phi_n(R) \exp\left[in\left\{ \tau + (2\alpha r_o R/\pi) Ln(n) \right\} - r^2 n/a^2(1-iR) \right] \right.$$

$$\left. + \phi_n^*(R) \exp\left[- in\left\{ \tau + (2\alpha r_o R/\pi) Ln(n) \right\} - r^2 n/a^2(1+iR) \right] \right\}$$

$$x \exp(-n\alpha r_o R)/\sqrt{1+R^2} \ .$$

Insertion of this relationship into Equation 2.5 gives the following expression for the variation of harmonic amplitude:

$$\frac{\partial \phi_n}{\partial \sigma} = \frac{i\phi_n}{\sigma_o \cosh[\{\sigma - \sigma(0)\}/\sigma_o]} + \frac{in}{4} \left\{ \sum_{k=1}^{\infty} \phi_k \phi_{n-k} \exp(-iA) \right.$$

$$\left. + 2 \sum_{k=1}^{\infty} \phi_k^* \phi_{n+k} \exp\left\{ iB - 2k\alpha r_o \sinh[(\sigma - \sigma(0))/\sigma_o] \right\} \right\} \qquad 2.15$$

$$A = [nLn(n) - kLn(k) - (n-k)Ln(n-k)] \ (2\alpha r_o/\pi) \sinh[(\sigma - \sigma(0))/\sigma_o]$$

$$B = [(n+k)Ln(n+k) - kLn(k) - nLn(n)] \ (2\alpha r_o/\pi) \sinh[(\sigma - \sigma(0))/\sigma_o]$$

and the other parameters are as defined in section 2.1.4. Equation 2.15 is solved by a numerical method, as described in section 2.2.1.

2.2 Methods of solution

There is no known exact solution, even of the approximate parabolic wave equation, Equation 2.3. For axial waveforms, it is possible to solve equations such as 2.6 and 2.8 to a high degree of accuracy, however, using numerical methods. Computation of these solutions can require considerable calculation time, so for many applications approximations are used which are valid under certain conditions. These numerical and approximate solutions will

now be discussed.

2.2.1 Numerical solution

Equations 2.6 and 2.8 can be solved using a numerical method similar to that described in [90]. If p is written in the following form:-

$$p = (1/2)\sum_{-\infty}^{\infty} \phi_n(R)\, e^{in\tau} \qquad e^{-n^2\alpha r_o R}\; p_o f_2(R)$$

where $f_2(R) \equiv f(z)$ and $\alpha \equiv \alpha(\omega_o)$, then Equation 2.6 becomes, on equating coefficients of $e^{in\tau}$

$$\frac{\partial \phi_n}{\partial R} = \frac{i\sigma_o}{4} f_2(R) n \left\{ \sum_{k=1}^{n-1} \phi_k \phi_{n-k} e^{2k(n-k)\alpha r_o R} + 2 \sum_{k=1}^{\infty} \phi_k^* \phi_{n+k} e^{-2k(n+k)\alpha r_o R} \right\} \qquad 2.16$$

for $n \neq 0$, where σ_o is given in Equation 2.9. Now $\partial \phi_o / \partial R = 0$, so it has been assumed in deriving the equation that $\phi_o = 0$. It has also been assumed that $f_2(R)$ is real, so Equation 2.16 cannot be used to account for phase variation. The solution is obtained using numerical techniques such as the Runge-Kutta method, and this has been implemented for several different forms of f(z). Equation 2.8 can also be solved by a similar method; this has the advantage that if a constant step size is used in the solution, then a roughly constant amount of nonlinear distortion is accounted for in each step. This feature is particularly advantageous when calculating the distortion of waves which vary in amplitude considerably due to diffraction or geometric spreading. The effect

of small-signal absorption has been allowed for in the definition of ϕ_n, and this makes it possible to use a relatively large step size. However, it also means that ϕ_n can become very large for large n, and so it is sometimes necessary to multiply by the factor $e^{-n^2 \alpha r_o R}$ at several values of R during a calculation.

The greatest difficulty in using Equation 2.16 results from the truncation of the series of harmonic components. The computing time increases as the square of the number of terms that are retained in the series, so there is a large incentive to keep this number as low as possible. However, the result of truncation is that the higher terms tend to grow too rapidly because part of their loss mechanism has been neglected, and this has a knock-on effect on the lower terms. In reference [90] this was overcome by requiring that each term should be no greater than the preceding one. The algorithm used here applies a similar criterion, requiring that all harmonics above a certain one (approximately the fiftieth) be smaller than the preceding one by the factor n/n+1, after having made allowance for the absorption factor. This criterion was only applied to the higher harmonics, as it was thought possible that the assumption that $\phi_{n+1} < \phi_n$ may be invalid for diffractive fields in certain cases. It was possible to use a different criterion to limit the truncation error, based on the Fay solution (section 2.2.3), but this was not normally used.

If a sufficiently large number of terms is retained in the series, there should be no error introduced by truncation, because absorption will have made the neglected terms very small. It is possible to estimate this absolute maximum number of terms by using the Fay solution (see section 2.2.3) as follows.

Implicit in the following calculation is the assumption that Γ is fairly large (eg greater than 20) and that $\sigma > 1$ - because otherwise the Fay solution is not valid. In this case, the higher harmonic amplitudes are approximately proportional to 1/n, and Equation 2.16 becomes, approximately:

$$\frac{\partial \phi_n}{\partial R} \simeq \sum_{k=1}^{n-1} \frac{1}{k(n-k)} + 2 \sum_{k=1}^{\infty} \frac{1}{k(n+k)}$$

If n is small, the second sum varies as 1/k and if n is large it varies as Ln(k); in either case the convergence is fairly slow. It is therefore necessary, if possible, to include terms up to the point where the 1/n dependence no longer holds. The Fay solution gives (see section 2.2.3):

$$\phi_n \simeq 1/\sinh[n(1 + \sigma)/\Gamma]$$

Consequently, the 1/n dependence ceases when $n(1+\sigma)/\Gamma \gtrsim 1$. As $\sigma > 1$ in the present discussion, the requirement that $n_{max}(1+\sigma)/\Gamma = 2$ means that the number of terms retained, $n_{max} = \Gamma$. This condition is applied in the programs, subject to an overriding maximum of between 115 and 256 terms. The error incurred by applying this condition can be estimated by approximating the summation in the loss term by an integral; this predicts a truncation error for $\sigma = 1$ of 9% for large n and 0.2% for small n. For $\sigma = 2$, the error is 4% for large n and 0.04% for small n. Since the truncation error is expressed as a fraction of the loss of the wave, the error in harmonic amplitude, which is expressed as a fraction of the amplitude, will usually be

significantly less than the values quoted above.

Table 1 Truncation errors of the numerical program.

The errors are expressed in percent relative to the most accurate calculation, which retained a hundred harmonics and used a step size of $x_s/50$. The calculations were made for $\sigma=3$ and $\Gamma=100$. The computing time (on the Tektronix 4052) for a propagation distance equal to x_s is also given.

Harmonic Number	50 Harmonics Retained			100 Harmonics Retained	
	Step $x_s/10$	Step $x_s/20$	Step $x_s/50$	Step $x_s/10$	Step $x_s/20$
1	0.019	0.014	0.009	0.002	<0.001
5	0.09	0.09	0.08	0.039	0.003
10	0.05	0.14	0.14	0.13	0.01
20	0.10	0.29	0.39	0.24	0.01
30	0.9	2.2	2.9	4.3	0.18
40	2.0	12	23	11	0.9
Time (mins.)	12	23	59	47	94

The dependence of accuracy on step size and number of retained harmonics was determined by using the program to calculate the harmonic content for a plane wave with $\Gamma = 100$ and $\sigma = 3$. Step sizes of 1/10, 1/20 and 1/50 times the shock formation distance

(x_s) and maximum harmonic numbers of 50 and 100 were used. The errors, expressed in percent relative to the most accurate calculation, are given in Table 1, along with the computing time required for each calculation. For all cases, the error in the twentieth harmonic amplitude was less than 1%. For the results reported in this thesis, a step size of $x_s/20$ was usually used. Comparing the errors given in Table 1 with those predicted from estimating the truncation error, agreement with the predictions for small n is obtained for the tenth harmonic, whilst agreement with the predictions for large n is obtained for the thirtieth harmonic. Calculations were also made of the harmonic content for $\Gamma = 100$ as far as $\sigma = 16$, using a step of $x_s/50$ and $n_{max} = 100$, to test for unforseen cumulative errors. The results were compared with the "Improved Fay" solution (see below) and there was no evidence of such problems.

Two computers were used in these calculations, the first being a Tektronix 4052 desktop controller, programmed in Basic. It is part of a dedicated system, being used to analyse and store the measurement results. Although it is not as fast as a larger machine, it can be left running for long periods, and its use has the additional advantage of avoiding the need for an interface with other equipment. Its speed was such that the calculation of one step in the solution of Equation 2.16 using 40 harmonics took 45 seconds. Equations 2.15 and 2.17 were solved using an IBM PC microcomputer with 8087 mathematics coprocessor, which was programmed in Pascal with double precision variables. These calculations involved many more operations than the solution of Equation 2.16 because of the need to take account of both

magnitude and phase, but the algorithms were optimised so that the calculation time was not greatly increased. For Equation 2.17 the evaluation of one step using 40 harmonics took 9 seconds, whereas the corresponding time for Equation 2.15 was 35 seconds.

Having described the general method of solving Equation 2.16, a second similar equation will be derived for a Gaussian beam profile, taking the effects of phase variation into account. The acoustic pressure p is written in terms of the following modes:

$$p = (p_o/2) \sum_{n=1}^{\infty} \exp(-n^2 \alpha r_o R) \left\{ \phi_n(R) \exp[in\tau - r^2 n/a^2(1-iR)] + \phi_n^*(R) \exp[-in\tau - r^2 n/a^2(1+iR)] \right\}$$

It should be noted that the radial variation of these modes is expressed as an eigenfunction of the operator $\nabla_\perp^2$ in Equation 2.3, as mentioned in section 2.1.2. Substituting into Equation 2.3 (the full parabolic equation, not the simplified one-dimensional form) results in the following equation:-

$$\frac{\partial \phi_n}{\partial R} - \frac{i}{1 - iR} \phi_n = \frac{i\sigma_o n}{4} \left\{ \sum_{k=1}^{n-1} \phi_k \phi_{n-k} e^{2k(n-k)\alpha r_o R} + 2 \sum_{k=1}^{\infty} \phi_{n+k} \phi_k^* e^{-2k(n+k)\alpha r_o R} \; e^{\frac{-2r^2 k}{a^2(1+R^2)}} \right\} \qquad 2.17$$

Comparing this with Equation 2.16, there is an extra term on the left hand side; this can be eliminated if a slightly different substitution is made. However, such a substitution introduces additional complexity into the other terms and so it is not used

in the numerical solution. The first term on the right hand side of Equation 2.17 is essentially the same as that obtained previously; this is because the formulation used satisfies the requirement of $\phi_n \simeq (\phi_1)^n$ which has the consequence that the harmonics are produced with the assumed profile. The second term on the right of Equation 2.17 represents the loss of energy to other harmonics, and has the extra factor of $\exp[-2r^2k/a^2(1+R^2)]$. This means that energy loss of a harmonic does not preserve the assumed beamshape. If the beamshape is changed from the assumed form, Equation 2.17 will no longer apply because the action of the $\nabla_\perp^2$ will be changed. However, if the change in beam profile is only small (eg if the change only occurs in the far field), then Equation 2.17 can still be applied to the field close to the axis. The energy loss term is only significant when the higher harmonics have acquired significant amplitudes, and so Equation 2.17 can be applied if the distortion within the near field is small. These conclusions are in agreement with the argument of section 2.1.2 thus justifying the method used there.

If it is assumed that the only part of the field that affects the axial pressure is that contained within the radius of the transducer, the value of r in Equation 2.17 may be set equal to a. If it is further assumed that R is large, then an expression corresponding to Equations 2.16 and 2.6 is obtained, thus confirming the conclusions of section 2.1.2. Equations 2.8 and 2.9 were obtained by Fenlon [34] for a piston source, using a similar approach to that given here; however there was no publication of the detailed derivation, making it necessary to repeat the work here.

The arguments given above to justify the neglect of the factor of $\exp[-2r^2k/a^2(1+R^2)]$ in Equation 2.17 have much less validity for focused fields because, if significant distortion is present, then the beam profile in the focal region will be modified which will in turn modify the subsequent diffraction of the wave. One possible method of overcoming this problem is to replace the mode amplitude, ϕ_n by $\phi_n = \phi_n(R) + \phi_n'(r,R)$, expressing the dependence of the amplitude on the radial co-ordinate. In the resulting nonlinear equation those terms that depend on r are separated out to determine the required variation of the diffraction term, and the main equation is then modified accordingly. In practice, this perturbation approach has to be developed further in order to achieve a stable and uniformly accurate solution and it is simpler to use a more ad hoc approach. One such method is to modify the diffraction term in Equation 2.17 (the second term on the left hand side) to account for the changing beam profile. One modification that has been tried successfully is to multiply the phase term (the imaginary part) by the extra attenuation of the fundamental component of the wave. The results obtained using this approach are compared with experiment in section 4.5.

2.2.2 Lossless solution

It is well known [16] that a solution of Equation 2.8 if the absorption term is neglected is:

$$P = g(\tau + \sigma P)$$

All of the work in this study relates to waves with an initially

sinusoidal waveform, and therefore the relevant form of the solution is:

$$P = \sin(\tau + \sigma P)$$

The utilisation of this implicit equation is straightforward for $\sigma < 1$, but for $\sigma > 1$ the equation becomes multiple valued for a range of values of τ, centred about $\tau = 0 + 2n\pi$. Such a solution is evidently impossible for longitudinal waves, and arises from the neglect of the attenuation term off Equation 2.8. However application of the results of weak shock theory [16] or the "equal area rule" [58] (which is a consequence of weak shock theory) allows one to arrive at the intuitively reasonable result for $\sigma > 1$:-

$$P = \theta/\sigma$$

where $\theta = \sin^{-1}\theta/\sigma \qquad 0 < \theta < \pi \qquad$ for $\tau = 0_+ + 2n\pi$

$\theta = \sin^{-1}\theta/\sigma \qquad -\pi < \theta < 0 \qquad$ for $\tau = 0_- + 2n\pi$

$P = 0 \qquad$ for $\tau = \pi + 2n\pi$

and P is continuous for $2n\pi < \tau < (2n+1)\pi$. The peak amplitude, P_p, of such a wave is therefore:

$$P_p = 1 \qquad \text{for } \sigma \leqslant \pi/2$$
$$P_p = (\sin^{-1}P_p)/\sigma \qquad 0 < \sin^{-1}P_p < \pi, \qquad \text{for } \sigma \geqslant \pi/2 \qquad 2.18$$

Blackstock [16] has obtained a Fourier series solution for P, valid for all values of σ:

$$\phi_n = \frac{2x_o}{n\pi} + \frac{2}{n\pi\sigma} \int_{\sin^{-1}x_o}^{\pi} \cos n(\theta - \sigma \sin\theta)\, d\theta \qquad 2.19$$

where $x_o = 0$ for $\sigma < 1$

and $x_o = (\sin^{-1}x_o)/\sigma$ for $\sigma > 1$ $\quad 0 < \sin^{-1}x_o \leq \pi$

and $P = \sum_{n=1}^{\infty} \phi_n \sin(n\tau)$.

Equations 2.18 and 2.19 are not new; however their application as solutions of Equation 2.8 demonstrates their utility in a wider range of practical situations than has been hitherto reported. Their relevance to this study is twofold. Firstly, the numerical computation of Equation 2.19 takes considerably less time than the solution of Equation 2.16, partly because Equation 2.19 gives each harmonic amplitude independently of the others. Secondly, Equation 2.18 is a very simple formula and so is useful in the description of the fields from medical ultrasonic equipment (section 2.1.4). The disadvantage of these solutions is obviously their failure to take explicit account of absorption. This omission becomes increasingly serious with increasing harmonic number; in fact there is no situation where Equation 2.19 is valid for arbitrarily large n. The general validity range of Equation 2.19 may be expressed as $n \ll \Gamma$, but a more precise statement may be obtained from the Fay solution (section 2.2.3, strictly valid for $\sigma \geq 3$):-

$$n < \sqrt{6\varepsilon}\ \Gamma/(1 + \sigma)$$

This is the condition for Equation 2.19 to be accurate within a

fractional error of ε, where Γ is the parameter occuring in Equation 2.8. This relationship shows that for n=7 and σ=2 an accuracy of 5% is achieved provided that Γ is at least 40. The accuracy of Equation 2.18 in the presence of absorption may be estimated in a similar manner by comparison with the time domain solution for sawtooth waves (Equation 2.23), giving the fractional error as

$$\varepsilon = -[(1+\sigma)/\pi^2\Gamma]\{1 + \mathrm{Ln}[2\pi^2\Gamma/(1+\sigma)]\}.$$

For σ = 2 this relationship requires that Γ should again be at least 40 to achieve an accuracy of 5% for the prediction of peak pressure, whereas for σ = 3 Γ must be 55.

Having demonstrated that Equation 2.18 is a solution of Equation 2.8, valid for Γ >40, it is now possible to complete the analysis of section 2.1.4 which treated the pulsed focused field of a piston transducer. In that section, it was shown that Equation 2.8 applies in this situation, with the relevant parameters being defined by Equation 2.12. The value of the shock parameter at the focus, σ_f is given by Equation 2.13 and the normalised peak pressure at the focus can now be obtained by substituting σ_f into Equation 2.18.

The formal treatment of the problem is now complete, but there are still some steps required to relate the solution to practically feasible measurements. Appendix 2 gives a number of experimental details and further explanation. What is required is a procedure for determining the amount of nonlinear distortion likely to be present in a particular field. For practical reasons, it is not desirable to characterise the shape of the waveform in a particular situation. Instead, the value of the shock parameter at

the focus (σ_f) is required. The fields from different diagnostic machines can then be separated into categories: $\sigma_f<0.5$, $0.5<\sigma_f<1.5$ and $\sigma_f>1.5$, thus allowing the likely extent of nonlinear effects to be assessed. It is essential that only a few measurements need be made, and also that the amplitude of the initial wave from the transducer should not have to be changed.

It is shown in Appendix 2 that the appropriate value of σ_f can be obtained from a parameter which can be determined practically, σ_m, using the following equations:

$$\sigma_f = \sigma_m/\sin(\sigma_m) \qquad \text{for } \sigma_m > \pi/2$$

$$\text{and } \sigma_f = \sigma_m \qquad \text{for } \sigma_m \leq \pi/2 \qquad 2.20$$

where

$$\sigma_m = \beta p_{o,m} kD \, \mathrm{Ln}(G + \sqrt{G^2 - 1})/\rho c^2 \sqrt{G^2 - 1}$$

Here, $p_{o,m}$ is the measured value of the peak pressure at the focus and the other parameters have been defined previously.

2.2.3 Approximate solution allowing for absorption

The solution of Equation 2.8 where all three terms must be taken into account will now be considered. The plane wave case, where $\Gamma(\sigma)$ is a constant will be dealt with first, because this problem has been studied extensively. Blackstock [13] demonstrated that a general solution due to Fay [17] could be expressed as an approximate solution of Equation 2.8, for the boundary condition of a sinusoidal wave, valid for $\sigma \gtrsim 3$:

$$P = (2/\Gamma) \sum_{n=1}^{\infty} \sin(ny)/\sinh[n(1 + \sigma)/\Gamma] \qquad 2.21$$

Recently, Parker [141] has demonstrated that the Fay solution is in fact an exact solution of Equation 2.8 for plane waves, and is the Fourier series representation of an infinite periodic array of well known time domain solutions (see Equation 2.23 below). Nevertheless, as a solution for the particular boundary condition that is considered here, Equation 2.21 is not accurate for small σ. Blackstock [13] verified the predictions of Equation 2.21 for the fundamental component of P, but he did not carry out the analysis for the harmonics. As the higher frequency components are of considerable interest in this study, further investigation of the accuracy of the Fay solution is required, and some results are reported in section 2.3.

Naugol'nykh et al [19], considered the solution of Equation 2.8 for cases with spherical symmetry, and demonstrated that an approximate time domain solution similar to that for plane waves could be obtained. The Fourier series representation of this solution [142] is again Equation 2.21, where Γ is now a function of σ, as in Equation 2.8. The extension of Equation 2.21 to other than plane geometries is possible because it describes the wave when a so-called "steady" shock exists. This situation was first treated by Taylor [143,12] and means that a balance exists between the forces of distortion (which tends to steepen the shock front) and absorption (which tends to smooth out the shock front). For a plane wave, these are the only effects present, but for a spherical wave, geometrical spreading is a third effect, which

acts to reduce (or increase) the wave amplitude. Consequently Equation 2.21 is not valid for abitrarily large ranges in this case [144,145]. Unfortunately there is some disagreement in the literature over the precise range at which Equation 2.21 ceases to apply for spherical waves, and so this topic will also be considered in section 2.3

From the above considerations, Equation 2.21 is felt to be justified for a wide variety of forms of $\Gamma(\sigma)$. In particular, if the variation of Γ with σ is no more severe than for spherical symmetry, then the solution is assumed to be valid. The only case where it may not be justified is in the rapidly varying near field structure of a piston source - however in this situation it is not usually necessary to take detailed account of absorption. An example of the valid use of Equation 2.21 is in the Gaussian beam case, where the axial field is characterised by a smooth transition from a plane wave to a spherical wave description. In this particularly simple case it is straightforward to estimate the validity range of Equation 2.21.

Blackstock [13] gives another Fourier series solution for the plane wave case which is a more accurate approximation than Equation 2.21 for an initially sinusoidal wave. This so-called "Improved Fay" solution is given below and can also be applied to non-plane waves:

$$P = (2/\Gamma) \sum_{n=1}^{\infty} \sin(ny)\left\{1 - (n/\Gamma^2)\coth[n(1+\sigma)/\Gamma]\right\}/\sinh[n(1+\sigma)/\Gamma] \qquad 2.22$$

This solution is somewhat more accurate than the Fay solution for

small σ, and approaches that solution as σ increases. As Equation 2.22 is again strictly applicable only for plane waves, or more generally for steady shocks, it has little advantage over Equation 2.21 when applied to other geometries. Consequently it is not very important whether Equation 2.21 or Equation 2.22 is used in a practical situation.

2.3 Accuracy of the solutions

As mentioned above, the accuracies of Equations 2.21 and 2.22 have not been previously determined in sufficient detail to permit reliable use of the formulae in many situations, particularly when predicting the amplitudes of harmonic components above the first. Consequently the accuracy of these equations has been investigated by comparison with the numerical solution of section 2.2.1 for a range of the parameters σ and Γ.

2.3.1 Accuracy for the plane wave case

Initially the relative accuracy of the Fay and Improved Fay solutions was considered. Inspection of Equations 2.21 and 2.22 indicates that the minimum discrepancy for a given n and Γ (as σ approaches ∞) is $100n/\Gamma^2$ %. A more useful guide, however, is the maximum discrepancy and this was determined by evaluating the expressions for $\sigma = 3$ and $\sigma = 4$ with the following results. For the fundamental component, the discrepancy is less than 1% for $\Gamma > 25$ and less than 5% for $\Gamma > 5$. For the twentieth harmonic component, the discrepancy is less than 1% for $\Gamma > 50$ and less than 5% for $\Gamma > 20$. Consequently, for most practical purposes, either equation may be used for values of Γ greater than fifty.

In the determination of the absolute accuracy of the equations, only the Improved Fay solution was used in the comparison with the numerical calculations since it is the most accurate relationship. A large amount of space would be required to present a complete range of results, so only the main features are given here. For many practical applications an accuracy of approximately 2% is required, so Figure 2 gives the values of σ and Γ for which this accuracy is achieved, for several harmonic numbers. For points lying above these curves the Improved Fay solution is more accurate than 2%. From Figure 2 it can be seen that the solution is fairly reliable for $\sigma > 4$ and $\Gamma > 50$, although this depends quite significantly on the harmonic number. If only the fundamental component is of interest, an accuracy of 1% is achieved for $\Gamma \gtrsim 10$, provided that $\sigma \gtrsim 4$. To supplement the information in Figure 2, Figure 3 gives the variation of the error as a function of σ, for $\Gamma = 50$. From these two curves, it is relatively straightforward to estimate the accuracy of Equation 2.22 for any value of σ and Γ.

2.3.2 Accuracy for the spherical wave case

The validity of Equations 2.21 and 2.22 will now be considered for the case of diverging spherical waves. This is of interest in its own right, but it is also important as a preliminary to the application of the equations to a transducer field. Although the subject has previously been considered [19,25,142,145] it has not been fully treated, and there is a certain amount of disagreement between different authors. The results of this earlier work are therefore summarised here, before giving details of the present study. It should be noted that the symbol Γ will be used here

(and elsewhere in this report) to denote the spatially varying $\Gamma(\sigma)$ of Equation 2.8, whereas Γ_o denotes the value of Γ at the source; the definitions of all the relevant parameters for spherical waves are given in Equations 1.17 and 1.18.

Naugol'nykh et al [19] showed that the following Taylor shock solution satisfies Equation 2.8 approximately (for $\sigma \gtrsim 2$),

$$P = \left\{ -\tau + \pi \tanh[\tau\pi\Gamma/2(1+\sigma)] \right\}/(1+\sigma) \qquad 2.23$$

They stated that this was valid provided that $\sigma_o\Gamma \gg 1$. Their discussion indicated that there were some situations where Equation 2.23 was still valid beyond the transition to the "old age" region (ie the region where the wave resumes a sinusoidal form) denoted by $(1+\sigma)/\Gamma > 1$. Cary [142] used Naugol'nykh's results to calculate the extra losses due to nonlinear effects. He noted that Equation 2.23 did not seem to be valid in the old age region because it predicted that the extra losses decreased with distance which was an incorrect result. Cary also used the Fourier expansion of Equation 2.23, which is Equation 2.21, the expansion being valid if $(1+\sigma)/\Gamma \ll 1$. He calculated the extra loss for the fundamental using Equation 2.21, assuming that it was valid at least up to $(1+\sigma)/\Gamma = 0.6$. Berktay [25] also performed similar calculations, and stated more precisely that Equation 2.21 was valid up to $(1+\sigma)/\Gamma = 0.6$ for spherical waves.

Scott [145] performed a more complete analysis of spherical wave propagation, defining a number of cases where different types of motion occurred. The case relevant to this discussion is his domain II, defined by $\exp(1/\sigma_o)/\Gamma_o\sigma_o^2 \ll 1$ and $\sigma_o/\Gamma_o \ll 1$. The first of these inequalities appears to ensure that a significant

amount of sawtooth propagation occurs, and the second that the effect of spherical spreading is important. Scott verified that a region governed by Equation 2.23 existed, and that this solution broke down when $(\sigma - \sigma_3)/\sigma_o \simeq 1$, where σ_3 is the larger root of the following equation:

$$\pi^2 \sigma_o \Gamma_o = (1 + \sigma_3)^2 \, e^{(\sigma_3/\sigma_o)}$$

This may be rewritten as follows:

$$\pi^2 e^{(1/\sigma_o)} \Gamma_o/\sigma_o = x^2 e^x$$

where

$$\sigma_3 = \sigma_o x - 1$$

and $(\sigma - \sigma_3)/\sigma_o \lesssim 1$ for Equation 2.23 to be valid. 2.24

From the above discussion, it is evident that three different conditions are given in the literature for the validity of Equation 2.23 and by implication Equation 2.21. Strictly speaking, Equation 2.24 only applies to Equation 2.23, but the relationship between Equation 2.23 and Equation 2.21 is very close and will not be discussed here. From the work of Cary [142] and Berktay [25] it seems that the condition given with Equation 2.23 is not reliable, and this observation was confirmed in this study by comparison with the results of numerical calculations. It therefore remains to compare the predictions of Equation 2.24 and Cary's condition.

If Cary's prediction is reliable, then the following parameter should be closely related to the error of Equation 2.21:-

$$g = \Gamma/(1 + \sigma) \qquad 2.25$$

If Scott's prediction is reliable, then another parameter should

be useful in predicting the error:-

$$h = (\sigma_3 - \sigma)/\sigma_o \qquad 2.26$$

Before considering the results of numerical calculation, these two conditions will be compared. First Equation 2.26 is solved for σ_3 and substituted in Equation 2.24

$$\pi^2\sigma_o\Gamma_o = (1 + \sigma + h\sigma_o)^2 e^h e^{(\sigma/\sigma_o)}$$

Substitution in Equation 2.25 and elimination of Γ gives:

$$e^h(1 + \sigma + h\sigma_o)^2/\pi^2\sigma_o = g(1 + \sigma)$$

$$g = e^h(1 + \sigma + h\sigma_o)^2/\pi^2\sigma_o(1 + \sigma)$$

If both Cary's and Scott's predictions were reliable, then one would expect a clear relationship to exist between g and h which did not involve the parameters such as σ_o and σ, at least in the situations when $g \simeq 2$ or $h \simeq 1$. Inspection of the above equation shows that no such relationship is apparent. The equation may be reduced further by noting that a significant sawtooth region must exist as a precondition for Equation 2.21 and hence Equations 2.25 and 2.26 to have any usefulness. If this is the case, and assuming that Equation 2.21 breaks down well into the sawtooth region, then $1 + \sigma \equiv 1 + \sigma_o \mathrm{Ln}(r/r_o) \simeq \sigma_o \mathrm{Ln}(r/r_o)$, giving

$$g = h \exp(h) \left[\sqrt{\mathrm{Ln}(r/r_o)/h} + \sqrt{h/\mathrm{Ln}(r/r_o)}\right]^2/\pi^2 \qquad 2.27$$

From the form of Equation 2.27 it can be seen that the two descriptions are roughly equivalent as long as $\mathrm{Ln}(r/r_o)$ is of order unity. This means that the effect of spherical spreading must be neither very great nor very small. The latter case

corresponds to the planar type of propagation rather than the spherical, and so is not relevant to the present discussion. For a given value of σ, the former case (ie a large amount of spherical spreading) corresponds to σ_o being small. Consequently it can be said that Equation 2.27 implies that Cary's and Scott's conditions are expected to be roughly equivalent as long as σ_o is not too small.

The validity of the two conditions was tested by plotting the error of Equation 2.21 as a function of g and h, as given in Equations 2.25 and 2.26. The error was determined by comparison with the results of numerical calculations as described in section 2.2.1. The range of σ_o was from 1 to 10 and the range of σ was usually 1 to 10 (sometimes from 1 to 15). The existence of a true spherical wave situation was ensured by requiring that $\sigma_o/\Gamma_o \ll 0.05$, and the range of Γ_o was from 100 to 7000. In general it was difficult to perform calculations for small σ_o because the requirement to obtain a significant region of sawtooth propagation meant that Γ_o must be very large. To preserve accuracy the algorithm requires the number of harmonic components retained to be of the same order as Γ_o, and consequently the calculations require too much computing time if Γ_o is very large. This problem was overcome in some cases by using the weak shock results (Equation 2.19) to calculate the harmonic amplitudes for some value of σ, and using the more complete numerical approach thereafter. If the value of σ is chosen so that $\Gamma \simeq 200$, then this hybrid calculation should be fairly reliable.

There are two effects causing Equation 2.21 to be inaccurate. The first has been discussed in the previous section (2.3.1) and

applies to the region of formation of a stable shock, ie $\sigma \lesssim 4$. The second applies to the region where a quasi-steady shock structure is breaking down and is the subject of the present discussion. The two effects have opposite sign and consequently it is fairly straightforward to distinguish between them. Only errors of the second kind are included in the results presented here.

Figure 4 gives the error as a function of g, for the first, fifth, tenth and thirtieth harmonics. It can be seen that the error of the fundamental is described very well, while that of the other harmonics is somewhat less well described. Nevertheless, the errors can be predicted quite reliably from the curves given. Figure 5 gives corresponding error curves as a function of h. Here the error of the fundamental shows poorer correlation than in Figure 4, whereas the correlation of the harmonics is slightly better. It must be remembered that Scott's predictions apply to Equation 2.23 and not strictly to Equation 2.21. For the fundamental, a given error occurs for greater propagation distances than for the other harmonics, and consequently the approximation of Equation 2.23 by Equation 2.21 is less reliable. The poorer correlation shown in Figure 5 for the fundamental is probably due to this reason, therefore, rather than to a weakness in Scott's results.

It should be noted that a common feature of the two sets of curves is that the error of Equation 2.21 is not the same for all of the harmonics. Instead, a given error occurs at smaller propagation distances for the higher harmonics than for the lower harmonics. This means that no single criterion can be applied to determine the validity of Equation 2.21; instead there are different

limiting values of g or h for each harmonic number. Figure 6 gives these values as a function of harmonic number for an error of 2%. From these curves it should be possible to estimate the range of validity of Equation 2.21 for a particular practical situation.

From the previous discussion it is somewhat surprising that Figures 4 and 5 indicate that good correlation is obtained between the error and both g and h. The main reason for this is that the range of values for σ_o was too small to show up any large discrepancies. Nevertheless, there are a number of points which lie a fair distance from the rest, and these mainly arise from the calculations for $\sigma_o = 1$ and $\Gamma_o = 7400$. Unfortunately the points for this case tend to lie on opposite sides of the curves in the two figures, and this makes it difficult to decide whether Scott's or Cary's method is the more useful. A further difficulty is that the numerical calculations for this case may be somewhat inaccurate, because it was necessary to use the hybrid method described above.

To conclude, it would be necessary to perform further calculations to decide conclusively whether Scott's or Cary's method is to be preferred. Such calculations would have to be performed with care, because of the difficulty of obtaining reliable results. For the practical situations arising in this study, however, either procedure may be used because the situation of small σ_o combined with large Γ_o does not arise. Although the results shown here relate to the situation $\sigma_o / \Gamma_o \leq 0.05$, they can be safely used for larger values of σ_o / Γ_o. In these cases the error will be less than expected, because the effect of spherical spreading is less significant. It should be noted that the results of this section

must be considered along with those of section 2.3.1, particularly for $\sigma<4$, because the errors described there occur in addition to those studied here.

2.3.3 Application to more general cases

The use of the results of the previous two sections in estimating the accuracy of Equation 2.21 (or Equation 2.22) when applied to the field of a transducer is largely a matter of common sense. If the results for a spherically spreading field are used, then a fairly conservative estimate of accuracy should be obtained. The application to the field of a piston transducer at distances beyond the Rayleigh length (Equations 2.8-2.10) will now be described briefly.

Inspection of Equations 2.9 and 2.10 indicates that if R is large, then the field is accurately modelled by that of a pulsating sphere of radius $r_o/2$, ie:

$$\sigma \simeq \sigma_o \mathrm{Ln}(2R) = \beta(2p_o)k\,(r_o/2)\mathrm{Ln}(2z/r_o)/\rho c^2$$

$$\text{and } \Gamma \simeq 2\Gamma_o\, e^{-(\sigma/\sigma_o)} = \beta(2p_o)k\,(r_o/2z)/\rho c^2$$

As R decreases, σ becomes greater than that given by the above equation, whereas Γ is less than would be expected. This means that for small R, the rate of change of Γ with respect to σ is less for a transducer field than for an equivalent spherical wave. It is the fact that Γ changes with σ that gives rise to the inaccuracy of Equation 2.21 as discussed in the previous section, and consequently the Equation should be more accurate for the transducer case than for a spherical wave of radius $r_o/2$. If the parameters defined by Equations 2.9 and 2.10 are used in

Equations 2.24-2.26, therefore, the curves of Figures 4 to 6 can be used to give a conservative estimate for the accuracy of the Fay solution as applied to this case. Similar arguments may be applied in other cases, but it will usually be obvious whether or not the results of section 2.3.2 will be of relevance.

3. EXPERIMENTAL METHOD

This chapter gives details of the equipment, along with the procedures necessary for its reliable operation. The calibration of the measurement system is discussed and an assessment of uncertainties given.

3.1 Hydrophone

Although a large number of experiments in nonlinear acoustics have been reported in the literature, only a few relate to the measurement of the harmonic components in detail (see section 1.4) and only recently have more than six harmonics been dealt with [5,133]. This is partly because there has been no strong requirement for such measurements, but also because it is difficult to obtain a hydrophone with a sufficiently broad-banded frequency response. The hydrophone used in this study has a response which varies by only 6 dB in the frequency range 0.5 to 100 MHz, and as it is a very important part of the measurement system, a number of its characteristics will be described here, although more complete details are given elsewhere [5,146].

The construction of the hydrophone is as follows (see Figure 7). A thin film of polyvinylidene fluoride (pvdf) is stretched over an annular frame which is large enough (100 mm in diameter) to allow the acoustic beam from a transducer to pass through its aperture. Each side of the membrane has a metal film lead evaporated onto its surface, and these two leads overlap only in a small central area, which becomes piezoelectrically active when the device is poled. The thin membrane introduces little acoustic perturbation

and so senses the free field acoustic pressure at the central element. At frequencies well below resonance the hydrophone has a flat frequency response, and does not introduce reverberation into the detected signal - features which are difficult to achieve at frequencies above 1 MHz. Even at frequencies close to resonance the frequency response is smooth (the quality factor Q of the resonance is less than 2) because the acoustic impedance of pvdf is fairly close to that of water.

3.1.1 Frequency response

An important aspect of this study is the measurement and theoretical modelling of acoustic waves with frequency components in the range 15 to 100 MHz. In this frequency range there are currently no standard methods for the absolute calibration of hydrophones, so it is necessary to infer the hydrophone response by less direct means. Four different methods of gaining the necessary information were used and will be described below. The first involves the formulation of a theoretical model to predict the frequency response based on a knowledge of the hydrophone's construction. The second is the comparison of the response of hydrophones made from different thicknesses of film, which makes it possible to determine the effect of the resonance in the hydrophone. The third is the measurement of the hydrophone's impedance as a function of frequency. The final method is to determine the frequency response of the hydrophone by placing it in an acoustic field whose frequency content can be predicted by theoretical means (see Chapters 2 and 4). This final method is inadequate when used alone, since the object of determining the

hydrophone's response is to test the accuracy of the theoretical models developed in Chapter 2. When used in conjunction with the other methods, however, it can provide additional confirmation of the results.

The active element of the hydrophone is suspended in the acoustic field without any backing material, so it is quite straightforward to describe its piezoelectric behaviour. The electric field in the hydrophone (in a direction perpendicular to its surface) is given by

$$E_3 = -g_{3i} T_i + D_3 / \varepsilon_T$$

where g_{3i} are the relevant piezoelectric coefficients, T_i are the components of the stress, D_3 is the electric displacement and ε_T the permittivity at constant stress. If the active element is connected to a load capacitance C_s, then the electric displacement will be determined by the charge transferred to it:

$$D_3 A = -VC_s$$

where V is the voltage across the active element. Integrating the previous equation over the thickness of the active element the following relationship is obtained:

$$V - D_3 t/\varepsilon_T = g_{3i} \int_o^t T_i \, dx = - g\bar{p}t$$

where t is the membrane thickness, $\bar{p}$ the mean pressure throughout the thickness of the membrane, and $g = g_{33} + \nu (g_{31} + g_{32})/(1 - \nu)$ with ν being Poisson's ratio for pvdf. Substituting for D_3 gives:

$$V(1 + tC_s/A\,\varepsilon_T) = -g\bar{p}t$$

Now $A\,\varepsilon_T/t$ is the capacitance of the active element (at constant stress), C_{el}, so that

$$V = -gt\bar{p}C_{el}/(C_{el} + C_s) \qquad 3.1$$

For the hydrophones used in this study, C_s is constant and considerably larger than C_{el}, so that the hydrophone frequency response is determined by the variation of g, $\bar{p}$ and C_{el}. It is known that the relative permittivity of pvdf decreases with frequency in the range 0.5 to 100 MHz [147-148], so that C_{el} is not constant. Unfortunately the variation of g has not been reported in the literature so far. Previously [5], it was necessary to develop two alternative models of hydrophone frequency response; one which assumed that g was constant, and one which assumed that $g\,\varepsilon_T$ was constant. Recently, however, more information has become available as a result of the calibration of membrane hydrophones in the range 0.5 to 15 MHz. At these frequencies, $\bar{p}$ is essentially constant, but the variation in ε_T is greatest. Consequently hydrophone calibrations in this frequency range can determine the variation of g quite reliably. In addition, because ε_T shows less variation at higher frequencies, any results obtained can be extrapolated to the range 15-100 MHz with a reasonable degree of confidence. A membrane hydrophone has been calibrated at eight frequencies from 0.5 to 15 MHz, using an interferometric method [149-150] and the results compared with the theoretical model that assumes that $g\varepsilon_T$ is constant. Agreement was obtained between the measured and predicted values, with the maximum deviation being 2%, whereas the

measurement uncertainties ranged from 2% at low frequencies to 7% at 15 MHz. By contrast, ε_T varies by 50% over this range. Consequently it appears that the model which assumes that $g\varepsilon_T$ is constant is confirmed, and that the hydrophone frequency response depends only on the variation of $\bar{p}$:

$$S(\omega) = (\text{Constant})\ V/p_o = \bar{p}/p_o$$

where p_o is the free field acoustic pressure amplitude at the angular frequency ω of an incident plane wave and $\bar{p}$ is the corresponding mean pressure amplitude averaged over the thickness of the active element. If the elastic properties of pvdf and the film thickness are known, then it is fairly simple to calculate $\bar{p}/p_o$. In principle these properties will depend on the loading conditions of the hydrophone, because the two stiffness constants C_D and C_E are not equal. However the electromechanical coupling constant, k_t^2, which determines the ratio C_D/C_E, is very small ($k_t^2 \simeq 0.012$ [151]), and so the difference between C_D and C_E is less than the experimental uncertainty for determining either of them. Calculation of the frequency response on this basis gives

$$S = t_1 \sin\theta\ /\theta(e^{-i\theta} - r_2 e^{i\theta}) \qquad 3.2$$

if the output voltage is described by $V_o e^{-i\omega t}$. If the acoustic losses in the film and the effect of the gold electrodes are ignored, then $\theta = \omega t/2c$, $t_1 = 2/(1 + z)$ and $r_2 = (z - 1)/(z + 1)$ where z is the ratio of the acoustic impedance of water to that of pvdf. If acoustic losses are included, then θ becomes complex and if the effect of the gold electrode is included, then t_1 and r_2 become complex. Both of these refinements are necessary to describe accurately the response of the hydrophone up to 100 MHz.

A value for the absorption coefficient in pvdf of 111 Np m^{-1} MHz^{-1} was used in the calculations [151,5].

Equation 3.2 was used to predict the relative sensitivity of hydrophones made from 25 μm and 9 μm film, and this ratio was compared with experiment [5]. Figure 8 gives the results of this comparison, and it can be seen that Equation 3.2 is thereby confirmed. Figure 9 gives the results of a similar comparison between the sensitivity of a hydrophone of thickness 50 μm and one of thickness 9 μm. The random uncertainty in the measurements is approximately 3% at the low frequencies and 6% at the higher frequencies. In this case a substantial part of the total capacitance is due to pvdf and so it was necessary to allow for the variation of the dielectric constant with frequency in the theoretical predictions. Good agreement is obtained for frequencies up to 16 MHz; above this the theoretical values are too high by about 10%. This discrepancy is probably due to the finite resistance of the gold electrodes. Such a resistance will be about 5 times larger in the hydrophone made from 50 μm film than in the other hydrophones. Nevertheless the response of the other hydrophones at frequencies between 20 MHz and 100 MHz could be between 5% and 10% lower than expected.

Measurements of the hydrophones' output impedances were made in the range 1 to 10 MHz by adding lengths of cable of known capacitance and noting the change in electrical signal level. These measurements indicated that the hydrophones behaved as capacitors, and further that their output impedances did not change with frequency below 10 MHz. More recent measurements of the impedance at the output terminals have indicated that the

phase departs from 90 degrees as the frequency increases. It is, however, difficult to determine an equivalent circuit, because there are a number of contributing factors, and consequently it is not yet possible to predict reliably the output impedance at frequencies above 10 MHz.

Measurements of the absolute hydrophone sensitivity at frequencies above 15 MHz are reported in Chapter 4. These indicate that the resonance predicted by Equation 3.2 exists and that there are no major deviations from the model described above. Nevertheless it is not possible to rule out relatively minor deviations from the model, particularly if they happened to possess a smooth variation with frequency.

The variation of the phase of the hydrophone response can be considered in a similar manner to that of the amplitude. Consideration of the electrical factors (such as the variation of the dielectric loss factor of pvdf [147-148]) shows that they should introduce negligible phase distortion into a waveform for the type of hydrophone used here. At high frequencies (approximately 40 MHz and above) there is some evidence that the resistance of the electrodes influences the response, but the measurements of phase that are presented here are at lower frequencies than this. The phase response of a hydrophone has not yet been measured at the NPL, but preliminary measurements [152] in the range 1 to 5 MHz indicate that the response is constant as expected.

3.1.2 Directional response

A model of the directional response of membrane hydrophones has been developed [5,146] which accurately describes the measured characteristics. A plot of the angle at which the response is predicted to be 6 dB below the peak is given in Figure 10 for a hydrophone with an active element 1 mm in diameter. Above about 2 MHz the directivity of a hydrophone with a 1 mm diameter active element behaves like a piston receiver, with the output voltage obeying the following equation:

$$V \simeq 2J_1(ka \sin \theta)/ka \sin \theta \qquad 3.3$$

where J_1 is the first order Bessel Function, a the element radius and θ the angle of incidence. For a frequency of 100 MHz, this equation predicts a drop in received signal of 50% for an angle of incidence of 0.5 degrees (see Figure 10). If the angle of incidence is 0.1 degrees, then the signal is reduced by 3%, so it is necessary to align the hydrophone with this precision to provide accurate measurements up to 100 MHz. When detecting a sawtooth wave, only a small fraction of the signal has this frequency, so it was necessary to use a special procedure to achieve the required alignment. One method was to rotate the hydrophone so as to minimise the apparent rise time of the shock front. As this risetime is essentially determined by the highest component frequency present, this technique is quite a sensitive one. An alternative method was to introduce an extra length of cable between the hydrophone and preamplifier. This set up a high frequency resonance in the cable, thus increasing the level of the components close to 100 MHz, and it was then possible to achieve

alignment by maximising the peak received signal. More recently, high pass signal filters have been obtained so as to permit the maximisation of the received high frequency components. Precision mounts were used to rotate the hydrophone; these are described in section 3.4.

At frequencies below 2 MHz, the hydrophone possesses sidelobes which can be larger than the main lobe of the directional response; in addition the main lobe is somewhat narrower than that predicted by Equation 3.3. The high sidelobes are caused by the propagation of Lamb waves in the membrane, and the narrower main lobe by the anisotropy of the piezoelectric properties of pvdf. A more complicated expression (which reduces to Equation 3.3 at higher frequencies) is required to predict the response in this instance [5]. A detailed knowledge of the directivity is not required at these low frequencies, however, as alignment is relatively straightforward. The main consequence of these considerations is that reliable measurements cannot be made at distances less than two transducer diameters from the source transducer. This is due to the wide range of propagation directions which occur in such a situation.

3.1.3 Signal quality

The hydrophone electrodes are exposed to its environment with little provision for screening and consequently the output signal is susceptible to radio frequency interference. This was reduced to some extent by connecting the ground electrode on the hydrophone to the metal mounting ring and by surrounding the acoustic tank with copper gauze. The electrical impedance of the

hydrophone has a significant loss tangent giving rise to a certain amount of intrinsic noise, and the preamplifier is a second source of wideband noise. In the measurements these effects were reduced by signal averaging and harmonic analysis to a level equivalent to approximately 50 Pa (peak) of acoustic pressure. The most obvious effect of noise is the introduction of random variations into the measured harmonic amplitudes, but there is a second, systematic effect which arises because the signal from the hydrophone is used to trigger the detection electronics. Noise on this signal will give rise to incoherence between successive samples and so reduce the measured amplitudes if signal averaging is applied. This effect decreases quadratically with increasing signal-to-noise ratio, so it is only significant when very low signals are being measured. The output impedance of the hydrophone is capacitative and so a high input impedance preamplifier is required to give accurate waveform reproduction. This preamplifier should be positioned very close to the hydrophone to avoid the problem of cable resonances. The preamplifier that was used had an input impedance of about 100 k ohm in parallel with a capacitance of 9.5 pF. The hydrophone had a cable which was 3 cm long and this allowed the preamplifier to be positioned just above the water surface. The output impedance of the preamplifier was 50 ohm so that it could be connected to the detection electronics with a matched cable.

3.1.4 Linearity

Since the measurements reported in this thesis concern the nonlinear characteristics of the propagation medium, it is of

prime importance that the measurement system be linear in its response. The linearity of the preamplifiers has been determined and they are operated in their region of linear performance. It is more difficult to determine the characteristics of the hydrophone, however, since any measurement procedure has to avoid or compensate for the nonlinear propagation characteristics of the medium used for testing. Measurements made close to the face of a transducer have shown that the level of spurious harmonic generation in the hydrophone is more than 40 dB below the fundamental level for amplitudes up to 0.4 MPa [5]. A similar technique has been used to show that the response is linear up to 1.5 MPa [130,146], but these levels are significantly less than the maximum amplitudes used in the present work (6 MPa). Tests using high amplitude pressure pulses have shown that the material used to fabricate the hydrophones is linear to better than 7% at levels of up to 65 MPa [153], and if the nonlinear response is assumed to have a quadratic variation with amplitude, this suggests that the linearity for the present measurements is better than 1%. This conclusion is supported by the fact that the distorted waveforms measured with a membrane hydrophone are in agreement with those determined by optical methods [130].

3.2 Hydrophone calibration

A crucial aspect of any experimental investigation of nonlinear propagation is the calibration of the hydrophone, since all measurements of absolute pressure amplitudes depend on it. Furthermore, calibration at megahertz frequencies is a very demanding exercise and it is difficult to achieve accuracies

better than 15%. The sensitivity of the hydrophone used here was traceable to three different absolute calibration methods, which will now be described briefly. All involve two stages - namely the calibration of the field of an auxiliary transducer followed by the measurement of the output voltage of a hydrophone which is placed in this known field.

In the first method, the auxiliary transducer is calibrated by self-reciprocity. A tone burst electrical drive is applied to the transducer and the input current measured. The acoustic wave is reflected from a plane surface and the received voltage produced by the transducer recorded. If the dimensions of the transducer are known and if it behaves as a plane piston, then the distribution of acoustic pressure in the field can be calculated. The propagation distance is then noted, and from these measurements the front face velocity of the transducer, and hence the pressure amplitude throughout its field can be calculated. The hydrophone is then calibrated by placing it in this field and measuring its output voltage. A major advantage of this method is that it is not necessary to measure voltages or currents absolutely, because the calibration is referred to a standard electrical impedance. Disadvantages are that the field distribution must correspond closely to the assumed distribution and that the circuits used for measuring voltage and current must be extremely well understood. The overall uncertainties of the method are currently estimated to range from 9% at 1 MHz to 20% at 15 MHz [154].

In the second method the transducer is given a continuous wave (CW) excitation and the output power measured using a radiation

pressure balance. The transducer is removed from the balance, placed in an acoustic tank and given a tone burst excitation. The hydrophone is placed in the field and scanned in a plane perpendicular to the acoustic axis. At each point the hydrophone output voltage is measured, and the integral of the square of the voltage over the entire plane evaluated. This integral is related to the total acoustic power in the beam with the conversion factor being the square of the hydrophone sensitivity, thus allowing the hydrophone to be calibrated. Advantages of this technique are that no assumptions are made about the pressure distribution in the field and that the acoustic power can be determined accurately. Disadvantages are the susceptibility to extraneous noise in the hydrophone signal and the possible change in transducer characteristics during transfer from the radiation pressure balance to the acoustic tank. The estimated overall uncertainties range from 6% at 1 MHz to 15% at 15 MHz [154].

The third method provided the calibration values for the hydrophone used to determine the field from the focused transducer (section 4.4) and has only recently been implemented. A thin, optically reflecting plastic pellicle is placed in the field of a transducer and the motion of its rear surface detected with a laser interferometer. A value for the acoustic displacement amplitude of the pellicle is derived from the measurement of the output signal of the interferometer and the acoustic pressure calculated from this value. The acoustic characteristics of the pellicle are known and thus the acoustic pressure amplitude of the acoustic wave in the tank is derived. The pellicle is then replaced with a hydrophone with the active element in the same

position in the acoustic field and the sensitivity determined from the ratio of its output signal to the acoustic pressure in the field. This method is significantly more accurate than the previous two, with the estimated overall uncertainties ranging from 2.1% at 1 MHz to 6.3% at 15 MHz [150]. It has been developed during the period of the work described in this thesis and consequently the calibration results have only been available for the most recent measurements; further details of the method are given in a separate report [150].

All of the methods described above are very time consuming to perform. Consequently, the sensitivity of the hydrophone used for most of the measurements was determined by intercomparison with a standard hydrophone which had previously been calibrated by the first two techniques described above. A substitution method was used for this and both low amplitude, (single frequency,) and sawtooth waveforms were employed. The random uncertainties involved were less than 4% (standard error of the mean), and so little extra error was introduced by this indirect procedure. The sensitivity determined in this way has a total spread of only 6% in the range 1 to 10 MHz. Consequently, when evaluating the results of a measurement in a nonlinear field (see Chapter 4) only the sensitivity at the fundamental frequency was used, the sensitivities at the other frequencies being obtained using the model of section 3.1.1. It has recently been possible to check the calibration of the hydrophone using results obtained with the interferometric technique, and the mean sensitivity over the frequency range 1 to 10 MHz was verified.

3.3 Measurement system

3.3.1 Electrical drive

A block diagram of the usual experimental arrangement is given in Figure 11, and Figure 12 gives a photograph of the equipment. The peak electrical power from the radio frequency source was in excess of 2 kW, so it was always necessary to use tone bursts with a very low duty cycle (greater than 1000:1) to avoid overheating the transducer. The tuned gated amplifier was a Matec model 5100 and had a frequency range of 0.5 to 25 MHz, and maximum output power in excess of 1 kW at all frequencies. It had the facility to produce double pulses, which could be used to test for possible artefacts due to the interaction of the primary acoustic beam with waves reflected from the hydrophone. The output impedance was 50 ohm, thus making it necessary to use an impedance matching network to drive a transducer. This network simply consisted of a number of inductors which could be switched into the circuit, with a variable capacitor to give fine tuning capability. An extra control was provided by the tuning capacitor of the Matec driver. Because the transducers had a significant resistive contribution to their impedance, large increases in drive voltage were not obtained by this method. Nevertheless the network made it possible to deliver a large amount of power without distortion of the voltage waveform. The drive voltage was measured with a 100 x probe which was connected to an oscilloscope. All absolute values of the experimental parameters were referred to hydrophone measurements, and so it was only necessary that the probe be linear and have properties which remained constant with time.

An alternative electrical source consisted of a broad-band amplifier (ENI model A150) with maximum output power of 250 W in the range 0.3 to 35 MHz. This could be driven with a Wavetek function generator to produce short pulses approximately one cycle in length.

3.3.2 Acoustic sources

The transducers were made from circular ceramic discs, with a matched absorbing backing and quarter wavelength layer on the front face to provide good coupling to the water. These transducers are designed principally to provide a broad-banded response, but their most important feature for the present investigation is their piston-like excitation function. Good acoustic coupling of the active disc to its environment results in both damping of the radial resonance modes and in a wide-band response, so the two properties are linked. A disadvantage of these transducers is their low efficiency, but this is not a problem except at 1 MHz where it is not possible to obtain a high enough source amplitude to produce a severely shocked waveform. There are two factors that limit the electrical drive which can be applied. At frequencies above about 5 MHz the maximum current which can be carried by the electrodes restricts the acoustic pressure at the transducer face to about 1 MPa, which is more than sufficient for the present investigation. At lower frequencies the limiting factor is the maximum voltage that can be withstood without breakdown of the electrical insulation. The transducer was specified to withstand at least 500 V peak, and the maximum peak voltage applied in practice was 650 V. At 1 MHz, the corresponding

pressure amplitude at the transducer face was 0.4 MPa, restricting the attainable value of σ to 1.4. The use of a longer acoustic tank would make it possible to attain a σ of 3, but a more efficient transducer would be required to achieve higher σ values.

A potential experimental difficulty which also could limit the acoustic pressures that can be obtained is cavitation. This was previously encountered in measurements with CW fields and can cause large fluctuations in the received hydrophone signal due to absorption and scattering by resonant bubbles. For pulsed fields the cavitation thresholds are considerably higher than for CW propagation, and there was no experimental evidence of these effects. Deionised and distilled water was used for all measurements and the water was changed approximately once a week. The maximum peak pressure produced at a field point was approximately 6 MPa, and recent theoretical work indicates that transient cavitation may occur at these levels, even in pulsed fields [155-156]. The cavitation threshold depends to some extent on the dissolved gas content, and although freshly distilled water contains relatively little gas, the water becomes saturated with air within approximately seven hours of filling the tank. From these considerations it is difficult to rule out the presence of cavitation but the measurements were reproducible and so this possibility is considered to be unlikely.

3.3.3 Receiving electronics

The preamplifiers and amplifiers for the hydrophone signal had a combined 3 dB bandwidth of approximately 80 MHz, so it was

necessary to calibrate the gain and phase lag as a function of frequency. It was necessary to take great care in these measurements, as the electromagnetic wavelength in the cable is about 2 m at 100 MHz. A connection to the oscilloscope was required and as the reactance of its input impedance (20 pF) was 80 ohm at 100 MHz these calibrations were carried out using exactly the same arrangement of cables as for the acoustic measurements. Details of the procedure are given in Appendix 3.

As mentioned above (Section 3.1.3) signal averaging was used in most of the measurements. The detection system was sensitive to phase and so it was necessary to provide an accurate trigger signal. One possible method was to use the trigger provided by the Matec amplifier, and rely on the propagation time of the acoustic wave to remain constant. To provide accurate measurements at 100 MHz, this would require the separation between the transducer and hydrophone to vary by less than 2 μm over a period of about 5 seconds. Because the membrane of the hydrophone follows the bulk motion of the water in the tank such stability would be difficult to achieve. Instead, a trigger signal was obtained from the received waveform using the retriggerable delayed time base of the oscilloscope. The oscilloscope trigger signal was then fed into the digitiser.

3.3.4 Digitiser

The digitiser was a Tektronix model 7912AD with programmable mainframe and plug-in units. Its operation is similar to that of an oscilloscope in that an electron beam is deflected to record the input signal on a 512 x 512 point diode array. The diodes

record the path of the writing beam, and a second beam is used to sense their status and so read off the recorded waveform. This mode of operation makes it possible to achieve very high sampling rates - up to 100 GHz. It is possible to digitise single shot waveforms, or to average up to 64 waveforms through an internal microprocessor. An IEEE bus facilitates transfer of data to the controlling Tektronix 4052 desktop computer.

The bandwidth is determined by the plug-ins to be 200 MHz, which is adequate for the present work, and the minimum sensitivity is 10 mV/division. The input impedance can be selected as either 50 ohm or 1 M ohm and 20 pF; usually an external 50 ohm terminator was used in conjunction with the 1 M ohm option. The 7912AD is virtually the only digitiser currently available with sufficient bandwidth, accuracy and speed to perform the required measurements. Nevertheless there are a number of features which could limit its performance. Examples of this are non-uniformity of sensitivity over different areas of the array, lack of alignment between the beam axis and the array axis and effects due to the thickness of the trace. All of these factors could distort measurements where a wide range of frequencies are present simultaneously. In a sawtooth wave, for example, the amplitudes of the higher harmonics are largely determined by the rise time of the shock front and by the curvature of the waveform immediately before and after the shock. A slight angular misalignment of the array axis could possibly give rise to a large error in the rise time of the shock, and a thick trace could restrict the maximum curvature that could be measured. It is not possible to investigate all of these features fully but measurements of

linearity and results obtained by using band limiting filters indicate that measurements of the first twenty harmonic components have an uncertainty due to these effects of approximately 3%.

The results from the digitiser were transferred into the controller, and the frequency components extracted using a Fast Fourier Transform routine. This algorithm requires the number of input values to be an exact power of two, corresponding to the 512 readings made by the digitiser. It is extremely important that an integral number of cycles be represented by this data, as otherwise frequency aliasing will occur in the analysis. The amplitudes of the first and last points of the waveform were therefore matched by the following method. The controller plotted out the last 50 points of the waveform on the left of its screen, and the first 50 points on the right of the screen, using a large vertical scale. It was then possible to adjust the fine control on the digitiser time base until a good match was obtained between the initial and final points.

The sweep rate of the time base could only be set to one of a range of fixed values, if the small variation obtainable with the fine control is neglected. Because of the requirement to include an integral number of cycles in the trace, the number of frequencies at which measurements can be made using this method is therefore very restricted. To perform measurements over a wider range of frequencies, the waveforms can be processed on the computer so as to obtain 512 points in a cycle. This is achieved by using the position of the zero crossings to determine the period and then altering the number of waveform points within this period using an interpolation routine.

The measurements in the field of a focused transducer (section 4.4) were performed using a Tektronix model 7D20 digitiser; this is a solid state device with 8 bit accuracy and a bandwidth of 70 MHz. Although the basic specification of this digitiser is inferior to that of the model 7912AD, it does not suffer from limitations due to distortion or trace thickness. The digitisation was performed by averaging 16 acquisitions of the waveform and the signal processing was performed as described above.

3.4 Acoustic tank

Most of the measurements reported here were made in an acoustic tank 0.9 m in length, but a second vessel of length 1.81 m was used in some cases, and this is shown in Figure 13. The two tanks had very similar features, so only the second is described here. The width is 0.295 m and the depth 0.315 m, these dimensions being limited by the quantity of distilled water that was available.

3.4.1 Hydrophone mounting arrangement

A meehanite optical bench with triangular cross-section is mounted above the tank, rigidly attached to a wooden frame by two substantial steel brackets. The optical bench supports carriers for the hydrophone and the emitting transducer. The carriers can slide along the bench, and then be clamped to it, using a retaining screw. Micromanipulation tables are screwed to the carriers, permitting fine adjustment of position and orientation of the components.

To describe the possible adjustments a set of cartesian axes may be defined with the z axis parallel to the optical bench and the y axis being vertical. The transducer can be translated under fine control in the z and x directions, and rotated about the y and x axes. Rotation about the x axis is achieved by a sine table mounted on the carrier which means that the axis of rotation is some 30 cm above the transducer face. The resulting compound motion does not cause any real difficulty, however, because this rotation is only used to align the transducer roughly with the z axis at the beginning of a set of measurements. The hydrophone can be moved in the x and y directions and rotated about the x and y axes. These mounts are designed so that the axes of rotation coincide with the active element of the hydrophone, so that the different adjustments can be made independently of each other. The hydrophone is supported in a metal ring, and held against five small steel balls by springs. The ring can rotate about the x axis with respect to a steel plate, which is rigidly connected to a pole. This pole is supported by a table which provides rotation about the y axis. The minimum rotation that can be achieved is approximately 5 minutes of arc (0.1 degrees), which is adequate for measurements at frequencies up to 100 MHz (see section 3.1.2).

The transducers have connectors fixed to them, and it is necessary to make a waterproof seal to the cable. For transducers with BNC connectors, the mount contains a perspex chamber with a rubber O-ring at one end. A metal plate is glued to the back of the transducer and this is screwed into a steel collar which presses the perspex chamber against the plate. A pole is screwed into the collar and this pole is supported from a rotation table. A second

type of transducer has UHF connectors and a built-in O-ring seal to the cable. In this case the transducer mount consists of a V-block with an adjustable clamp, and can again be screwed onto the pole. Although attention has been paid to making the mounts as rigid as possible there is an inevitable conflict between achieving rigidity, providing a large number of adjustments and making the system easy to use. The arrangement described here represents a compromise between these considerations and has the added advantage of utilising a number of commercially available components.

3.4.2 Echo suppression

It is desirable to make the acoustic tank as long as possible, to obtain the maximum distortion of a wave for a given initial pressure amplitude. An opposing constraint is that the volume must not be too large, because the availability of distilled water is limited. Consequently the tank has small cross-sectional dimensions compared with the length. One difficulty in using such a tank, however, is that reflections occurring at the tank walls and the water surface can interfere with the main signal. If the tone burst length is sufficiently short these signals can be separated out because of their longer propagation paths. Alternatively, if the source has narrow directivity characteristics, then these reflections have low amplitudes because they arise from the side lobes of the field distribution. For these reasons the reflections do not affect the measurements at frequencies above 2 MHz. At 1 and 2 MHz, however, some of the transducers have a directivity which is sufficiently broad to give

reflections which are up to 10% of the main signal amplitude. The tone bursts are too long for these reflections to be separated out, because the electrical source has a narrow bandwidth and the signal must be twenty to thirty cycles long. Fortunately these problems do not occur for short propagation distances and do not affect measurements where the distances are less than 0.7 m. To utilise the available path length, however, it is necessary to reduce the amplitude reflection coefficient of the walls and water surface to 0.1.

Although it is relatively straightforward to obtain such a reflection coefficient for normal incidence, the task is much more difficult for grazing angles of approximately 10 degrees. The longitudinal wave velocity of most solids is greater than that of water, and consequently, for angles of incidence above the critical angle, the reflection coefficients for plane solid surfaces will be too large. If a scattering surface is used, the spacing between scatterers must be extremely large compared with the acoustic wavelength, as otherwise foreshortening will result in a large diffracted signal. After some consideration it was felt that the best approach was to line the walls with wooden baffles (see Figure 14). These were made from a light wood, to make their reflectivity as high as possible, and they were varnished to prevent absorption of water. They were stuck to the tank walls with their length perpendicular to the propagation, and they were angled so as to trap the incident wave by multiple reflection. It was impossible to prevent scattering from the edges of the baffles, but this was kept to a minimum by using as few baffles as possible. To preserve the maximum "free space" along the centre of

the tank the width of the baffles could not be too large. The spacing between them was 150 mm, which was thought to be large enough to avoid constructive interference occurring at the hydrophone. To cover the water surfaces, the baffles were stuck to sheets of perspex which were supported from the tank walls, and could be removed if necessary. The reflection coefficient of the assembly has been determined for grazing incidence to be approximately 0.05 at a frequency of 1 MHz, confirming that the system meets the design requirements.

3.4.3 Other details

The absorption coefficient of water changes with temperature, and such variations can affect the amplitudes of the higher harmonic components of a wave significantly. A thermometer was therefore placed in the tank and the temperature noted for each measurement. The accuracy was approximately 0.1 K. The distance from the transducer to the hydrophone was not measured directly because this would be quite a time consuming procedure. Instead the propagation time of the wave was noted from the oscilloscope, and the distance derived using the wave velocity. The same time base was used for these measurements as for determining the diffraction lengths of the transducers so as to reduce the effect of calibration errors.

3.5 Experimental procedure

The bulk of the experimental work reported here consists of a set of measurements of the harmonic amplitudes on the axis of a piston transducer, for different source amplitudes and frequencies and at

a range of distances from the transducer. This was primarily to provide a set of data to test the model developed in section 2.1.3, but obviously the results have a number of uses and are of some intrinsic interest. Fundamental frequencies of 1, 2, 5 and 10 MHz were used; at the lower frequencies small-signal absorption was not very significant whereas at 10 MHz absorption was quite large. Details of the transducer sizes, and of the other measurement parameters, are given in Table 2.

Table 2 Details of Transducer characteristics

	Frequency (MHz)	Diameter (inches)	r_o (m)	Maximum R	Maximum σ_o	Maximum Γ_o	Maximum σ
1.	1	1	0.34	1.9	0.91	105	1.4
2.	2	0.75	0.42	1.6	4.8	108	5.9
3.	2	0.5	0.18	3.8	1.7	97	3.7
4.	5	0.5	0.41	1.6	8.5	33	12.3
5.	5	0.25	0.11	5.7	2.6	38	6.5
6.	10	0.25	0.20	1.3	13.3	26	17.5

To characterise the measurements for a particular transducer it

was necessary to obtain two properties of the transducer, namely the Rayleigh distance and the ratio of the pressure at the radiating surface to the drive voltage. The Rayleigh distance was determined by performing a plot of the axial pressure at low amplitudes as a function of distance from the transducer, beginning at the position of the last axial maximum. The Rayleigh distance (r_o) was then determined by fitting the measurement values to the function $p/p_o = 2 \sin(r_o/2z)$, after having compensated for the effect of small-signal absorption. The sensitivity of the hydrophone is known (see section 3.2) so that the pressure at the transducer face can also be evaluated from the above formula, once the Rayleigh distance is determined. Usually the pressure at the transducer face was determined from the pressure at the last axial maximum ($z = r_o/\pi$). In this case the formula gives $p_o = p/2$, but in practice p_o is slightly larger than this because of spatial averaging over the hydrophone active area and because of transducer imperfections. These effects were estimated from the curves of reference [157] and from previous measurements of the axial beam profiles of similar transducers. Having determined p_o and r_o, the measured values of p at different values of z were compared with those obtained from the above equation to check the validity of the method. The drive voltage (V_{in}) was noted so that the ratio p_o/V_{in} could be obtained. The values of p_o for other drive voltages were calculated by assuming that the transducer was linear; this assumption was verified by a separate series of measurements.

For each transducer, measurements were made at distances corresponding to $z = nr_o/\pi$ where n is an integer. Generally

measurements were made for each value of n (n=1,2,3 etc), but for some transducers with small values of r_o the spacings were larger than this. For each distance the minimum drive voltage was determined by the smallest pressure that could be measured by the hydrophone (with a signal-to-noise ratio of approximately five). The drive voltage was increased in steps of approximately 3 dB until the maximum allowable voltage was reached. The hydrophone was aligned carefully (section 3.1.2) and 64 averages of the signal made by the digitiser. This process was repeated for different distances, with the drive voltages having similar values for each distance. A number of repeat measurements were made to determine the reproducibility and consistency of the results.

The Fourier coefficients of the hydrophone voltage (amplitude and phase) were recorded on magnetic tape, after allowing for the gains and phase delays of the amplifiers. If the measurement time for each signal sample was more than one acoustic period, then some of the Fourier coefficients should be zero due to the periodicity of the wave. In practice these redundant coefficients were not zero, and they were used to provide estimates of the random uncertainty at each harmonic frequency, this information being stored on the tape along with the measurement results. Up to 256 harmonic components were evaluated for each measurement and obviously only a few of these results were reliable. The number of results to be stored was therefore determined by the program on the basis of the relative amplitudes of the harmonics, subject to an overriding maximum of fifty.

With each set of results the following measurement parameters were stored: fundamental frequency, propagation distance, near field

distance (equal to r_o/π), pressure amplitude at the transducer face and the number of harmonics that were retained. Each tape contained a file which was used as an index where further parameters were recorded for each measurement: nominal transducer diameter, hydrophone serial number, page number in measurement book, the date, transducer serial number, water temperature and approximate values of σ_o and Γ_o. At a later date calculations were made corresponding to each measurement and these could be initiated automatically using these records. The results of the calculations were stored along with equivalent records which included the file number of the measurement, and the program ensured that only corresponding files could be compared. This careful book-keeping was required because over 350 measurements were made.

To provide a value for the pressure at the transducer it was necessary to use the sensitivity of the hydrophone at the fundamental frequency. The measurements of pressure were recorded in terms of the voltage from the hydrophone, so that no other assumptions about the hydrophone's response were made. Consequently it is straightforward to perform calculations based on different values for the hydrophone sensitivity and frequency response. This flexibility is important because the procedures for hydrophone calibration are continually being improved and more accurate values for the sensitivity are being obtained. An alternative way of using the measurement results is in calibrating the hydrophone, as described in Chapter 4.

The focused transducer had a resonant frequency of 3.5 MHz, a diameter of 10 mm and focal point located 39 mm from the front

face. The procedure for determining the required input parameters for the theoretical calculations is described in detail in Appendix 2, and involves determining the normalised distance R from the ratio of the transducer area to the 1/e beam area at the focus. It should be noted that the procedure of Appendix 2 permits this determination to be made at high amplitudes, where significant nonlinear propagation may occur, however, for these measurements it was possible to alter the source level and therefore R was determined at low amplitudes. The value of the source amplitude was also determined in a slightly different manner from that described in Appendix 2. At low levels, the ratio of the pressure amplitude at the focus (p_o) to the voltage across the transducer was found, and this ratio was used to predict the amplitude at higher levels, assuming that the transducer behaved linearly. The maximum value of p_o was 6 MPa, which gives values for σ and Γ_o of 3.6 and 500 respectively. These experimental conditions are similar to those pertaining to the fields radiated by diagnostic ultrasound equipment, where the highest peak-positive acoustic pressure that has been measured is approximately 10 MPa.

3.6 Measurement uncertainties

In assessing the accuracy of the theory presented in Chapter 2 it is necessary not only to compare the calculated results with experiment but also to determine the uncertainty in the measurements. In addition it is necessary to determine the accuracy to which certain properties of water are known, as these values will affect the comparison of theory with experiment. This

second consideration will be dealt with in section 3.7.

It is of interest here to determine the probable uncertainty in the measurements rather than the absolute maximum uncertainty. The absolute maximum uncertainty would be obtained by adding linearly the contributing systematic uncertainties, whereas the probable uncertainty will be defined here to mean that there is a given probability (usually 68% here) of the error being less than the stated value. This definition, while being unsatisfactory for standards work, is useful in providing a realistic guide to the reliability of the results. In principle each contributing uncertainty may be represented by a probability distribution, and they may be combined by repeated convolution to give an overall distribution. If the number of contributions is large and they are roughly equal in size, then this process will give an overall uncertainty which is approximately the quadrature sum of the individual components. This applies even if the distribution is not Gaussian. If the contributions are dissimilar in size, however, then the overall uncertainty at the 68% confidence level for a square function probability distribution will be closer to that obtained by linear summation. Consequently the overall uncertainty was obtained here by dividing the contributions into groups of similar size (differing by no more than a factor of two). Within each group, the uncertainties were summed in quadrature, and then the group values were added linearly.

Table 3 gives twelve sources of uncertainty that were identified, along with their estimated sizes. The values were obtained wherever possible by direct measurement, and correspond to a confidence level of 68%. Combining them in the manner described

above gives an overall value of 10.5% for frequencies up to 10 MHz and 12.5% for frequencies between 10 MHz and 50 MHz. For the later measurements, where interferometry was used as the reference calibration method, the corresponding uncertainties are 5.7% and 10.2% respectively. For low amplitudes there is an additional contribution of 50 Pa (peak) in the measurement of pressure, due to noise. If measurements of relative pressure amplitudes at any particular frequency are considered, (see section 4.2,) then the contributions arising from the hydrophone calibration can be neglected and the uncertainty is 5% of the pressure amplitude plus 50 Pa.

3.7 Other uncertainties

Three properties of water could potentially affect the comparison of theory with experiment, namely the sound velocity, the attenuation coefficient and the value of β. The velocity of sound is known to approximately 0.01% [158] and has little significance because all distances are measured in terms of propagation time. The variation in water temperature during the measurement period gives rise to an uncertainty in distance of about 0.5 %, which is a small effect compared with the other uncertainties.

The attenuation coefficient of water is less accurately known, the standard reference being to the work of Pinkerton in 1947 [159]. He made measurements at seven frequencies between 7 and 70 MHz, and from the self-consistency of these results, he derived a probable error which was less than 2%. Unfortunately, very few experimental details were given and it is difficult to assess his work from a modern standpoint. An additional difficulty is that

Table 3 Measurement Uncertainties

Source	Standard deviation (%, in amplitude)	Comments
1) Transducer non-linearity	1.5	Limited by measurement resolution, obtained by measuring hydrophone voltage/ drive voltage for very short propagation distances
2) Oscilloscope non-linearity	1.5	Compared with a calibrated attentuator
3) Variation of field from predictions (at low amplitudes)	2	Performed a beam plot with a hydrophone
4) Interference due to echoes from tank walls	1.5	Only affects fundamental component at maximum propagation distance
5) Reproducibility of measurements	2	ie measurement resolution
6) Noise (peak)	50 Pa	
7) Linearity of hydrophone	-	Included in 1) above; too small to measure from other experiments; theoretically estimated to be negligible.
8) Hydrophone calibration	6	Typically, for 68% confidence, between 1 and 10 MHz
(Interferometry)	(3)	For values from interferometry
9) Hydrophone frequency response	5	Estimated contribution in addition to 8) at frequencies from 10 to 50 MHz.
10) Amplifier calibration	1.5	
11) Thickness of trace	1.5	See section 3.3.4; this is for first 15 harmonic components
12) Calibration of digitiser	2	One of the methods of hydrophone calibration relies on this, so it is partly cancelled out

Pinkerton's measurements were made at only a few temperatures in the range of interest, and the accuracy of interpolation is therefore difficult to determine. Recent measurements made with an acoustic interferometer have given results that are some 3.2% less than Pinkerton's [160], but the work was only performed at 25 ^{o}C and so it is difficult to apply the results at different temperatures. A second difficulty that is encountered in using any published results for the attenuation is the fact that the attenuation coefficient is increased if the water is not completely clean and the likely size of this effect is not known.

In an attempt to resolve some of these difficulties, the attenuation coefficient was measured at a frequency of 10 MHz by determining the variation of acoustic pressure on the acoustic axis of a transducer with a hydrophone. The temperature was 18.9 ^{o}C and the random uncertainty at the 95% confidence level was 1.1% whereas the estimated systematic uncertainty (obtained by linear summation of the component contributions) was 0.9%. The water had been in the tank for a week and so was relatively contaminated; no contribution due to this cause was included in the estimates of overall uncertainty as the measurements were made partly to investigate this effect. The measured coefficient was 4% below the value given by Pinkerton [159], in agreement with the more recent results of Uhlendorf et al [160]. Since the measured coefficient is not greater than the published values, it is reasonable to assume that the uncleanliness of the water does not significantly affect the attenuation coefficient under the present experimental conditions. Taking these factors into consideration, the attenuation coefficient used in the calculations [159] is

probably reliable to within 4%. In many experimental situations this coefficient has little effect on the harmonic amplitudes, so the extra uncertainty in the comparison of theory with experiment is usually very much less than 4%.

There are several ways of determining the parameter β for water, but the highest accuracy is obtained with the thermodynamic method. This involves the measurement of the velocity of sound as a function of temperature and pressure. The derivative of the sound velocity with pressure (at constant temperature) is then derived, and a small correction applied to obtain the adiabatic derivative. The value of β is then obtained from the relationship:

$$\beta = 1 + \rho c \left(\frac{\partial c}{\partial p} \right)_s$$

Applying this calculation to the data of Wilson [158] gives a value for β of 3.52, which Beyer [161] estimates to have an uncertainty of 2%; this value is in agreement with results obtained from studying second harmonic generation at finite amplitudes [30]. A similar value for β can be obtained from more recent data [162], but these measurements were not made at room temperatures.

4. RESULTS

Various measurements have been made, some to test the theory developed in chapter 2 directly, and some which utilise either the theoretical results or the experimental capability described in chapter 3.

4.1 Plane piston transducer

Measurements were made using the transducers listed in Table 2, and the results compared with the predictions of Equations 2.8-2.10 (sections 2.1.2 and 2.1.3). As many measurements were made, it is not possible to reproduce all of the results here. Instead, a thematic approach is taken, with the accuracy of the model being determined as the various parameters of Equation 2.9 are varied. It is expected that the model will be fairly reliable if $\sigma_o<3$, $R>1$ and $\Gamma_o>40$, so it is possible to choose situations where all but one of these conditions are met, and in this way to study the accuracy as a function of each of these parameters independently of the others. Table 2 is particularly useful in making these choices.

4.1.1 Variation of σ_o

The effect of diffraction within the transducer near field is only approximately allowed for by the theory, and consequently the model is expected to break down if the distortion occurring in this region is significant. The parameter related to the near field distortion is σ_o, so this section describes the accuracy of the model as σ_o is varied. To keep the ratio of σ/σ_o fixed, the

normalised range (R) must be constant. The value of R chosen was 1.27: this was thought to be large enough for the model to be reasonably valid, but small enough to show up any deficiencies. The measurements for transducers 2 and 4 were used: these had maximum σ_o values of about 5 and 9 respectively (see Table 2). Figure 15 gives the results for transducer 2. The experimental uncertainty of approximately 10% (one standard deviation) is equivalent to about twice the extent of the crosses. Figure 15a is typical of the results for low amplitudes ($0.1 < \sigma_o \leq 1.1$), and shows that the theoretical harmonic values are too small by a factor which increases with the harmonic number. Figure 15b shows that as σ_o approaches 1.5 this divergence disappears and good agreement is obtained. Figure 15c shows that as σ_o increases the first twenty or so harmonic amplitudes are accurately predicted, whereas the predictions for the higher harmonics are 20-30% too low. The size of this discrepancy is close to the measurement uncertainty since the digitising error and noise level are significant for the higher harmonics. A similar feature is evident in Figure 15d for $\sigma_o \simeq 5$. These results indicate that the amplitude of the fundamental is predicted very reliably, even though nonlinear effects have caused an extra attenuation of a factor of three. This means that the value of σ_o used describes the situation well.

To explain the discrepancy at low amplitudes it is necessary to consider two effects due to the diffraction of the harmonics, namely the phase variations that occur within the near field region of the transducer and the different diffractive characteristics of the Gaussian and the piston source. For R = 1.27 and if the amplitude is low, the effect on the second

harmonic level due to the neglect of phase variations in Equation 2.16 is to make the predictions about 3.5% too high. It is rather more difficult to estimate the effect due to the diffractive characteristics of a piston source, but a published graph of calculations for low amplitudes [79] gives a value for the second harmonic amplitude that is significantly higher than predicted by the matched Gaussian model. Thus, the discrepancy at low amplitudes is probably due to this second cause, although the difference between theory and experiment (approximately 15% for the second harmonic) is less than the difference predicted from [79]. The behaviour of the twentieth and higher harmonics for large σ_o may be explained by a similar effect, although the difference between theory and experiment may not be significant in this case. An alternative explanation for the discrepancy at low amplitudes is that the nonlinear distortion is inadequately accounted for. This is thought to be unlikely, however, since the behaviour of the fundamental at higher amplitudes is described accurately.

The agreement obtained for $\sigma_o > 1.5$ for the first twenty harmonics is explained by the existence of the shock front in this case. The shock introduces a rapid transfer of energy from the lower to the higher harmonic components. Consequently, the effect of harmonic generation over the entire pre-shock region becomes less important, and effects in the region close to the field point become more important. As a result, the diffraction of the harmonics is less important, and so the behaviour is more like that of a one-dimensional wave.

A similar behaviour to that in Figure 15 is shown in Figure 16 for

transducer 4. These results have been corrected for an error in the determination of distance. The higher frequency of 5 MHz means that absorption is more important. This explains the fact that agreement is not obtained until $\sigma_o \simeq 2.5$, since absorption prevents the establishment of a well-formed shock front for lower values of σ_o, and it is the existence of a shock which reduces the influence of harmonic diffraction. The maximum value of σ_o is approximately 12, and it is evident that the model is still reliable, even though the fundamental component has incurred an extra attenuation of about five. The model is therefore reliable up to at least $\sigma_o = 12$, with the main difficulty occurring at low amplitudes.

4.1.2 Variation of σ

The previous section examined the accuracy of the model as a function of σ_o, and it was seen that there is a critical value of σ_o above which the model is reliable. The results presented were for a fixed value of the normalised distance (R) from the transducer, and this means that it was not possible to distinguish between the effect of varying σ_o and that of varying σ, since $\sigma = \sigma_o \mathrm{Ln}(R + \sqrt{1+R^2})$. Put another way, it was not possible to tell which factor determines the accuracy: the near field distortion or the total distortion.

To answer this question, measurements for R=3.82 were examined, as in this case $\sigma \simeq 2\sigma_o$. Figure 17 presents the results, which are for transducer 3. The transition between the low and high amplitude regions is clearly shown in this figure, although the maximum value of σ_o is about 1. The transition occurs at $\sigma \simeq 1.5$,

which is a similar value to that in Figure 15b. A similar result is obtained for transducer 3, at a distance of R=2.55. The parameter which is important in determining the model's accuracy is therefore σ, which describes the total distortion of the wave. This conclusion is consistent with the explanation for the discrepancies that was given in section 4.1.1.

The above conclusions were checked using the 1 MHz transducer (number 1) for R=1.91. Here the maximum value of σ was approximately 1.5, and the expected variation of the accuracy of the model for $\sigma \leqslant 1.5$ was obtained.

4.1.3 Variation of R

Figure 18 gives the results for transducer 3, for R=0.64, 1.3, 2.5 and 3.8 in the form of plots of the harmonic amplitudes as a function of σ. Figure 18a is particularly interesting, as the propagation distance is less than the Rayleigh length. As in the previous cases, agreement is obtained for $\sigma \simeq 1.5$. For $\sigma \leqslant 1$, the predicted amplitudes are generally slightly higher than the measured values and for the highest σ there is some evidence that the predicted fundamental level is too low. It is therefore quite probable that the theoretical value of σ is too high for R<1. This conclusion is very reasonable in view of the approximations made in the model. In Figure 18a there is also evidence that at high amplitudes the predicted levels for harmonics 2 to 15 are too low. The results for transducer 2 at R=0.64 (Figure 19) are similar to those shown in Figure 18a thus confirming these conclusions.

Figures 18b-d demonstrate the features discussed in the previous two sections, in that the theoretical predictions are seen to be accurate for $\sigma \geqslant 1.5$. In particular, the behaviour of the fundamental component is described very well (as long as $R \geqslant 1$) for a wide range of values for σ, Γ and R. These results suggest that the model can be used in calibrating hydrophones, as will be discussed in section 4.2.

4.1.4 Variation of Γ_o

For given values of σ and R, the variation of Γ_o corresponds to variation of the absorption coefficient. The effect of decreasing Γ_o is twofold - firstly the "extra attenuation" of the fundamental (due to nonlinear distortion) decreases, and secondly the amplitudes of the harmonic components relative to the fundamental decrease. The theoretical model should predict both of these effects accurately.

Figure 20 gives the comparison of the predicted and measured amplitudes, for four different transducers (numbers 2, 4, 5 and 6), with $R \simeq 1.2$ and $\sigma \simeq 2.3$. The values of Γ_o are 50, 34, 8 and 4, so that absorption is fairly unimportant in the first case and very important in the last case. Figures 20a and 20b give typical results for the high Γ_o case in that good agreement is obtained for the first twenty harmonics. In Figure 20c agreement is obtained within the measurement uncertainty (of 12.5% + 50 Pa) for all the harmonics shown, although a certain amount of deviation is present. Figure 20d indicates that the model does not predict the measured amplitudes reliably for $\Gamma_o = 4.4$, although the disagreement is only just outside the estimated uncertainties.

This discrepancy may be accounted for within the context of the explanations given in previous sections as follows. When Γ_o is large, a full shock occurs at $\sigma = 1.5$, but for smaller Γ_o, the effect of absorption is to increase the value of σ for which a full shock occurs. Thus, for $\Gamma_o = 4.4$ a full shock will probably be only in its formation stage in Figure 20d (for which $\sigma \simeq 2.2$) and so the theoretical model is only on the edge of its region of validity. This observation is supported by inspection of Figure 1 in [13], where the extra attenuation of the fundamental for $\Gamma_o = 50$ and $\sigma = 1.5$ is given as approximately 1.8 dB, for plane waves. For $\Gamma_o \simeq 4.4$, this amount of extra attenuation is achieved at $\sigma \simeq 2.9$.

The explanation given above implies that the model should be more reliable for $\Gamma_o = 4$ if σ is larger than in Figure 20d. Unfortunately it is not possible to test this prediction, as measurements were not made with transducer 6 at the required propagation distances. Nevertheless, it is possible to conclude from these results that the model is accurate for a wide range of values for Γ_o - at least for $\Gamma_o > 8$.

4.1.5 Spherical wave solution

For comparison purposes the results obtained using a model based on the spherical wave analogue of Burgers' equation are presented in this section. There is more than one way of utilising this equation to describe a transducer field, but one common method [22-23] was described in section 2.1.3 and will be used here. In the method, the field is modelled by that of a sphere of radius $r_o/2$ (where r_o is the Rayleigh length) and source amplitude $2p'_o$ (where p'_o is the effective pressure amplitude at the transducer).

If the measurement point is sufficiently far from the transducer, then the values of σ and Γ given by this method approach those of Equations 2.9-2.10 (which represent the matched Gaussian model) but, for smaller propagation distances, the two approaches diverge. Apart from the differences outlined above, the numerical algorithm used to calculate the spherical wave amplitudes was the same as that employed in the previous work.

Results for transducer 2 at R=1.3 are presented in Figure 21a and 21b. The measurements are the same as in Figure 15a and 15d, respectively, so a direct comparison can be made. It is evident that the accuracy of this method is considerably less than that of the matched Gaussian model for R=1.3, and that the value of σ is too small. Inspection of the results for R=0.64 for transducer 2 confirms the expectation that the accuracy of the spherical wave model is poorer for smaller propagation distances.

To see how the accuracy varies for larger propagation distances, calculations were made for transducer 3. Figure 22a gives the results for R=2.5 at the highest source amplitude. Although the spherical wave approach is not as accurate as the matched Gaussian model, the first ten harmonics agree with the measurements within the uncertainties. The fundamental in particular seems to be slightly high for the spherical wave model, although it is still within the uncertainty. The results for R=3.8 are presented in Figure 22b, and both models perform well even at the fundamental frequency. The uncertainty in the absorption coefficient has a larger effect on the calculated values for the higher harmonics and, allowing for this, both methods are in agreement with experiment.

4.1.6 Summary

To sum up, the results of this section demonstrate that whereas the matched Gaussian model can be used for R>0.64, the spherical wave approach is only accurate for R>2.5. Thus the approach derived in this report is a considerable improvement on previous methods, giving reliable predictions at propagation distances less than the Rayleigh length.

The matched Gaussian model has been verified for $\sigma > 1.5$ and $\Gamma_o > 8$. It is probable that the model is also reliable for $\Gamma_o < 8$, as long as σ is high enough, but it has not yet been possible to verify this conjecture. In general, the first 20 or so harmonics are reliably predicted if the model is used in its domain of reliability.

An important topic for further research would be to improve the accuracy of the predictions for $\sigma < 1.5$. Nevertheless, the current model is still useful for many applications, as is illustrated in the next section. A possible criticism of the conclusions presented here is that the experimental results at frequencies above 15 MHz rely on hydrophone sensitivities which are not determined directly, but are predicted using a theoretical model. This argument may be countered in three ways. Firstly, the major conclusions can be obtained from the results obtained at 15 MHz and below. Secondly, there is considerable redundancy in the results, as there are measurements for four different fundamental frequencies and for two types of transducer at two of the frequencies and this has permitted their self-consistency to be verified. Thirdly, the model of hydrophone response has

significant independent support, as outlined in section 3.1.1.

4.2 Hydrophone calibration

In the previous section the accuracy of the matched Gaussian model was investigated as a function of various relevant parameters and to do this it was necessary to know the sensitivity of the hydrophone at all the harmonic frequencies. In the range 1 to 15 MHz there are calibration data available, but at higher frequencies it was necessary to use a theoretical model of the hydrophone frequency response (see section 3.1.1). Although there is significant evidence to support this model, it has not yet been thoroughly verified. It is therefore of interest to reverse the process of the previous section and to use the matched Gaussian model in calibrating the hydrophone, assuming that this model of the nonlinear propagation is reliable.

Yet another way of using the measurement results would be to rely on the independently obtained hydrophone sensitivities (section 3.2) and use the matched Gaussian model to determine the nonlinearity parameter (β) for water. Unfortunately the measurement uncertainties are larger than the uncertainty in β (sections 3.6 and 3.7) so this approach has little usefulness. Nevertheless the good agreement obtained in section 4.2 provides confirmation of the value of β which was used. Recently, a method has been reported for determining β[30], which is similar to that suggested above. As the uncertainties of hydrophone calibration were large the overall uncertainty of the method was estimated to be 17 % [30]. However, in view of the close agreement obtained with the accepted values of β for three liquids, the author

suggested that an accuracy of 4% was achieved in practice.

A preliminary report of the hydrophone calibration method described below was given previously [35] and an earlier form of the method has been reported as part of a discussion of hydrophone characteristics [5].

4.2.1 Calibration method

To apply the method it is necessary to make measurements in the field of a transducer at low amplitudes (where negligible loss of fundamental amplitude has occurred) and at high amplitudes (for $\sigma \geq 2$). For ease of explanation it will be assumed that only two measurements are made, for transducer drive voltages (peak) of U_1 and U_2 ($U_1 < U_2$), where sinusoidal excitation is also assumed. The corresponding output voltages from the hydrophone will be denoted V_1 and V_2 at the fundamental frequency, with $V_2(n)$ being the amplitude of the n^{th} harmonic at high levels.

The procedure consists of two stages - initially the hydrophone is calibrated at the fundamental frequency, and then it is calibrated at the harmonic frequencies. The first stage involves determining the loss of fundamental amplitude that has occurred due to nonlinear distortion, and inferring from this the absolute amplitude of the wave. This extra loss, L, is given by:

$$L = V_2 U_1 / V_1 U_2 \qquad (0 < L < 1)$$

There are several possible ways of relating L to the pressure amplitude, and these will be discussed later. To illustrate the general approach, the Fay solution (Equation 2.21) is used here,

with the matched Gaussian model to give:

$$L = 2 \exp(\alpha_o r_o R_m)/\Gamma \sinh[\alpha_o r_o \sqrt{1+R_m^2}\, \mathrm{Ln}(R_m + \sqrt{1+R_m^2}) + 1/\Gamma] \qquad 4.1$$

Here $\alpha_o = \alpha(\omega_o)$, and the other symbols are defined in sections 2.1.2 and 2.1.3. The values of r_o and R_m can be determined by a separate set of measurements at low amplitudes, and α_o is determined by the frequency, so that Equation 4.1 can be solved for Γ by iteration. The local fundamental pressure amplitude p_1 is then obtained from

$$p_1 = L \exp(-\alpha_o r_o R_m)\Gamma\alpha_o\rho c^2/\beta k \qquad 4.2$$

The hydrophone sensitivity at the fundamental frequency, S_1, is then given by:

$$S_1 = V_2/p_1 \qquad 4.3$$

or, in dB relative to 1 V/μPa:-

$$S_1 = 20\ \mathrm{Log}_{10}\ (V_2/p_1) - 120$$

Having obtained the sensitivity at the fundamental frequency the known values of p_1 and Γ are used in Equation 2.21 to obtain the sensitivity, S_n, at each of the harmonic frequencies:-

$$S_n = V_2(n)L\Gamma \exp(-\alpha_o r_o R_m) \sinh\{n[\alpha_o r_o \sqrt{1+R_m^2}\,\mathrm{Ln}(R_m + \sqrt{1+R_m^2}) + 1/\Gamma]\}/2p_1 \qquad 4.4$$

where $n = 2, 3, 4 \ldots\ldots\ldots$

As explained in section 2.2, there are several alternative approaches to solving the matched Gaussian equations, Equations 2.8-2.10, and each of these approaches can be used to give values for the hydrophone sensitivity.

The weak shock solution (Equation 2.19) gives

$$L = 2x_o/\pi + (2/\pi\sigma)\int_{\sin^{-1}x_o}^{\pi} \cos(\theta - \sigma\sin\theta)d\theta \qquad 4.5$$

with $x_o = 0$ for $\sigma \leqslant 1$

and $x_o = (\sin^{-1}x_o)/\sigma$ for $\sigma > 1$

Here, small-signal absorption has been neglected in the expression for L, since the weak shock solution neglects such effects. Equation 4.5 is again solved by iteration, to obtain a value for σ. The hydrophone sensitivity at the fundamental frequency is then:

$$S_1 = V_2\beta k r_o \exp(\alpha_o r_o R)\sqrt{1+R_m^2}\,\mathrm{Ln}(R_m + \sqrt{1+R_m^2})/\rho c^2 \sigma L \qquad 4.6$$

Attenuation is included in Equation 4.6 and neglected in Equation 4.5, because it has a direct effect on the fundamental amplitude, but only a secondary effect on the loss (see, for example, [69]). The sensitivity at the harmonic frequencies is then

$$S_n = S_1 L V_2(n)/V_2\phi_n \qquad 4.7$$

where ϕ_n is obtained from Equation 2.19. The Improved Fay solution (Equation 2.22) may be applied in an identical manner to the Fay solution; the only change is in Equations 4.1 and 4.4, where $\sinh(.)$ is replaced by $\sinh(.)/[1-(1/\Gamma^2)\coth(.)]$ and $\sinh(.)/[1-(n/\Gamma^2)\coth(.)]$ respectively.

The most accurate way of calibrating the hydrophone using the general technique described above is to use the numerical solution of Equation 2.16. The procedure is to start out with an assumed hydrophone sensitivity at the fundamental (obtained using one of

the methods described above), use Equation 2.16 to compute L, and alter S_1 until the experimental value of L is obtained. This method has the disadvantage that it demands a potentially large amount of computing time. For this reason a hybrid approach was formulated [35], whereby one of the approximate solutions (Equations 4.1-4.7) is used to compute S_1, and hence the source pressure p_o. It is then possible to determine the values for S_n using a single numerical evaluation of Equation 2.16. The numerical calculation also makes it possible to check the value of S_1 by comparing the computed and measured value of L . A comparison of the various methods is given in [35] for three different fundamental frequencies, from which it is apparent that it is usually necessary to use the numerical solution to obtain reliable results for S_n.

Since the calibration method depends critically on the accuracy of the various approximate solutions, it is necessary to consider the relative merits of Equations 4.1-4.7, and how to decide which one to use. If the loss factor L is greater than 0.5 (which implies that $\sigma<3$), then Equations 4.5 and 4.6 must be used since Equations 4.1-4.4 are inaccurate (see Figure 2). However if attenuation is too large, then Equation 4.5 is not valid, so for 1% accuracy, the following condition must be met:-

$$\alpha_o r_o < 0.01/R_m \qquad 4.8$$

If Equation 4.8 is not satisfied, and L>0.5, then the numerical solution of Equation 2.16 must be used to calculate L. Fortunately (so long as $\alpha_o r_o$ is not too small), the time taken for the numerical calculations is relatively short in this case.

If $L<0.5$, then Equations 4.1-4.4 may be used; these have the advantages of allowing for absorption and also of being simple to evaluate. If $L\simeq 0.5$, and particularly if $\Gamma \lesssim 20$ in Equation 4.1, then it is advantageous to use the Improved Fay solution in Equations 4.1 and 4.4, because of its increased accuracy for low σ and low Γ. The accuracy of the equations diminishes if the combined effects of attenuation and geometrical spreading are too great; in this case section 2.3.2 (Figure 4) indicates that the fundamental has a 1% error for $\Gamma/(1+\sigma) \simeq 2.2$. Substitution for Γ and σ gives the following condition which must be met for $\sigma>3$:

$$\alpha_o r_o \sqrt{1+R_m^2}\, \mathrm{Ln}(R_m + \sqrt{1+R_m^2}) < 0.34 \qquad 4.9$$

For R_m = 1,2 and 3, this gives maximum values for $\alpha_o r_o$ of 0.27, 0.11 and 0.06 respectively. If Equation 4.9 is violated, then Equation 2.16 must be used to calculate S_1, but again this procedure should not require too much computing time, since absorption is significant and hence only a few harmonics have to be retained.

Table 4 summarises the above conclusions, demonstrating how they could be incorporated into a computer program. For the measurements reported here, the weak shock solution is normally used to calculate S_1 at 1 MHz, the Fay solution at 2 and 5 MHz, and the numerical method at 10 MHz.

An experimental aspect that is very important in this method is the linearity of the hydrophone and transducer, since these properties are crucial in the determination of L. This is not a problem for the present measurements as linearity has been checked

Table 4 Flow diagram for hydrophone calibration

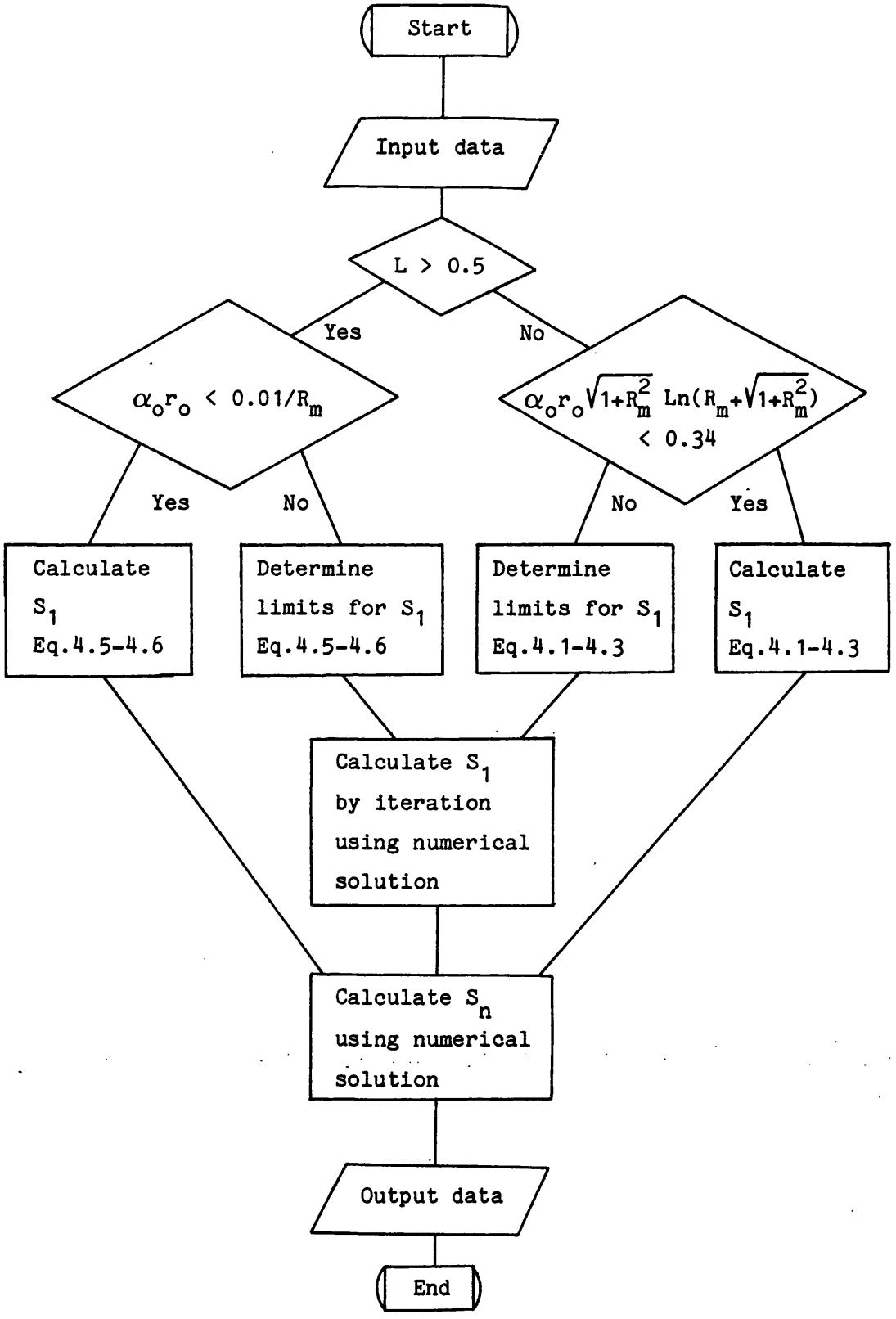

by a separate set of measurements (section 3.1.4). Alternative methods of calibration also require the hydrophone to be linear, and a device with a nonlinear response has little practical use. In addition, the pressure amplitudes used in this technique are below those frequently encountered in diagnostic ultrasound, so there is no requirement for linearity over an increased dynamic range. If measurements should reveal that the source transducer has a nonlinear response, then the loss may be determined by placing a hydrophone close to the transducer face, and using its output voltages instead of U_1 and U_2 in the expression for L.

4.2.2 Results

A hydrophone was calibrated using the procedure described above along with the measurement data discussed in Section 4.1. The measurements were not made with hydrophone calibration as their primary objective, and so there is scope for obtaining improved results by optimising the experimental method.

The hydrophone sensitivity at the fundamental frequency was calculated using the approximate solutions as described in section 4.2.1. Values were obtained for several propagation distances, subject to the condition that the approximate solutions be accurate to within 2% (see section 2.3). These results are presented in Figure 23a, where it is possible to compare the values for different propagation distances and for different transducers. At 2 MHz and 5 MHz the results from transducers with different sized active elements are available, and it is evident that there is no significant variation in the result obtained with different transducers.

The number of separate measurements used to obtain each point in Figure 23a varied from one to five, and the scatter of the results at a particular frequency seems to correlate quite well with the number of measurements available. This suggests that the uncertainty associated with measuring the loss L is significant - giving rise to variations in S_1 of approximately 0.5 dB. Here it should be noted that the calibration procedure is particularly sensitive to the uncertainty in L, as is illustrated by considering the case where attenuation is negligible. If L = 0.5 (which means that $\sigma \simeq 3$) then, from Equation 4.5, (or Figure 4 of [16],) a 1% change in L causes a 1.5% change in σ. In this case the change in hydrophone sensitivity would be 1.5%, since it is obtained directly from σ (nb in Equation 4.6 V_2/L is constant, since L is derived from V_2). As L becomes smaller, this effect decreases, but for most practical situations the measurement uncertainty is magnified when applied to hydrophone calibration. For this reason, it is important to determine L as accurately as possible. A significant improvement in measuring accuracy could be achieved if L was determined separately from the analysis of harmonic amplitudes. A low pass filter could be used to isolate the fundamental frequency component, and the relative voltage determined using a calibrated attenuator.

Figure 23b gives a comparison of the hydrophone sensitivites determined using the present method with those obtained with the techniques of reciprocity, beam plotting and interferometry as described in section 3.2. Both the beam plotting and the present methods rely on the calibration factor of the digitiser, so this was allowed for in calculating the results. It should be noted

here that the results derived from interferometry were obtained somewhat indirectly, being based on early intercomparison data that were acquired before the primary calibration was made. Agreement within the uncertainties is obtained for each of the four frequencies where the nonlinear propagation method has been applied. One exception is the result at 1 MHz, which is just outside the range of agreement with the beam plotting method. However, more recent measurements with the beam plotting method have given lower hydrophone sensitivities, which differ by only 3% from the nonlinear propagation results at 1 MHz. The most accurate results are those derived from interferometry, and the difference between these and the results of the nonlinear propagation method is less than 5% at all frequencies.

In Figure 24, the calibration results are presented for the first fourteen harmonics, using the results from transducers 1, 3 and 5. Where more than one value is available at a particular frequency, the arithmetic mean has been taken. The results are compared in Figure 24a with those of the three other methods and again the agreement is satisfactory. At frequencies between 20 and 30 MHz, it is possible to see the difference between results obtained with a 2 MHz fundamental and those with a 5 MHz fundamental. The amplitudes of the harmonics of the 2 MHz wave are approximately a twentieth of the fundamental, so the difference of 7% between the two sets of values is well within the measurement uncertainties.

No independent calibration data are available for frequencies above 15 MHz but the results can be compared with the predictions of the model of hydrophone frequency response that was presented in section 3.1.1. The model predictions were normalised to the

mean of the experimental data, and the two sets of results are plotted in Figure 24b. The agreement obtained indicates that the calibration technique is reliable at frequencies up to 70 MHz.

The results of this section indicate that the calibration technique is reliable over the frequency range 1 to 70 MHz. The overall accuracy appears to be limited by the measurement uncertainties at present, and so it would be desirable to improve the experimental method. The systematic uncertainty is difficult to determine independently because of the nature of the mathematical propagation model. Nevertheless the agreement obtained with other calibration methods indicates that any systematic uncertainty is probably less than 10%.

4.3 Intercomparison of hydrophone responses

An application of sawtooth wave formation which utilises the experimental capability outlined in chapter 3 is the intercomparison of the sensitivities of different hydrophones. The existence of many frequency components in a sawtooth wave makes it possible to compare hydrophone responses at several frequencies simultaneously. Such a capability is important because it is very time consuming to perform intercomparisons on a point by point frequency basis. As hydrophones frequently have considerable structure in their frequency response curves, many measurements are often required, and the use of a sawtooth wave can provide more results in less time.

The procedure is straightforward: a replacement method is used, and care is taken that the propagation distance and transducer

drive voltage are the same for each of the hydrophones. After making measurements with each hydrophone in turn, the first one is returned to the tank, to check that the acoustic field has not changed.

Some results have already been presented in Figures 8 and 9, where they were used to confirm the theoretical model of frequency response for membrane hydrophones. In this section the accuracy and reproducibility of the method as currently employed will be examined, using results obtained with a fundamental frequency of 1 MHz.

In a sawtooth wave the harmonic amplitudes are inversely proportional to the harmonic number, and as a consequence the frequency range for the intercomparison of hydrophones is limited. This range depends on the accuracy required for the intercomparison, and is limited by the noise and digitising error of the measurement system. Consideration of the sampling error shows that a 9 bit digitiser such as used here should give an accuracy of approximately 5% for the first 17 harmonics if the noise is negligible. The above uncertainties can be reduced by signal averaging and Fourier analysis but they still contribute significantly to the overall uncertainty.

Two systematic uncertainties arise from imperfections in the performance of the digitiser, namely the possible nonlinearity of its response and the non-zero width of its trace. The first of these has a nominal magnitude of 2%, but it depends significantly on the position of the waveform on the diode array due to imperfections in the deflection system for the electron beam (see

section 3.3.4). The second uncertainty is discussed below. Another potential source of disagreement between the results obtained here and those derived from other methods is the finite size of the active element of the hydrophones. As the acoustic beam is not planar, methods which use different beams will give slightly different results, due to spatial averaging. Extra difficulties could be caused if areas other than the active element are acoustically sensitive - either in the hydrophone itself or in its connecting cable.

An indication of the reproducibility and self-consistency of the method is given in Figure 25. Here the sensitivities of two hydrophones are compared using fundamental frequencies of 1 MHz and 0.9091 MHz, so that the results can be compared directly at 10 MHz and 20 MHz. Over the range 0.9 to 25 MHz the agreement between the two sets of data is better than 7%, and up to 17 MHz it is better than 3.5%. In general the agreement becomes worse with increasing frequency, as expected, but it is interesting to note that one of the largest differences occurs at 1 MHz. A possible reason for this is the presence of reflections from the tank walls.

The measurement uncertainty due to the non-zero width of the digitiser trace was investigated in the following manner. The effect would be expected to be greatest when a wide range of frequency components is present in the signal, since this introduces the most rapid oscillations into the trace. To achieve this situation a hydrophone amplifier with a wide bandwidth is obviously required, but the waveform is most difficult to capture when a hydrophone with a long cable (65 cm) is also used. The

electrical resonance in such a cable occurs at about 70 MHz, and this introduces oscillations into the waveform. To investigate the effect of finite trace width, the response of a hydrophone made from 9 micron film with a long cable was compared with that of an identical hydrophone which had a stub cable (3 cm long). The relative sensitivities obtained using the full system bandwidth of approximately 100 MHz were then compared with those obtained when a 20 MHz filter was introduced. Figure 26 gives the two sets of results which are in agreement within 3% over the frequency range 1 to 20 MHz. Although the consistency of the results is thus as good as in Figure 25, there is evidence of a small systematic difference between the two sets of data. Although this difference is relatively small it is probably wise to limit the system bandwidth to the minimum required for a particular intercomparison.

To verify the absolute accuracy of the technique, the sensitivities of two hydrophones were compared using sinusoidal waves by measuring the peak-to-peak output voltages produced when they were placed in a certain position in the field. One of the hydrophones was a bilaminar design (50 micron total thickness) and the other was a coplanar type (made from 9 micron film). These were chosen so that the frequency responses and acoustical reflection coefficients were significantly different. An initial set of results is presented in Figure 27a, where the points obtained with a sawtooth wave represent the means of readings made with different system bandwidths. In general the agreement between the two methods is better than 4%, which is consistent with uncertainties of between 2% and 3% (68% confidence level) for each

of the techniques. At 7.5 MHz, however, the results differ by about 10%. This comparison was made by interpolating between the 7 MHz and 8 MHz readings from the sawtooth wave method, so there is a small possibility that the hydrophone has a peak in its response. However it is more likely that the results obtained with the single frequency method are in error, because all calibrations of membrane hydrophones made to date indicate that their responses vary smoothly with frequency. As the radiating transducer used at 7.5 MHz has a relatively complex field structure, an error of alignment seems to be the most likely cause of the observed discrepancy. This observation underlines one of the advantages of the method described here, since the method requires fewer alignments of hydrophone and transducer.

The results of a more complete intercomparison between the two alternative methods are presented in Figure 27b. Here the sinusoidal wave method was repeated some 15 times (7 times at 15 MHz) over a period of 3 years to obtain the final result, with the random uncertainty being 1.5% and the estimated overall uncertainty, including systematic components being typically 3% (95% confidence level). Again agreement is obtained within the random uncertainties at all frequencies, except at 15 MHz where the agreement is within the overall uncertainty of the sinusoidal wave method and the random uncertainty of the sawtooth wave method.

From the results of this section it is concluded that hydrophone sensitivities can be compared with an accuracy of approximately 3% using the first 10 to 15 harmonic components of a sawtooth wave. The results obtained to date indicate that the uncertainty of the

method at the fundamental frequency is larger than would be expected, and this effect is currently being investigated by using a different digitiser to capture the waveforms and by redesigning the acoustic baffles to have a lower reflection coefficient. In future work the use of high pass filters may be investigated as a means to measure the higher harmonic components more accurately. A further possible development is to use different waveforms to drive the transducer so as to cover either a wider frequency range, or intermediate frequency points within a given range.

4.4 Pulsed focused field

Some measurements have been made in the field of a focused transducer under pulsed excitation to test the theoretical development presented in sections 2.1.4, 2.2.2 and Appendix 2, which neglects the effect of phase variations on the observed waveform. The purpose of this work was to examine the usefulness of this relatively simple model in describing the nonlinear distortion that occurs in the fields produced by medical diagnostic equipment, and the results were published in 1984 [55].

The characteristics of the transducer have been described in section 3.5. A buffer preamplifier was positioned close to the hydrophone and, as this had a slight resonance at 85 MHz, a 50 MHz low pass filter was inserted to smooth the frequency response. The signal was recorded with the transient digitiser (Tektronix 7912AD) and a typical waveform is given in Figure 28. The most obvious effect due to nonlinear distortion is the difference between the rise time and the decay time for the peak positive pressure. The time delays between the 10% and 90% points of peak

to peak amplitude for the relevant half cycles are 33 ns and 122 ns respectively. This effect was not noticeable either when the hydrophone was placed close to the transducer or when the amplitude of the drive voltage was reduced. The linearity of the transducer was determined from measurements at a distance of 2.4 mm from the transducer face and was found to be better than 2 %. From studies of the linearity of similar hydrophones [5,130,146] it was estimated that any spurious harmonics introduced were at least 30 dB below the amplitude of the fundamental (see also section 3.1.4).

To test the validity of the mathematical model, the harmonic content of the peak cycle of the waveform was determined by Fourier analysis as a function of the drive amplitude. It was possible to compare these results with the predictions of Equation 2.19, by assuming that the waveform of the peak cycle of the pulse was sinusoidal for low acoustic pressures. In Figure 29 the variation of the fundamental frequency component (first harmonic) is presented as a function of σ. The experimental points are obtained from the ratio of the measured amplitude to that obtained by extrapolation from low amplitudes. The characteristic decrease in the measured pressure as the drive level is increased is observed, with the agreement between theory and experiment being better than 5%.

The relative amplitudes of the harmonic components can give a sensitive indication of the accuracy of the theoretical model since, for $\sigma \ll 1$, they are proportional to $\sigma^{(n-1)}$ (Equation 1.10) where n is the harmonic number. Figure 30 gives the amplitudes (relative to the fundamental level) of harmonics 2, 3 and 4, and

the agreement is approximately 10%. An exception to this is the level of the second harmonic for low values of σ; this lack of agreement probably arises from a non-sinusoidal initial wave. Such an explanation seems reasonable since the pulse is only about two cycles long.

The variation of the normalised peak-to-peak pressure as given in Equation 2.18 is compared with experiment in Figure 31. For $\sigma < 0.6$, the observed normalised pressure is roughly constant, as expected, but for greater values of σ the pressure increases contrary to predictions. There are three possible reasons for this result. Firstly, the amplitudes of the harmonic components may be incorrectly described by the model, however such an explanation is doubtful because of the agreement obtained in Figures 29 and 30. Secondly, the relative phases of the harmonics may not be as predicted. This is quite plausible since phase variations are not fully accounted for in the derivation of Equation 2.8. Thirdly, distortion caused by overshoot in the detection electronics may have given rise to errors in the measurement of peak-to-peak pressure. In the next section, comparison is made with theoretical predictions that take account of the phase variations that occur in the field, demonstrating that the second explanation given above is the correct one.

4.5 Waveforms in a focused field

To test the predictions of Equation 2.17 for a focused field a second set of measurements was made in the field of the transducer used in the previous section. The transducer was driven with a tone-burst electrical waveform, and a different detection system

was employed which incorporated a 65 MHz bandwidth preamplifier and 70 MHz bandwidth digitiser (Tektronix 7D20). The field at the focus was characterised more fully than in the previous work, with peak-positive and peak-negative acoustic pressures being recorded along with the phases of the frequency components in addition to their amplitudes. In the previous measurements the highest source amplitude corresponded to a value for σ at the focus of 1.4, whereas here the maximum value of σ was 3.6, making it possible to test the model under conditions of significant saturation and beam broadening.

Calculated and measured waveforms are given in Figures 32-34 for σ values of 1.4, 2 and 3.6 respectively. In Figure 32 the agreement is good, with both waveforms showing a sharp positive peak and rounded negative peak and a similar amount of asymmetry, defined as the ratio of the peak-positive pressure to the peak-negative. It should be noted that there is evidence of ringing in both of the waveforms occurring immediately after the shock front. This is caused by the finite bandwidth of the measurement system and the limited number of harmonics (up to 256) retained in the calculations. The ringing has been reduced in the calculated waveforms by using a smoothing algorithm; to eliminate the effect from the measurements completely it would be necessary to increase the bandwidth approximately thirty times to over 2 GHz. The positive portions of the measured waveforms show little variation with increasing σ, but the shape of the negative portions does change, with the region immediately before the shock front initially having a positive gradient, then zero slope and finally a negative gradient. This trend is not seen in the predicted

waveforms, although there is a small change in the shape. This deficiency in the model is due to the neglect of changes in the beam profile (and therefore of diffraction characteristics) with increasing amplitude.

A crude method of accounting for these changes in beam profile is described in section 2.2.1 and it involves reducing the diffraction term in the governing equation by an amount equal to the extra attenuation of the fundamental component of the wave. The predictions of this method are presented in Figure 35 for moderate and high amplitudes and it can be seen that the deficiencies noted above have been overcome and the waveforms agree qualitatively with experiment. For ease of reference, in the rest of this thesis, the method of calculation used in Figure 35 will be referred to as the modified theory, whereas that used to obtain Figures 32-34 will be called the simple theory. Unless it is stated to the contrary, the simple theory will be used for comparisons with experiment.

The magnitude of the fundamental frequency component of the wave, normalised to the source level, is shown in Figure 36, where it can be seen that the predicted and measured values agree for all amplitudes. Agreement at low amplitudes ($\sigma<1$) is again shown in Figure 37 for the magnitude of the harmonic components expressed as a ratio of the fundamental component. When σ is greater than 1, the predicted amplitudes can be as much as 15% lower than the measured values, with this difference becoming less as σ increases further. It is of interest to note that the measured amplitudes can be slightly greater than the values that are obtained for a perfect sawtooth wave with 1/n dependence of amplitude on harmonic

number. The relative phases of the harmonic components are plotted in Figure 38 as a function of σ. When σ is less than 1 the variation is relatively small, with the most rapid change occurring for σ values between 1 and 2, after which the phase increases at a slower rate. Both the measured and predicted curves show this trend, although the amount of predicted variation is too small. For low values of σ the agreement for the size of the relative phases is 10-15% for the first five harmonics, which is remarkable considering that the phase characteristics of a focused Gaussian and a focused piston field are very different.

Having examined the theoretical predictions in the frequency domain, the next series of graphs give the variation of some parameters obtained from the time domain waveform. In presenting these results the parameter under consideration is normalised to the value that would be expected for linear propagation, derived by extrapolation from the measurements at low amplitude. The variation in peak-to-peak amplitude is shown in Figure 39; for $\sigma<1.4$ the amplitude increases due to the increasing asymmetry associated with the nonlinear propagation. For higher source levels saturation becomes the dominant effect, giving rise to a decrease in the normalised amplitude, although the corresponding absolute value never decreases. Similar behaviour is demonstrated in Figure 40 for the peak-positive pressure of the waveform, although the increase in amplitude is greater, being 80% for $\sigma = 1.4$. In general, the predicted values are again in agreement with the measurements, although at high source levels they are some 10% too high. The effect of asymmetry in the waveform is to decrease the value of the peak-negative pressure, and so this

parameter shows a monotonic decrease in normalised amplitude, as shown in Figure 41. For low amplitudes, the predicted and measured curves agree, but for high amplitudes there are differences of up to 17%. The experimentally determined curve shows a feature which is not predicted in that there is a point of inflexion at the point where the shock becomes fully developed ($\sigma = 1.4$), with the decrease in amplitude becoming less marked. This effect is probably due to the change in beam profile due to saturation, because it can be predicted using the modified theory.

The differences between theory and experiment are most marked in Figure 42a where the asymmetry ratio, defined as the ratio of peak-positive and peak-negative pressures, is plotted as a function of σ. The measured asymmetry decreases once the shock has fully formed, whereas the predicted curve remains essentially constant. As indicated previously, the most likely cause for this discrepancy is the failure of the model to account for changes in the beam profile with amplitude. Justification for the measured behaviour of the asymmetry can be obtained by considering a simple plane wave propagation model, which predicts the following relationship for the rate of change of the asymmetry, A:

$$\frac{\partial A}{\partial \sigma} = -(A^2 - 1)/2(1 + \sigma) \qquad 4.10$$

This formula predicts a decrease in A that is about twice the measured rate, which is a reasonable result since in practice the decrease in asymmetry will be moderated by the effects of diffraction. To confirm this conclusion, the variation in asymmetry was also calculated using the modified theory and these predictions are compared with experiment in Figure 42b. The

results show a marked improvement in the agreement with experiment, with the variation in asymmetry being predicted to within 5%, which is to be compared with the previous differences of up to 35%. The modified theory also shows an improved agreement with the measured values for the peak-positive and peak-negative acoustic pressures, although the improvement is less marked in this instance since the simple theory is more accurate in predicting these parameters.

To sum up the results of this section, the predictions of the theoretical model have been verified at the focus of a transducer by comparison with experiment. Most of the features of the field are predicted by the model, although as expected the predictions are less reliable for $\sigma>1.4$ than they are for lower amplitudes. This conclusion is particularly significant when the approximations made in the model are considered, particularly the use of a Gaussian beam profile to model the field of a piston source. For $\sigma>1.4$ the shortcomings of the simple theory are overcome by the modified theory, which takes account of the changing beam profile at high amplitudes.

4.6 Waveforms in tissue and tissue-mimmicking gels

The method described in section 2.1.5 was used to predict the acoustic field of the focused transducer when radiating into liver tissue. The acoustical parameters used in the calculations were those measured by Cobb for normal, fresh human liver [163], with the additional assumption of a linear dependence of the attenuation coefficient on frequency. Unfortunately, Cobb did not measure the dispersion of liver, however the theoretical model

allows this to be calculated from the attenuation coefficient, giving a variation in the velocity of 0.26% per frequency decade. This figure is significantly less than the figure of 0.7% per decade reported by Wells [140,164] for soft tissue and which was used in initial calculations [78], but the discrepancy is explained by the facts that Wells assumed a higher value for the attenuation coefficient than was measured by Cobb [163] and that his formula is only an approximate one, with the numerical factor being given to one significant digit.

A typical calculated waveform is given in Figure 43a and apart from the smoothing of the shock front due to the high attenuation of the medium, the most obvious feature is the comparative symmetry between the positive and negative parts of the curve. This reduction in asymmetry is caused by the dispersion of the medium as is illustrated in Figure 43b where the same input parameters were used for the calculations, but the dispersion was set to zero. The asymmetry in this case is 1.6, compared with the value in the previous curve of 1.3. In certain circumstances it is possible for the asymmetry of the waveform to be reversed as demonstrated in Figure 43c where the higher value of dispersion, quoted by Wells [140,164], was used in the calculations, resulting in an asymmetry ratio of 0.87.

It is of interest to estimate the conditions for an asymmetry ratio of less than unity to occur, and this is achieved by noting the physical processes that determine the shape of the waveform. For convenience, in the following discussion, the term 'harmonic components' will be used to refer to all of the frequency components in the wave apart from the fundamental. To explain the

profiles it should be noted that both diffraction and dispersion lead to an increase in the phase velocity of the wave when compared to the plane-wave or low-frequency value, but that the velocity due to diffraction decreases with harmonic number whereas that due to dispersion increases. Thus, in the absence of dispersion, the harmonic components, which determine the position of the shock front, travel more slowly than the fundamental, and are delayed in time with respect to it. As the shock front occurs at a point in the waveform where the acoustic pressure is increasing, this delay gives rise to an increase in the value of the peak-positive pressure and a corresponding decrease in the value of the peak-negative. The opposite behaviour occurs if dispersion is the dominant effect, because in this case the harmonic components are advanced in time with respect to the fundamental and consequently the peak-negative acoustic pressure is larger than the peak-positive. To determine the point of balance, where the phase shifts due to dispersion and diffraction cancel each other out, it is convenient to consider the velocity of the second harmonic with respect to the fundamental component. The balance point is then determined by equating the decrease in speed due to diffraction with the increase due to dispersion. As the speed due to diffraction is not constant during the propagation it is necessary to use an average value and this is obtained by weighting the average with the rate of production of the second harmonic, that is with σ. Utilising the relationship between attenuation and dispersion that was derived in Appendix 1, the condition for the asymmetry ratio to be less than unity (reversed asymmetry) is:

$$D > \frac{\pi R_o \, \mathrm{Ln}\sqrt{1+R_o^2}}{2\,\alpha\,\mathrm{Ln}(2)\,\mathrm{Ln}^2\,(R_o+\sqrt{1+R_o^2})} \qquad 4.11$$

where D and R_o have been defined in section 2.1.4 and α is the attenuation coefficient at the fundamental frequency. For a typical medical transducer with R_o = 3 Equation 4.11 predicts that the wave must be attenuated by a factor of at least 10 in travelling to the focus (αD = 2.4) before the asymmetry of the wave can be reversed. For tissue with an attenuation of 1 dB cm^{-1} MHz^{-1}, this corresponds to a propagation distance of 6 cm at 3.5 MHz and 4 cm at 5 MHz; these distances are typical of the focal lengths used in diagnostic ultrasound and so one would expect the waveforms produced in tissue to be fairly symmetrical. One would expect there to be some cases of reversed asymmetry, but the effect would not be great because the nonlinear distortion would be relatively slight, due to the large attenuation of the wave. The implications of these theoretical predictions for the way in which measurements of the output of diagnostic ultrasound scanners should be interpreted will be discussed later in this section; now the reliability of the predictions will be examined.

The theoretical model was tested by comparison with measurements for propagation in a tissue-mimmicking gel [165]. A slab of the gel 4 cm thick was obtained and the attenuation coefficient measured to be approximately 0.9 dB cm^{-1} MHz^{-1} in the frequency range 2.25 to 5 MHz; the sound velocity was given as 1540 ms^{-1} and the density determined as 1.11 g cm^{-3}. The sample of material was immersed in a water bath and the transducer pressed against one face, while a membrane hydrophone was positioned approximately 3 mm from the other face. The hydrophone was thus placed close to

the focus of the beam, and for the purpose of the calculations it was assumed that it was actually at the focus. The focal gain G of the beam was determined in the manner described in section 2.1.4 and a series of measurements of the waveform was made for increasing source amplitude. To compare the the predictions with the measurements it was necessary to know the nonlinearity parameter β, of the gel; this was determined from the extra attenuation of the fundamental component by choosing a value for σ which gave agreement with the calculated extra attenuation. The value of β obtained in this way was 4.6.

The predicted and measured waveforms are given in Figure 44 for the highest amplitude that was achieved. Qualitatively the waveforms are similar, with asymmetry close to unity, although the rise-time of the measured waveform (40 ns) is slightly greater than that of the calculated profile (30 ns). A more quantitative comparison of the results is given in Figure 45, where the asymmetry and normalised peak-to-peak amplitude are plotted as a function of sigma. The peak-to-peak amplitude behaves in accordance with the predictions, but the asymmetry is slightly greater than expected, although it is a lot less than would be expected if the dispersion was negligible (dashed curve). Since the influences of dispersion and diffraction on the profile are roughly balancing each other out, the asymmetry is particularly sensitive to the value assigned to each effect. This is illustrated in Figure 46, where the assymmetry and peak-to-peak amplitude are compared with predictions which used a value for the focal gain G that was obtained from the calculated beam profile at the focus, rather than the measured profile. Here agreement is

obtained for both of the parameters under study and consequently this new value of G was used in subsequent calculations.

Figure 47 gives the amplitudes of the first four harmonic components, normalised to the amplitude that the fundamental would have for linear propagation. The measured amplitudes are somewhat less than the predicted values, particularly for the higher harmonics. There are a number of explanations for this, but most of the discrepancy can be explained by the effect of the thin (0.025 mm) plastic film that was used to protect the surfaces of the gel, which tended to filter out the higher frequency components in the wave. The phases of harmonic components 2, 3 and 4 are presented in Figure 48, where it can be seen that the measured phase differences are greater than the predicted values with the absolute differences between theory and experiment being similar to those for measurements in water (Figure 38). It is interesting to note that the calculated phase differences increase with increasing amplitude, whereas the measured values decrease, although this latter effect could be an artefact of the experimental procedure. The reason for the behaviour of the predicted curves is that for high amplitudes the harmonic components produced close to the focus (where the phase shifts due to diffraction are greatest) are most important in determining the field at the focus. On the other hand, the behaviour of the experimental data is due to the effect of saturation in modifying the beam profile and consequently reducing the phase shifts due to diffraction when the amplitude is high.

The theoretical model has now been verified by comparison with experiment; to conclude this section the implications of the

results will be discussed. It is currently the accepted practice to characterise the output of diagnostic ultrasound equipment by measuring the field radiated into water and, if predictions of the field in the patient are required, to derive acoustic parameters in tissue on the basis of linear propagation theory [166]. The validity of this procedure is examined in Figure 49, where the calculated value for the peak-positive acoustic pressure in liver tissue is plotted as a function of the corresponding parameter for propagation in water (with the same transducer output conditions). The graph demonstrates that the relationship between the two parameters is far from straightforward, with the value in tissue varying from 0.6 to 1.2 times the value that would be expected if the propagation were linear. The initial part of the curve is due to the fact that the peak-positive pressure in water is greater than the predictions of linear theory for moderate amounts of distortion (see Figure 40). At higher amplitudes, however, saturation of the wave occurs much more rapidly for propagation in water than for tissue and so the pressure in tissue becomes greater than expected. If the amplitude of the initial wave were increased still further, so that saturation occurs in tissue as well as in water, then the absolute acoustic pressures in the two media would be expected to be similar (to within a factor of two for the conditions under consideration). In this case the errors involved in making predictions based on linear theory would be even larger than demonstrated in Figure 49, being similar in size to the small-signal attenuation of the wave.

In Figure 50, a similar comparison of the peak-positive acoustic pressures in water and in the tissue-mimmicking gel is given, only

here the measured parameters are plotted rather than the calculated ones. The same features can be noted here as were seen in Figure 49, although the maximum source amplitude attained was slightly less.

The calculated peak-negative acoustic pressure in liver tissue is plotted in Figure 51 as a function of the corresponding value in water and it is evident that errors of greater than 40% can occur if predictions of the levels are made on the basis of linear propagation theory. The shape of the curve is less complex than for the case of the peak-positive pressure because the normalised peak-negative pressure in water shows a monotonic decrease with increasing source amplitude (Figure 41). However, this effect suggests that the maximum deviation from a linear relationship is probably greater in this case than in the previous one. A comparison of the measured peak-negative pressure in tissue-mimmicking gel with the corresponding value in water is given in Figure 52, which demonstrates similar features to the curve for liver tissue. The departure from linearity is greater in this case (about 60%) because the slightly greater dispersion of the gel gives rise to larger peak-negative pressures.

Since the behaviour of the ultrasonic wave in tissue is significantly different from the behaviour in water, it is of interest to develop a procedure to predict the field in tissue, based on measurements in water. The main difficulty in developing such a technique is that when saturation occurs in water, the measured amplitude does not change significantly with increasing source amplitude, whereas the level in tissue can continue to increase still further. This effect is illustrated in Figure 53,

where the calculated amplitude in gel is plotted as a function of the corresponding amplitude in water. If a procedure was developed that was based on using the measured amplitude in water as a predictive parameter, then small deficiencies in the calculations or the measurements would give rise to large errors in the predicted level in tissue. This difficulty can be overcome by noting that when saturation occurs, the asymmetry of the waveform can still change significantly if the source amplitude is increased still further (see Figure 53). Consequently, a more reliable procedure would be to base the predictions on the measured amplitude in water for small signal amounts of distortion ($\sigma < 2$), but to use the asymmetry of the wave for $\sigma > 2$. The modified theory of section 2.2.1 should be used to make these predictions, since the simple theory does not account for changes in the asymmetry at high amplitudes. This method was used with the results obtained for the focused transducer and the predictions are compared with the measured amplitudes in gel in Figures 54-55. Although there is some scatter in the results, the agreement with the measured values is satisfactory, indicating that the method is of practical use. By contrast, the predictions based on linear theory are shown to be in error.

The results presented above show that it is not valid to predict the acoustic field in tissue on the basis of measurements made in water and a simple attenuation correction, and that nonlinear propagation effects must be taken into account. It is however possible to predict the effects of nonlinearity and so to obtain more reliable calculations of the true field in tissue, if the basic focusing characteristics of the transducer are known. The

peak-positive pressure in tissue can be greater or smaller than the value predicted by linear propagation theory, whereas the peak-negative pressure is always greater. This second observation is of particular concern, since the peak-negative acoustic pressure is a very important parameter in predicting the possibility of biological hazard due to the occurrence of cavitation.

5. CONCLUSION

The main purpose of this chapter is to outline the areas for future work, since the results obtained so far have been discussed in the main text, but a brief summary of the principal achievements is given below. The matched Gaussian model of the field of a piston transducer has been shown to give reliable predictions of the true field for propagation distances greater than two thirds of the Rayleigh length, for $\sigma > 1.5$ and for $\Gamma_o > 8$. This model has been employed in developing a method of calibrating ultrasonic hydrophones. The method relies on measuring the variation in amplitude of the fundamental component in the field as a function of source level and comparing this with the theoretical predictions. It is then possible to determine the acoustic amplitude at the transducer and to predict the spectrum of the wave that is incident on the hydrophone. The hydrophone is calibrated by comparing the frequency content of its output voltage with the incident spectrum. With this method it is possible to obtain values of the sensitivity over a wide frequency range in a single calibration. The results have been shown to compare well with those from independent calibration techniques and with predictions of the frequency response of the hydrophone. A rapid method of intercomparing hydrophone sensitivities has also been demonstrated, which relies on the fact that a sawtooth waveform contains many frequency components.

To describe the field of a focused transducer, a simple model was developed that neglected the phase variations which occur in such fields. This model was able to predict the spectral content of the

wave but could not account for the observed asymmetry in the waveforms. This deficiency was overcome with a second model, which accounted for phase variations and, by modifying the algorithm slightly, it was also possible to account for the effect of the changing beam profile of the wave at high amplitudes. In a further development it was possible to describe the field in tissue-mimmicking gel. These theoretical models were then used to develop a procedure for predicting the ultrasonic field in tissue on the basis of measurements that are made in water. For several of the theoretical models it was possible to employ some previously known solutions for nonlinear waveforms as approximations to the true solution. To examine the usefulness of these formulae for this application, numerical studies were performed to determine their range of validity.

In the following two sections suggestions are made for further research based on the work that has been presented in this thesis.

5.1 Theory

The matched Gaussian model for the field of a piston transducer has been shown to be generally reliable for $\sigma > 1.5$ and $R > 1$ (section 4.1). To improve this model, it would be trivial to include the effects of phase variations within the near field, but the most significant limitation is the use of a Gaussian profile to describe the beam. To overcome this problem it would be of value to develop the method of section 2.1.2 for non-Gaussian beam profiles, but an earlier analysis based on these concepts was not successful, because it neglected phase changes. The main difficulty to be overcome is the characterisation of the beam

profile of the harmonic components, which is required in order to determine the diffractive term in the propagation equation. Progress has already been made by using a Green's function approach for the second harmonic component (this work is not presented here), but it will be extremely difficult to extend the analysis to describe the higher harmonics. To complete the treatment it will probably be necessary to derive the appropriate terms using a less rigorous approach. Measurements of the finite amplitude near field of a piston transducer have shown that as the harmonic number increases the axial beam profile quickly reaches a limiting form, suggesting that such a simplified approach to this problem could be successful.

In applying the theory of section 2.1.4 to focused beams, the main difficulty lies in describing the change in the beam profile that occurs due to the increased loss of energy on the axis. Nevertheless, a simple ad hoc approach to this problem has been very successful in improving the agreement with experiment, suggesting that a completely rigorous method is not necessary to overcome this problem. In section 2.1.5, the effect of dispersion in the propagating medium is taken into account, permitting the prediction of fields in tissue and in tissue-mimmicking materials. This model has been shown to agree with experiment, the main difficulty lying in the determination of the relevant characteristics of the medium rather than in applying the theoretical model. Future studies in the modelling of pulsed focused fields may include the comparison of the measured focal beam profiles for the harmonic components with theoretical predictions. Although the theoretical description of focused

fields given here permits a much more rapid calculation of the waveform than was previously possible, there is still a requirement for simpler and quicker methods which could be applied to estimate the effect of nonlinear propagation on the peak-positive and peak-negative acoustic pressures. Such a procedure would be of great use in the characterisation of diagnostic ultrasound equipment. One approach could be to derive characteristic curves using the theory described here, but another possibility is to modify the theory of Sutin [26, 27] or the simplified approach due to Lucas and Muir [38].

In section 2.3.2 it was noted that further calculations were required to examine the accuracy of the approximate solution Equation 2.21 in more detail for the spherical wave case. Although this is not strictly required for the present work, such an investigation is desirable to make the study complete.

It seems possible to develop the calibration method of section 4.2 to obtain the relative response of a hydrophone at a number of different frequencies. To obtain an absolute calibration, the hydrophone would have to be calibrated by a separate method at one frequency. The advantage of such a technique is that it would not be necessary to derive a model which can predict the detailed field structure of a transducer. This method would be based on the observation that certain scaling laws apply to the finite amplitude field of an axisymmetric radiator. A further method which is under active consideration is to develop the absolute calibration method by applying it to a plane wave field and so bypass the difficulty of having to describe a diffractive field theoretically. Initial tests have demonstrated the feasibility of

this method by isolating the plane-wave component in a pulsed field from the edge-wave component, but considerably more work is required to establish this technique.

5.2 Experiment

An experimental system has been set up which works well and the associated measurement uncertainties have been assessed. An aspect of the measurement system that has not been studied in sufficient detail, however, is the effect that the resistance in the hydrophone output leads may have on the frequency response of the hydrophone. To examine this effect it is hoped to use the interferometric calibration method to determine the phase reponse of the hydrophones and to use these results in the development of an improved model of their frequency response.

It would be of great interest to obtain a transducer with a Gaussian source shading function, so that the theoretical calculations for this field profile could be compared directly with experiment. Such a transducer has in fact been purchased and preliminary measurements have been made with it. Unfortunately, the axial beam profile is not as smooth as it should be to conform to the theoretical model, so there is a requirement for an improved transducer. This could possibly be obtained by using a lens structure to selectively attenuate certain parts of the beam profile. Such a design would have the advantage of giving an inherently smooth structure to the source beam profile and not requiring low coupling to radial modes of vibration in the transducer element.

The calibration method of section 4.2 could be improved if a better theoretical model were available; this subject has already been discussed in the previous section. Another important development is to establish an integrated computer program, following the outline of Table 4, which could calculate hydrophone sensitivities with a minimum of user interaction. Repeated and extended experimental measurements would be useful to check the self-consistency of the method more completely. It is of particular interest to use the absolute calibration method with a fundamental frequency of 1 MHz, because then the hydrophone can be calibrated at 1 MHz frequency intervals over the main range of interest (1-15 MHz) and because the method can then be validated by comparison with the interferometric technique. With the equipment available for the present study such calibrations are difficult to achieve, because the value of σ that can be achieved is too low, but new transducers have recently been obtained with longer Rayleigh lengths and these should be capable of producing the required fields.

The technique for hydrophone intercomparison (section 4.3) is currently being implemented using a digitiser (Tektronix 7854) that has a superior performance to the model 7912AD, and the method is being validated by comparing the results with those from the single frequency technique. The initial results show agreement between the two methods, indicating that the small inconsistencies that were previously observed at the fundamental frequency of the calibration field were indeed due to the inadequacies in the performance of the digitiser.

To examine the usefulness of the models for focused acoustic beams

it is important to perform measurements on several different transducers, operating over a range of frequencies. Such measurements would need to be made in a dispersive medium as well as in water, and the propagation characteristics of the medium would have to be determined more precisely. It would be of particular interest to verify the prediction that under certain circumstances in tissue the asymmetry of the wave can be reversed (ie the peak-negative acoustic pressure can be greater than the peak-positive) and these measurements could also be used to determine the reliability of the procedure for predicting the field in tissue from measurements performed in water.

REFERENCES

1. STOKES, G.G. On a difficulty in the theory of sound. Phil. Mag., (Series 3) 1848, 33, 349-356.

2. DE REGGI, A.S., ROTH, S.C., KENNEY, J.M., EDELMAN, S. and HARRIS, G.R. Polymeric ultrasonic probe. J. Acoust. Soc. Am., 1978, 64 (S1), S55-S56 (A).

3. SHOTTON, K.C., BACON, D.R. and QUILLIAM, R.M. A pvdf hydrophone for operation in the range 0.5 MHz to 15 MHz. Ultrasonics, 1980, 18, 123-126.

4. DE REGGI, A.S., ROTH, S.C., KENNEY, J.M., EDELMAN, S and HARRIS, G.R. Piezoelectric polymer probe for ultrasonic applications. J. Acoust. Soc. Am., 1981, 69, 853-859.

5. BACON, D.R. Characteristics of a pvdf membrane hydrophone for use in the range 1-100 MHz. IEEE Trans. Son. Ultrason., 1982, SU-29, 18-25.

6. LEWIN, P.A. Miniature piezoelectric polymer ultrasonic hydrophone probes. Ultrasonics, 1981, 19, 213-216.

7. MUIR, T.G. Nonlinear effects in acoustic imaging. 9th Int. Symp. on Acoustical Imaging, (Ed. K Wang), Plenum, New York. 1980.

8. MUIR, T.G. and CARSTENSEN, E.L. Prediction of nonlinear acoustic effects at biomedical frequencies and intensities. Ultrasound Med. Biol., 1980, 6, 345-357.

9. CARSTENSEN, E.L., LAW, W.K., McKAY, N.D. and MUIR, T.G. Demonstration of nonlinear acoustical effects at biomedical frequencies and intensities. Ultrasound Med. Biol., 1980, 6, 359-368.

10. BACON, D.R. Nonlinear propagation and the characterisation of medical ultrasonic equipment. Ultrasound Med. Biol., 1982, 8, (S1), 8(A).

11. BLACKSTOCK, D.T. Propagation of plane sound waves of finite amplitude in nondissipative fluids. J. Acoust. Soc. Am., 1962, 34, 9-30.

12. LIGHTHILL, M.J. Viscosity effects in sound waves of finite amplitude. Surveys in Mechanics.(ed. Batchelor and Davies) Cambridge Univ. Press. 1956, 250-351.

13. BLACKSTOCK, D.T. Thermoviscous attenuation of plane, periodic, finite-amplitude sound waves. J. Acoust. Soc. Am., 1964, 36, 534-542.

14. POISSON, S.D. Memoire sur la Theorie du Son. J. Ecole polytech. (Paris), 1808, 7, 319-392.

15. GHIRON FUBINI, E. Anomalie nella propagazione di onde acustiche di grande ampiezza. Alta Frequenza, 1935, 4, 530-581.

16. BLACKSTOCK, D.T. Connection between the Fay and Fubini solutions for plane sound waves of finite amplitude. J. Acoust. Soc. Am., 1966, 39, 1019-1026.

17. FAY, R.D. Plane sound waves of finite amplitude. J. Acoust. Soc. Am., 1931, 3, 222-241. .

18. SOLUYAN, S.I. and KHOKHLOV, R.V. Propagation of acoustic waves of finite amplitude in a dissipative medium. (in Russian). Vestnick Moscow State Univ., (Ser. III Fiz. Astron). 1961, 3, 52-61.

19. NAUGOL'NYKH, K.A., SOLUYAN, S.I. and KHOKHLOV, R.V. Spherical waves of finite amplitude in a viscous thermally conducting medium. Sov. Phys. Acoust., 1963, 9, 42-46.

20. BLACKSTOCK, D.T. History of nonlinear acoustics and a survey of Burgers' and related equations. Nonlinear Acoustics, (ed. T G Muir) Texas University at Austin, Applied Research Labs., 1970, (AD 719 936), 1-27.

21. RUDNICK, I. On the attenuation of high amplitude waves of stable saw-tooth form propagated in horns. J. Acoust. Soc.

Am., 1958, 30, 339-342.

22. LOCKWOOD, J.C., MUIR, T.G. and BLACKSTOCK, D.T. Directive harmonic generation in the radiation field of a circular piston. J. Acoust. Soc. Am., 1973, 53, 1148-1153.

23. SHOOTER, J.A., MUIR, T.G. and BLACKSTOCK, D.T. Acoustic saturation of spherical waves in water. J. Acoust. Soc. Am., 1974, 55, 54-62.

24. OSTROVSKII, L.A. and FRIDMAN, V.E. Directionality of high-intensity acoustic radiation. Sov. Phys. Acoust., 1973, 18, 478-481.

25. BERKTAY, H.O. Finite-amplitude effects in acoustic propagation in fluids. New Directions in Physical Acoustics, (Soc. Italiana di Fisica, Bologna, Italy), 1976, 369-408.

26. OSTROVSKII, L.A. and SUTIN, A.M. Focusing of finite-amplitude acoustic waves. Sov. Phys. Dokl., 1975, 20, 275-277.

27. SUTIN, A.M. Influence of nonlinear effects on the properties of acoustic focusing systems. Sov. Phys. Acoust., 1978, 24, 334-339.

28. GOULD, R.K., SMITH, C.W., WILLIAMS, A.O. Jr and RYAN, R.P. Measured structure of harmonics self-generated in an acoustic beam. J. Acoust. Soc. Am., 1966, 40, 421-427.

29. INGENITO, F. and WILLIAMS, A.O. Jr. Calculation of second-harmonic generation in a piston beam. J. Acoust. Soc. Am., 1971, 49, 319-328.

30. COBB, W.N. Finite amplitude method for the determination of the acoustic nonlinearity parameter B/A. J. Acoust. Soc. Am., 1983, 73, 1525-1531.

31. KUNITSYN, V.E. and RUDENKO, O.V. Second harmonic generation in the field of a piston radiator Sov. Phys. Acoust., 1978, 24, 310-313.

32. LAPIDUS, Y.R. and RUDENKO, O.V. New approximations and

results of the theory of nonlinear acoustic beams. Sov. Phys. Acoust., 1984, 30, 473-476.

33. BURVINGT, R. Solution non lineaire approchee pour le rayonnement acoustique d'une source Gaussienne monochromatique. Rev. du Cethedec - Ondes et Signal, 1984, 79, 167-174.

34. FENLON, F.H. and KESNER, J.W. Saturated parametric receiving arrays. Procs. 7th Int. Symp. Nonlinear Acoustics, Blacksburg VA, 1976, 125-128.

35. BACON, D.R. A new method for ultrasonic hydrophone calibration. IEEE Ultrasonics Symposium Procs, 1982, 700-704.

36. GINSBERG, J.H. Nonlinear King integral for arbitrary axisymmetric sound beams at finite amplitudes. I. Asymptotic evaluation of the velocity potential. J. Acoust. Soc. Am., 1984, 76,1201-1207.

37. GINSBERG, J.H. Nonlinear King integral for arbitrary axisymmetric sound beams at finite amplitudes. II. Derivation of uniformly accurate expressions. J. Acoust. Soc. Am., 1984, 76, 1208-1214.

38. LUCAS, B.G. and MUIR, T.G. Field of a finite-amplitude focusing source. J. Acoust. Soc. Am., 1983, 74, 1522-1528.

39. RUGAR, D. Resolution beyond the diffraction limit in the acoustic microscope: a nonlinear effect. J. Appl. Phys., 1984, 56, 1338-1346.

40. GINSBERG, J.H. Transition from the nonlinear King integral to spherical propagation for a finite amplitude sound beam. J. Acoust. Soc. Am., 1983, 74, S24.

41. HAMILTON, M.F., TJOTTA, J.N. and TJOTTA, S. Nonlinear effects in the farfield of a directive sound beam. J. Acoust. Soc. Am., 1985, 78, 202-216.

42. ZABOLOTSKAYA, E.A. and KHOKHLOV, R.V. Quasi-plane waves in the nonlinear acoustics of confined beams. Sov. Phys.

Acoust., 1969, 15, 35-40.

43. ZABOLOTSKAYA, E.A. and KHOKHLOV, R.V. Convergent and divergent sound beams in nonlinear media. Sov. Phys Acoust., 1970, 16, 39-42.

44. VOROB'EV, E.M. and ZABOLOTSKAYA, E.A. Propagation of high frequency sound beams, Sov. Phys. Acoust., 1974, 19, 523-525.

45. VOROB'EV, E.M. and ZABOLOTSKAYA, E.A. Propagation of high-frequency quasispherical waves in nonlinear media. Sov. Phys. Acoust., 1974, 20, 191-192.

46. VOROB'EV, E.M. and SLAVIN, A.R. Scale invariance and asymptotic solutions of the Zabolotskaya-Khokhlov equation. Sov. Phys. Acoust., 1976, 22, 190-193.

47. RUDENKO, O.V. Exact solutions of the Zabolotskaya-Khokhlov equations. Sov. Phys. Acoust., 1975, 21, 196-197.

48. VINOGRADOV, A.M. and VOROB'EV, E.M. Use of symmetries to find exact solutions of the Zabolotskaya-Khokhlov equation. Sov. Phys. Acoust., 1976, 22, 12-15.

49. RUDENKO, O.V., SOLUYAN, S.I. and KHOKHLOV, R.V. Confinement of a quasiplane beam of periodic perturbations in a nonlinear medium. Sov. Phys. Acoust., 1974, 19, 556-559.

50. RUDENKO, O.V., SOLUYAN, S.I. and KHOKHLOV, R.V. Nonlinear theory of paraxial sound beams. Sov. Phys. Dokl., 1976, 20, 836-837.

51. LAPIDUS, Y.R. and SOLUYAN, S.I. Evolution of nonlinear waves along the axis of slightly diffracted and focused beams. Sov. Phys. Acoust., 1985, 31, 368-370.

52. OSTROVSKII, L.A. and SUTIN, A.M. Diffraction effects in finite-amplitude sound beams. Sov. Phys. Acoust., 1977, 23, 100-101.

53. NAUGOL'NYKH, K.A. and ROMANENKO, E.V. Amplication factor of a focusing system as a function of sound intensity. Sov. Phys.

Acoust., 1959, 5, 191-195.

54. SMITH, C.W. and BEYER, R.T. Ultrasonic radiation field of a focusing spherical source at finite amplitudes. J. Acoust. Soc. Am., 1969, 46, 806-813.

55. BACON, D.R. Finite amplitude distortion of the pulsed fields used in diagnostic ultrasound. Ultrasound in Med. & Biol., 1984, 10, 189-195.

56. GINSBERG, J.H. Recent developments for the nonlinear distortion of non-dispersive acoustic waves I. Shock Vib. Dig., 1979, 11 (7), 3-8.

57. GINSBERG, J.H. Recent developments for the nonlinear distortion of non-dispersive acoustic waves II. Shock Vib. Dig., 1979, 11, (8), 3-12 (1979).

58. WHITHAM, G.B. The flow pattern of a supersonic projectile. Commun. Pure Appl. Math., 1952, 5, 301-348.

59. GINSBERG, J.H. Multi-dimensional non-linear acoustic wave propagation; Part II. J. Sound Vib., 1975, 40, 359-379.

60. GINSBERG, J.H. Uniformly accurate description of finite amplitude sound radiation from a harmonically vibrating planar boundary. J. Acoust. Soc. Am., 1981, 69, 929-936.

61. GINSBERG, J.H. A singular perturbation analysis of axisymmetric, finite amplitude sound beams. 9th Int Symp. Nonlinear Acoustics, book of abstracts, 1981, 29-30.

62. KELLY, S.G. and NAYFEH, A.H. Non-linear propagation of directional spherical waves. J. Sound Vib., 1980, 72, 25-37.

63. BAKHVALOV, N.A., ZHILEIKIN, YA.M., ZABOLOTSKAYA, E.A. and KHOKHLOV, E.A. Nonlinear propagation of a sound beam in a nondissipative medium. Sov. Phys. Acoust., 1976, 22, 272-274.

64. BAKHVALOV, N.S., ZHILEIKIN, YA.M., ZABOLOTSKAYA, E.A. and KHOKHLOV, R.V. Focused high-amplitude sound beams. Sov. Phys. Acoust., 1978, 24, 10-15.

65. BAKHVALOV, N.S., ZHILEIKIN, YA.M. and ZABOLOTSKAYA, E.A. Nonlinear propagation of Gaussian beams. Sov. Phys. Acoust., 1979, 25, 458-460.

66. BAKHVALOV, N.S., ZHILEIKIN, YA.M. and ZABOLOTSKAYA, E.A. Nonlinear propagation of sound beams with a uniform amplitude distribution. Sov. Phys. Acoust., 1980, 26, 95-100.

67. ZHILEIKIN, YA.M. and RUDENKO, O.V. Nonlinear and diffraction transformation of acoustic pulses. Sov. Phys. Acoust., 1981, 27, 200-202.

68. ZHILEIKIN, YA.M. Programs for numerical solution of the equation for acoustic beams in a nonlinear medium. (in Russian) Comp. Meth. and Programming, 1979, 31, Izd. Mosk. Univ., Moscow, 166-173.

69. LOCKWOOD, J.C. Approximate time-domain solution for finite-amplitude spherical waves in an absorbing medium. Finite amplitude effects in fluids, (ed. L. Bjorno), IPC Science and Tech. Press, 1973, 55-58.

70. MERKLINGER, H.M., MELLEN, R.H. and MOFFETT, M.B. Finite-amplitude losses in spherical sound waves. J. Acoust. Soc. Am., 1976, 59. 755-759.

71. MOFFETT, M.B. Measurement of fundamental and second harmonic pressures in the field of a circular piston source. J. Acoust. Soc. Am., 1979, 65, 318-323.

72. MERKLINGER, H.M., BERKTAY, H.O. and SAFAR, M.H. Finite-amplitude losses in the field of a real transducer. Ref [69], 1973, 168-173.

73. KUZNETSOV,V.P. Equations of nonlinear acoustics. Sov. Phys. Acoust., 1971, 16, 467-470.

74. FENLON, F.H. and KESNER, J.W. Finite-amplitude radiation fields of a plane-piston projector. J. Acoust. Soc. Am., 1976, 60 (S1), S98-S99 (A).

75. FENLON, F.H. On the role of the second-order parabolic wave

equation in non-linear acoustics, proceedings of the conference on underwater applications of nonlinear acoustics, University of Bath: Institute of Acoustics, ch. 3.3, 1979.

76. SWINDELL, W. A theoretical study of nonlinear effects with focused ultrasound in tissues: an "Acoustic Bragg Peak". Ultrasound in Med. & Biol., 1985, 11, 121-130.

77. SWINDELL W. Nonlinear effects with focused ultrasound in tissues: an improved model. Proc. Inst. Acoust., 1986, 8(2), 79-84.

78. BACON, D.R. Nonlinear ultrasonic fields: theory and experiment. Proc. Inst. Acoust., 1986, 8(2), 39-46.

79. BERNSTEN, J., TJOTTA, J.N. and TJOTTA, S. Nearfield of a large acoustic transducer. Part IV: Second harmonic and sum frquency radiation. J. Acoust. Soc. Am., 1984, 75, 1383-1391.

80. BAKHVALOV, N.S., ZHILEIKIN, YA.M., ZABOLOTSKAYA, E.A. and KHOKHLOV, R.V. Propagation of finite-amplitude sound beams in a dissipative medium. Sov. Phys. Acoust., 1978, 24, 271-275.

81. BAKHVALOV, N.S., ZHILEIKIN, YA.M., ZABOLOTSKAYA, E.A. and KHOKHLOV R.V. Harmonic generation in sound beams. Sov. Phys. Acoust., 1979, 25, 101-106.

82. McKENDREE, F.S. A numerical solution of the second-order nonlinear acoustic wave equation in one and in three dimensions. Ph. D. Thesis, Pennsylvania State University, NTIS:AD A103148, 1981.

83. AANONSEN, S.I., BARKVE, T., TJOTTA, J.N. and TJOTTA, S. Distortion and harmonic generation in the nearfield of a finite amplitude sound beam. J. Acoust. Soc. Am., 1984, 75, 749-768.

84. AANONSEN, S.I. Numerical computation of the nearfield of a finite amplitude sound beam. Report 73, 1983, Dept. Applied Math., University of Bergen, Norway.

85. AANONSEN, S.I., HAMILTON, M.F., TJOTTA, J.N. and TJOTTA, S.

Nonlinear effects in sound beams. Proc. 10th. Int. Symp. Nonlinear Acoustics, 1984, 45-48.

86. COOK, B.D. New procedure for computing finite-amplitude distortion. J. Acoust. Soc. Am., 1962, 34, 941-946.

87. CARY, B.B. Prediction of finite-amplitude distortion with dissipation and spreading loss. J. Acoust. Soc. Am., 1968, 43, 1364-1372.

88. FENLON, F.H. A recursive procedure for computing the nonlinear spectral interactions of progressive finite-amplitude waves in nondispersive fluids. J. Acoust. Soc. Am., 1971, 1299-1312.

89. HENNION, P.Y. and LA GREVE, M.L. Calcul de l'attenuation non lineaire d'une onde acoustique plane d'amplitude finie. Acustica, 1981, 48, 44-49.

90. TRIVETT, D.H. and VAN BUREN, A.L. Propagation of plane, cylindrical and spherical finite amplitude waves. J. Acoust. Soc. Am., 69, 1981, 943-949.

91. HARAN, M.E. and COOK, B.D. Distortion of finite amplitude ultrasound in lossy media. J. Acoust. Soc. Am., 1983, 73, 774-779.

92. HARAN, M.E. and LEWIN, P.A. Application of a nonlinear layered model to hyperthermia. J. Acoust. Soc. Am., 1984, 75(S1), S4.

93. POLYAKOVA, A.L., SOLUYAN, S.I. and KHOKHLOV, R.V. Propagation of finite disturbances in a relaxing medium. Sov. Phys. Acoust., 1962, 8, 78-82.

94. SOLUYAN, S.I. and KHOKHLOV, R.V. Finite amplitude acoustic waves in a relaxing medium. Sov. Phys. Acoust., 1962, 8, 170-175.

95. KHOKHLOV, R.V. and SOLUYAN, S.I. Propagation of acoustic waves of moderate amplitude through dissipative and relaxing media. Acustica, 1964, 14, 241-247.

96. WEBSTER, D.A. and BLACKSTOCK, D.T. Finite-amplitude saturation of plane sound waves in air. J. Acoust. Soc. Am., 1977, 62, 518-523.

97. BLACKSTOCK, D.T. Generalized Burgers' equation for plane waves. J. Acoust. Soc. Am., 1985, 77, 2050-2053.

98. KORPEL, A. Frequency approach to nonlinear dispersive waves. J. Acoust. Soc. Am., 1980, 67, 1954-1958.

99. GONGHUAN D. Fourier series solution of Burgers' equation for nonlinear acoustics. J. Acoust. Soc. Am., 1985, 77, 924-927.

100. THURAS, A.L., JENKINS, R.T. and O'NEIL, H.T. Extraneous frequencies generated in air carrying intense sound waves. J. Acoust. Soc. Am., 1935, 6, 173-180.

101. HUBBARD, J.C., FITZPATRICK, J.A., KANKOVSKY, B.T. and THALER, W.J. Distortion of progressive ultrasonic waves. Phys. Rev., 1948, 74, 107-108.

102. MENDOUSSE, J.S. Nonlinear dissipative distortion of progressive sound waves at moderate amplitudes. J. Acoust. Soc. Am., 1953, 25, 51-54.

103. FOX, F.E. and WALLACE, W.A. Absorption of finite amplitude sound waves. J. Acoust. Soc. Am., 1954, 26, 994-1006.

104. KRASSILNIKOV, V.A., SHKLOVSKAYA-KORDY, V.V. and ZAREMBO, L.K. On the propagation of ultrasonic waves of finite amplitude in liquids. J. Acoust. Soc. Am., 1957, 29, 642-647.

105. BUROV, V.A. and KRASIL'NIKOV, V.A. Direct observation of the deformation of intense ultrasonic waves in liquids. Sov. Phys. Dokl., 1958, 3, 173-176.

106. RYAN, R.P., LUTSCH, A.G. and BEYER, R.T. Measurement of the distortion of finite ultrasonic waves in liquids by a pulse method. J. Acoust. Soc. Am., 1962, 34, 31-35.

107. NAUGOL'NYKH, K.A. and ROMANENKO, E.V. On the propagation of finite-amplitude waves in a liquid. Sov. Phys. Acoust., 1958,

4, 202-204.

108. LESTER, W.W. Experimental study of the fundamental frequency component of a plane, finite-amplitude wave. J. Acoust. Soc. Am., 1966, 40, 847-851.

109. BERKTAY, H.O. Some finite-amplitude effects in underwater acoustics. Nonlinear Acoustics, (ed. T G Muir), Texas University at Austin, Applied Research Labs. (AD 719 936), 1970, 29-55.

110. BROWNING, D,G, and MELLEN, R.H. Finite-amplitude distortion of 150 kHz acoustic waves in water. J. Acoust. Soc. Am., 1968, 44, 644-646.

111. MOFFETT, M.B. and GINSBERG, J.H. Finite-amplitude waveforms produced by a circular piston projector. J. Acoust. Soc. Am., 1982, 72 (S1), S40 (A).

112. PESTORIUS, F.M. and BLACKSTOCK, D.T. Propagation of finite-amplitude noise. Ref. [69], 1973, 24-29.

113. ANDREEV, V.G., KARABUTOV, A.A. and RUDENKO, O.V. Experimental study of the propagation of nonlinear sound beams in free space. Sov. Phys. Acoust., 1985, 31, 252-255.

114. BASIN, Y.A. and KRYACHKO, V.M. Experimental study of the propagation of compression and expansion pulses in a sound beam in a highly nonlinear medium. Sov. Phys. Acoust., 1985, 31, 255-257.

115. ROMANENKO, E.V. Experimental investigation of the propagation of finite-amplitude spherical waves. Sov. Phys. Acoust., 1959, 5, 100-104.

116. BJORNO, L. and LEWIN, P.A. Nonlinear focusing effects in ultrasonic imaging. IEEE. Ultrasonics Symp. Procs., 1982, 659-662.

117. McLENNAN, D.D., NGOC, T.D.K. and MAYER, W.G. Measurements of harmonic profiles of a bounded ultrasonic beam in a liquid medium. Ultrasonics, 1983, 21, 103-106.

118. BREAZEALE, M.A. and GONGHUAN, D. Diffraction of Gaussian beams: linear and nonlinear. Proc. Ultrasonics International, 1985, 145-150.

119. ALLEN, C.H. Nonlinearity in free progressive sound waves. Procs. 7th Int. Symp. Nonlinear Acoustics, Blacksburg VA, 1976, 226-229.

120. CAMPANELLA, A.J. Finite amplitude distortion of spherically diverging intense sound waves in air. J Acoust. Soc. Am., 1980, 67, 6-14.

121. MARSH, H.W. Non-linear effects at range from underwater explosions. Procs. 3rd. Int. Symp. Nonlinear Acoustics, University of Birmingham, 1971, 24-35.

122. GALLEGO-JUAREZ, J.A. and GAETE-GARRETON, L. Propagation of finite-amplitude ultrasonic waves in air - 1. Spherically diverging waves in the free field. J. Acoust. Soc. Am., 1983, 73, 761-767.

123. CARSON, P.L., FISCHELLA, P.R. and OUGHTON, T.V. Ultrasonic power and intensities produced by diagnostic ultrasound equipment. Ultrasound in Med. & Biol., 1978, 3, 341-350.

124. DUCK, F.A. and STARRITT, H.C. Acoustic shock generation by ultrasonic imaging equipment. B. J. Radiol., 1984, 57, 231-240.

125. DUCK, F.A., STARRITT, H.C., AINDOW, J.D., PERKINS, M.A. and HAWKINS, A.J. The output of pulse-echo ultrasound equipment: a survey of powers, pressures and intensities. B. J. Radiol., 1985, 58, 989-1001.

126. LIVETT, A.J. and PRESTON, R.C. A comparison of the AIUM/NEMA, IEC and FDA (1980) definitions of various acoustic output parameters for ultrasonic transducers. Ultrasound in Med. & Biol., 1985, 11, 793-802.

127. DUCK, F.A. and STARRITT, H.C. The locations of peak pressures and peak intensities in finite amplitude beams from a pulsed focused transducer. Ultrasound in Med. & Biol., 1986, 12,

403-409.

128. KOSSOFF, G. and CARPENTER, D.A. A reflection technique for measurement of high acoustic intensities. Ultrasound in Med. & Biol., 1984, 10, 197-199.

129. DUCK, F.A. Finite amplitude distortion and pvdf hydrophone response. Ultrasound in Med. & Biol., 1984, 10, L643-L644.

130. BACON, D.R. The observation of distorted waveforms - nonlinear propagation or hydrophone overload? Ultrasound in Med. & Biol., 1984, 10, L639-L642.

131. BACON, D.R. A comparison of displacement and pressure waveforms of a nonlinear ultrasonic field. J. Ultrasound in Med., 1984, 3 (9, Suppl.), 73.

132. PARKER, K.J. Observation of nonlinear acoustic effects in a B-scan imaging instrument. IEEE Trans. Son. Ultrason., 1985, SU-32, 4-8.

133. HUMPHREY, V.F., BURGESS, M. and SAMPSON, N. Harmonic generation due to nonlinear propagation in a focused ultrasonic field. Proc. Inst. Acoust., 1986, 8(2), 47-54.

134. GOSS, S.A and FRY, F.J. Nonlinear acoustic behaviour in focused ultrasonic fields: observations of intensity dependent absorption in biological tissue. IEEE Trans. Son. Ultrason., 1981, SU-28, 21-26.

135. CARSTENSEN, E.L., BECROFT, S.A., LAW, W.K. and BARBEE, D.B. Finite amplitude effects on the thresholds for lesion production in tissues by unfocused ultrasound. J. Acoust. Soc. Am., 1981, 70, 302-309.

136. CARSTENSEN, E.L., MCKAY, N.D., DELECKI, D. and MUIR, T.G. Absorption of finite amplitude ultrasound in tissues. Acustica, 1982, 51, 116-123.

137. AKIYAMA, I., NISHIDA, Y., NAKAJIMA, M. and YUTA, S. On the measurement of frequency dependent attenuation in biological tissues using broadband pulsed ultrasound. Proc. IEEE

Ultrasonics Symp., 1983, 800-805.

138. STARRITT, H.C., PERKINS, M.A., DUCK, F.A. and HUMPHREY, V.F. Evidence for ultrasonic finite amplitude distortion in muscle using medical equipment. J. Acoust. Soc. Am., 1985, 77, 302-306.

139. DUCK, F.A., STARRITT, H.C. and HAWKINS, A.J. Observations of finite amplitude distortion in tissue. Proc. Inst. Acoust., 1986, 8(2), 71-77.

140. WELLS, P.N.T. Biomedical Ultrasonics, 1977, Academic Press, 131.

141. PARKER, D.F. The decay of sawtooth solutions to the Burgers' equation. Proc. R. Soc. Lond. A, 1980, 369, 409-424.

142. CARY, B.B. Nonlinear losses induced in spherical waves. J. Acoust. Soc. Am., 1967, 42, 88-92.

143. TAYLOR, G.I. The conditions necessary for discontinuous motion in gases. Proc. R. Soc. Lond. A, 1910, 84, 371-377.

144. CRIGHTON, D.G. and SCOTT, J.F. Asymptotic solutions of model equations in nonlinear acoustics. Phil. Trans. R. Soc. Lond. A, 1979, 292, 101-134.

145. SCOTT, J.F. Uniform asymptotics for spherical and cylindrical nonlinear acoustic waves generated by a sinusoidal source. Proc. R. Soc. Lond. A, 1981, 375, 211-230.

146. PRESTON, R.C. BACON, D.R., LIVETT, A.J. and RAJENDRAN, K. PVDF membrane hydrophone performance properties and their relevance to the measurement of the acoustic output of medical ultrasonic equipment. J. Phys. E, 1983, 16, 786-796.

147. CALLERAME, J, TANCRELL, R.H and WILSON, D.T. Comparison of ceramic and polymer transducers for medical imaging. Proc. IEEE Ultrasonics Symp., 1978, 117-121.

148. LEUNG, W.P. and YUNG, K.K. Internal losses in polyvinylidene fluoride (PVF_2) ultrasonic transducers. J. Appl. Phys., 1979,

50, 8031-8033.

149. BACON, D.R., DRAIN, L.E., MOSS, B.C. and SMITH, R.A. A new primary standard for ultrasonic hydrophone calibration. Physics in Medical Ultrasound, 1986, IPSM Report 47, 30-35, (Institute of Physical Sciences in Medicine).

150. BACON, D.R. The improvement and evaluation of a laser interferometer for the absolute measurement of ultrasonic displacements in the frequency range up to 15 MHz. NPL Report, 1986, to be published.

151. BUI, L, SHAW, H.J. and ZITELLI, L.T. Study of acoustic wave resonance in piezoelectric PVF_2 film. IEEE Trans. Son. Ultrason. SU-24, 1977, 331-336.

152. REIBOLD, R and MOLKENSTRUCK, W. Interferometrische Untersuchungen des Impulsverhaltens von Ultraschallsondenhydrophonen. Fortschritte der Akustik - FASE/DAGA, 1982.

153. MEEKS, S.W. and TING, R.Y. Effects of static and dynamic stress on the piezoelectric and dielectric properties of PVF_2. J. Acoust. Soc. Am., 1983, 74, 1681-1686.

154. PRESTON, R.C., LIVETT, A.J. and BACON, D.R. Absolute calibration of hydrophones in the frequency range 0.5 MHz to 15 MHz. Proc. Inst. Acoust., 1984, 6(5), 60-67.

155. FLYNN, H.G. Generation of transient cavities in liquids by microsecond pulses of ultrasound. J. Acoust. Soc. Am., 1982, 72, 1926-1932.

156. CARSTENSEN, E.L. and FLYNN, H.G. The potential for transient cavitation with microsecond pulses of ultrasound. Ultrasound Med. Biol., 1982, 8, L720-L724.

157. BRENDEL, K. and LUDWIG, G. Calibration of ultrasonic standard probe transducers. Acustica, 1976, 36, 203-208.

158. WILSON, W.D. Speed of sound in distilled water as a function of temperature and pressure. J. Acoust. Soc. Am., 1959, 31,

1067-1072.

159. PINKERTON, J.M.M. A Pulse method for the measurement of ultrasonic absorption in liquids: results for water. Nature, 1947, 160, 128-129.

160. UHLENDORF, V., RICHMANN, K.H. and BERGER, W. Ultrasonic absorption and velocity measurements at mW peak power level in the range 50-500 MHz with variable pathlength cell. J. Phys. E: Sci. Instrum., 1985, 18, 151-157.

161. BEYER, R.T. Parameter of nonlinearity in fluids. J. Acoust. Soc. Am., 1960, 32, 719-721.

162. HOLTON, G., HAGELBERG, M.P., KAO, S. and JOHNSON, W.H. Jr. Ultrasonic-velocity measurements in water at pressures to 10,000 kg/cm^2. J. Acoust. Soc. Am., 1968, 43, 102-107.

163. COBB, W.N. Measurement of the acoustic nonlinearity parameter for biological media. PhD Thesis, 1982, Yale University.

164. WELLS, P.N.T. Absorption and dispersion of ultrasound in biological tissue. Ultrasound in Med. & Biol., 1975, 1, 369-376.

165. Attenuation coefficient measured by Dr. B Zeqiri.

166. US Department of Health and Human Services, Food and Drug Administration, 510(K) Guide for measuring and reporting acoustic output of diagnostic ultrasound devices. 1985.

A1 APPENDIX 1

In this section it is shown that Equation 2.4 predicts a linear dependence of the attenuation on frequency and a logarithmic variation of the dispersion with frequency, provided that the propagation is linear, and the method of deriving Equation 2.5 is indicated. From Newton's third law and the (linearised) equation of continuity, the following relationship between the acoustic pressure, p, and the density perturbation, ρ, is obtained:

$$\nabla^2 p = \frac{\partial^2 \rho}{\partial t^2}$$

and inserting this into Equation 2.4 gives the following wave equation:

$$\frac{\partial^2 \rho}{\partial t^2} - c_\infty^2 \nabla^2 \rho + m c_o^2 \nabla^2 \int_{-\infty}^{t-\tau_1} \frac{\rho(t')}{(t - t')} dt' = 0 \qquad \text{A.1}$$

where $c_\infty^2 = c_o^2 \left[1 + m \, \mathrm{Ln}(\tau_2/\tau_1)\right]$.

If a one-dimensional propagating wave, described by the function $\exp\{i(\omega t - kx)\}$, is assumed then the dispersion relation becomes:

$$\omega^2 = c_\infty^2 k^2 - m c_o^2 k^2 e^{-i\omega t} \int_{-\infty}^{t-\tau_1} \frac{e^{i\omega t'}}{(t - t')} dt'$$

If m is small compared with unity, then the following relationships can be derived for the velocity and attenuation coefficients, which have the required dependence on frequency:

$$\alpha = \frac{m\omega\pi}{4c_o}$$

$$c = c_o\left[1 + \frac{m}{2}\,\mathrm{Ln}\,(\omega\tau) + \frac{c_\infty^2 - c_o^2}{2\,c_o^2}\right] \qquad \text{A.2}$$

where $\tau = \tau_1 e^{C_E}$ and C_E is Euler's constant.

These relationships also demonstrate that it is possible to predict the dispersion if the attenuation of the wave is known (and vice versa), since the parameter m appears in both equations.

Equation 2.5 is derived by rearranging Equation 2.4 to give ρ in terms of p, and using the first equation above to rewrite Equation A.1 in terms of p. Next, c_∞^2 is rewritten in terms of c_o^2 and the same change of variables and approximations are made that were used in deriving Equation 2.3. This procedure gives the linear form of Equation 2.5; to obtain the full relationship the nonlinear term is added by analogy with Equation 2.3, since the additional terms in the equation of state are both independent and small.

A2 APPENDIX 2

Extract from "Finite amplitude distortion of the pulsed fields used in diagnostic ultrasound" (reference 55).

A2.1 Theory

A form of Burgers' equation which applies to the axial field of a plane transducer has been derived by Fenlon and Kesner [34,74]. This was obtained from an equation of Kuznetsov [73], using a Gaussian distribution as an approximation to the beam profile. Kuznetsov's equation was rewritten by describing the field in terms of Gaussian modes and neglecting the influence of variations in the off-axis beam profile on the axial profile. A further approximation involved neglecting a term related to the phase variation in the near field, and this introduced an error into the solutions of less than 10%. Although strictly valid only for Gaussian radiators, the equation was found to be useful in describing the fields of plane piston transducers. The variation of acoustic pressure with distance and time is described [34] by:

$$\frac{\partial P}{\partial \sigma} - P\frac{\partial P}{\partial \tau} - \left\{\Gamma_o^{-1}\cosh(\sigma/\sigma_o)\right\}\frac{\partial^2 P}{\partial \tau^2} = 0 \qquad \text{A.3}$$

where $P = p\sqrt{1+R^2}/p_o$, $R = r/r_o$, $r_o = ka^2/2$

$\sigma = \sigma_o \sinh^{-1} R$, $\sigma_o = \beta k p_o r_o/\rho c^2$, $\Gamma_o = \sigma_o/\alpha_o r_o$ and $\tau = \omega(t-r/c)$.

Here p is the instantaneous acoustic pressure at a point on the axis at a distance r from the transducer, and time t; p_o is the amplitude of p at the transducer (i.e. at R=0); a is the radius of the beam at R=0; $k = \omega/c$ where ω is the acoustic angular frequency

and c the speed of sound; β is the nonlinearity parameter (3.5 for water); ρ is the density of the undisturbed medium, α_o is the absorption coefficient (in Np m^{-1}) at the fundamental frequency, r_o is the Rayleigh length and R is a normalised distance. Equation A.3 describes the way in which the waveform changes with σ and thus σ is a nonlinear propagation parameter describing the extent to which distortion has occurred. Equation A.3 applies to an unfocused transducer situated at the origin of the co-ordinate system. It may be applied to a focused radiator by changing the position of the transducer with respect to the origin (R=0) by a distance equal to the focal length. An equivalent method of obtaining the required equation is to expand the field in terms of converging Gaussian modes, and then apply the same analysis that led to Equation A.3. The result is as follows:

$$\frac{\partial P}{\partial \sigma} - P\frac{\partial P}{\partial \tau} - \left\{\Gamma_o^{-1}\cosh\left[\frac{\sigma-\sigma(o)}{\sigma_o}\right]\right\}\frac{\partial^2 P}{\partial \tau^2} = 0 \qquad \text{A.4}$$

where $R=(r-D)/r_o$, $R_o=D/r_o$, D is the focal distance, $\sigma = \sigma_o \sinh^{-1}(R) - \sigma_o \sinh^{-1}(-R_o)$; $\sigma(0)$ is the value of σ at R=0; a and p_o are still the values of the beam radius and pressure at R=0, except that they are obtained by extrapolation from those at low amplitudes, and the other parameters are as defined previously.

Equation A.4 is expected to be valid as long as σ is not too large (eg. for $\sigma<3$) since it does not allow for large changes in the beam profile due to nonlinear distortion. It is also not expected to account for phase changes which may occur between the harmonic components in the vicinity of the focus. The use of this equation

to describe acoustic fields which do not have a Gaussian profile will be discussed later. For significant nonlinear distortion to occur in water at the frequencies and propagation distances used in diagnostic ultrasound, it can be shown that Γ_o must be large (approximately 50 or greater). In this case it is possible to neglect the third term of Equation A.4, leading to a form which has the well-known solution (e.g. [16]):

$P = f(\tau+\sigma P)$ where f is an arbitrary function, determined by the initial conditions,

and $P = \sin(\tau+\sigma P)$ for the present case. A.5

From this equation the peak amplitude of the wave (P_p) is as follows:

$$P_p = 1 \qquad \text{for } \sigma \leq \pi/2$$

$$\text{and } P_p = \sin(\sigma P_p) \qquad \text{for } \sigma > \pi/2 \ (\pi/2 < \sigma P_p < \pi).$$

The product σP_p corresponds to the value of σ calculated using the actual value of the peak pressure at the focus, rather than the value extrapolated from low amplitudes. It is therefore convenient to obtain the following expression for the decrease in measured pressure amplitude at the focus of the transducer (R = 0)due to nonlinear distortion:

$$x = 1 \qquad (\text{for } \sigma_m \leq \pi/2)$$

$$x = \sin \sigma_m \qquad (\text{for } \pi/2 < \sigma_m < \pi)$$

$$\text{and } x = P_{o,m} \qquad \text{A.6}$$

$$= p_{o,m}/p_o$$

where $p_{o,m}$ is the measured peak pressure amplitude at the focus, $P_{o,m}$ is the corresponding normalised amplitude and σ_m is the value of σ calculated using $p_{o,m}$ instead of p_o. The value of σ

can then be calculated from:

$$\sigma = \sigma_m / x \qquad \text{A.7}$$

Alternative equations to those above have been derived by Sutin [26,27] by assuming that the effect of diffraction at the focus is large compared with that of nonlinear distortion. Unfortunately, Sutin's approach cannot be applied for the present purposes since it gives physically unreasonable results for $\sqrt{1+R_o^2} \lesssim 2\pi$. The validity of Sutin's equations has recently been questioned [38] and its relevance to pulsed fields has not been determined, so only Equations A.6 and A.7 will be used in this study.

A2.2 Experimental requirements

Application of Equations A.4-A.7 requires the knowledge of several parameters of the acoustic field: the distance to the focus, fundamental frequency, peak pressure and effective Rayleigh length (r_o). The focal distance is equal to the distance from the transducer face to the field point where the maximum peak-to-peak acoustic pressure is measured. The peak pressure may be defined as half of this peak-to-peak pressure, such a definition compensating for possible asymmetric distortion of the waveform due to diffraction. The frequency is given by the inverse of the period of the peak cycle of the pulse, measured between zero pressure points.

The effective Rayleigh length (r_o) determines the degree of diffraction present, and could be obtained by predicting the focal beam radius from the propagation distance, frequency and dimensions of the radiating surface, if ideal focusing is assumed.

A better procedure, however, may be to determine it from the geometry of the actual transducer beam by determing the focal gain (G), which is the ratio, at low amplitudes, of the pressure at the focus of the beam to that at the radiating surface. This is achieved by noting that G is related to the parameter R_o by $G = \sqrt{1+R_o^2}$. The Rayleigh distance is then the quotient of the propagation distance and R_o. In practice G may be derived from the ratio of the focal area to the radiating area, such a procedure being particularly reliable if $\sigma<1$. The relevant focal area should be that over which the maximum peak-to-peak pressure in the pulse is greater than exp(-1) times the value at the focus. If the 6 dB, 10 dB or 20 dB areas are known instead, then they should be multiplied by 10/3Ln(10), 2/Ln(10) and 1/Ln(10) respectively. G is then given as the square root of the quotient of the radiating area and the focal area.

A2.3 Summary of the procedure

Figure A.1 illustrates the measurements that are required in the mathematical model. The parameter σ_m is given by:

$$\sigma_m = \frac{\omega\beta p_m D \, \mathrm{Ln}(G+\sqrt{G^2-1})}{\rho c^3 \sqrt{G^2-1}} \qquad \text{A.8}$$

where p_m is the measured peak pressure at the focus, and D is the focal distance. x and σ can be obtained from Equations A.6 and A.7 respectively. It should be noted that only a few simple measurements are required by the procedure.

The parameter x can be regarded as an estimate of the maximum error introduced into measurements of peak pressure by finite

amplitude propagation. The second parameter, σ, may be considered as an indicator of the extent to which nonlinear distortion is present. As the two are related, and as x is constant for $\sigma \leq \pi/2$, σ is the more useful and can be used to define the experimental procedures necessary to quantify accurately a particular ultrasonic field. Typical acoustic waveforms for various values of σ are given in Figure 1 for plane wave propagation. If σ is less than about 0.5, then there is little distortion. Only small errors will be introduced into the measurements if a hydrophone with finite bandwidth (eg twice the fundamental frequency) is used. If σ is larger - between 0.5 and 1.5 - then the distortion is significant, but little attenuation of the peak pressure occurs (see Figure 1). Nevertheless, there will be considerable introduction of higher harmonics into the signal, and a broad bandwidth hydrophone would be required to obtain accurate results. This bandwidth should be seven to ten times the fundamental frequency or about 35 MHz, whichever is the lesser. If σ is greater than 1.5, then the extra attenuation of the wave due to nonlinear effects becomes significant. It is not only necessary to use a broad bandwidth hydrophone to measure the peak pressure, but it may also be necessary to correct the measurement using formulae such as those given above.

A2.4 Reappraisal of the method

The mathematical model has been given some degree of justification, and it has been shown how to apply it in practice. It may now be useful to consider the assumptions of the method, their justification and the possible alternatives. The neglect of

absorption has already been justified for propagation in water (Γ_o is large); its inclusion would add considerable complication to the analysis. A more significant assumption is the approximation of the beam profile by a Gaussian distribution. This permits the use of Equation A.4, and implies that there are no subsidiary maxima or minima of acoustic pressure, except at the focus. This assumption cannot be valid for all cases, but may be justified as follows. Firstly, the application is to pulsed fields where most of the energy is contained in one or two cycles, and so the wave will have insufficient coherence length to give rise to significant diffractive structure. Secondly, the beam profiles encountered in practice may vary considerably, particularly in transducer arrays which may use several elements in each excitation, each element being separately phased. Consequently, any alternative model which took the beam structure into account in great detail could not be valid for all the types of transducer which are likely to be encountered.

Another implicit assumption of the model is that the degrees of focusing in the two directions perpendicular to the beam axis are equal. This is only true for a circular transducer with a single radius of curvature. It would be possible to allow for non-uniform focusing explicitly in the model, but, for simplicity, this has not been done.

One final possible limitation is the use of Equations A.3 and A.4 to describe a Gaussian beam. If G is large, then the equations are similar to those for a spherically converging beam [19]. In the opposite limit, as G approaches 1, Equation A.8 agrees with the corresponding formula for plane waves [16], and hence the

procedure is reasonably well justified. Diffraction may in some instances considerably affect the value of the peak pressure at the focus [26,27], and has only been partially accounted for in Equation A.4. However, recent work [38] has questioned the accuracy of this theory [26,27], so that its relevance is currently uncertain. It therefore seems reasonable to apply Equations A.4 to A.8, particularly for the calculation of σ.

A3 APPENDIX 3

Amplifier Calibration

Figure A2 gives the circuits that were used. The circuit for determining the input to the amplifier had to be slightly different from that for determining the output, since the digitiser was used for both measurements. Nevertheless the electrical characteristics of the two circuits were made as similar as possible so as to minimise the error of measurement.

The method relied on the digitiser having a linear response over a dynamic range equal to the amplifier gain. The linearity of the digitiser for different calibrated voltage ranges was checked using an attentuator in a separate experiment; the linearity within a particular range was found to be about 0.1%. It was possible to use a different method of calibrating the amplifiers, by altering the attenuator setting in circuit B so as to obtain the same digitiser reading as for circuit A. This method relied on the amplifier having a linear response over a dynamic range equal to the gain, and so was generally less useful than the first technique.

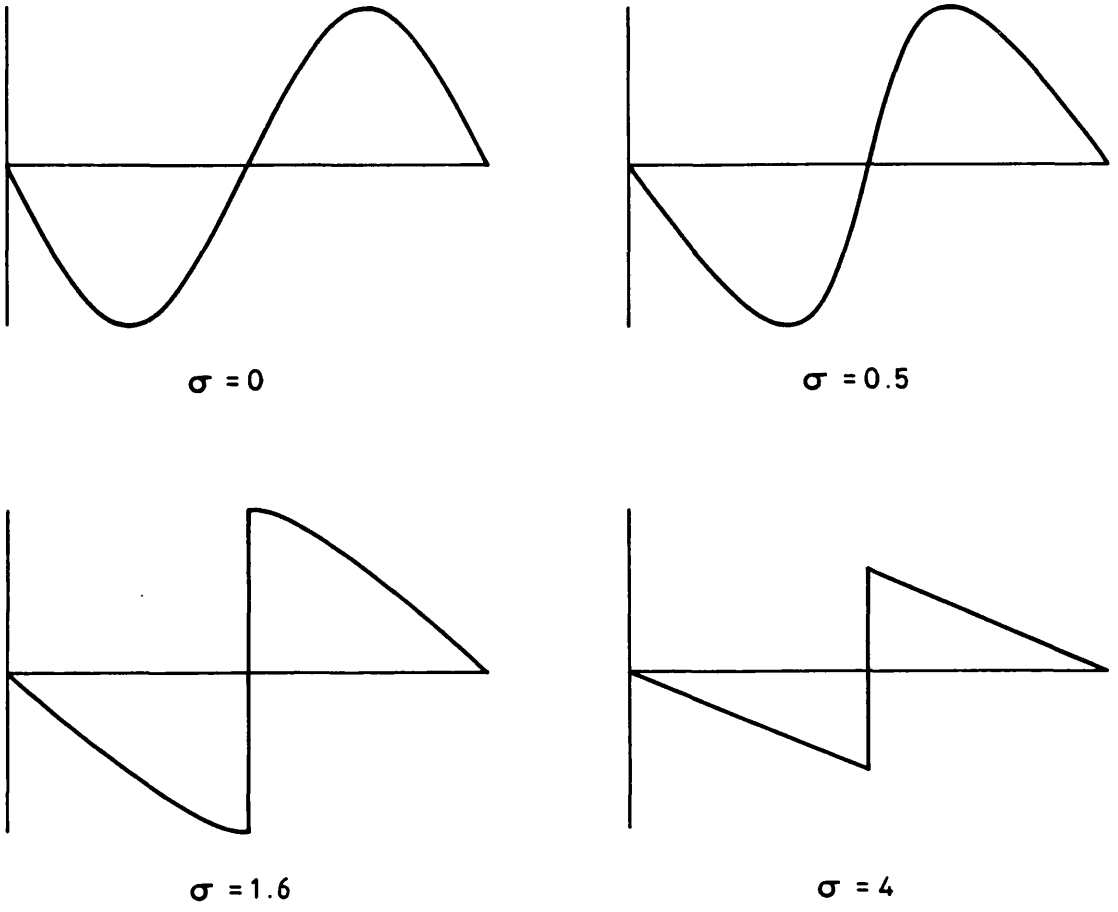

Figure 1 Acoustic waveforms for various values of σ, assuming an initial sinusoid and lossless plane-wave propagation.

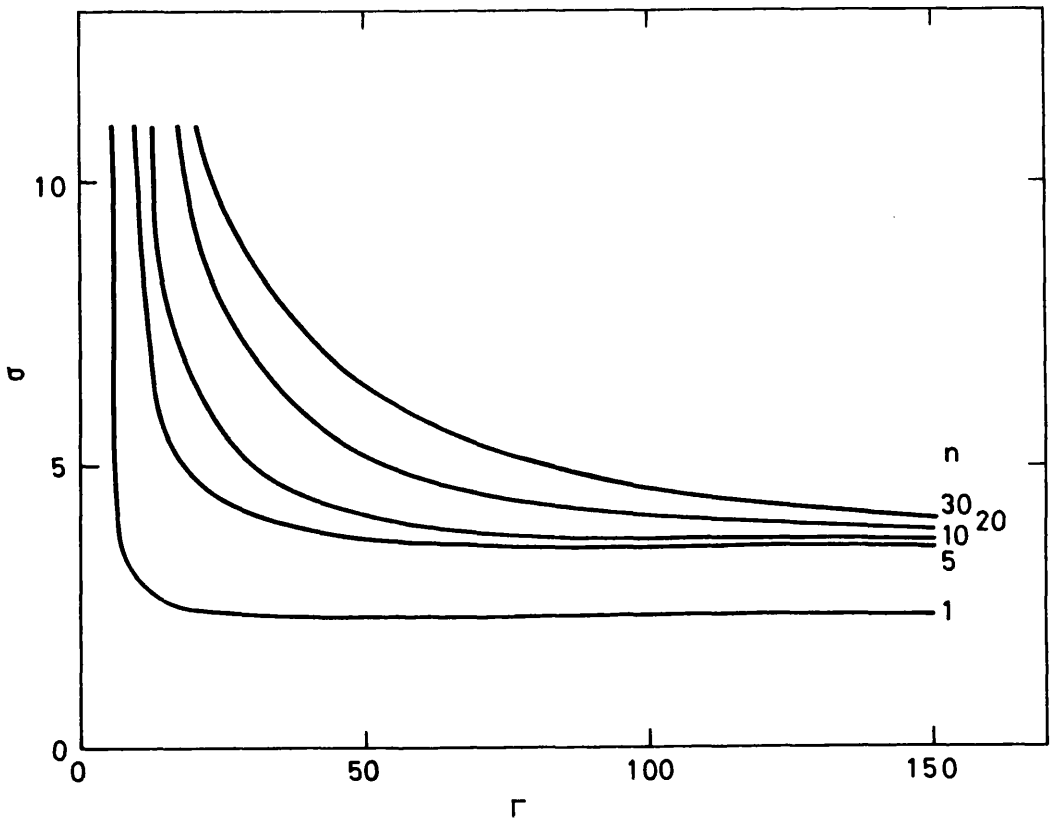

Figure 2 The relationship between σ and Γ for Equation 2.22 to have an accuracy of 2%, for various harmonic numbers (for a plane wave). In the region above the curves, the accuracy is better than 2%.

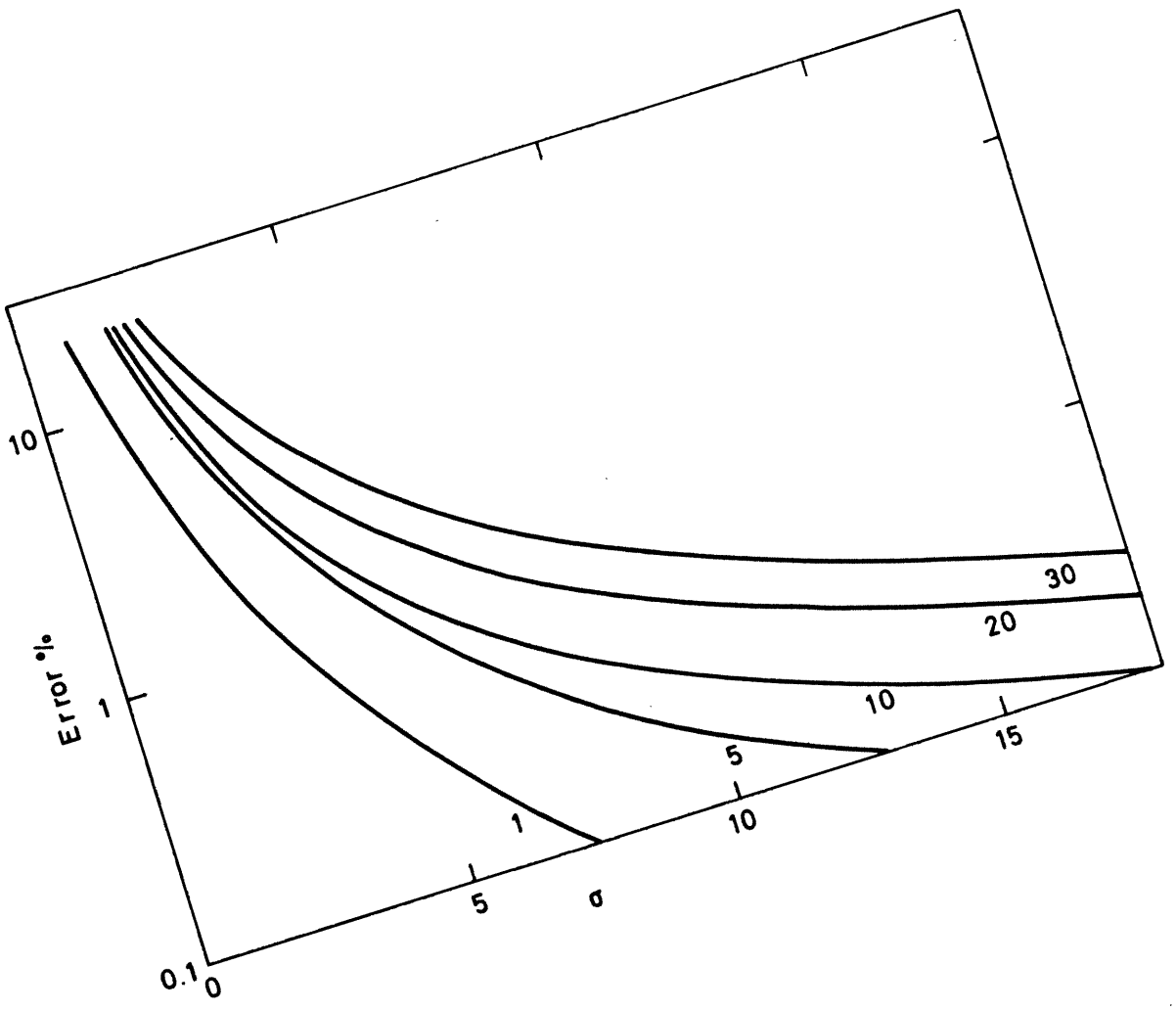

Figure 3 Error of Equation 2.22 as a function of σ for various harmonic numbers - for plane waves, $\Gamma = 50$.

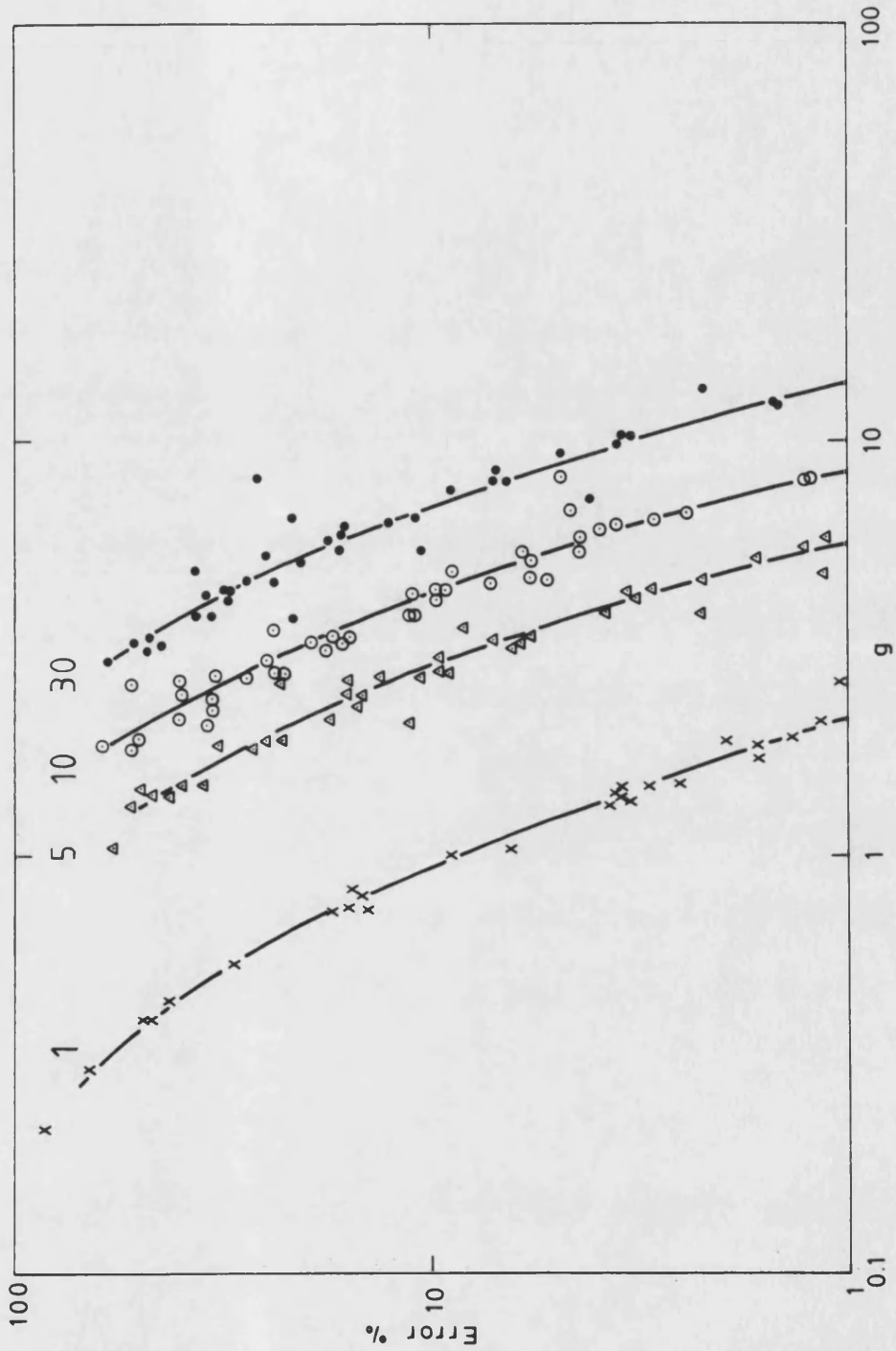

Figure 4 Error of Equation 2.21 applied to spherical waves, as a function of g (Equation 2.25). The parameter is the harmonic number.

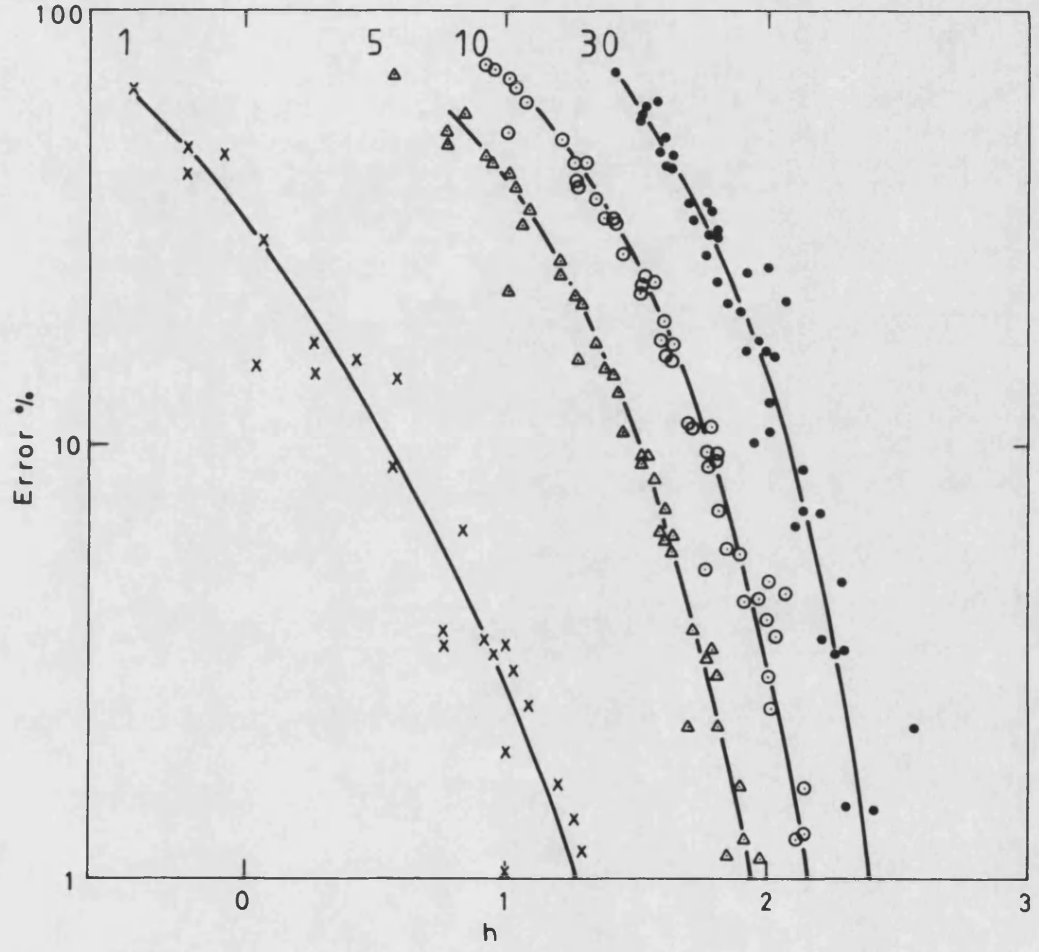

Figure 5 Error of Equation 2.21 applied to spherical waves, as a function of h (Equation 2.26). The parameter is the harmonic number.

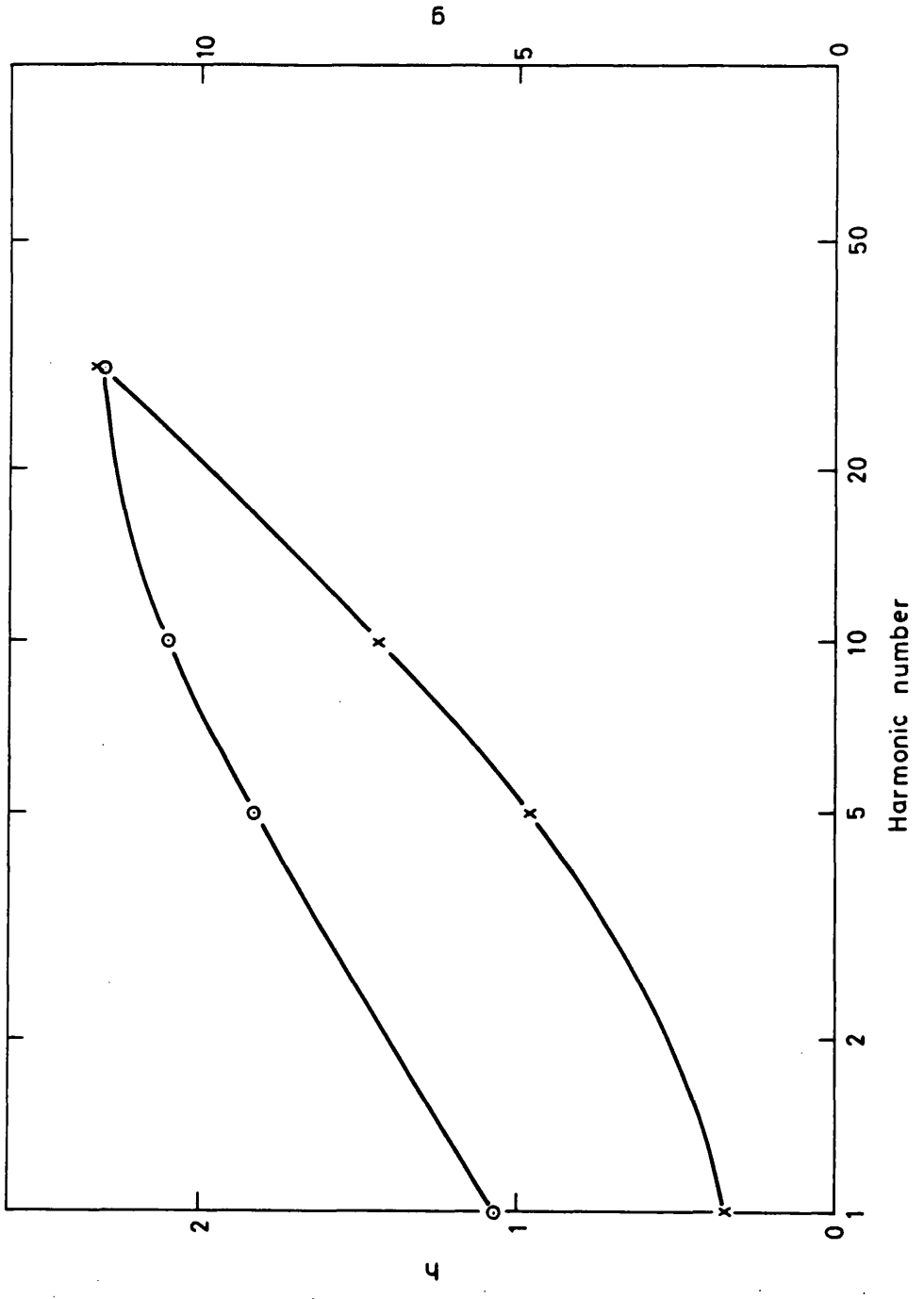

Figure 6 Variation of h (upper curve) and g (lower curve) with harmonic number for Equation 2.17 to have an accuracy of 2%. for spherical waves. An error of less than 2% occurs in regions above the curves.

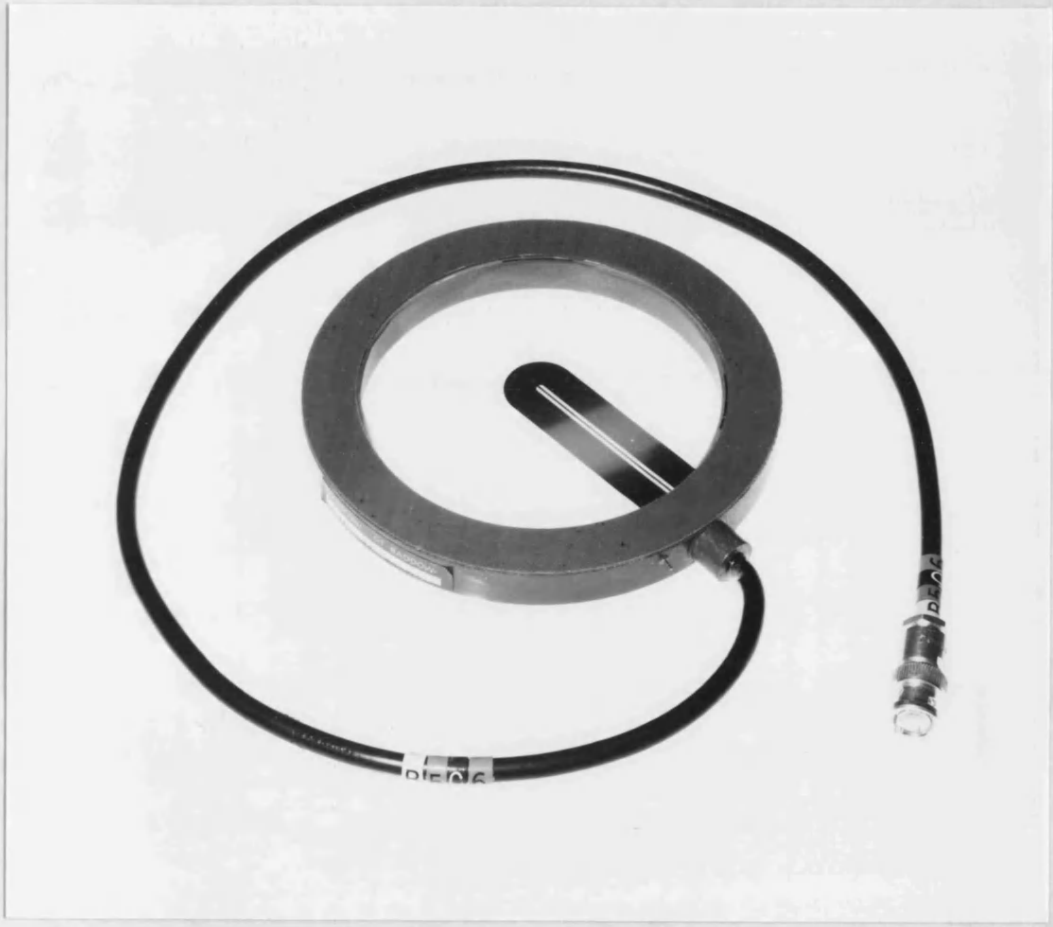

Figure 7 Coplanar shielded membrane hydrophone with an active element 0.5 mm in diameter.

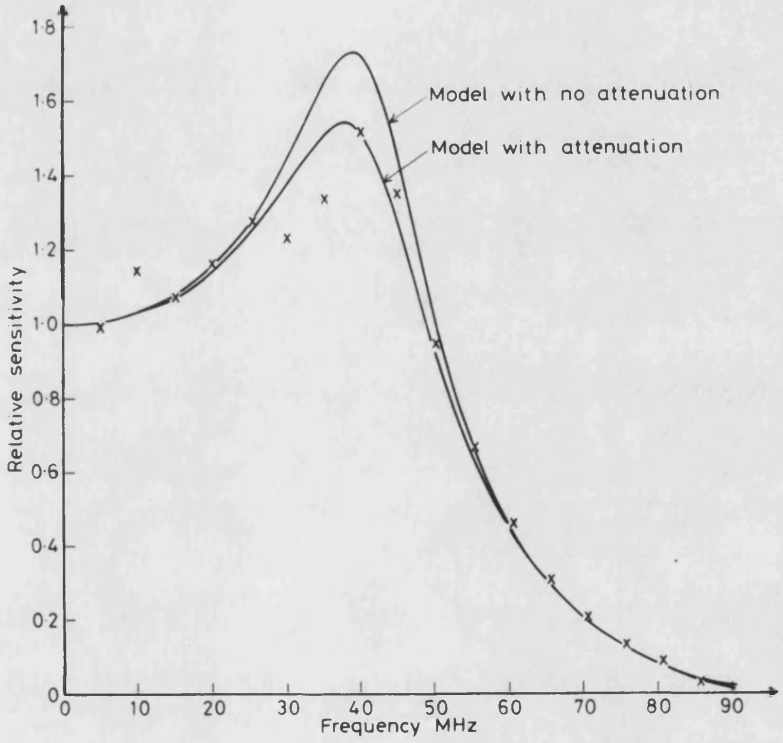

Figure 8 Sensitivity of a hydrophone made from 25 μm film relative to a hydrophone made from 9 μm film (normalised at 5 MHz), - theory (Equation 3.2), x experiment.

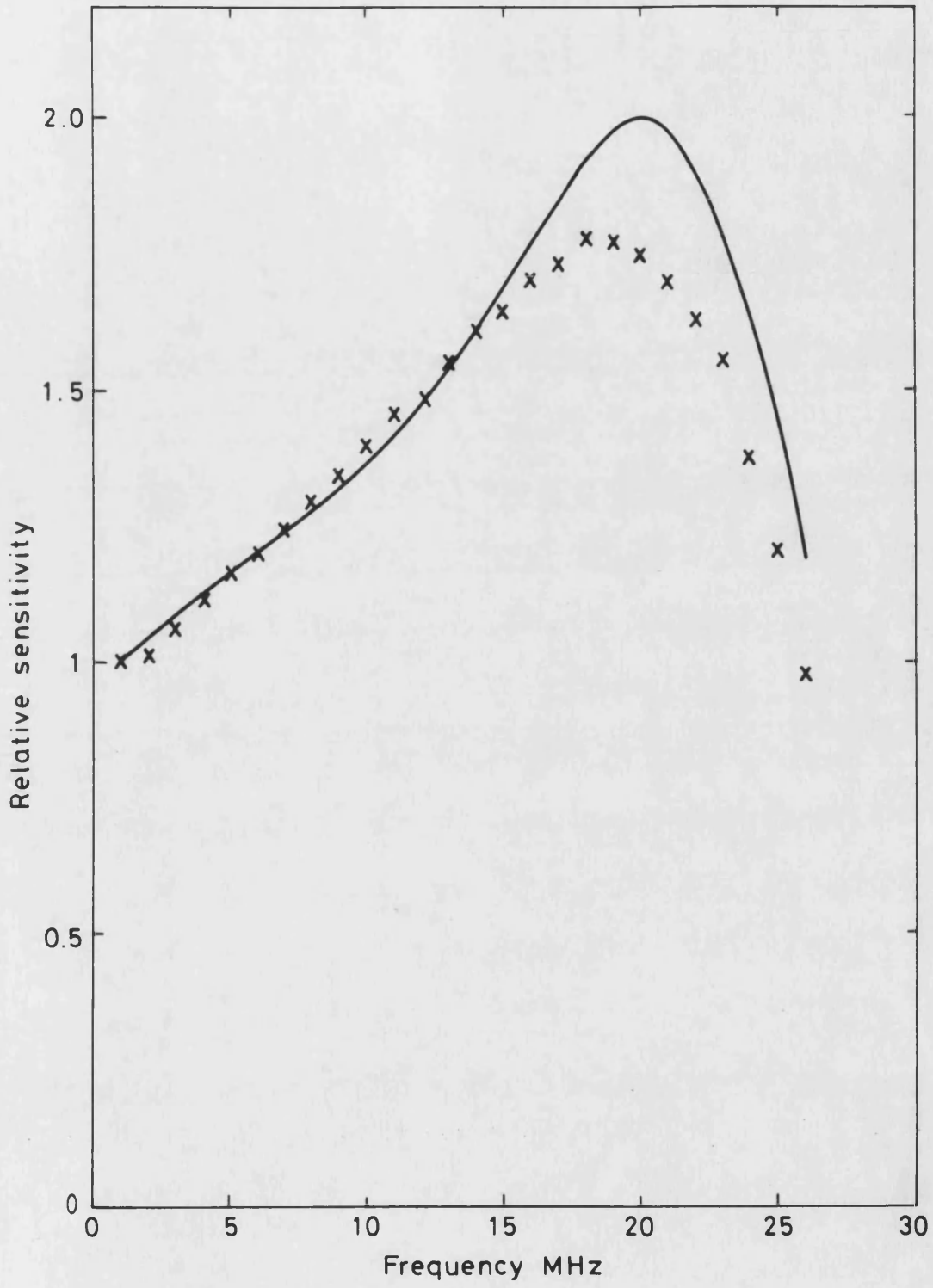

Figure 9 Sensitivity of a hydrophone of thickness 50 μm relative to hydrophone of thickness 9 μm (normalised at 1 MHz): — theory (Equation 3.2), x experiment.

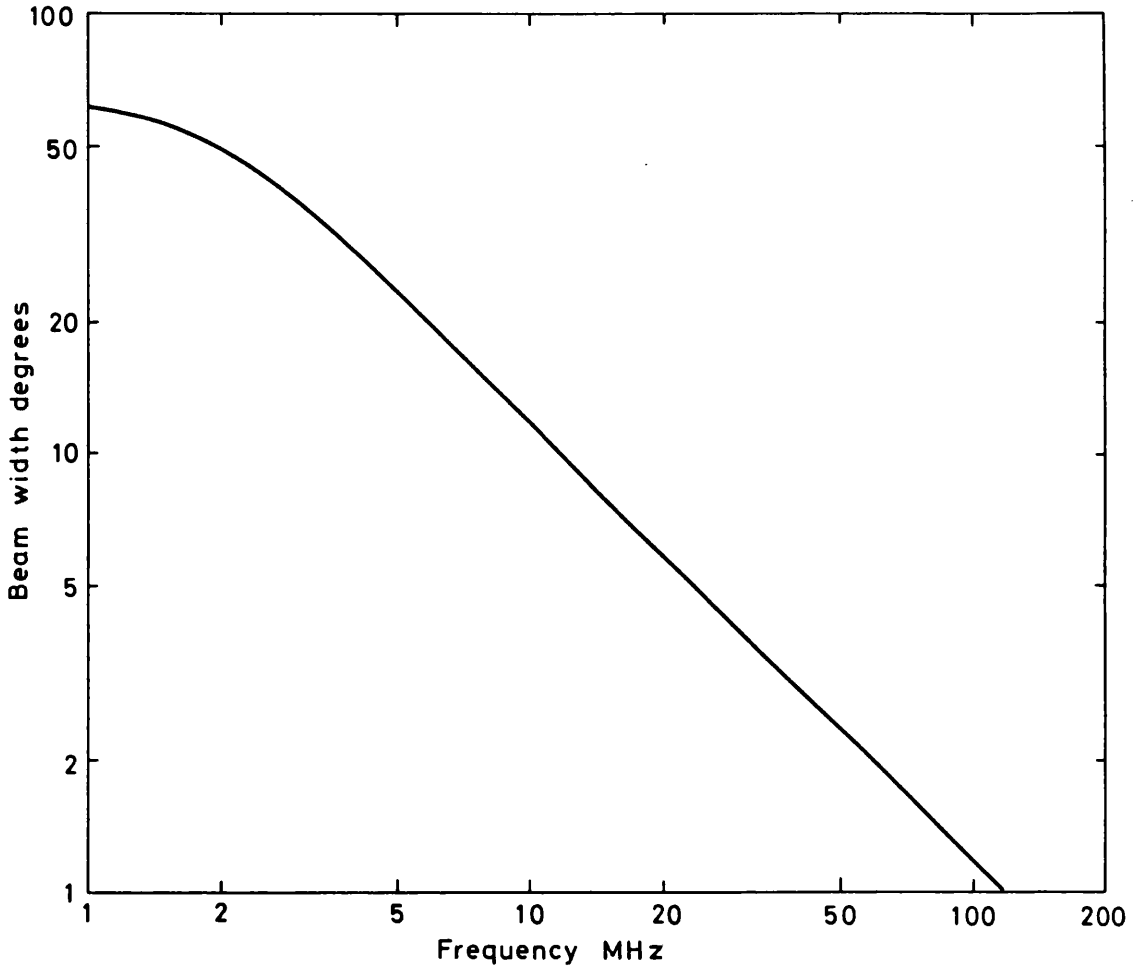

Figure 10 Variation of the angular diameter of the directional response at 6 dB below the peak level - according to the theory of reference [5].

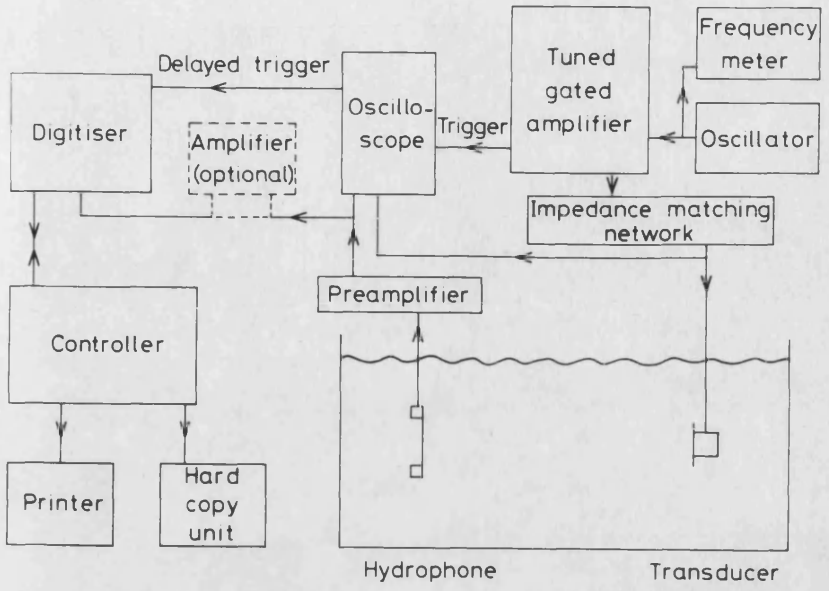

Figure 11 Block diagram of experimental apparatus.

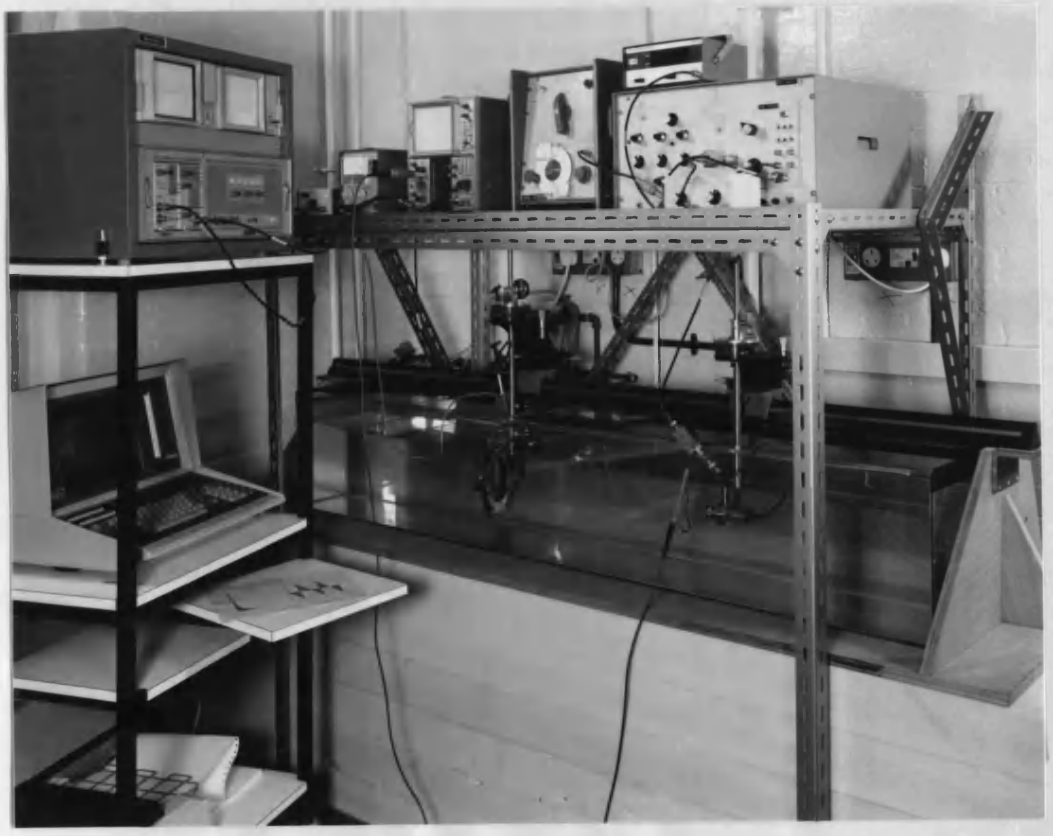

Figure 12 Photograph of experimental arrangement.

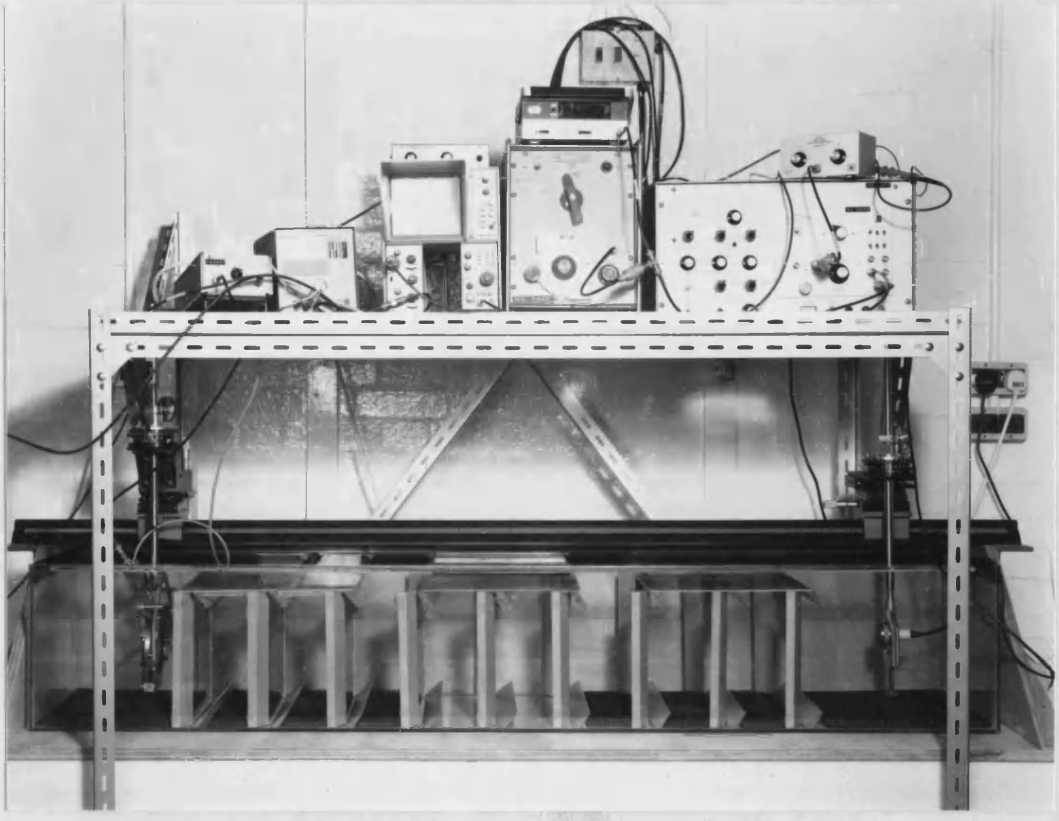

Figure 13 Acoustic tank.

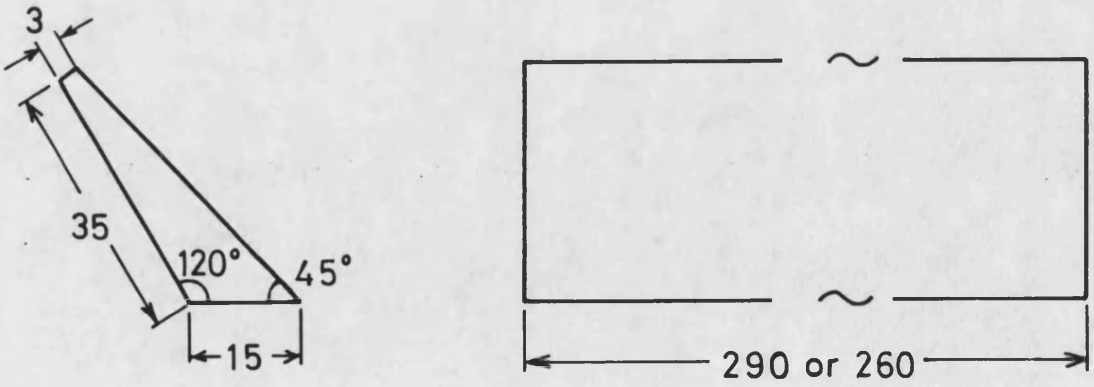

Figure 14 Diagram of acoustic baffles - dimensions are in mm.

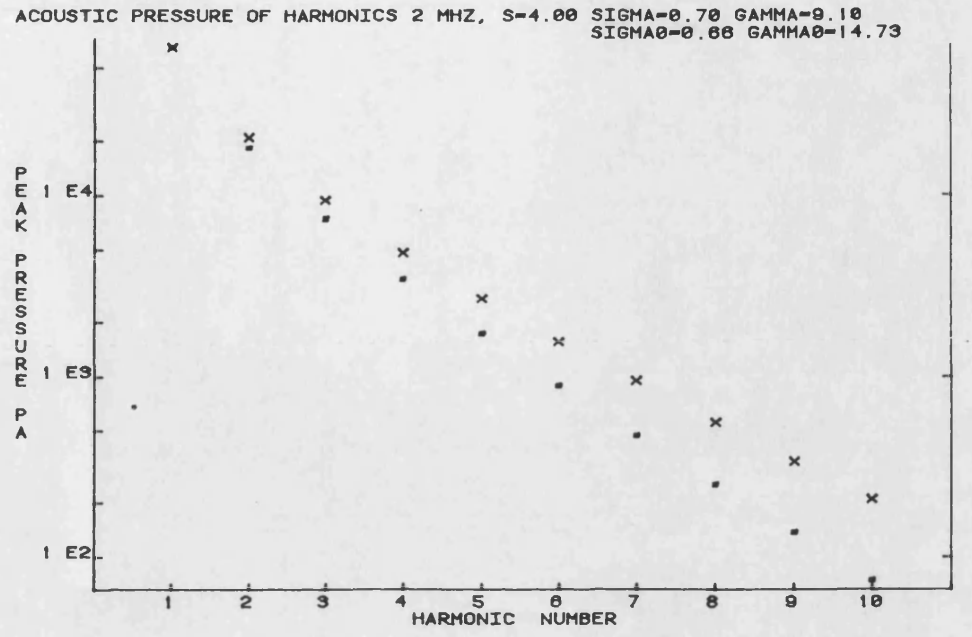

Figure 15a

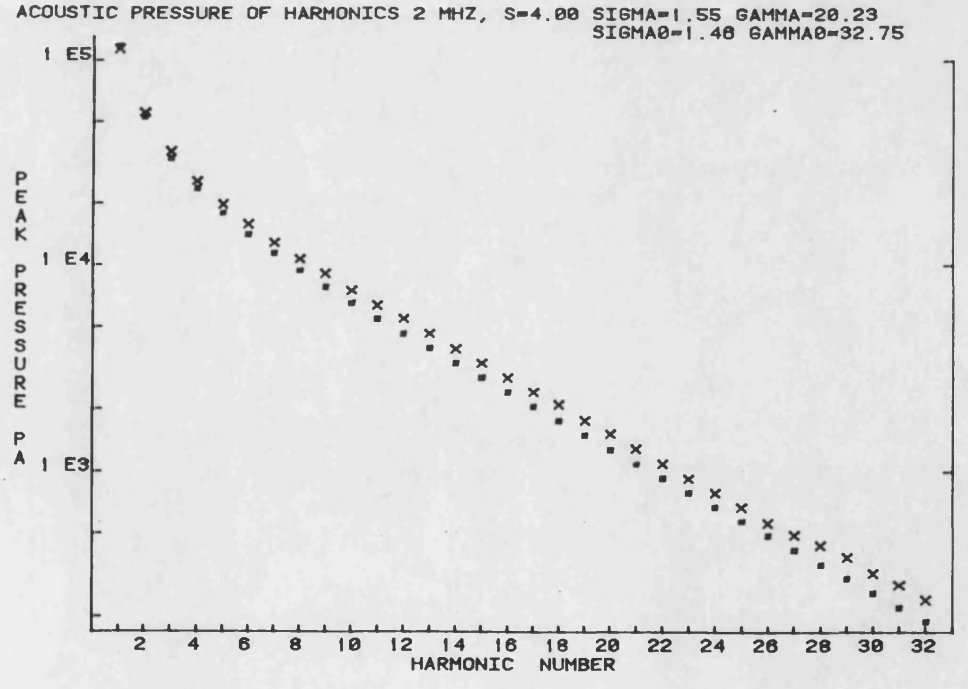

Figure 15b

Figure 15 Results for transducer 2, R = 1.27, for increasing values of the source amplitude. ■ theory (matched Gaussian), x experiment.

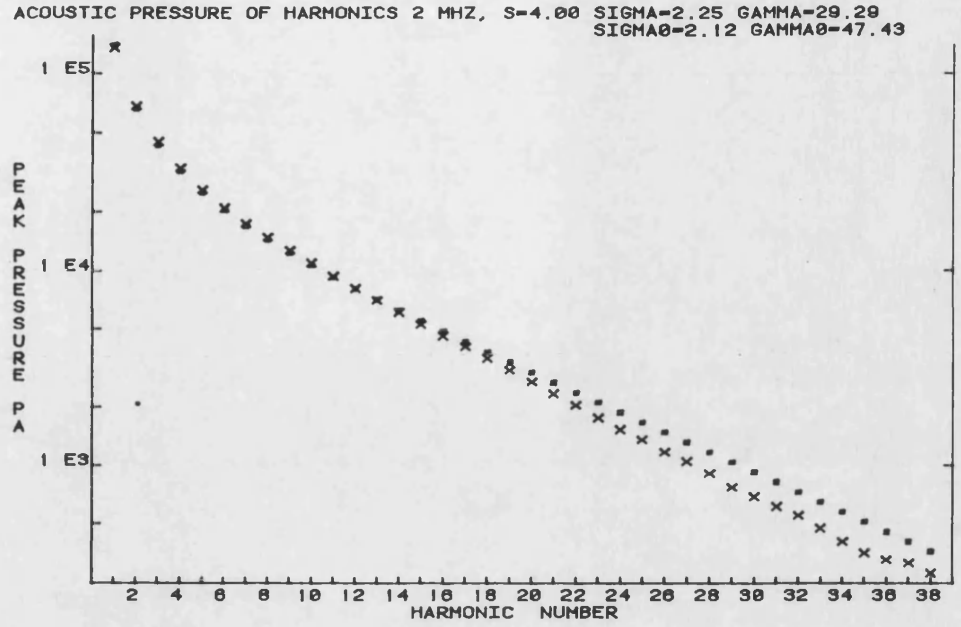

Figure 15c

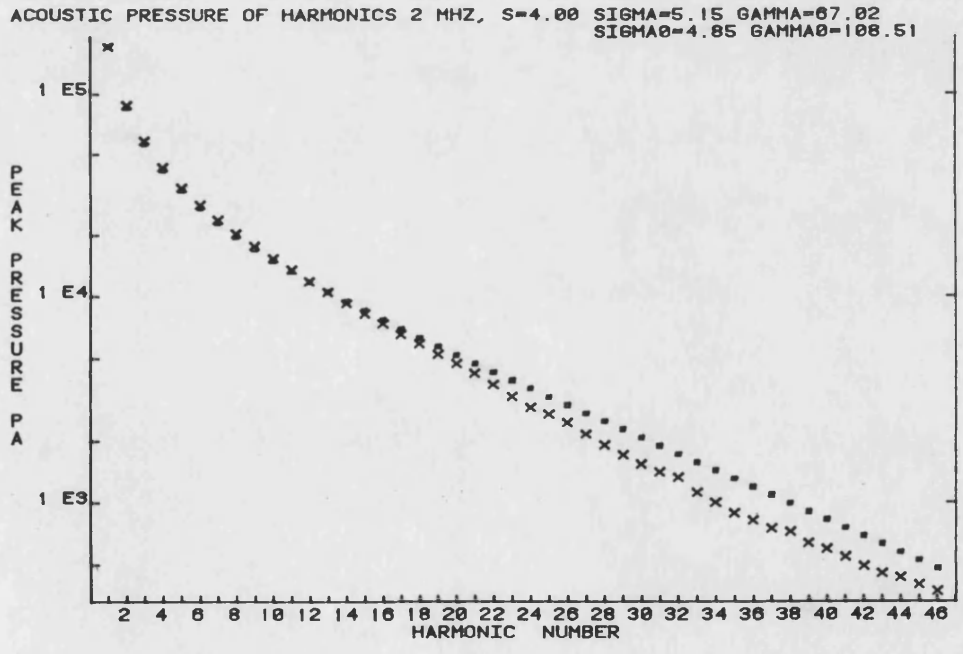

Figure 15d

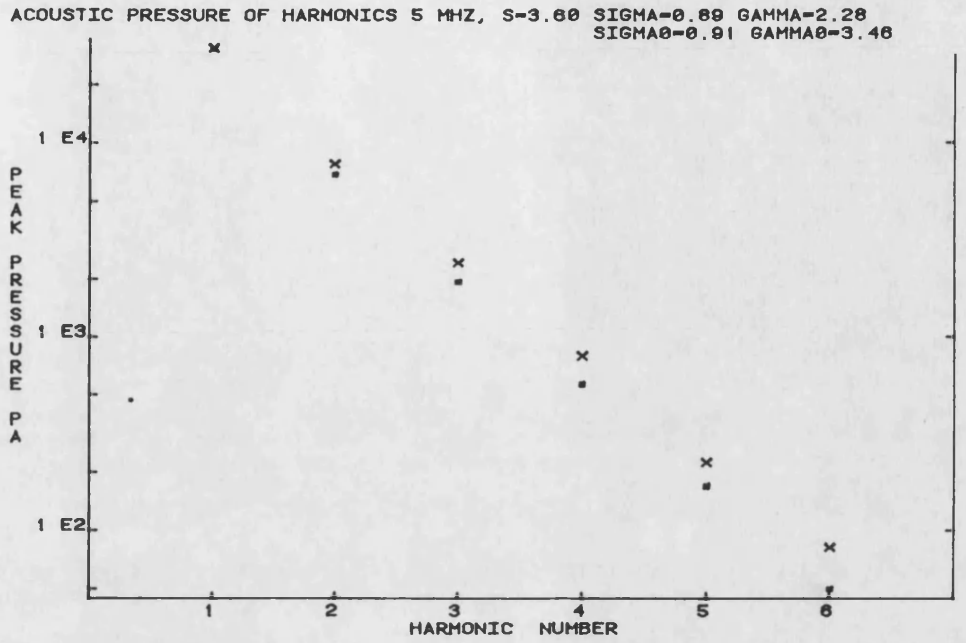

Figure 16a

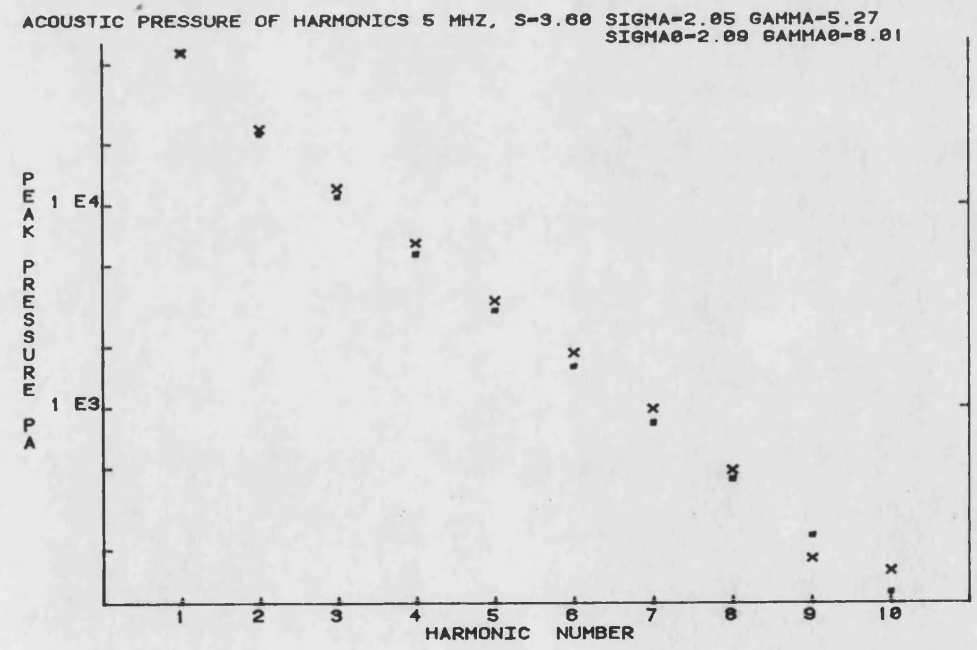

Figure 16b

Figure 16 Results for transducer 4, R = 1.15, for increasing values of source amplitude. ■ theory (matched Gaussian), x experiment.

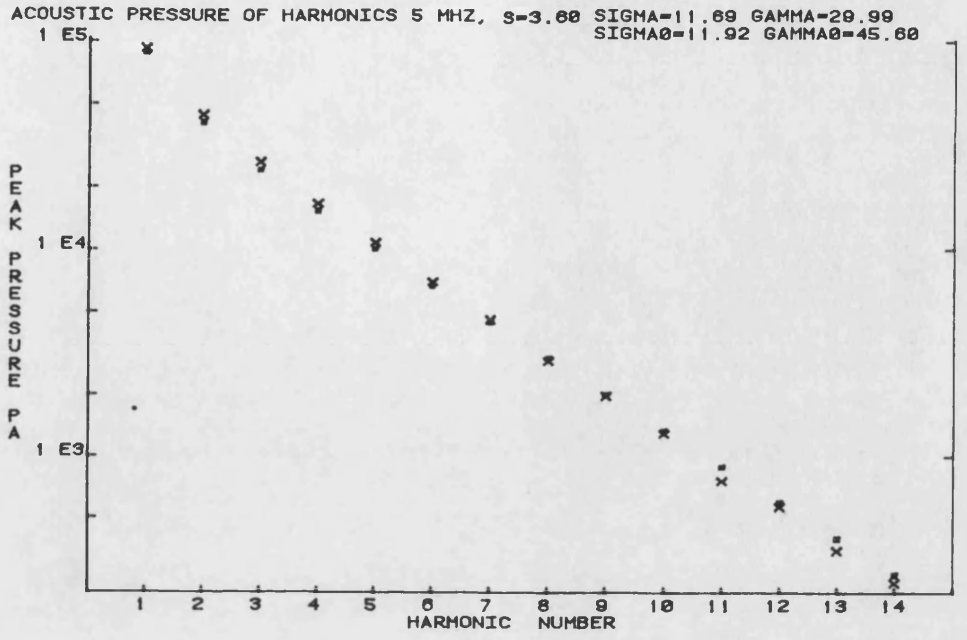

Figure 16c

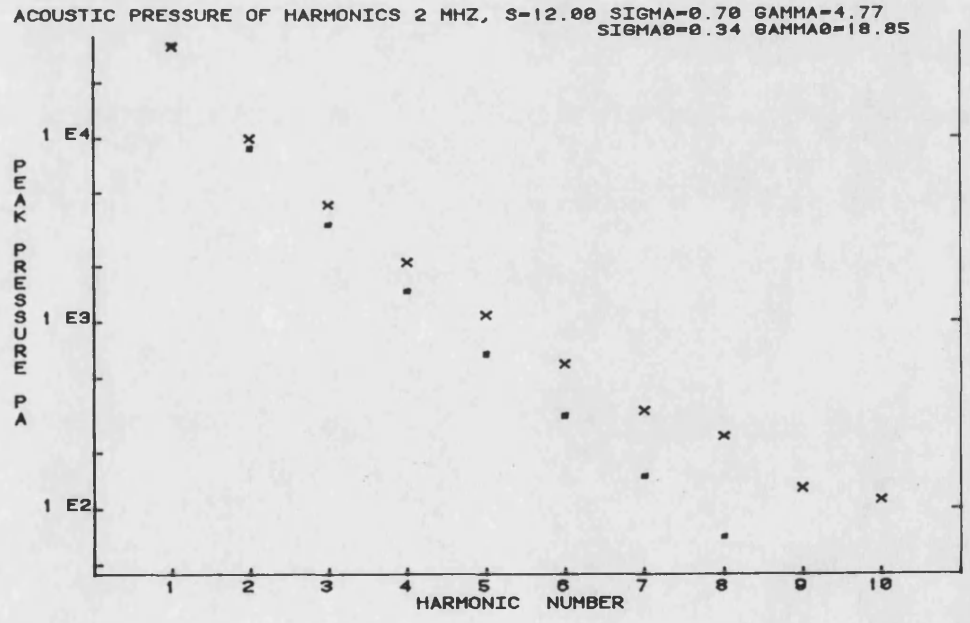

Figure 17a

Figure 17 Results for transducer 3, R = 3.82 ;for increasing source amplitude. ■ theory (matched Gaussian), x experiment

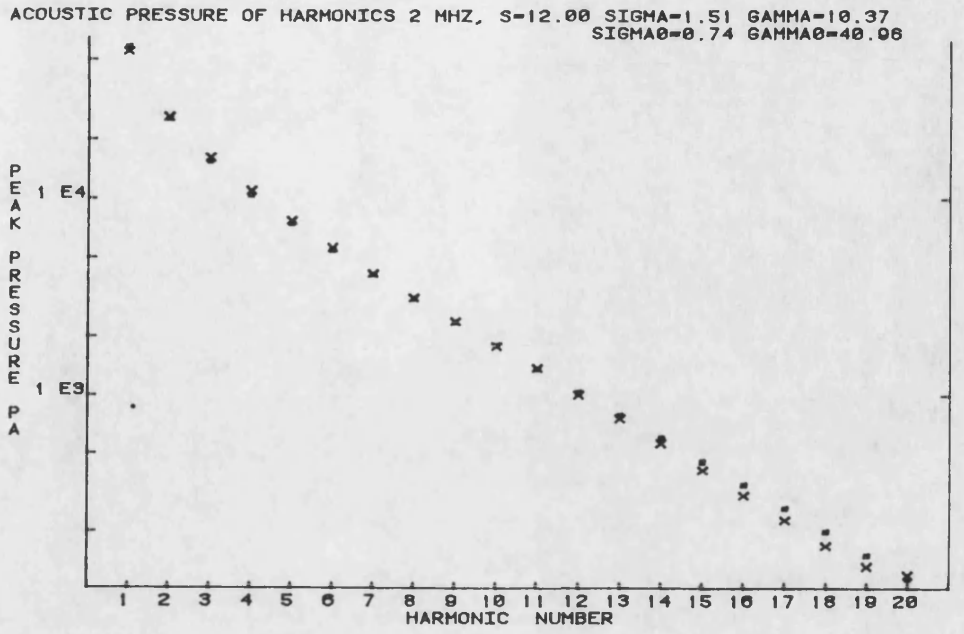

Figure 17b

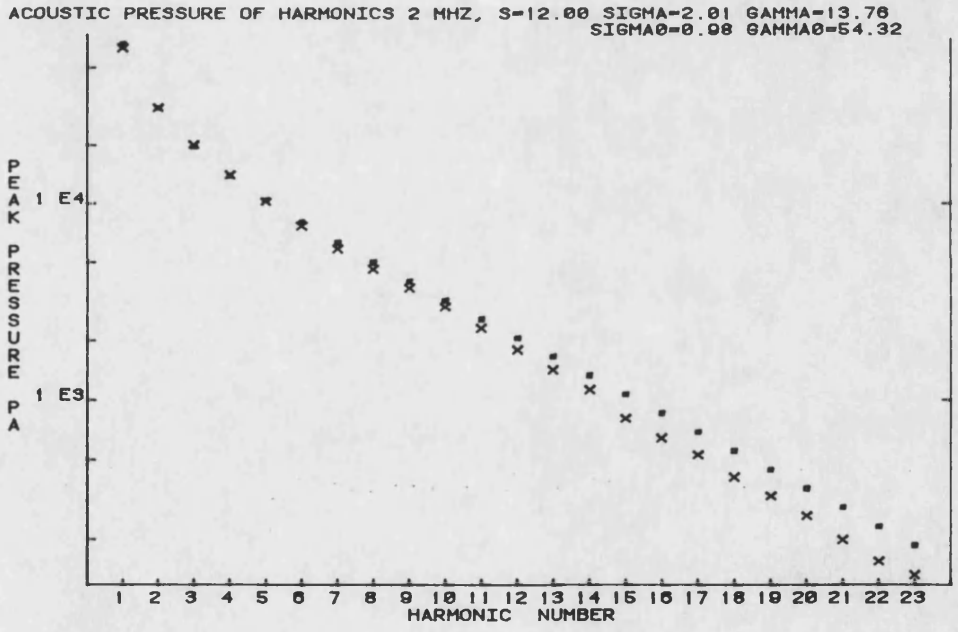

Figure 17c

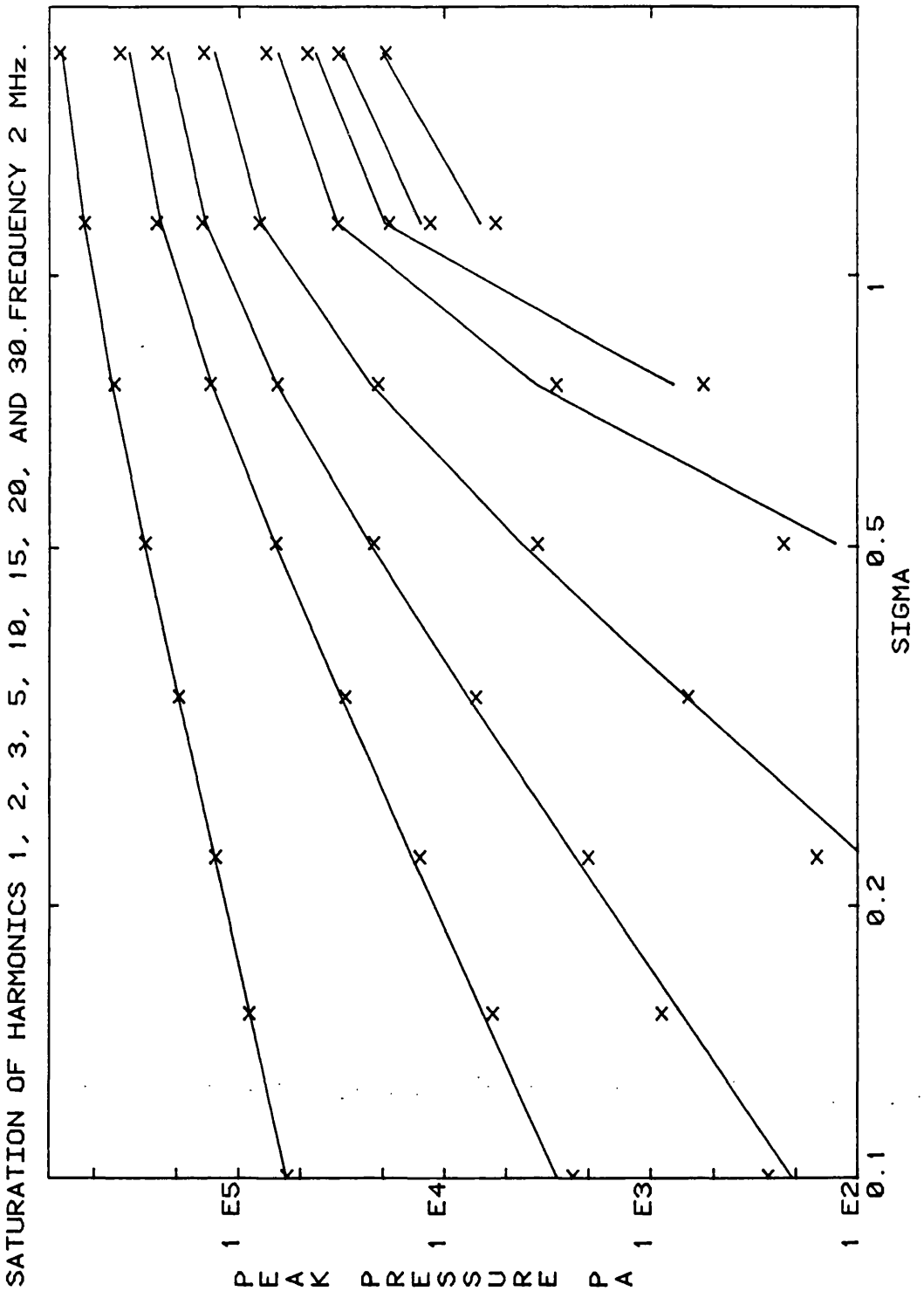

Figure 18a Transducer 3, R = 0.64, - theory (matched Gaussian), x experiment.

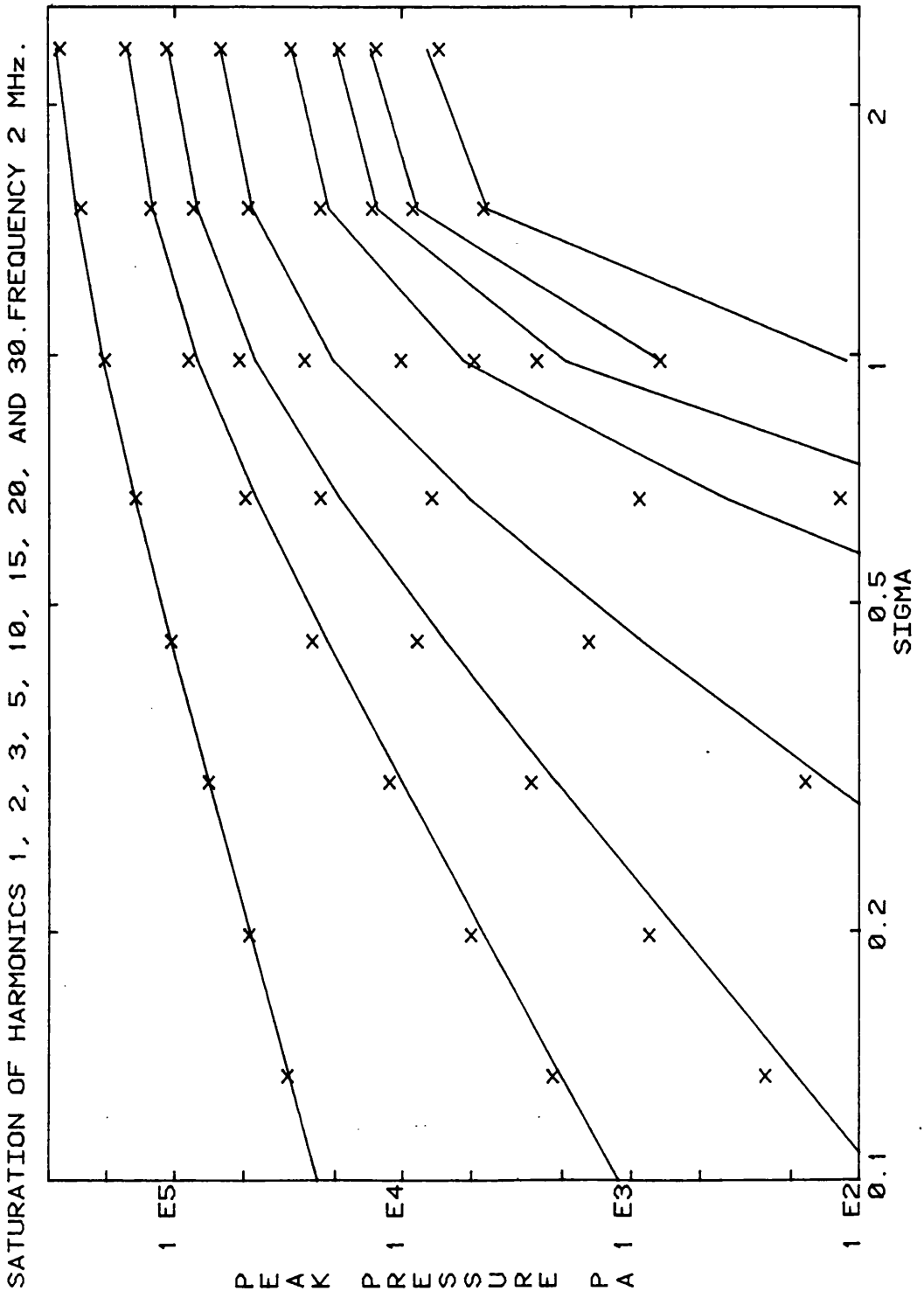

Figure 18b Trandsucer 3, R = 1.27, - theory (matched Gaussian), x experiment.

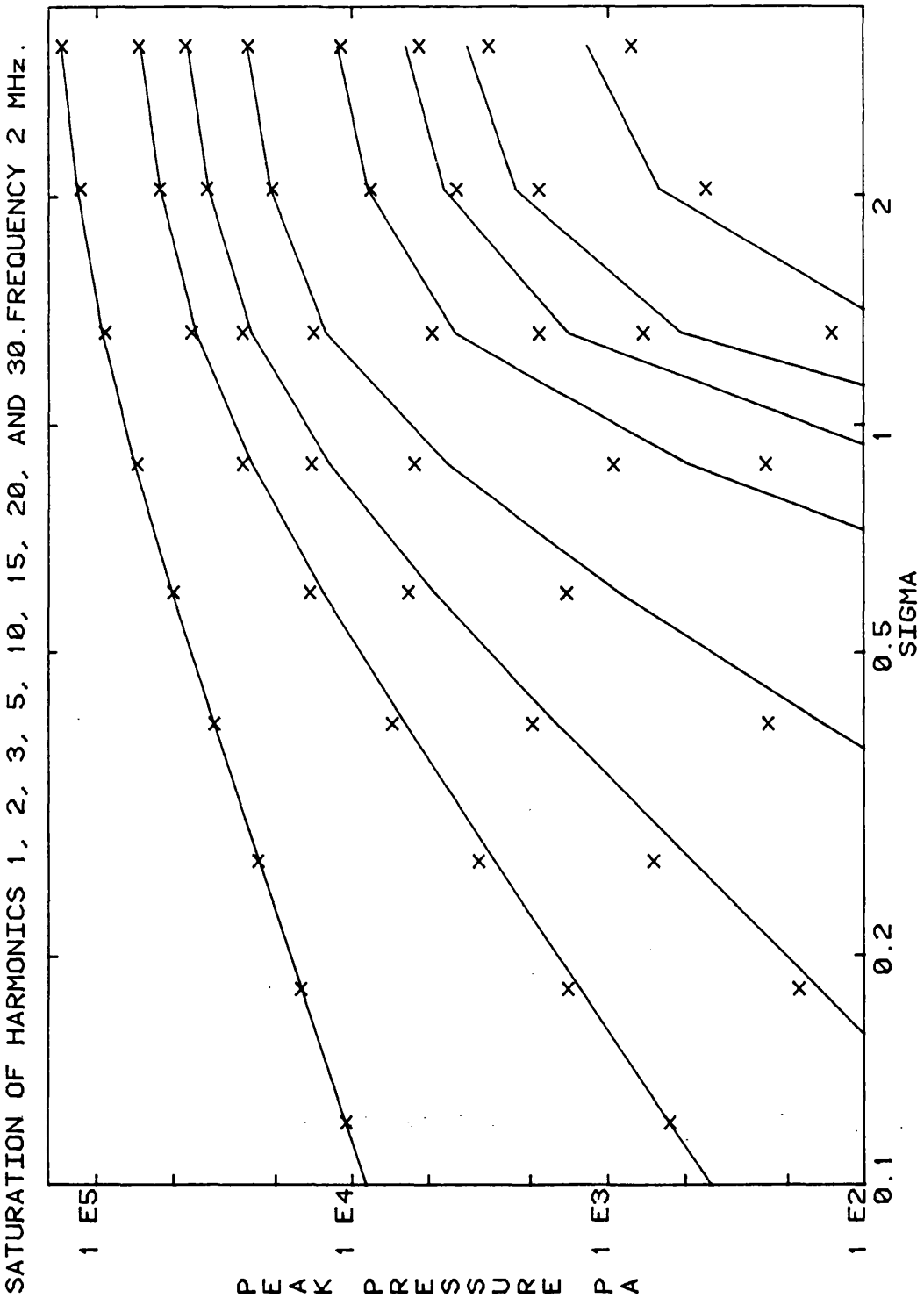

Figure 18c Transducer 3, R = 2.55, - theory (matched Gaussian), x experiment.

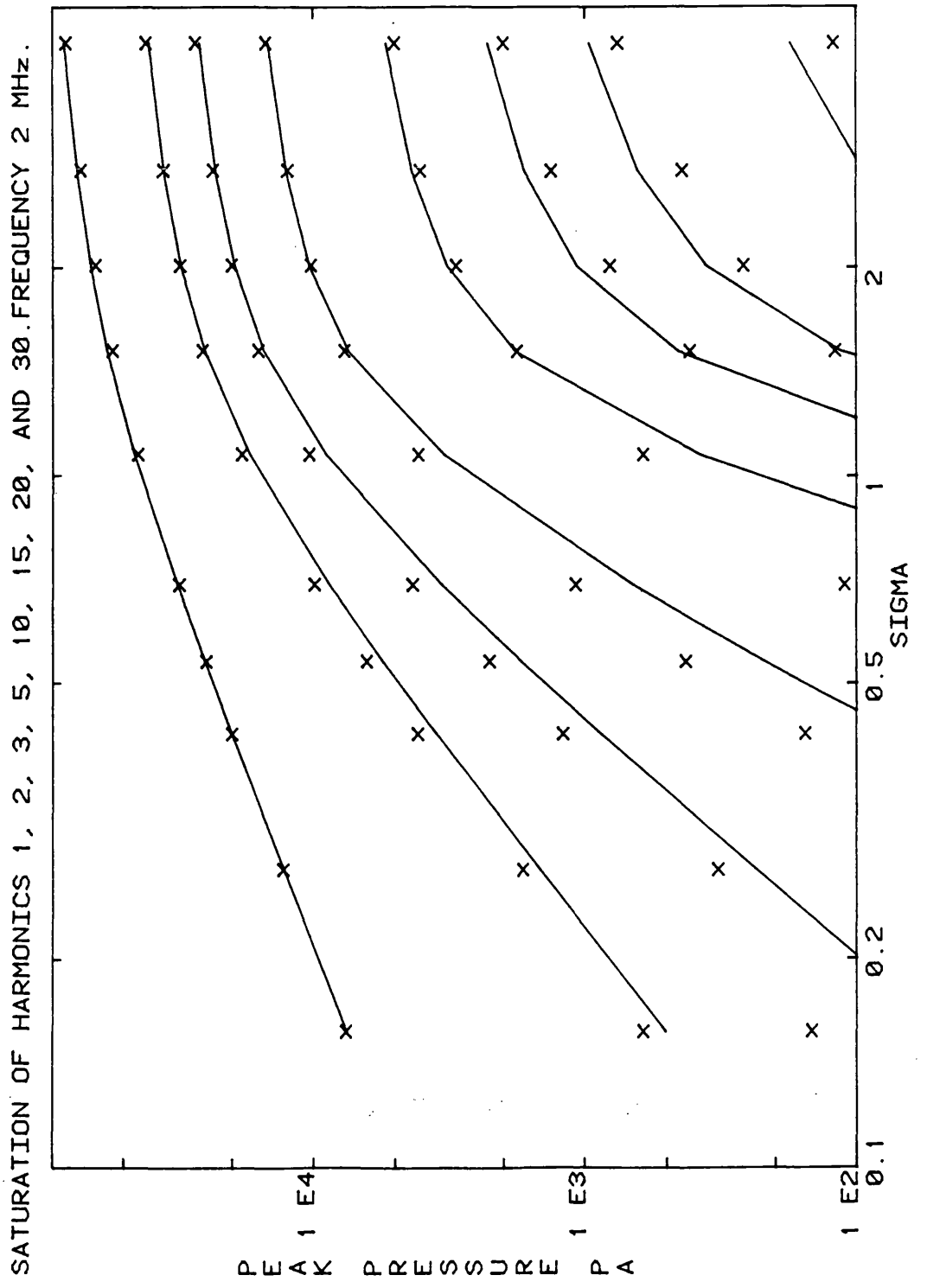

Figure 18d Transducer 3, R = 3.82, - theory (matched Gaussian), x experiment.

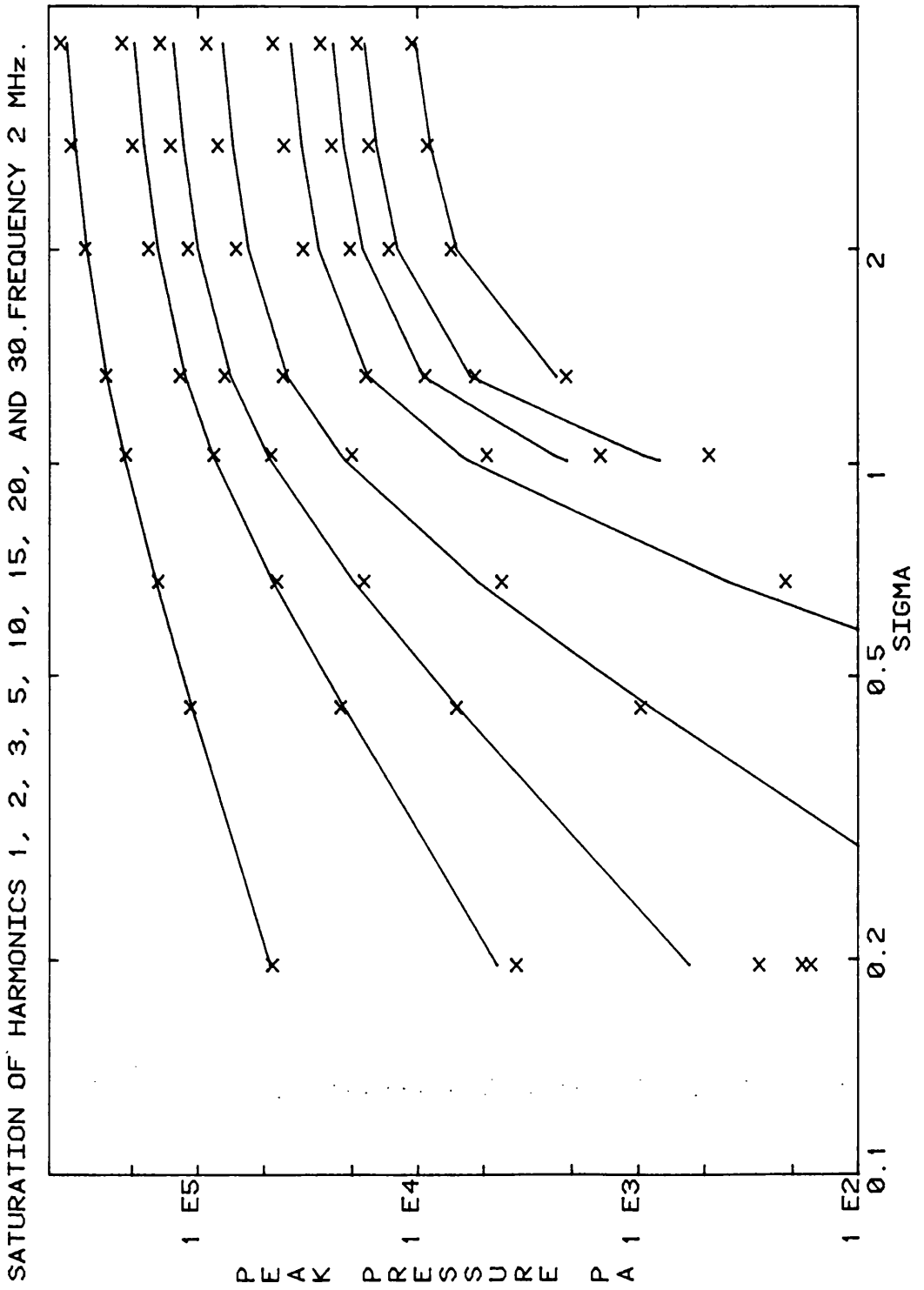

Figure 19 Transducer 2, R = 0.64, - theory (matched Gaussian), x experiment.

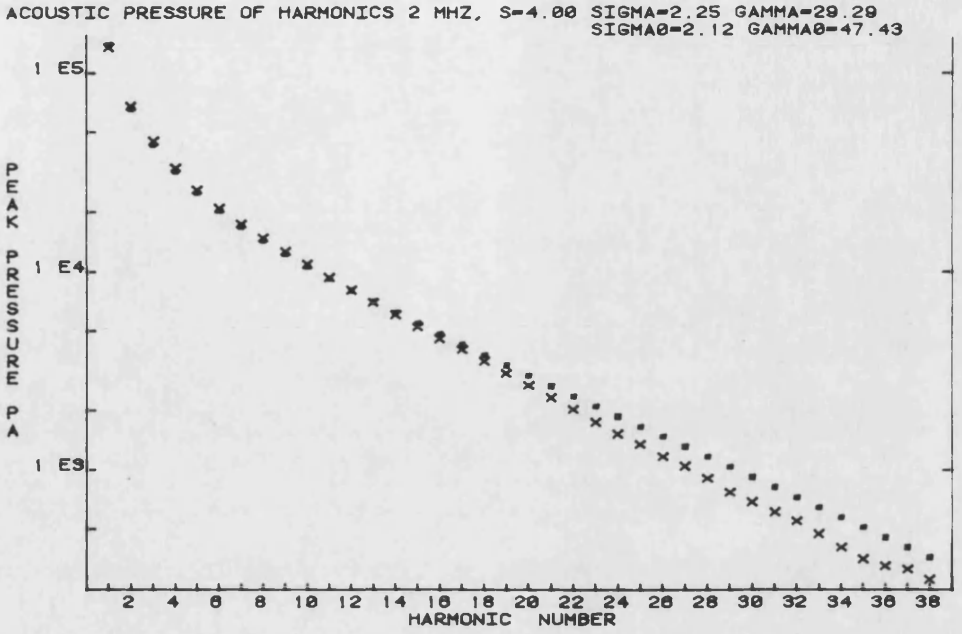

Figure 20a Transducer 2.

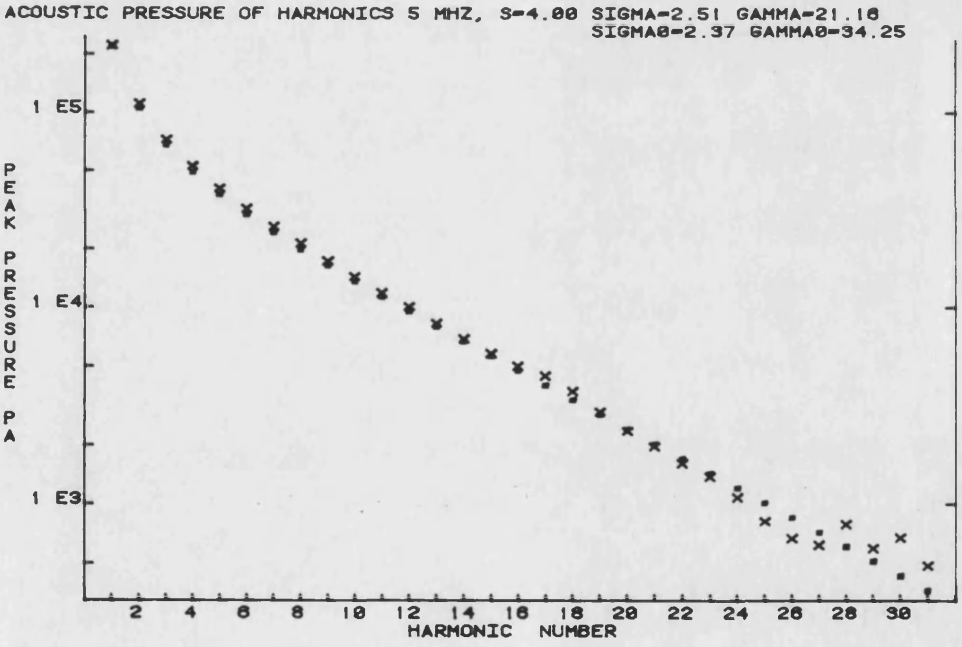

Figure 20b Transducer 5.

Figure 20 Comparison of theory (■) with experiment (x) for $\sigma \simeq 2.3$ and $R \simeq 1.2$ for different values of Γ_0.

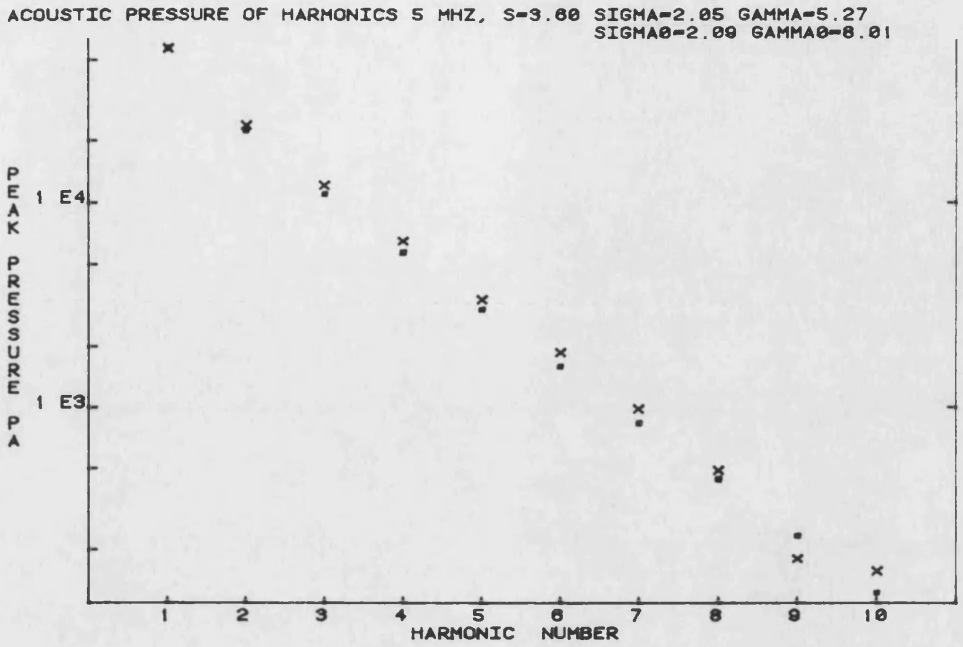

Figure 20c Transducer 4.

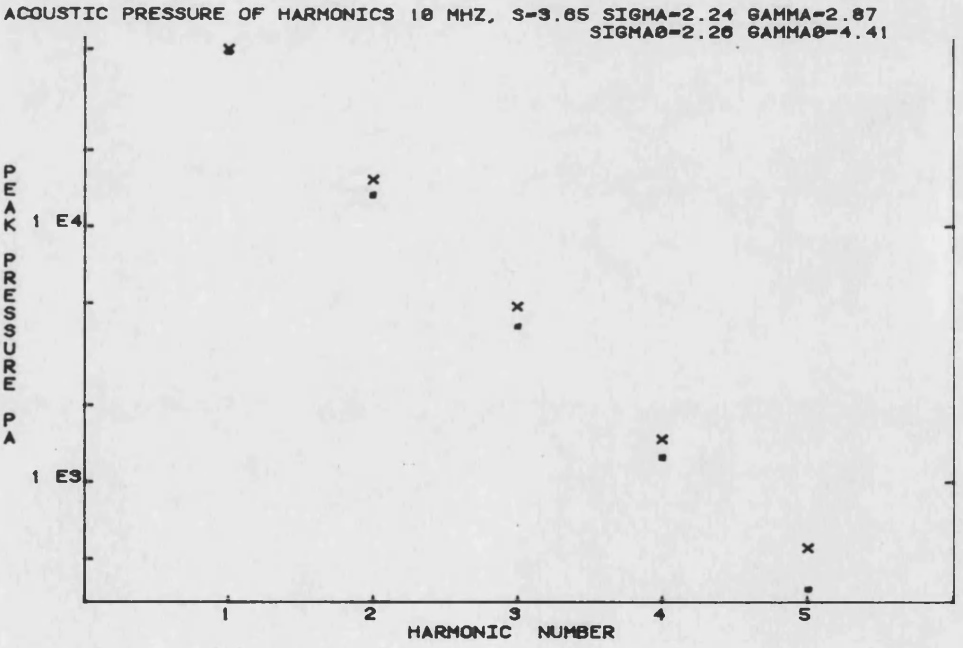

Figure 20d Transducer 6.

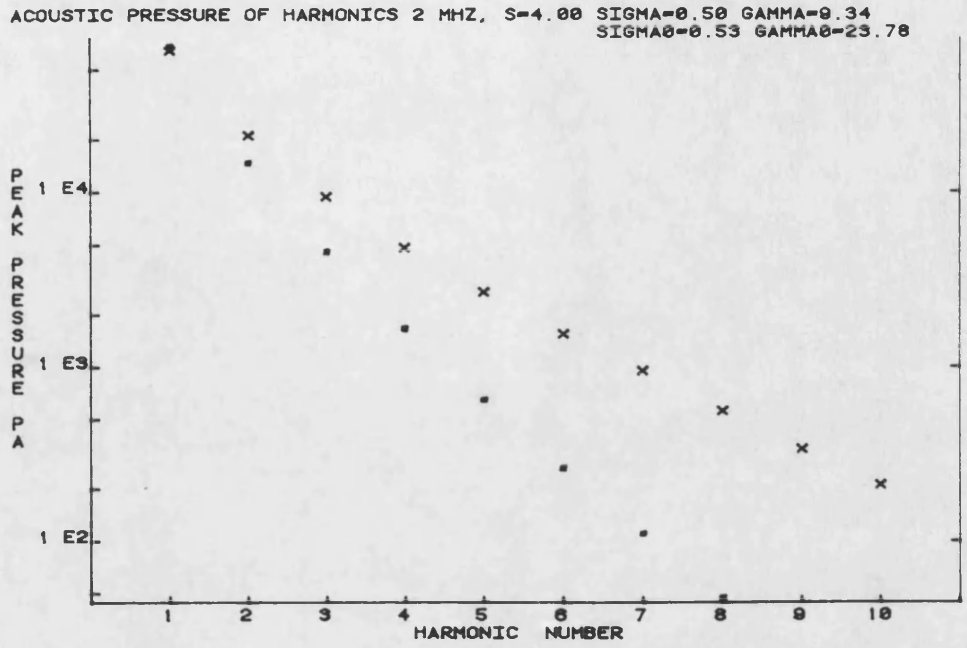

Figure 21a

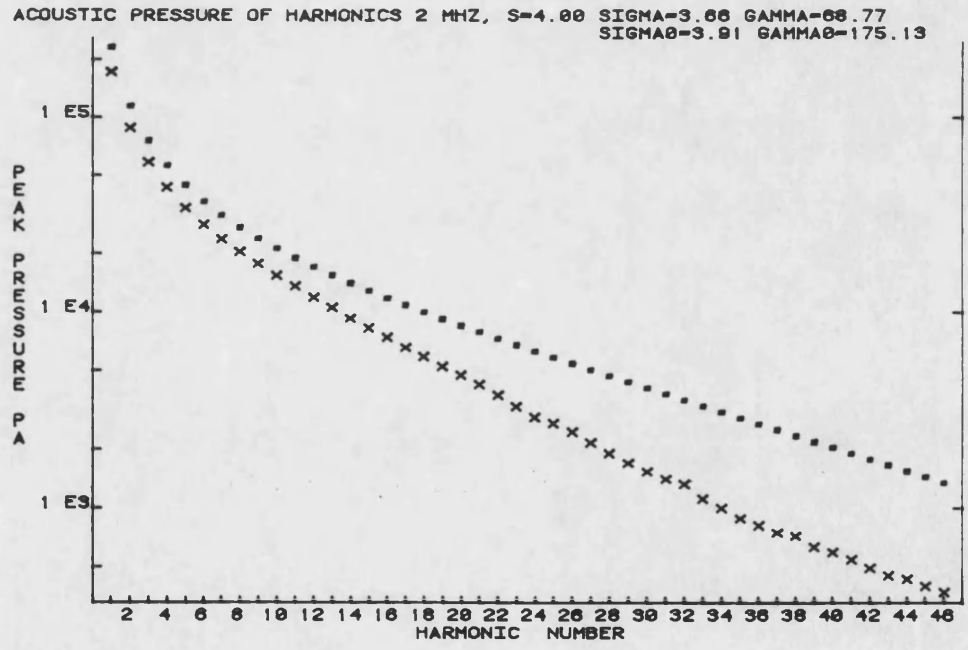

Figure 21b

Figure 21 Comparison of spherical wave theory with experiment for transducer 2, R = 1.27, ■ theory, x experiment.

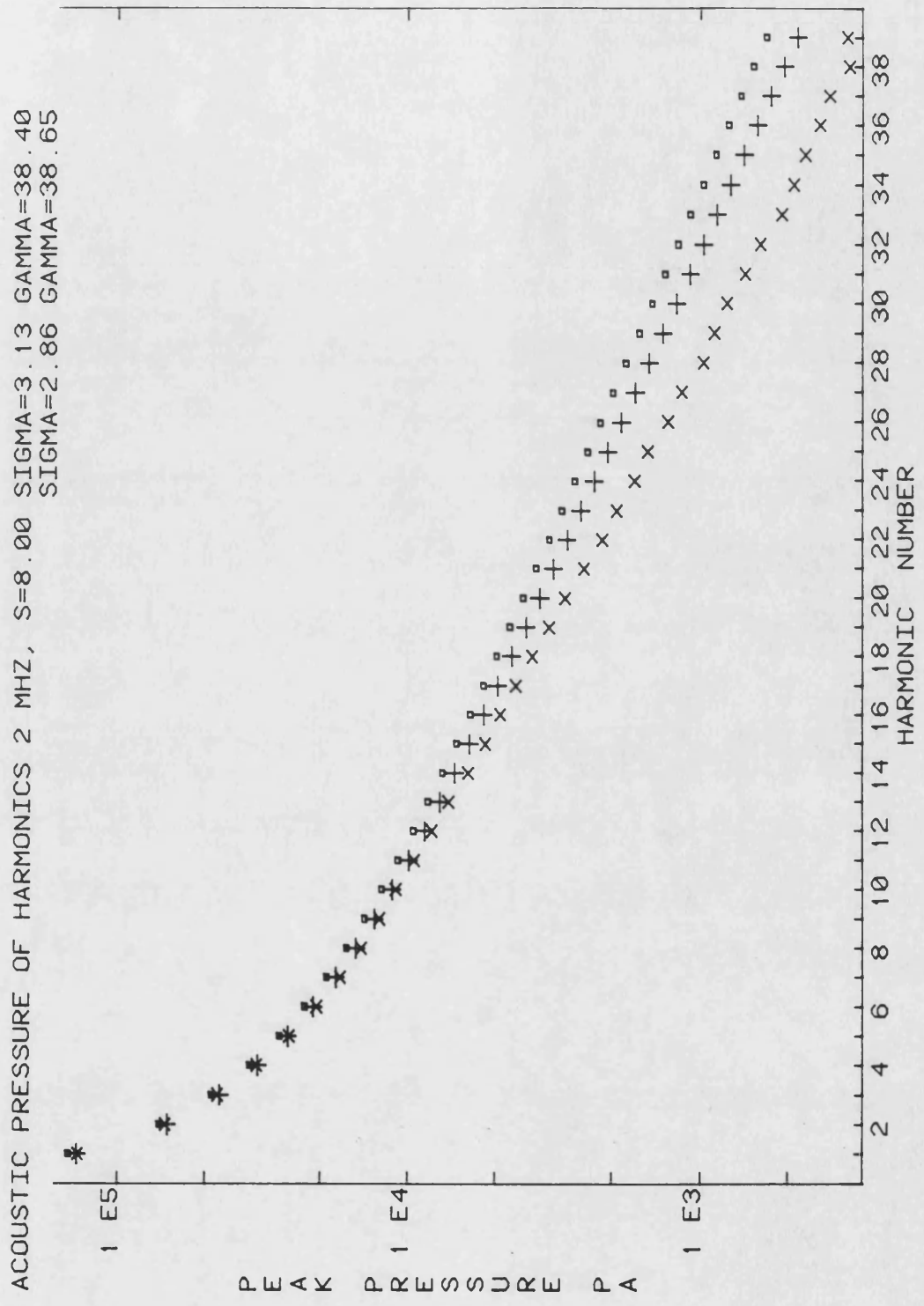

Figure 22a Comparison of theories with experiment for R = 2.55. □ spherical wave model, + matched Gaussian model, x experiment.

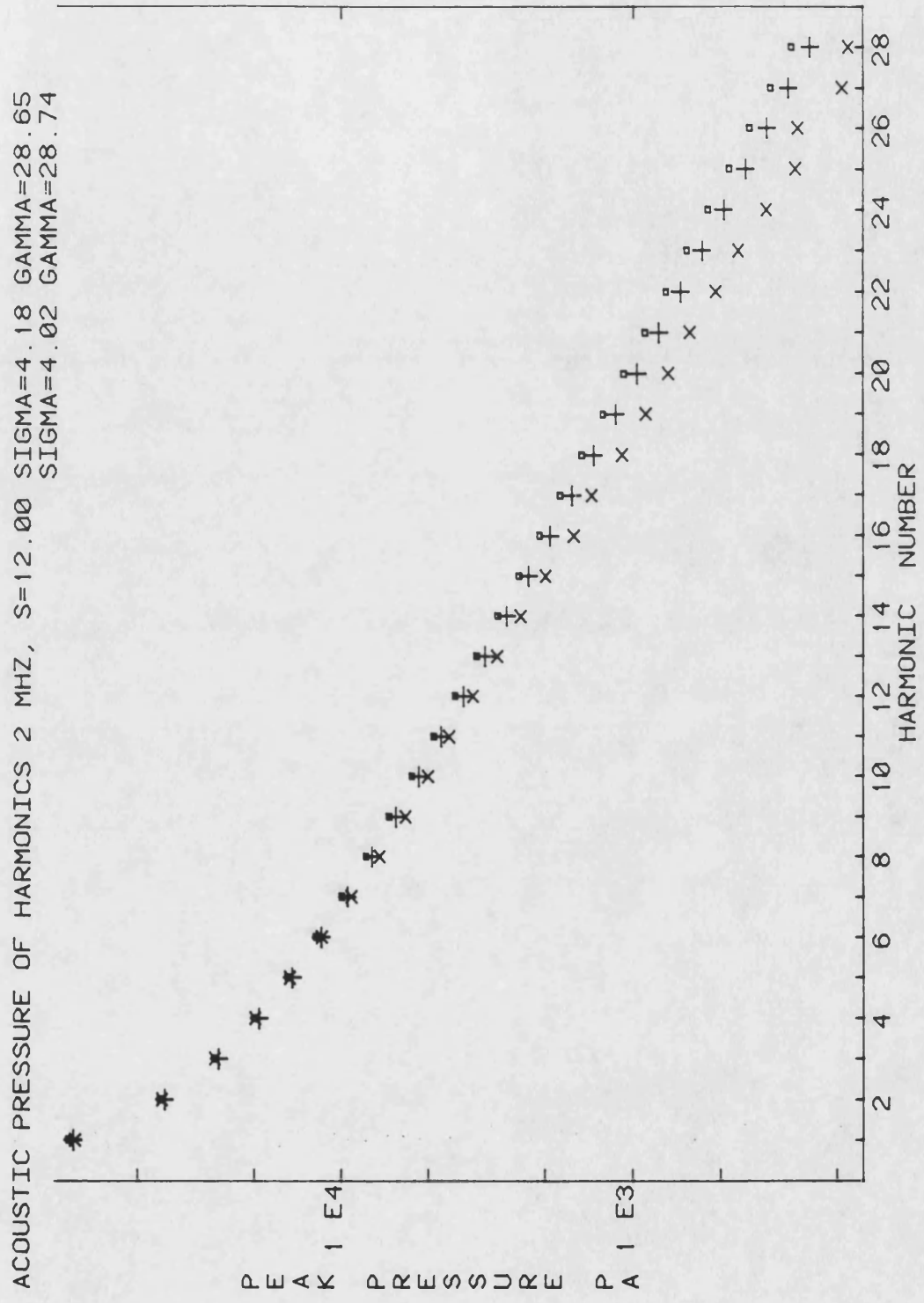

Figure 22b Comparison of theories with experiment for R = 3.82. □ spherical wave model, + matched Gaussian model, x experiment.

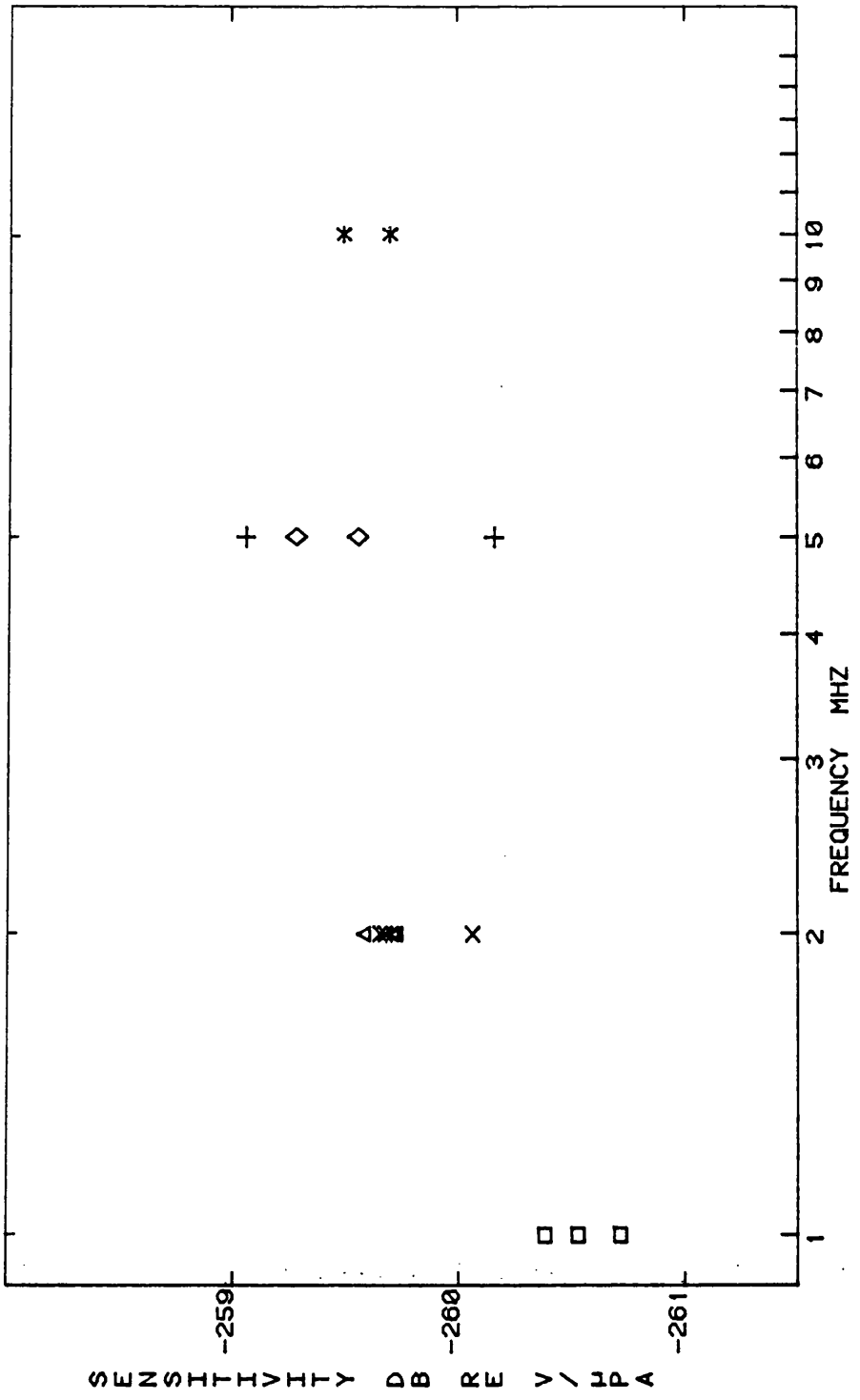

Figure 23a Hydrophone sensitivities determined at the fundamental frequency, using several different transducers. Each symbol corresponds to a particular propagation distance.

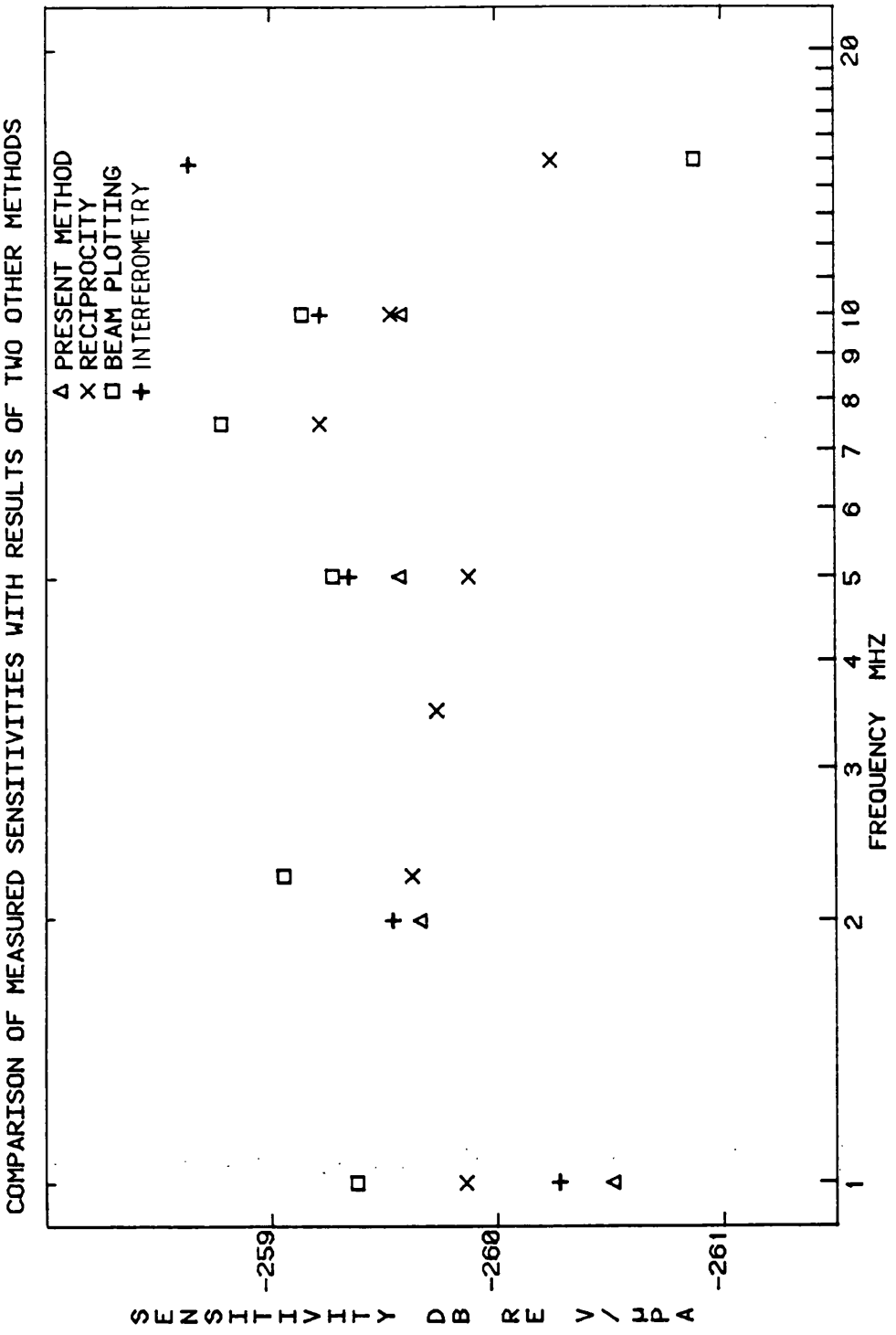

Figure 23b Comparison of the results of different calibration methods. The results of the present method are obtained for the fundamental component only.

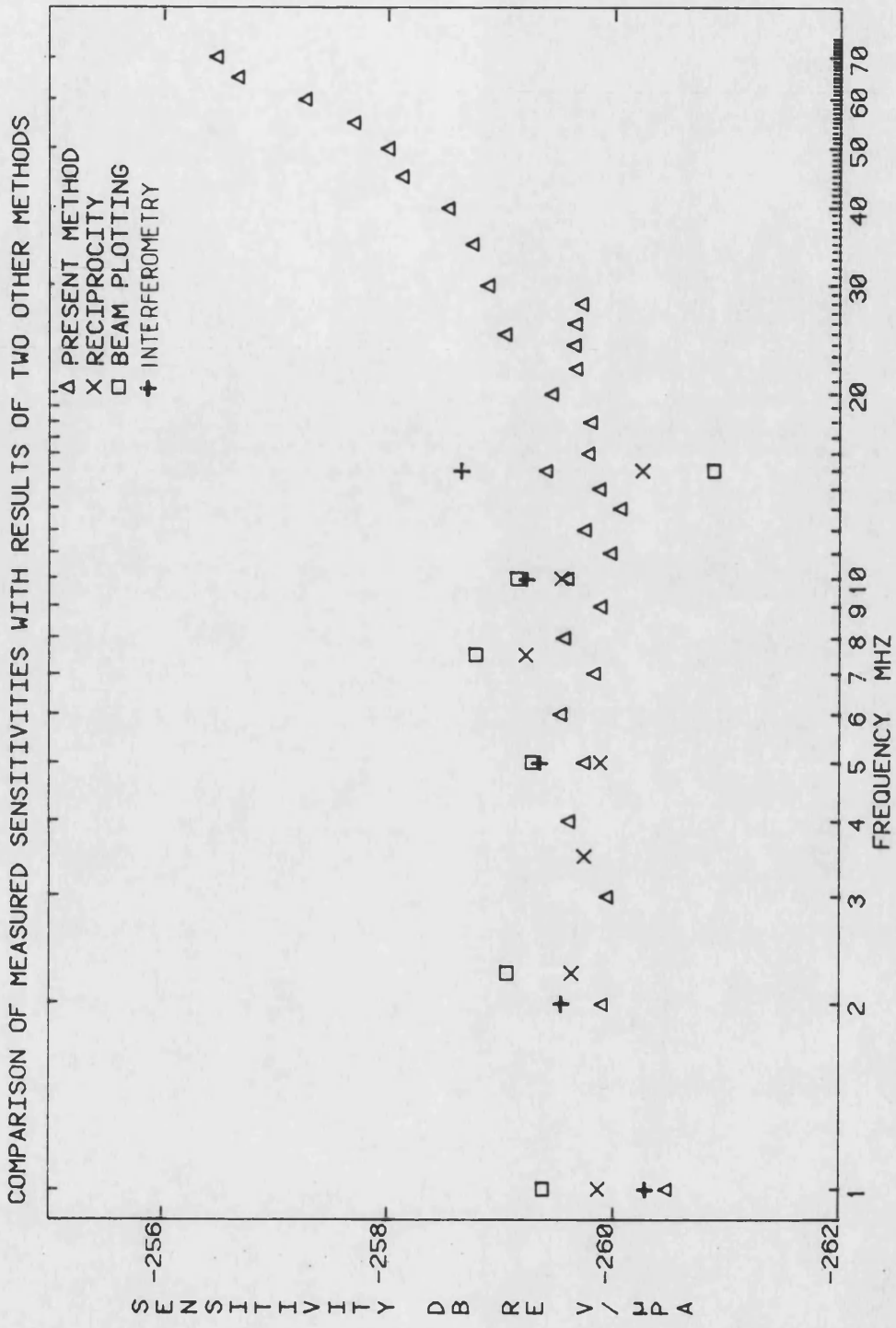

Figure 24a Comparison of the results obtained from different calibration methods. The results of the present method are derived from the measurement of the first fourteen harmonic components.

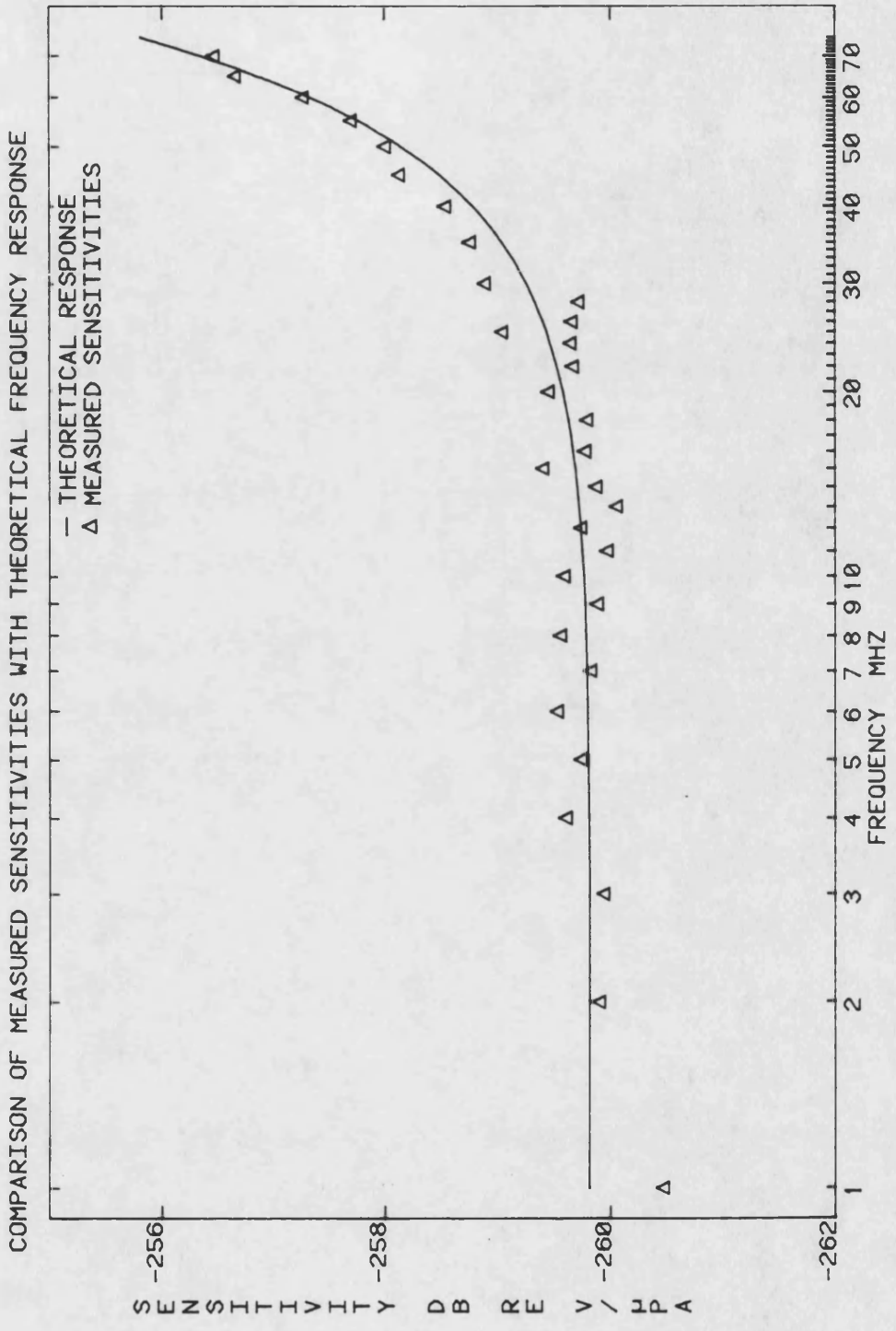

Figure 24b Comparison of the frequency response measured using the nonlinear calibration method, with that predicted using the theory of section 3.1.1.

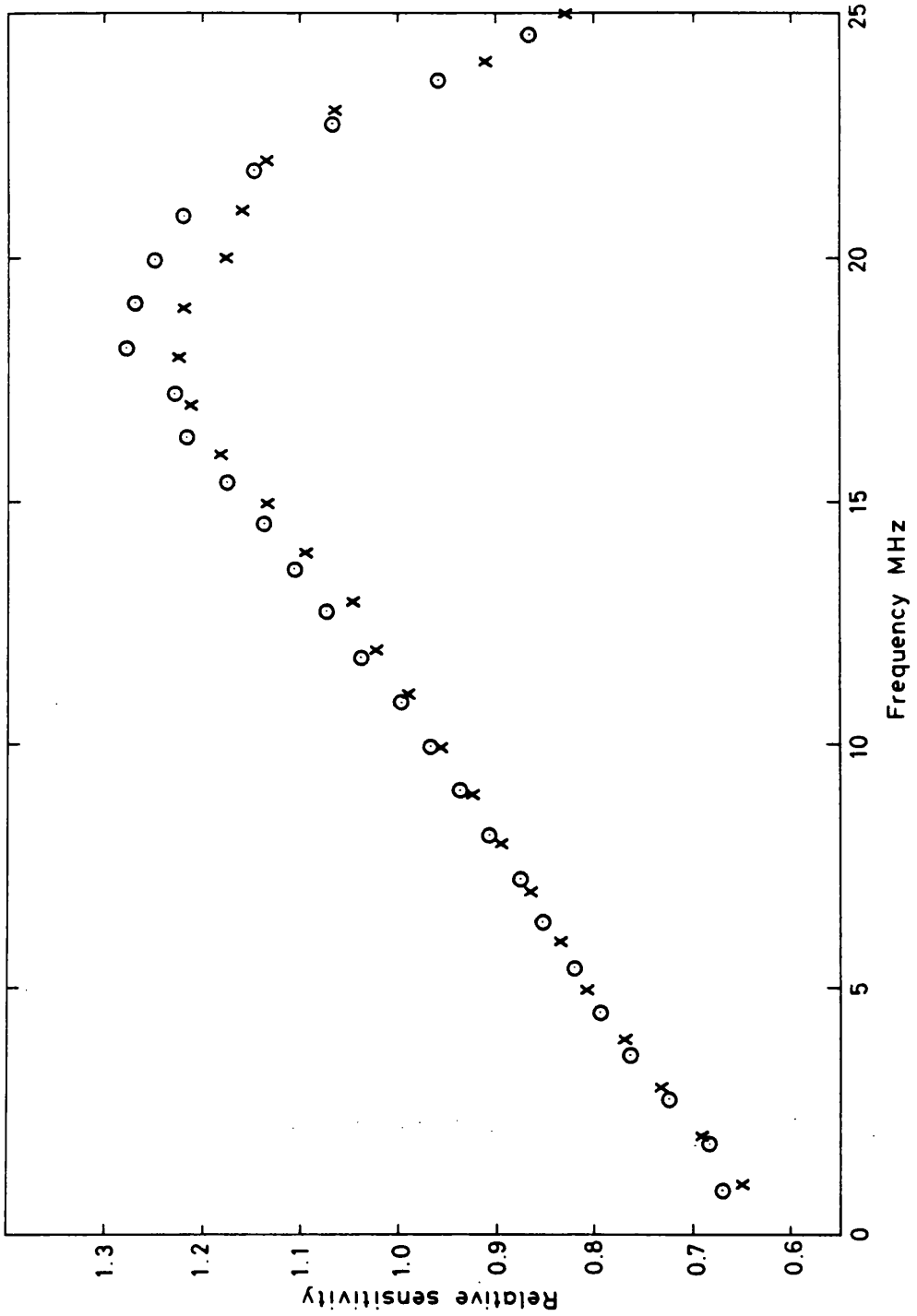

Figure 25 Relative sensitivities of two hydrophones. o measured using a fundamental frequency of 0.9091 MHz, x measured using a fundamental frequency of 1 MHz.

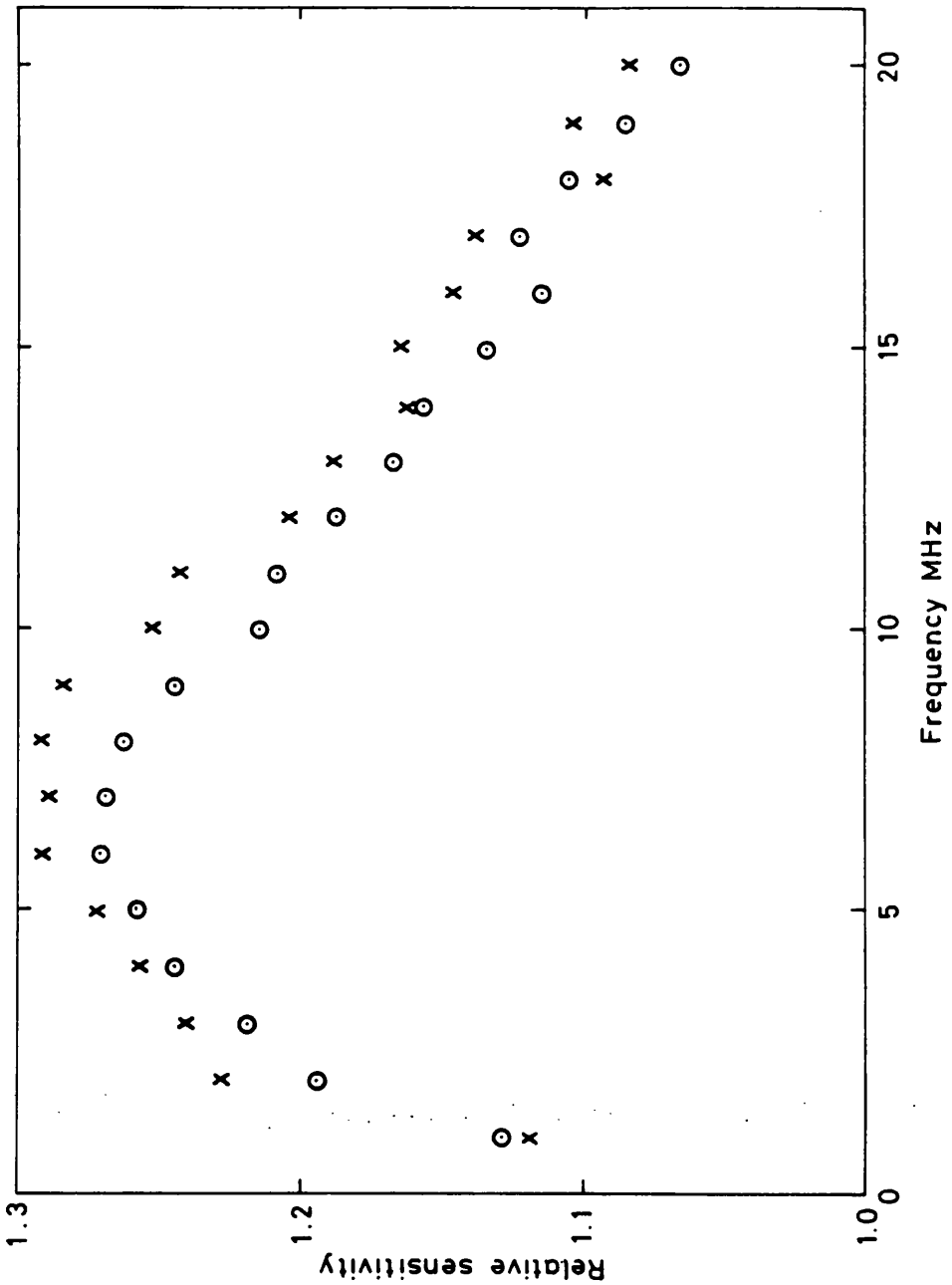

Figure 26 Relative sensitivities of two hydrophones. ⊙ measured using a 20 MHz bandwidth, x measured using a 100 MHz bandwidth.

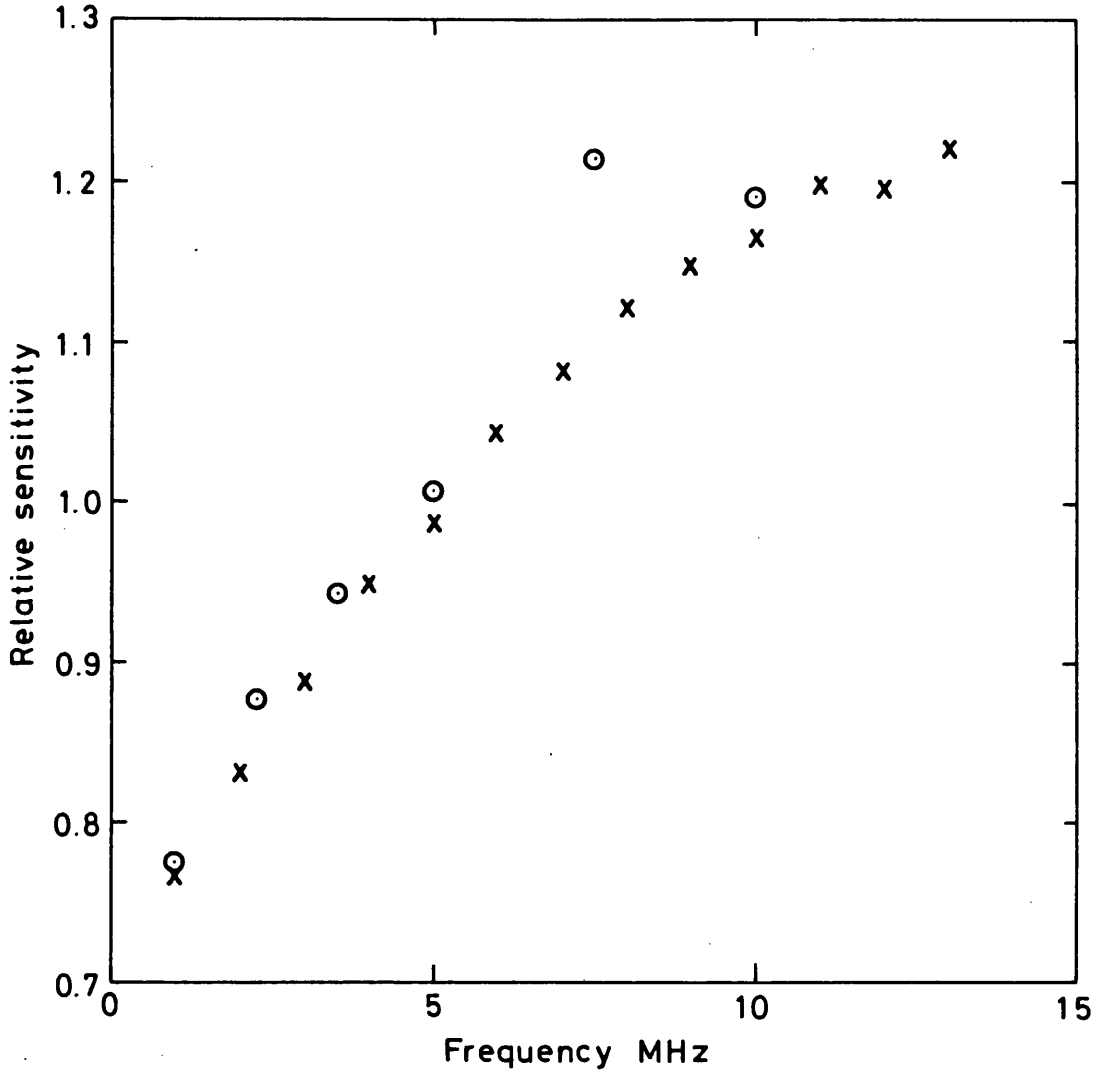

Figure 27a Relative sensitivities of two hydrophones. o measured using a single frequency wave, x measured using a sawtooth wave.

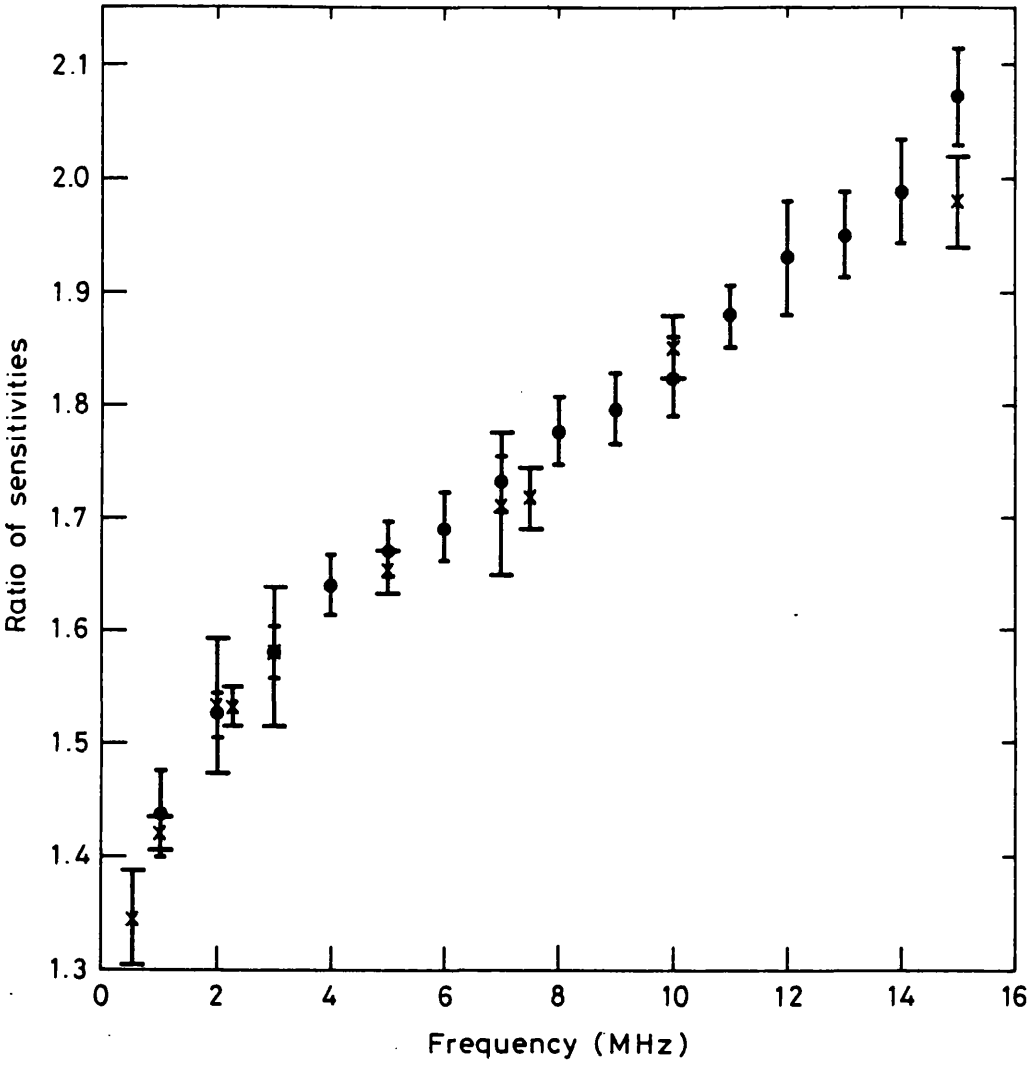

Figure 27b Relative sensitivities of two hydrophones. x measured using a single frequency wave, • measured using a sawtooth wave. The error bars correspond to the random uncertainty at the 95% confidence level.

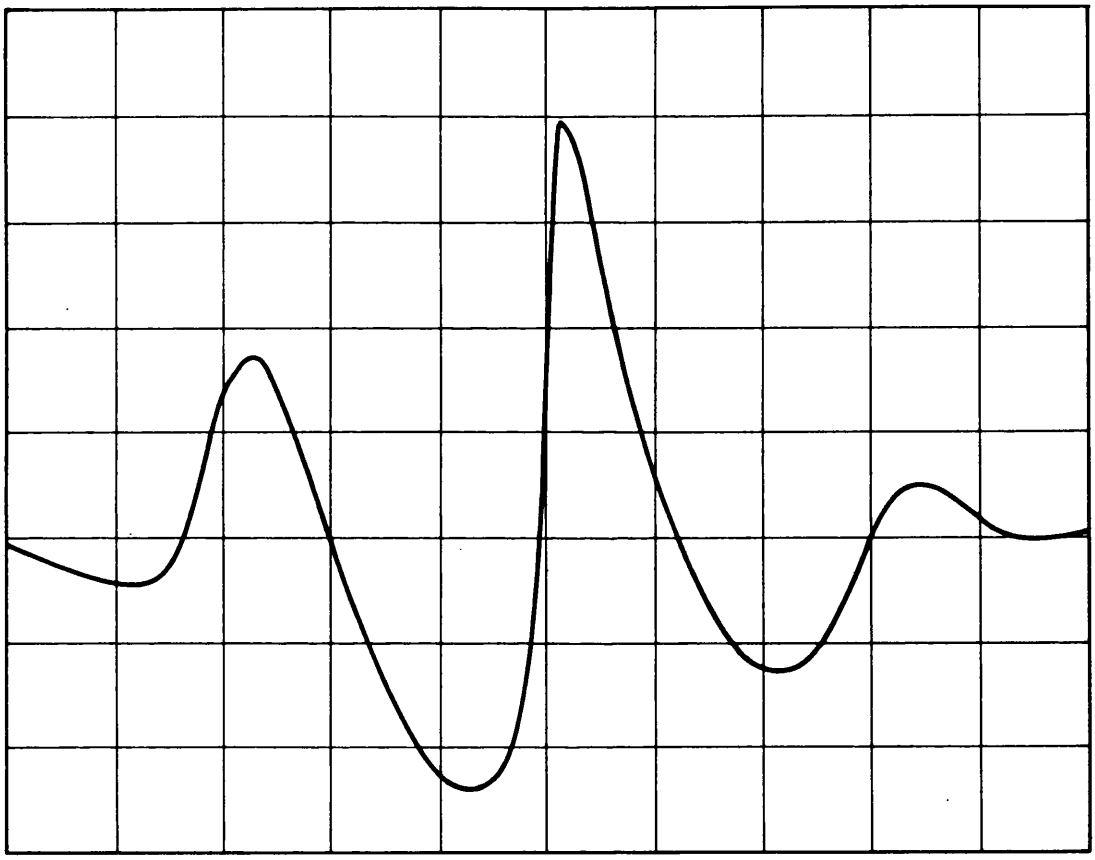

Figure 28 Typical distorted acoustic waveform measured at the focus of the transducer. Time scale: 100 ns/div, vertical scale: 0.72 MPa/div.

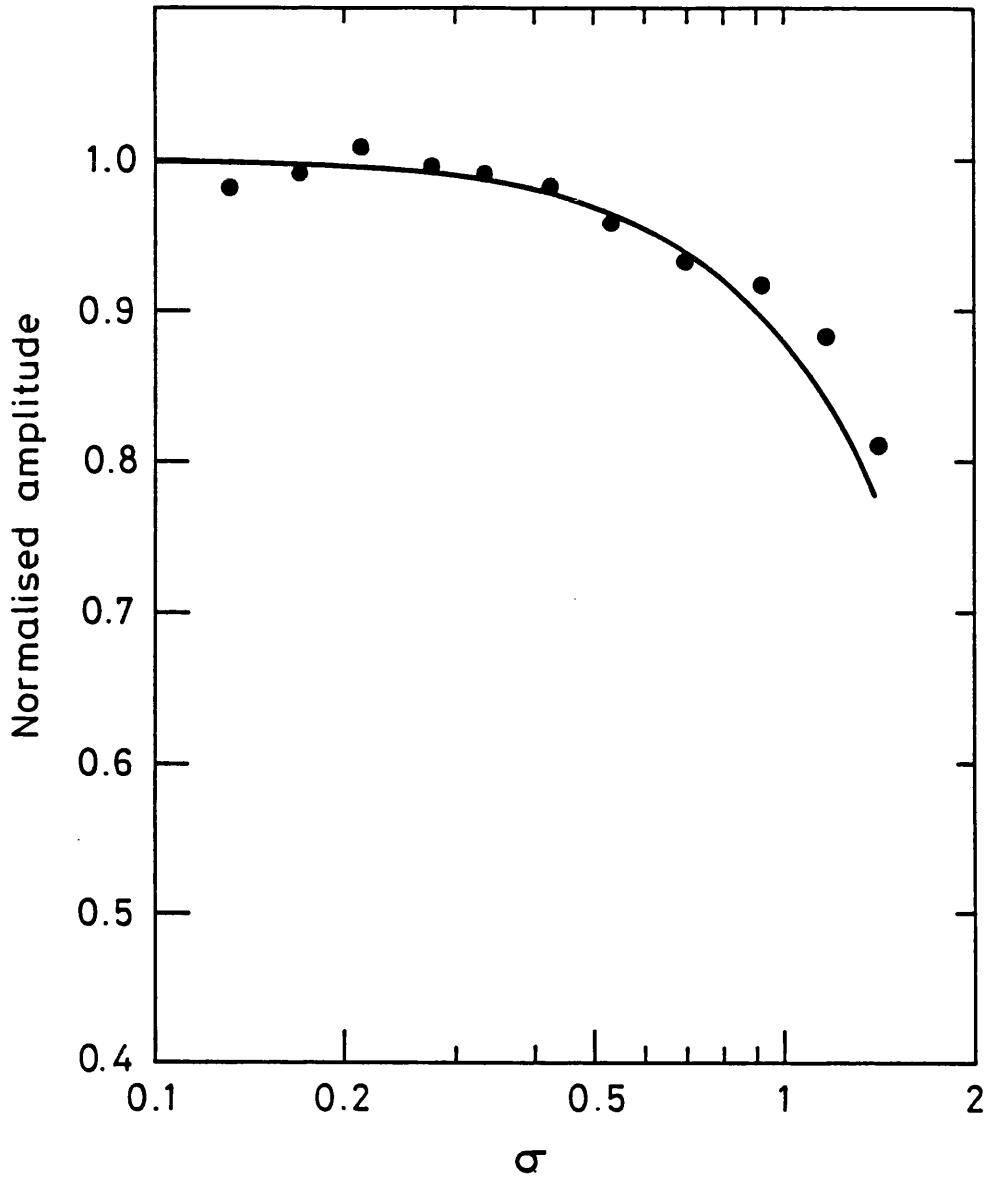

Figure 29 Variation of the pressure amplitude at the fundamental frequency as the source amplitude is varied. The amplitude is normalised to that expected for linear propagation and is measured at the focus for the peak cycle of the pulse. σ is calculated from Equation 2.13. - theory ● measured values.

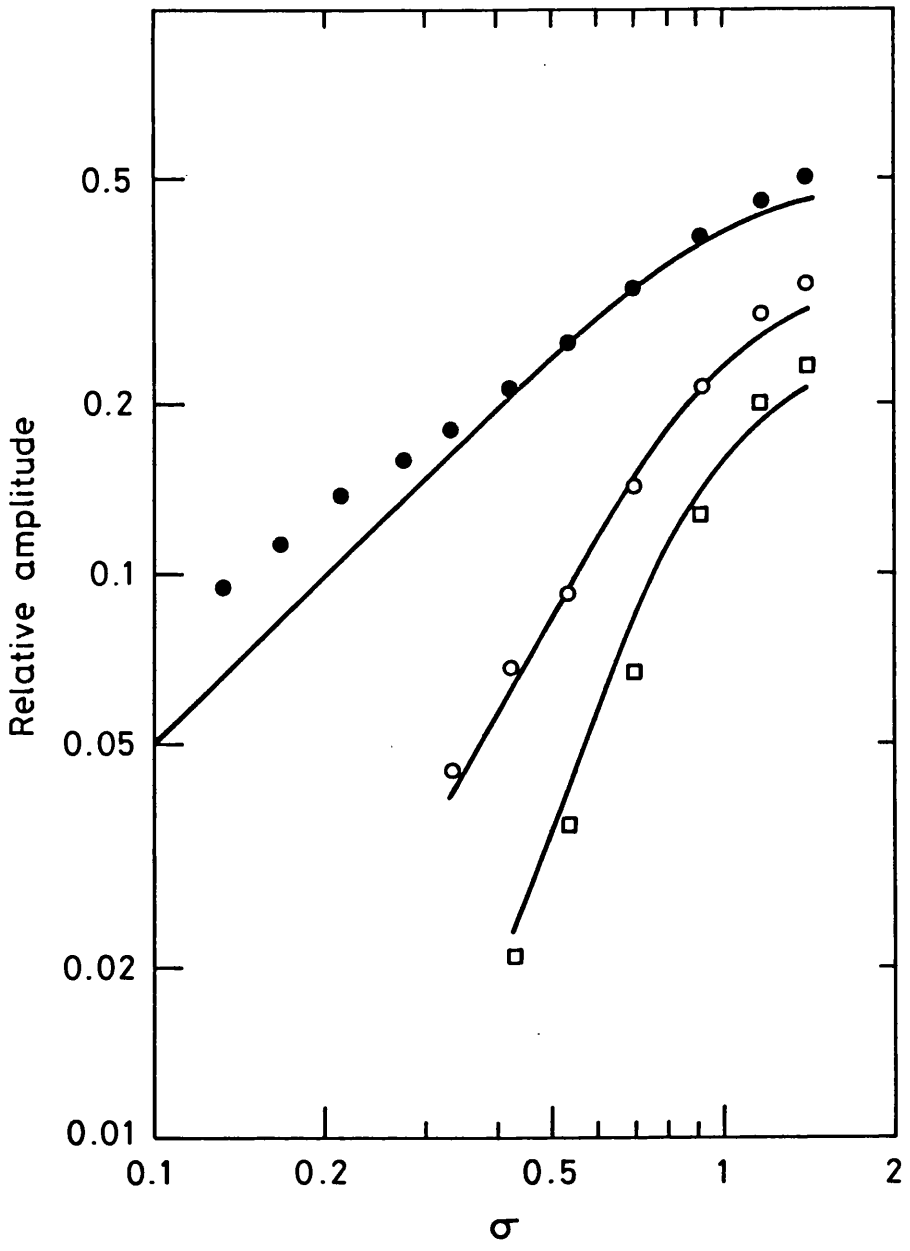

Figure 30 Variation of the amplitudes of the harmonic components as the source amplitude is varied. The values are expressed as fractions of the amplitude of the fundamental frequency and are measured for the peak cycle of the focal waveform. - theory; ●, o, □ experiment, for harmonics 2, 3 and 4 respectively.

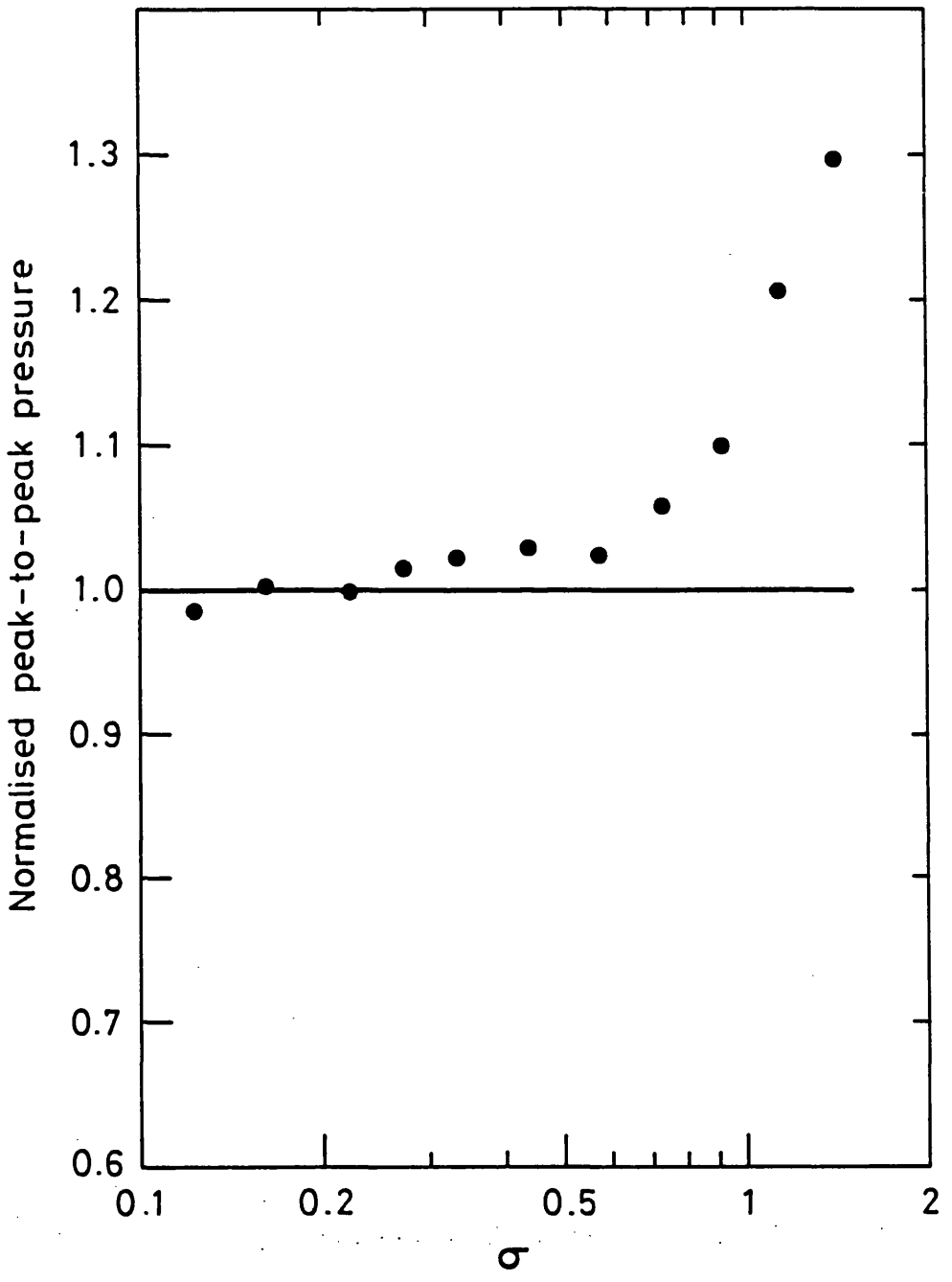

Figure 31 Variation of the peak-to-peak acoustic pressure at the focus. The pressure is normalised to that expected for linear propagation and is equivalent to $P_{o,m}$ (Equation A.6). σ is calculated from Equation 2.13. - theory, • experiment.

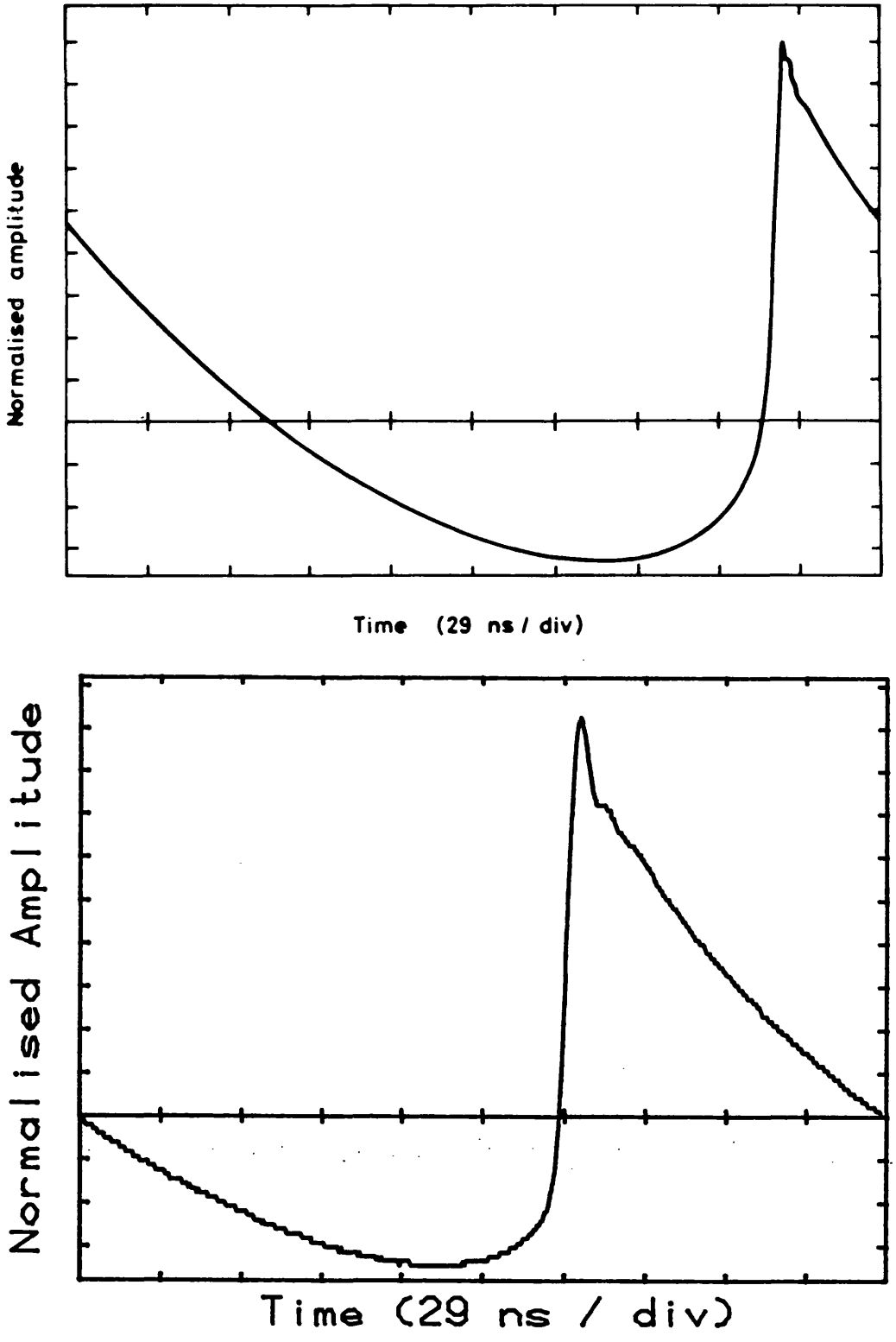

Figure 32 Waveforms for propagation of 3.5 MHz focused ultrasound in water, sigma 1.4. Upper curve: predicted waveform, (section 2.1.4), lower curve: measured waveform.

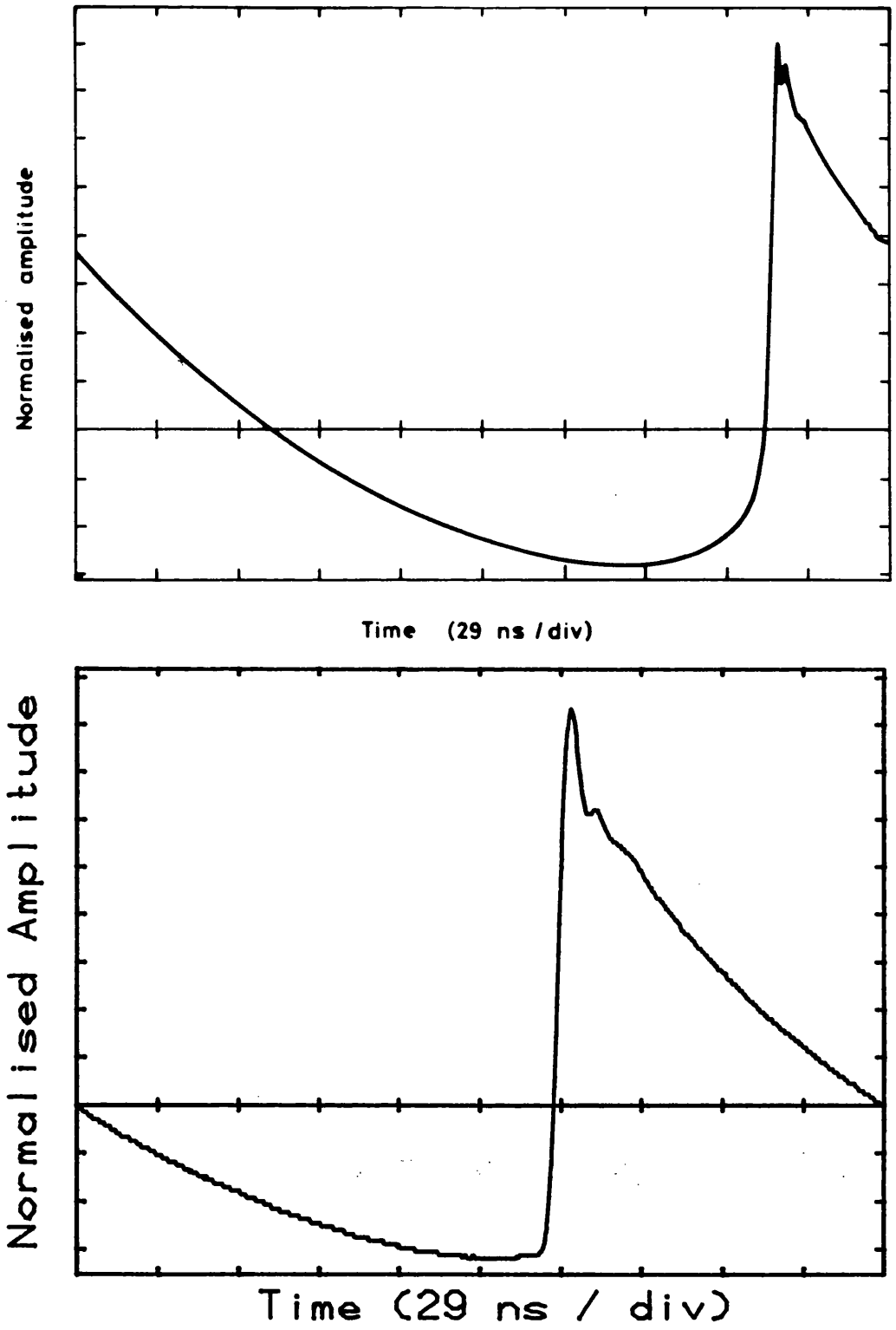

Figure 33 Waveforms for propagation of 3.5 MHz focused ultrasound in water, sigma 2. Upper curve: predicted waveform (section 2.1.4), lower curve: measured waveform.

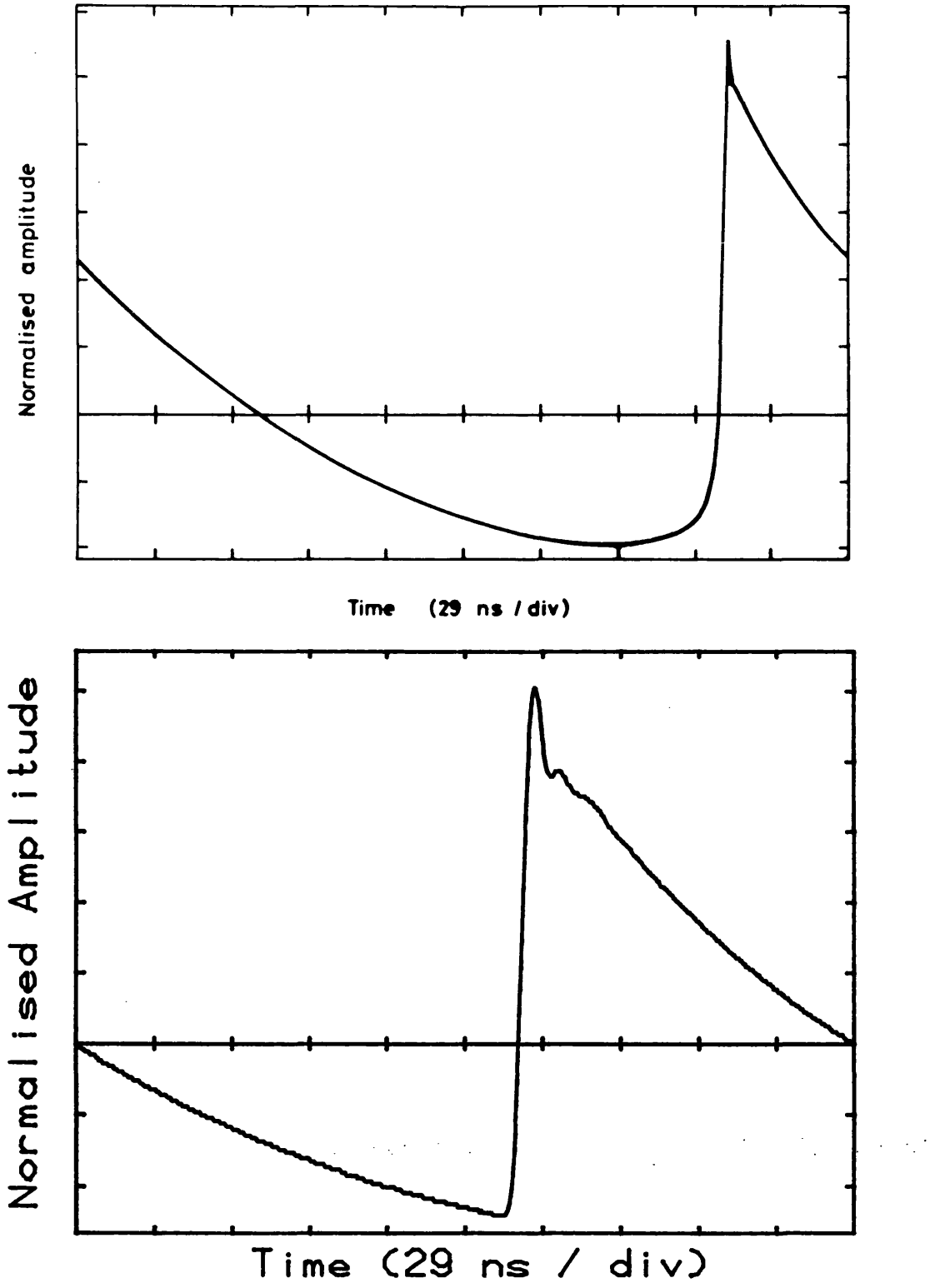

Figure 34 Waveforms for propagation of 3.5 MHz focused ultrasound in water, sigma 3.6. Upper curve: predicted waveform (section 2.1.4), lower curve: measured waveform.

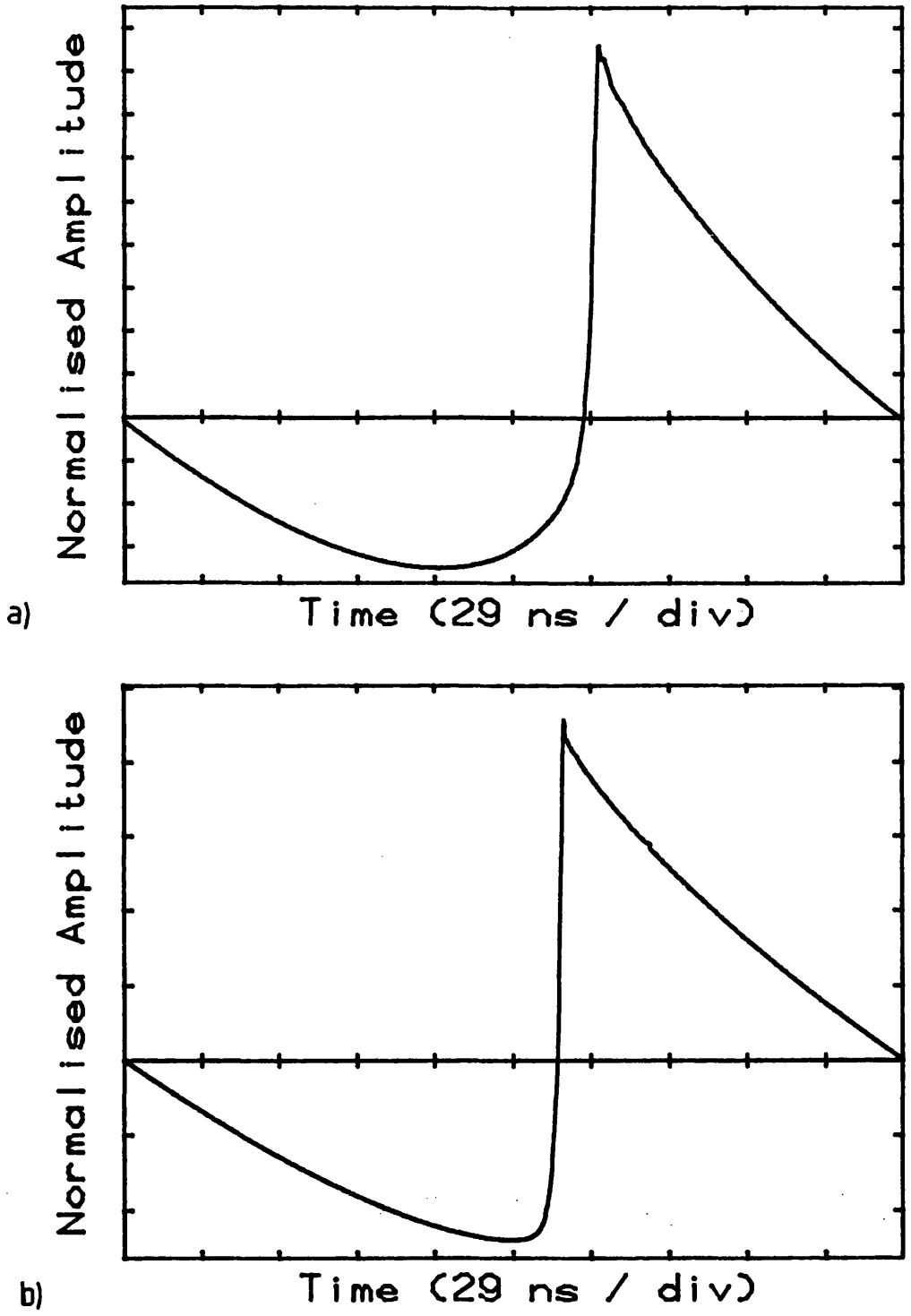

Figure 35 Calculated waveforms for propagation of 3.5 MHz focused ultrasound in water, a) sigma 1.4, b) sigma 3.6. The calculations were performed using the modified theory as described in section 2.2.1.

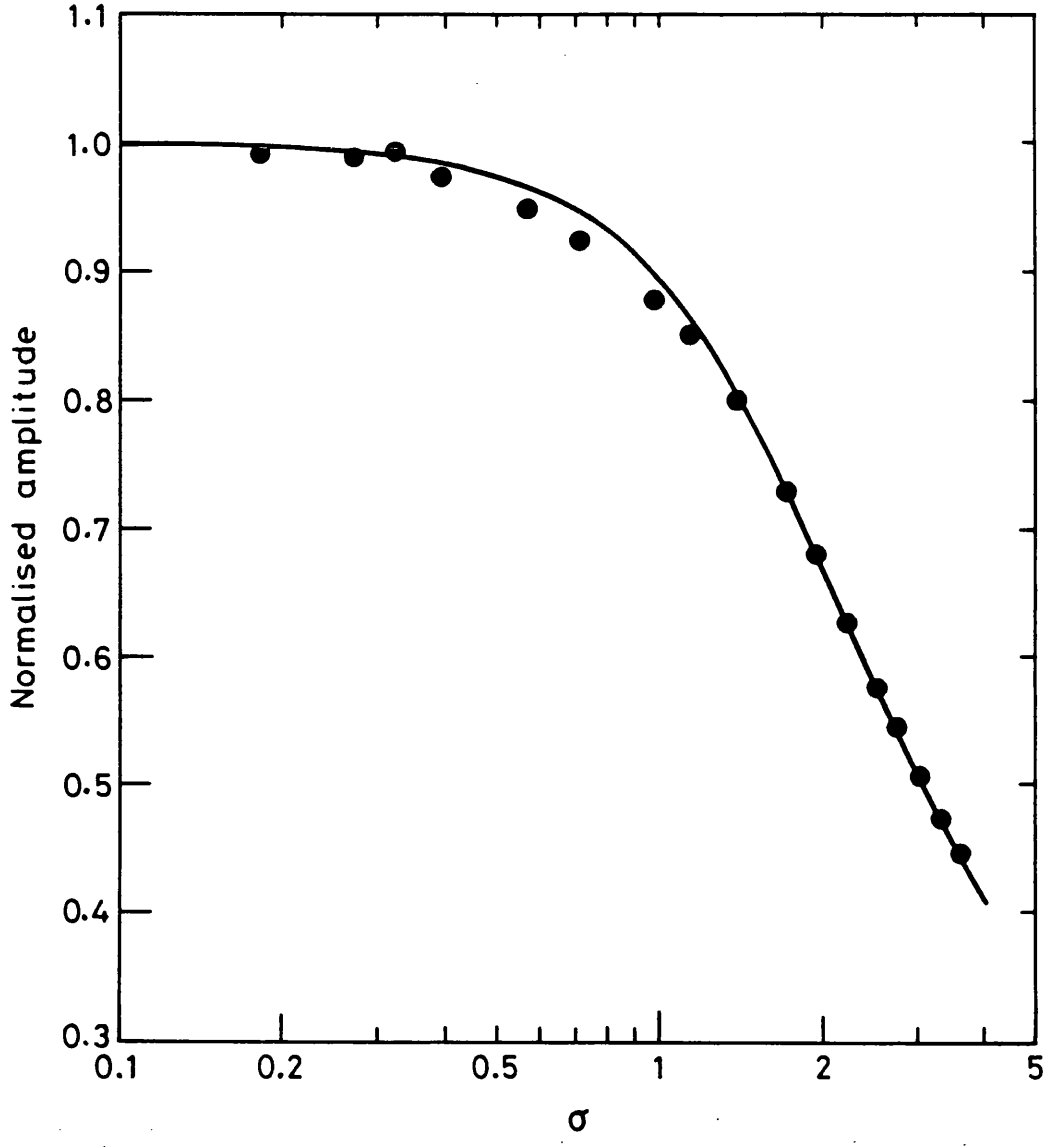

Figure 36 Variation of the amplitude of the fundamental component, normalised to the value expected for linear propagation, for a focused field in water, as a function of sigma. - theory (section 2.1.4), • measured values.

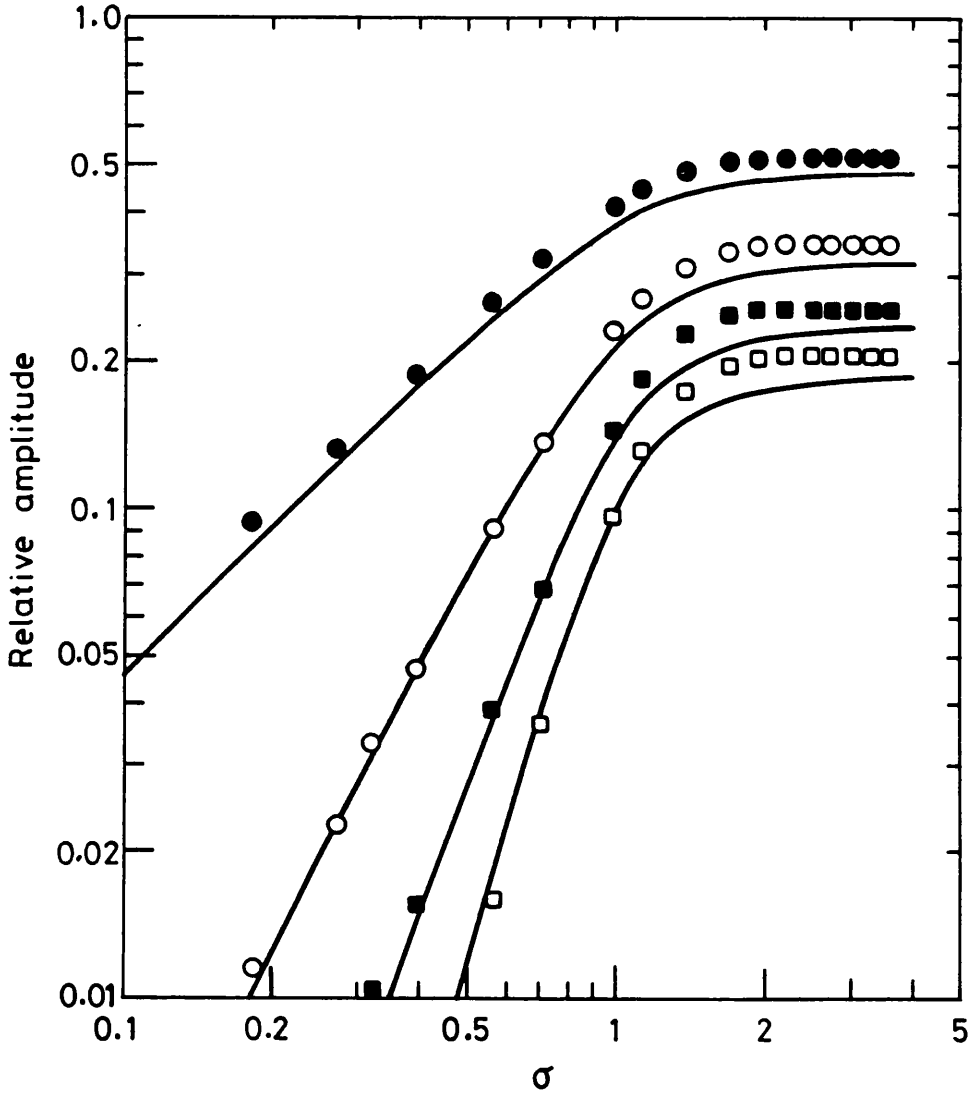

Figure 37 Variation of the amplitude of the harmonic components, normalised to the fundamental amplitude, for a focused field in water, as a function of sigma. - theory (section 2.1.4), ●, o, ■, □ experiment, for harmonics 2, 3, 4 and 5 respectively.

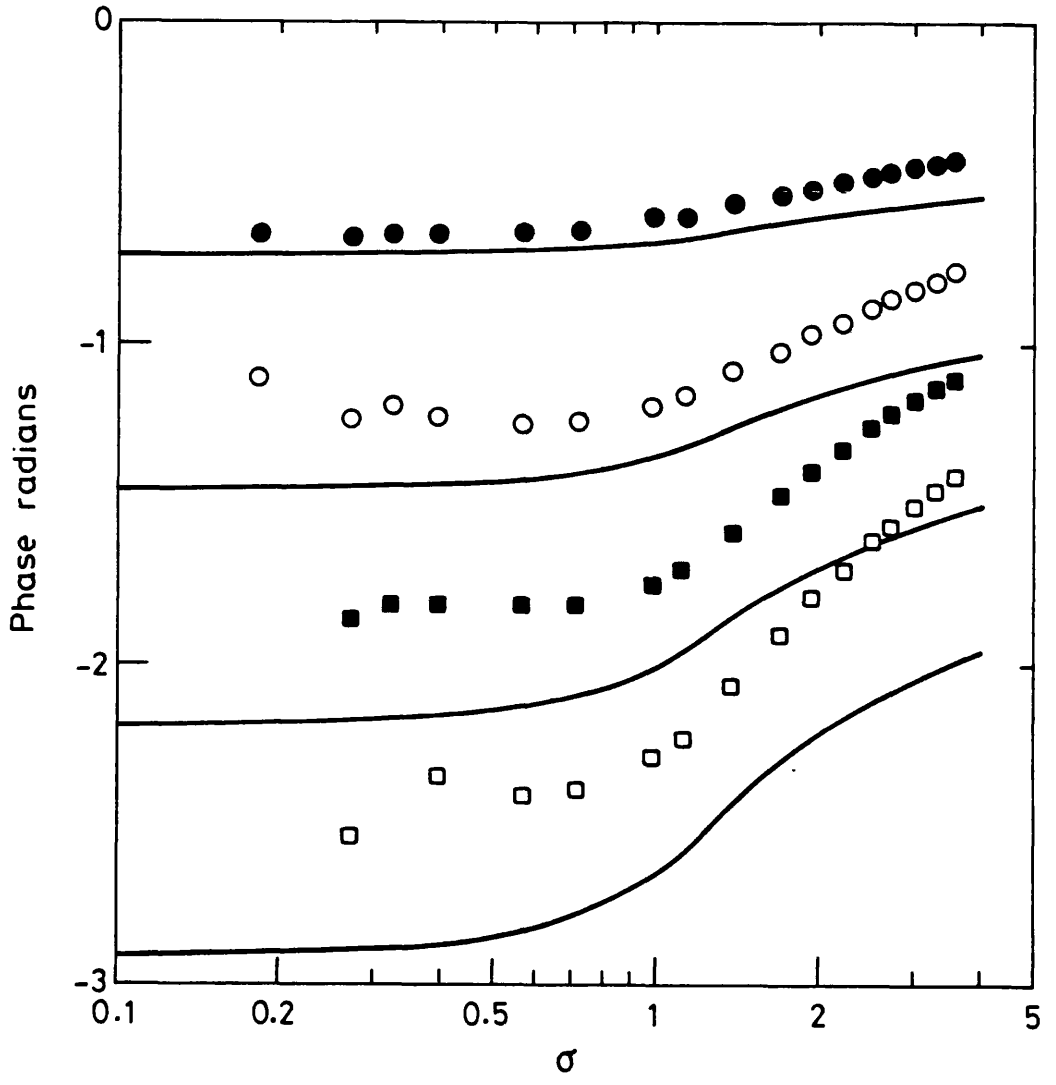

Figure 38 Variation of the phase of the harmonic components relative to the phase of the fundamental, for a focused field in water, as a function of sigma. - theory (section 2.1.4), ●, ○, ■, □ experiment, for harmonics 2, 3, 4 and 5 respectively.

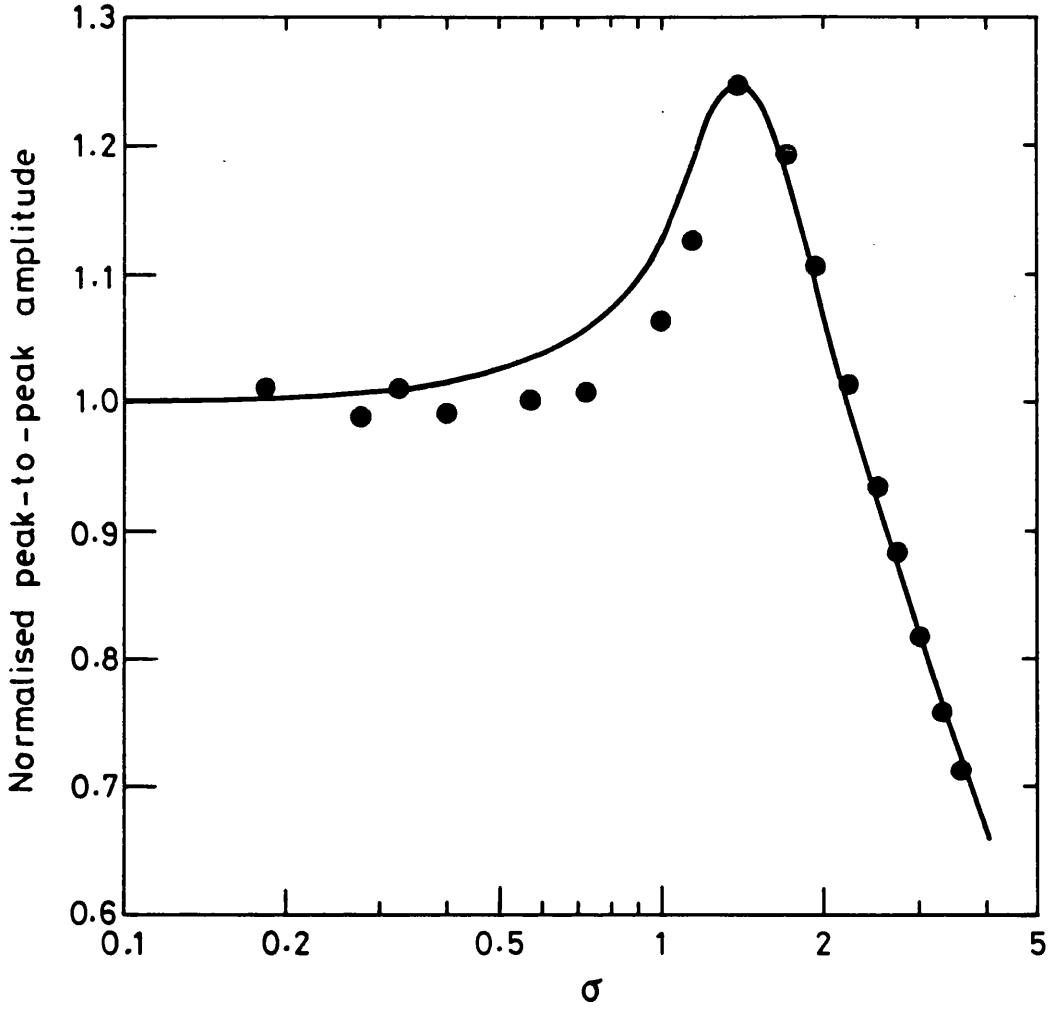

Figure 39 Variation of the peak-to-peak acoustic pressure, normalised to that expected for linear propagation, for a focused field in water, as a function of sigma. - theory, • experiment.

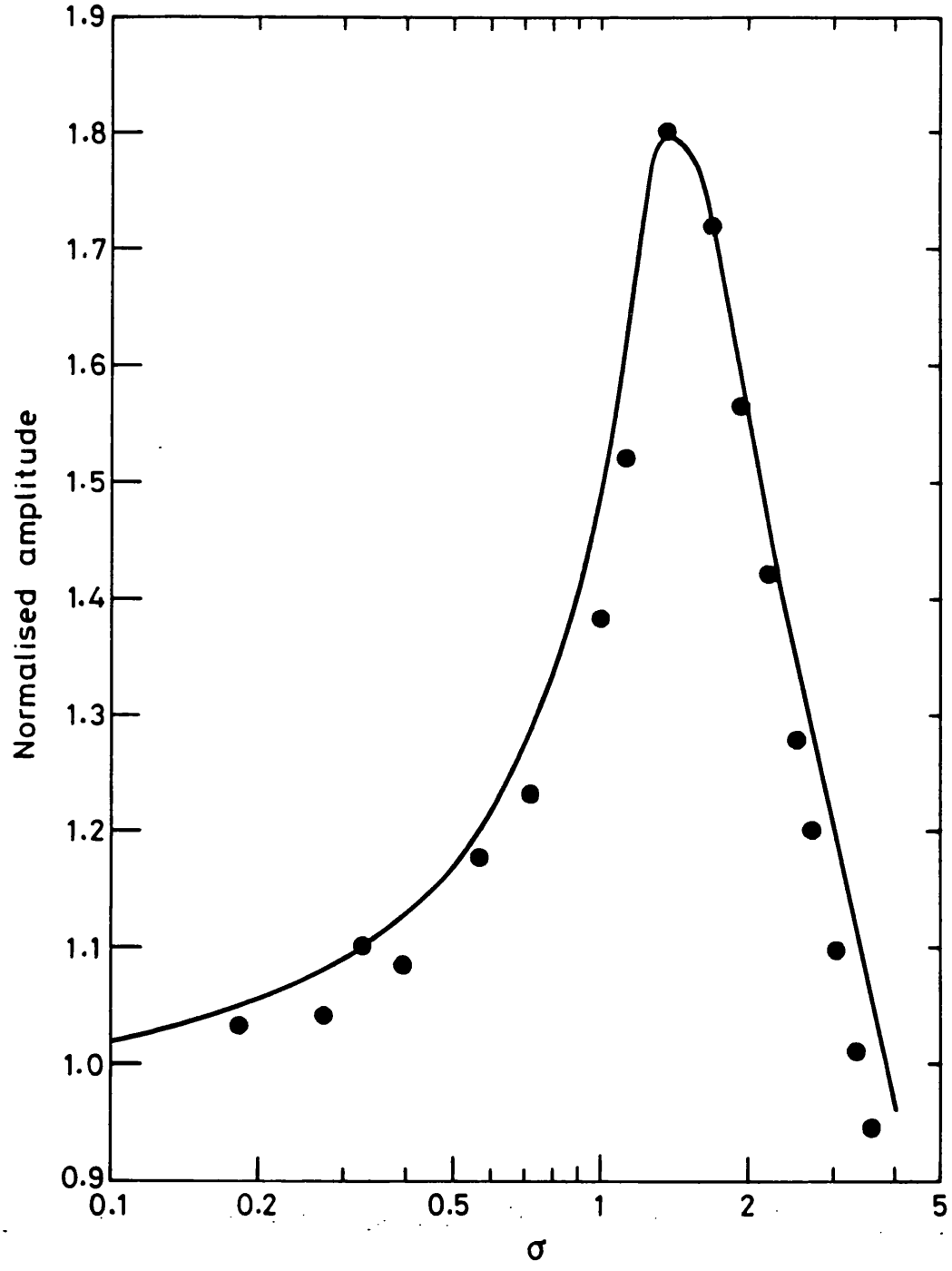

Figure 40 Variation of the peak-positive acoustic pressure, normalised to that expected for linear propagation, for a focused field in water, as a function of sigma. - theory, • experiment.

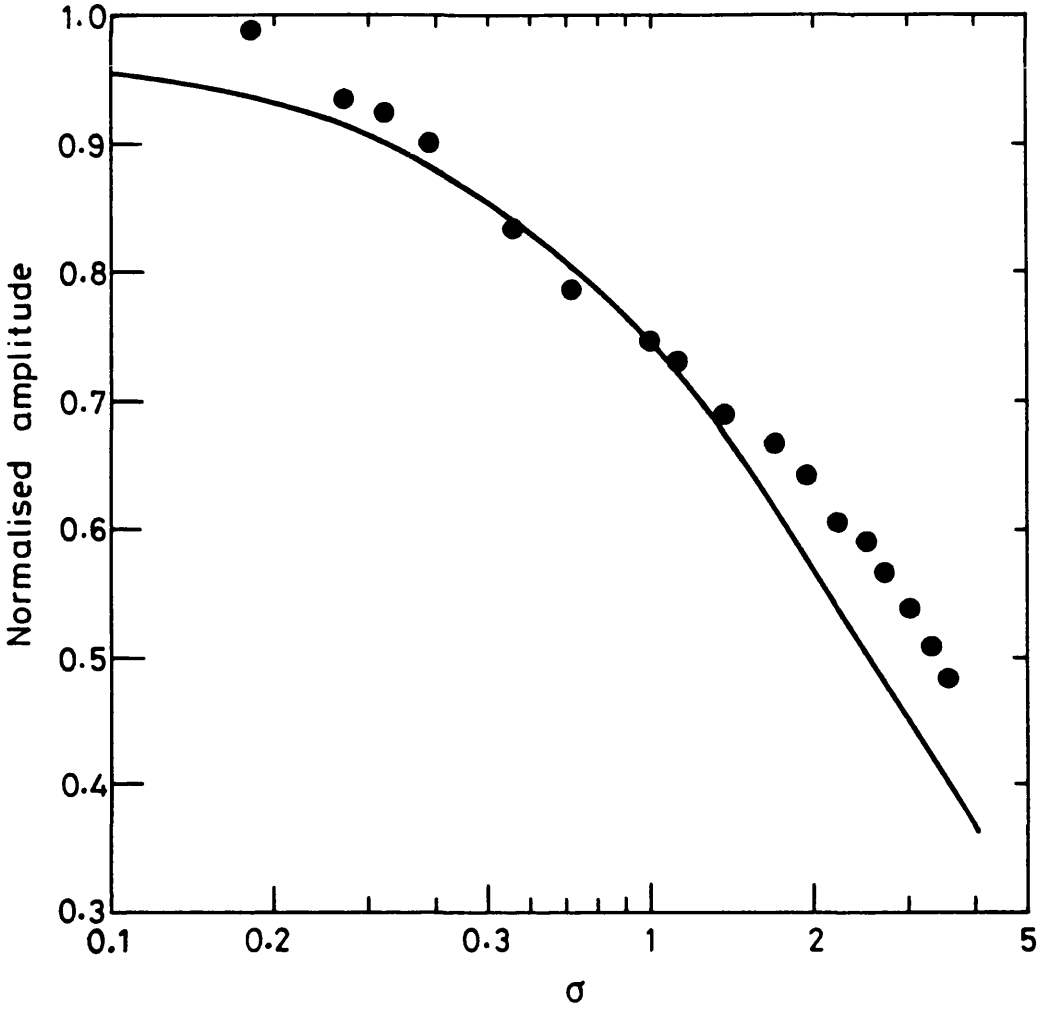

Figure 41 Variation of the peak-negative acoustic pressure, normalised to that expected for linear propagation, for a focused field in water, as a function of sigma. - theory, • experiment.

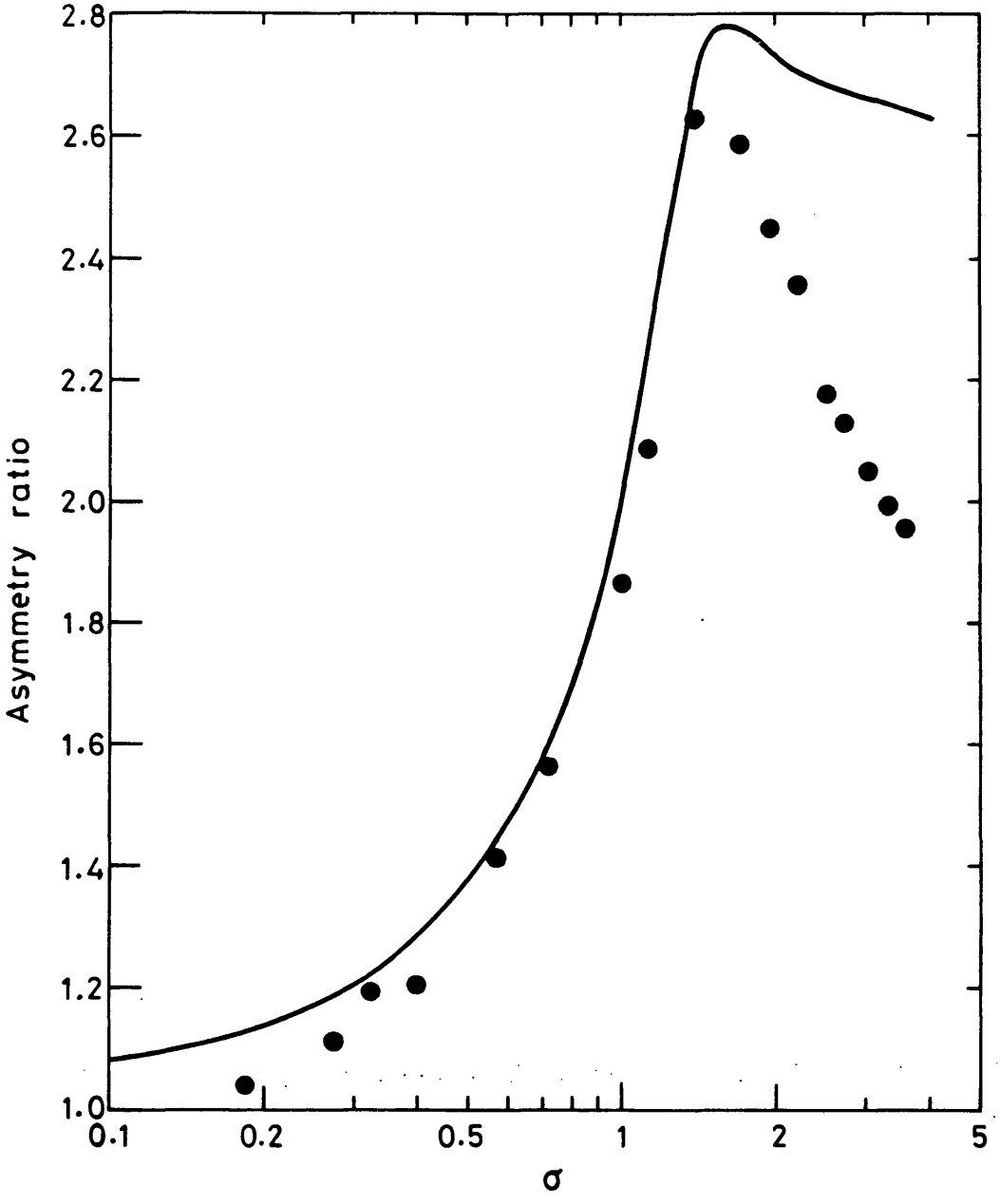

Figure 42a Variation of the asymmetry ratio (p_+/p_-) for a focused field in water, as a function of sigma. - simple theory, • experiment.

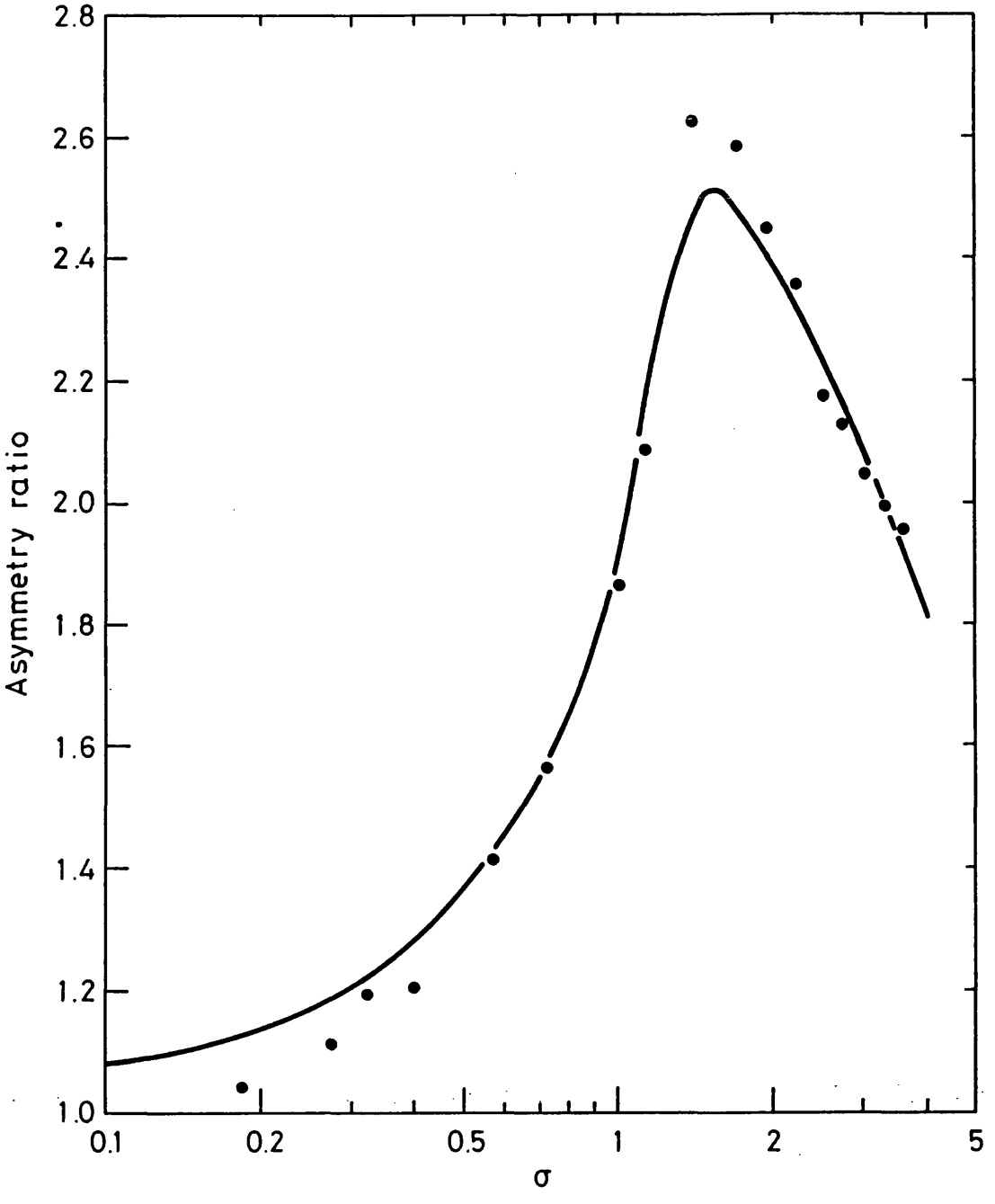

Figure 42b Variation of the asymmetry ratio (p_+/p_-) for a focused field in water, as a function of sigma. - modified theory (section 2.2.1), • experiment.

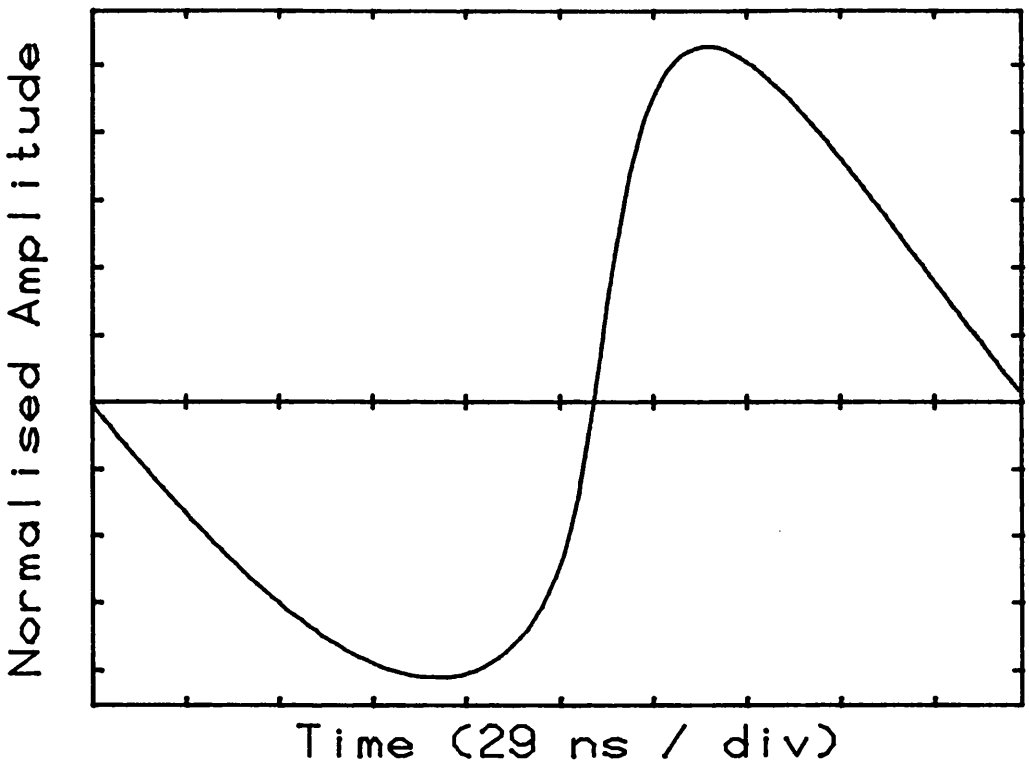

Figure 43a Calculated waveform for propagation of a focused field in tissue for a sigma of 2, according to Equation 2.15, with the dispersion calculated from the attenuation (Equation A.2).

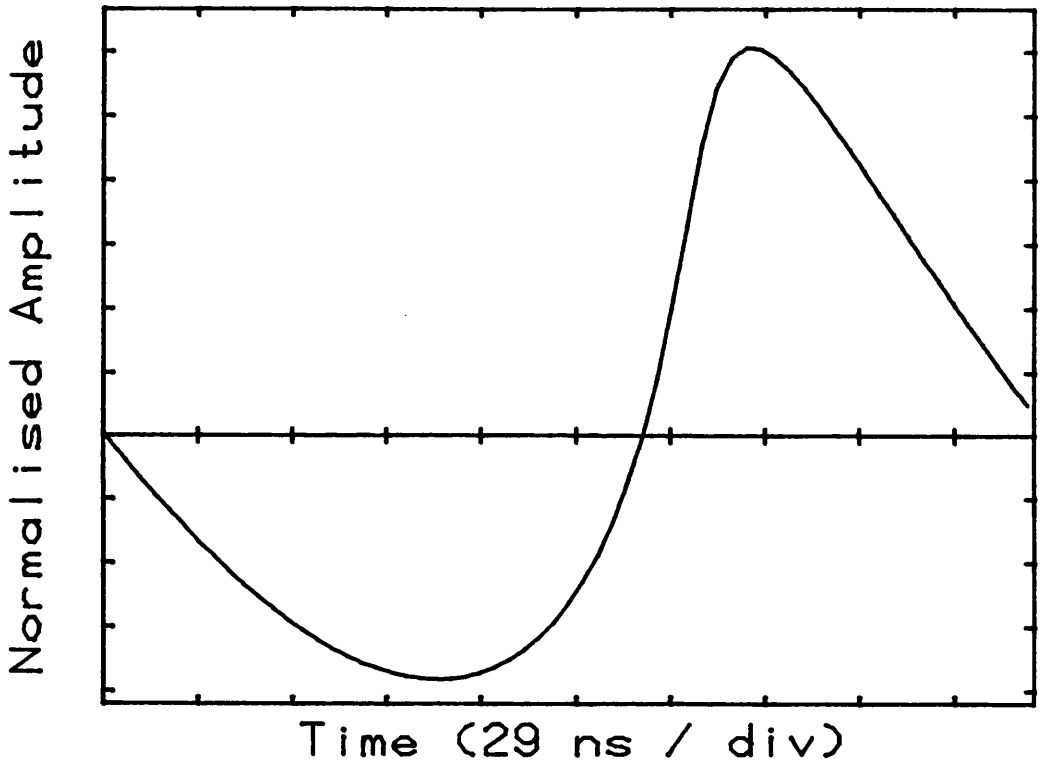

Figure 43b Calculated waveform for propagation of a focused field in tissue for a sigma of 2, according to Equation 2.15, with the dispersion set equal to zero.

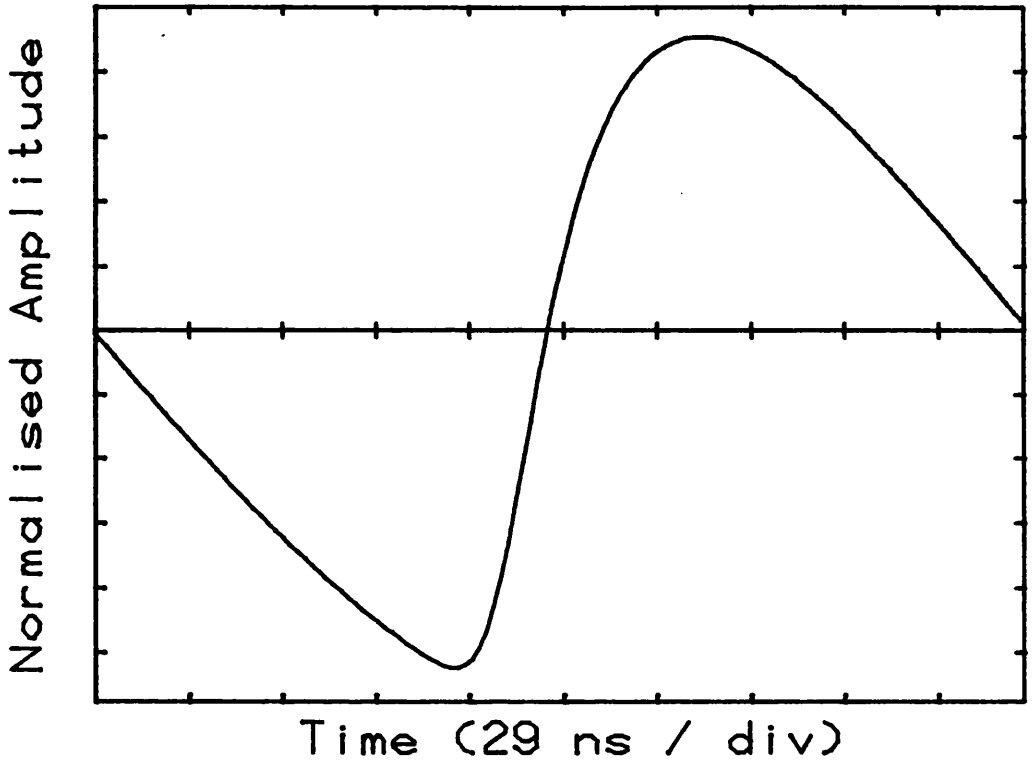

Figure 43c Calculated waveform for propagation of a focused field in tissue for a sigma of 2, according to Equation 2.15, with the dispersion equal to the value given by Wells.

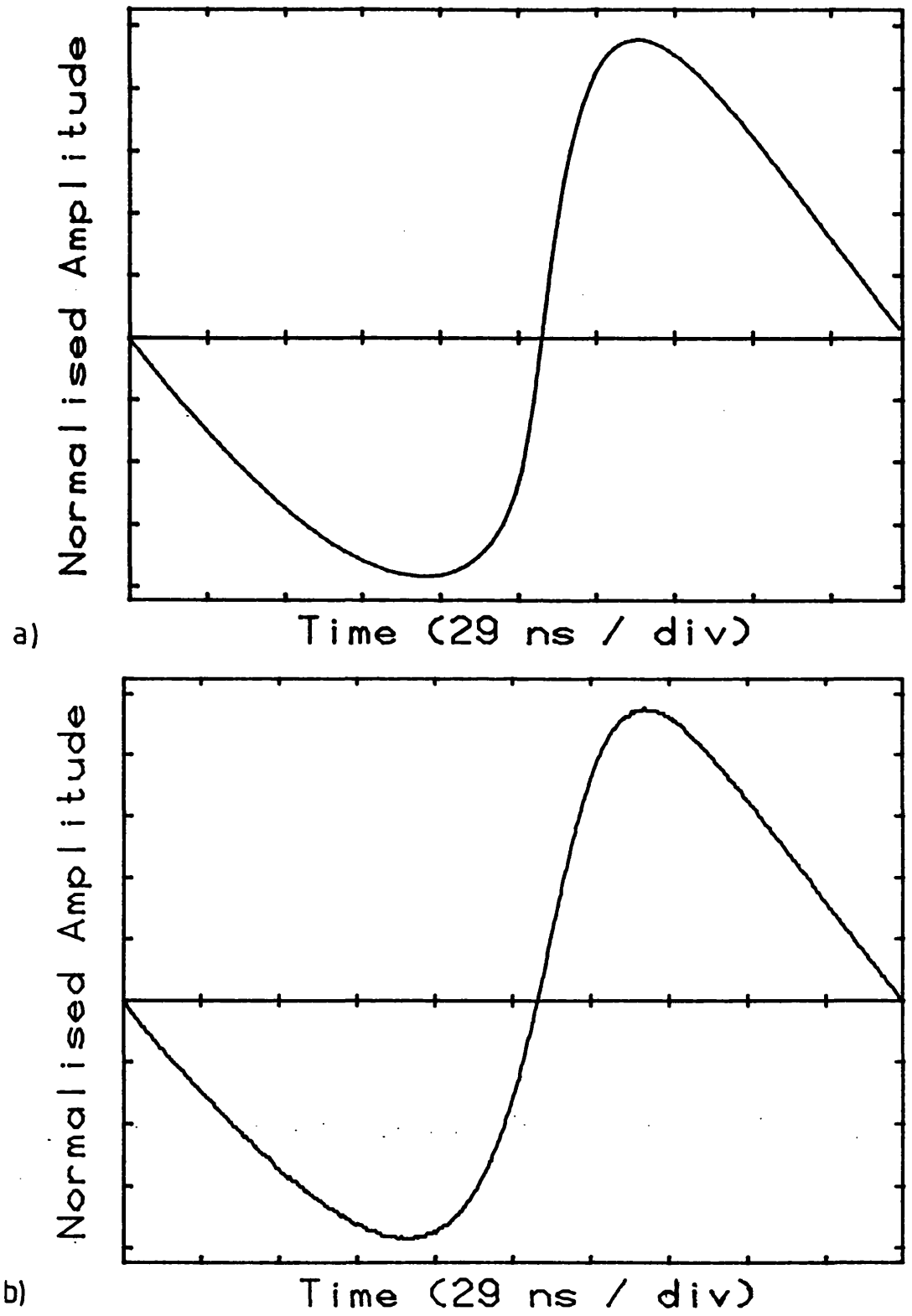

Figure 44 Waveforms for propagation of a focused field in gel for a sigma of 4: a) calculated from Equation 2.15; b) measured.

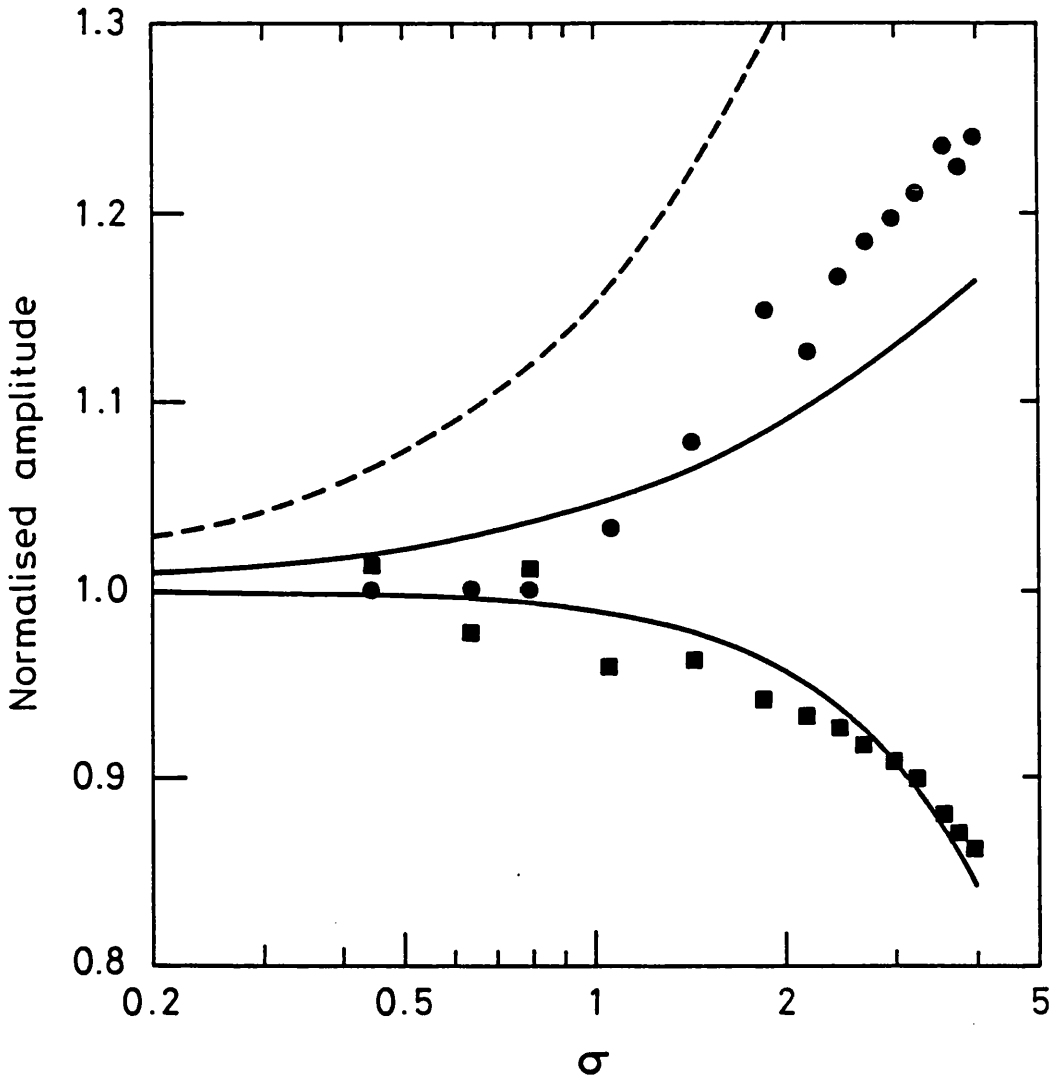

Figure 45 Variation of the asymmetry and normalised peak-to-peak amplitude for a focused field propagating in gel, as a function of sigma. Upper solid curve: calculated asymmetry, lower curve: calculated peak-to-peak amplitude, dashed curve: calculated asymmetry if dispersion is neglected, circles: measured asymmetry, squares: measured peak-to-peak amplitude.

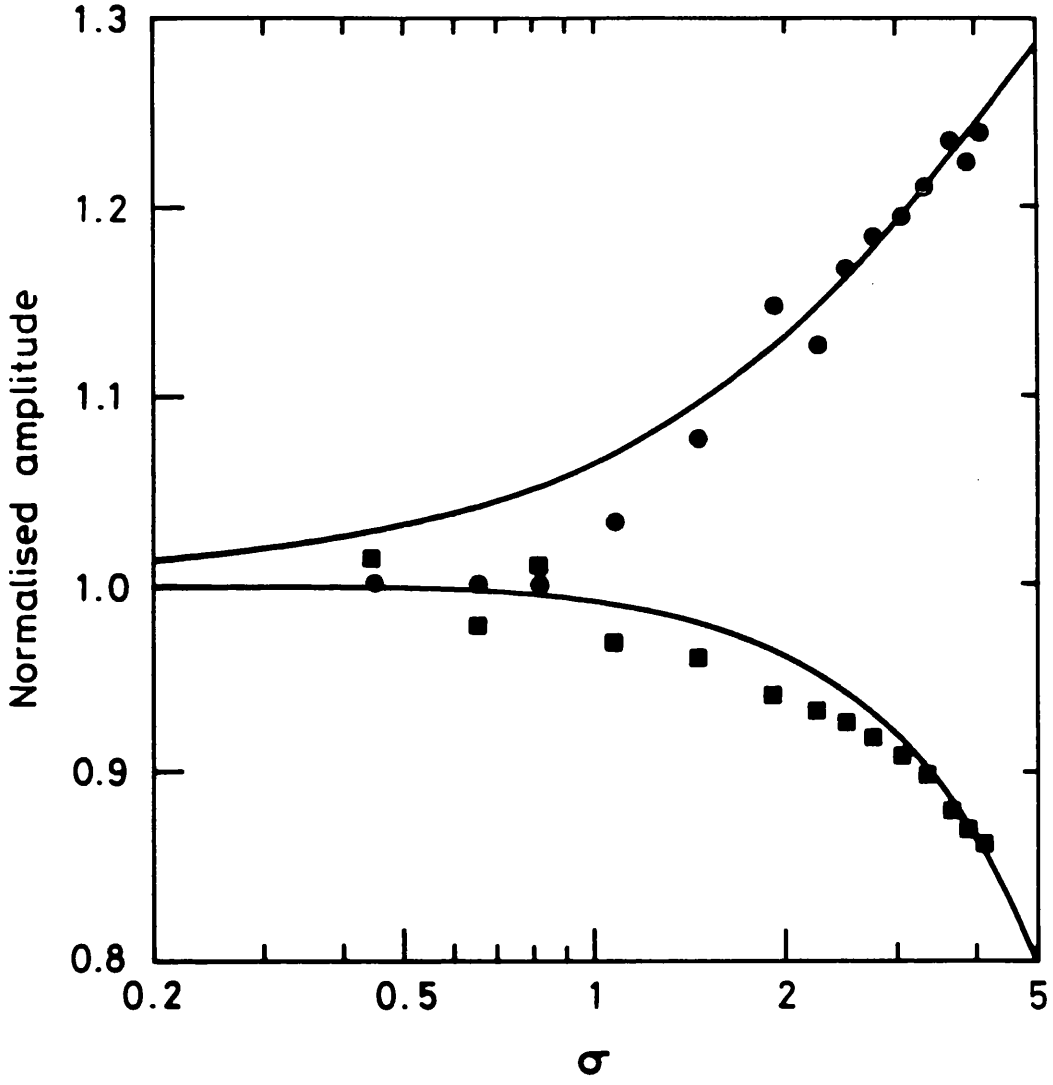

Figure 46 Variation of the asymmetry and normalised peak-to-peak amplitude for a focused field propagating in gel, as a function of sigma. The focal gain used was obtained by calculating the beam profile at the focus. Upper curve: calculated asymmetry, lower curve: calculated amplitude, ● measured asymmetry, ■ measured amplitude.

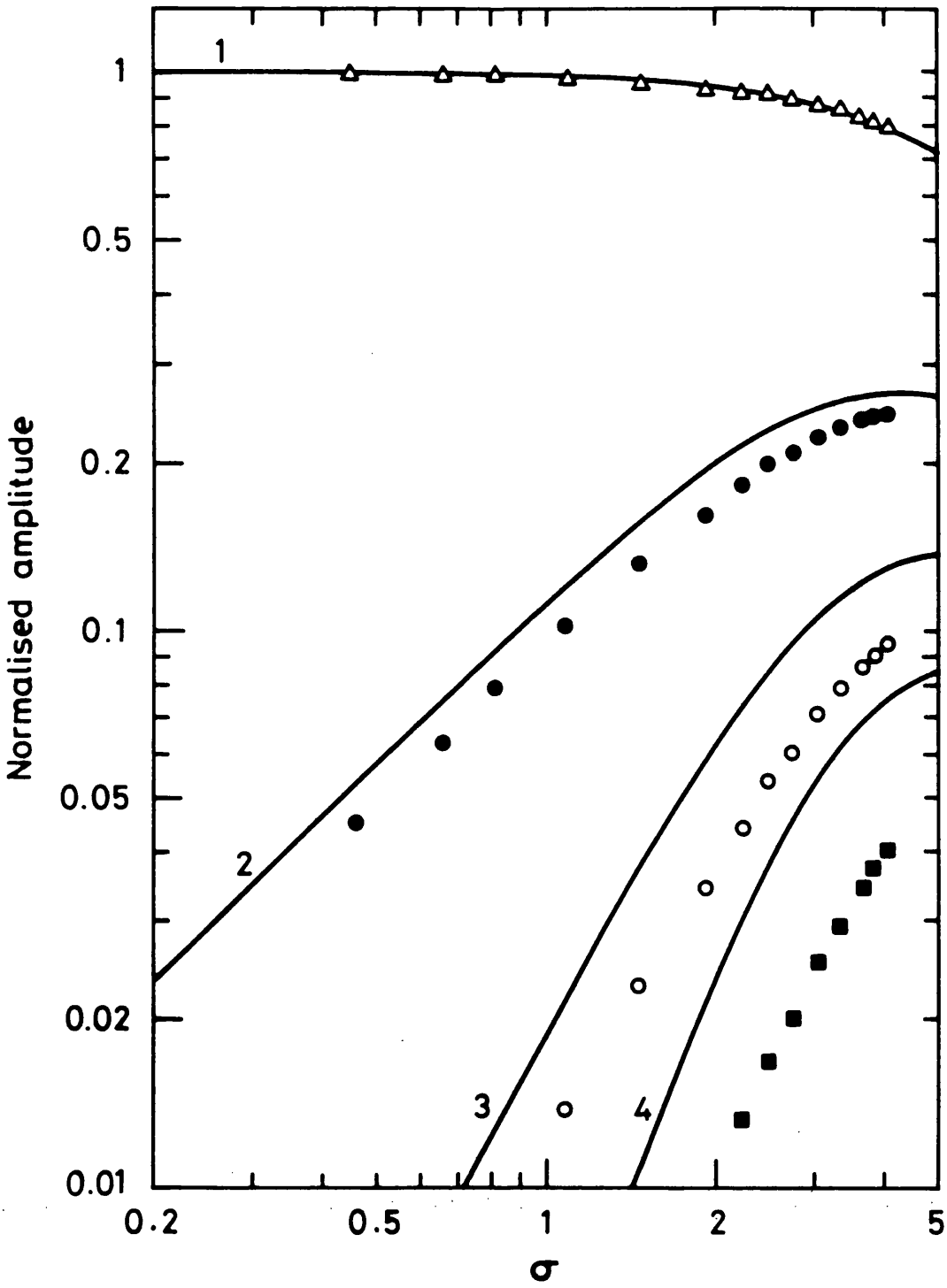

Figure 47 Variation of the amplitude of the first four harmonics, normalised to the value of the fundamental amplitude expected for linear behaviour, for propagation of a focused field in gel. - theory (harmonic number as indicated on the curve), symbols: measured values.

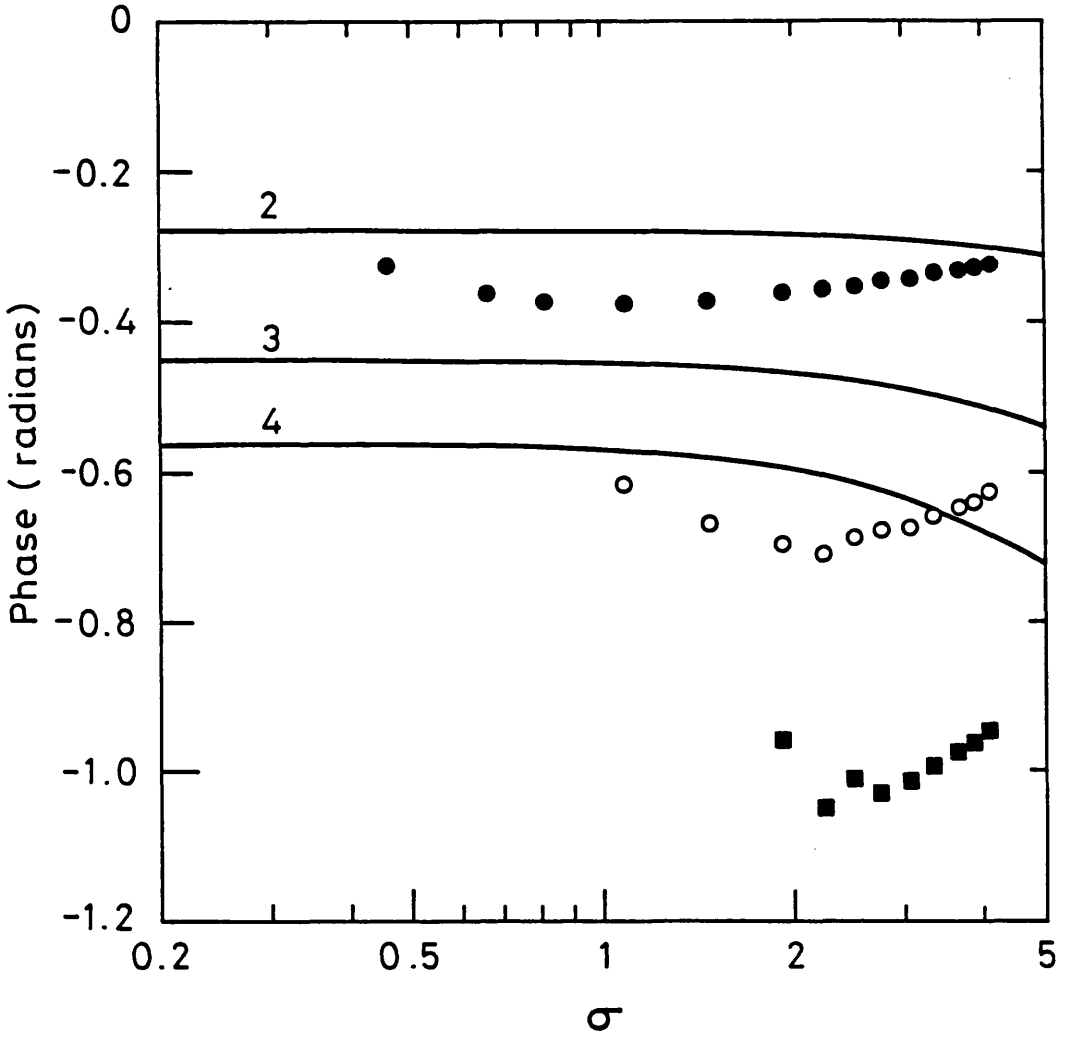

Figure 48 Variation of the phase of the second, third and fourth harmonics relative to that of the fundamental, for propagation of a focused field in gel. - calculated phases (harmonic number as indicated), symbols: measured values.

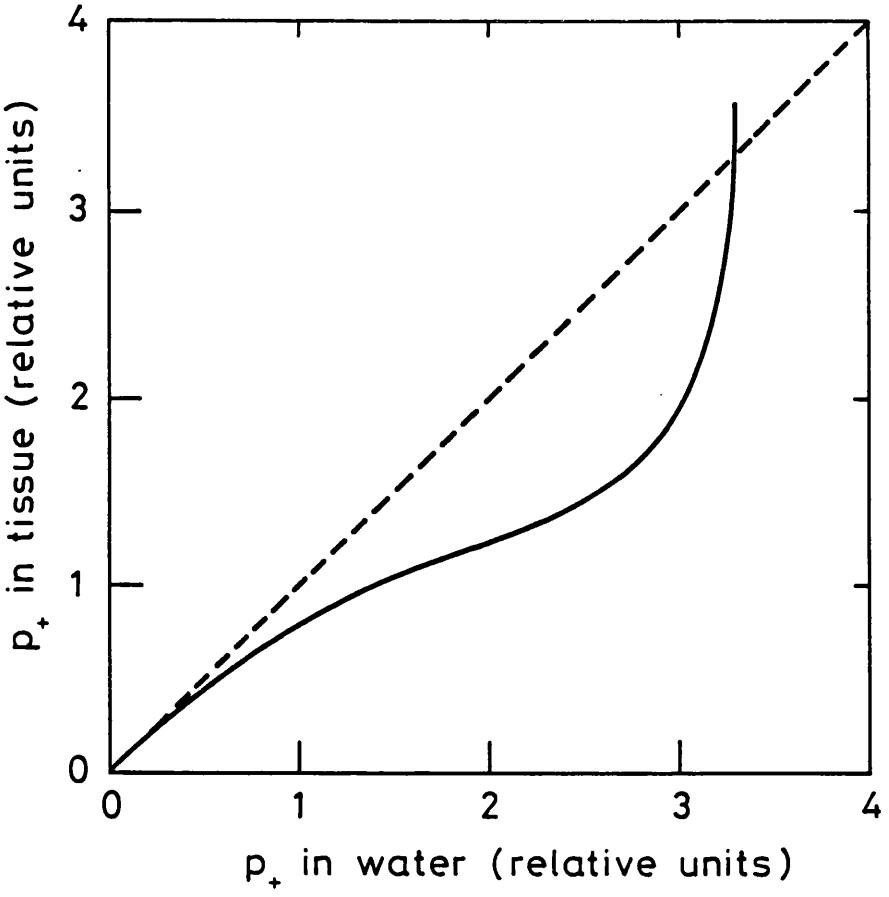

Figure 49 Variation of the calculated peak-positive pressure in tissue as a function of the corresponding value for propagation in water, for a focused field. The dashed line corresponds to the linear behaviour.

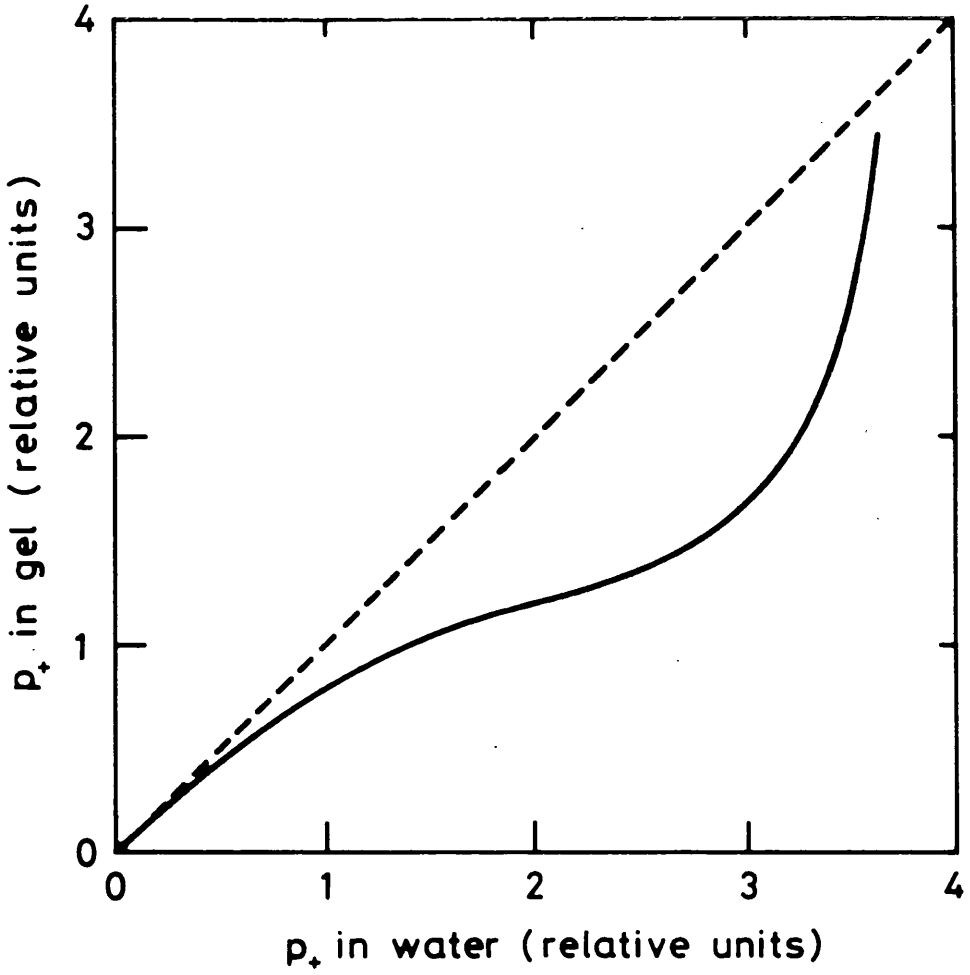

Figure 50 Variation of the measured peak-positive pressure in gel as a function of the corresponding value for propagation in water, for a focused field. Again, the dashed curve corresponds to the predictions of linear theory.

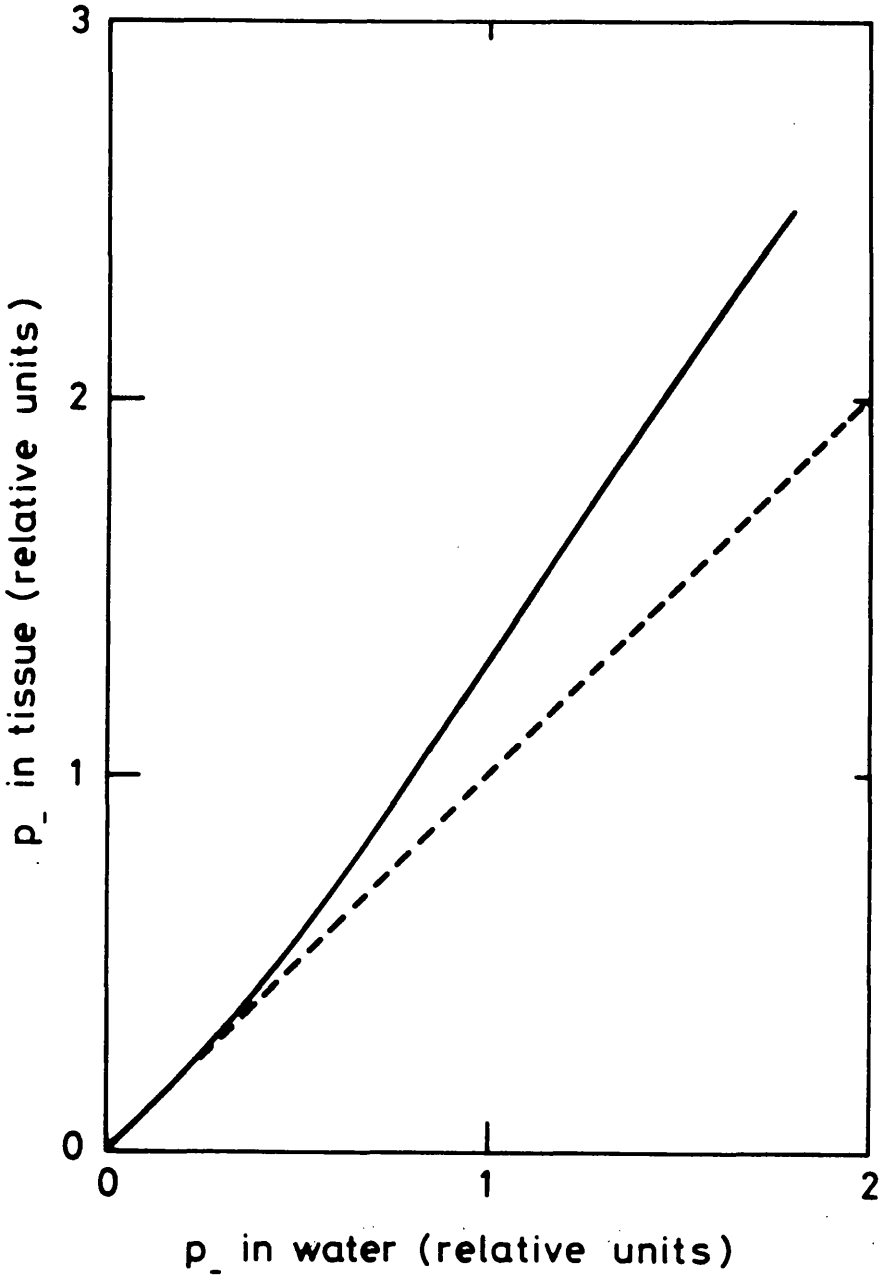

Figure 51 Variation of the calculated peak-negative pressure in tissue as a function of the corresponding value for propagation in water, for a focused field. The dashed curve corresponds to the predictions of linear theory.

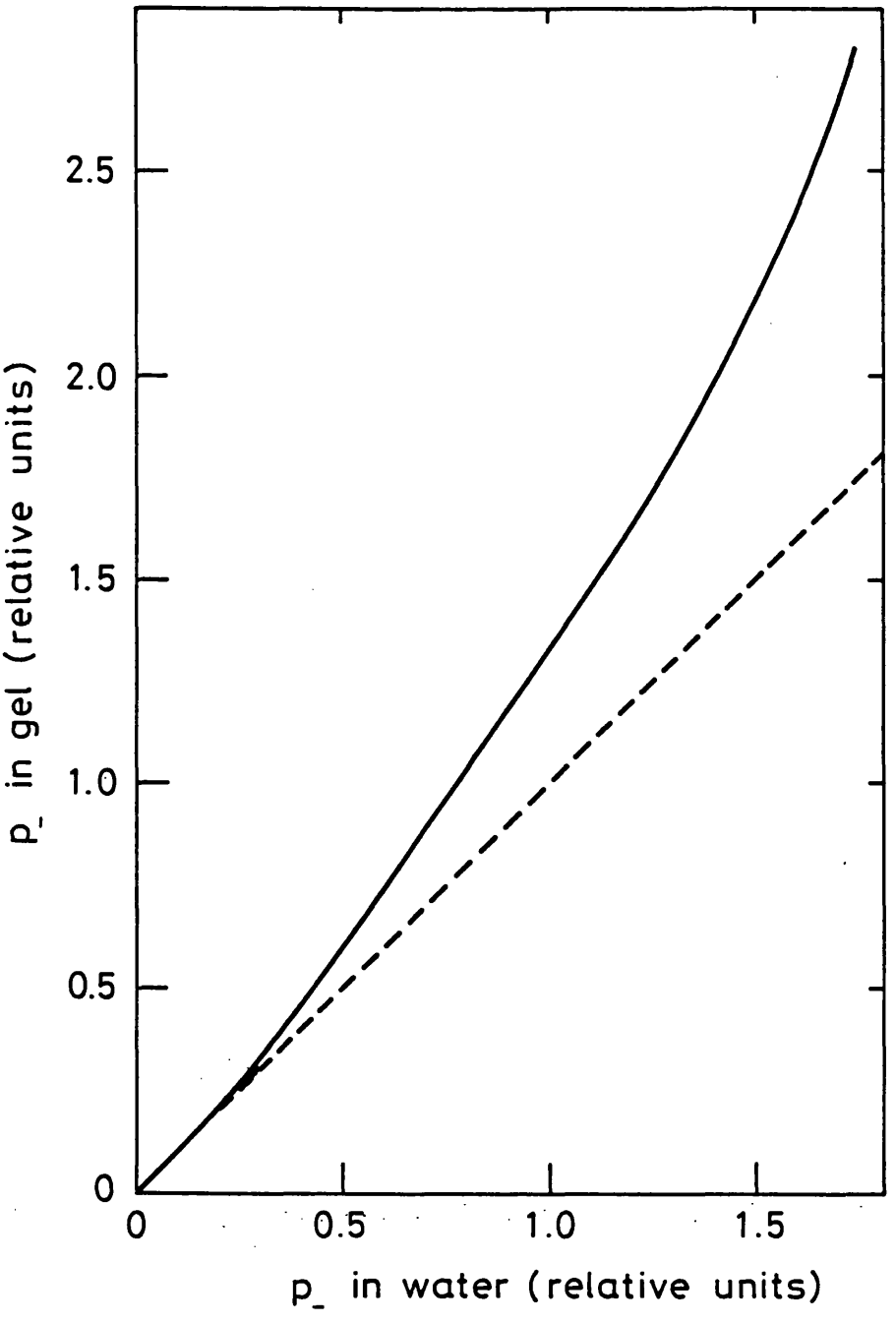

Figure 52 Variation of the measured peak-negative pressure in gel as a function of the corresponding value for propagation in water, for a focused field. The dashed curve gives the predictions of linear theory.

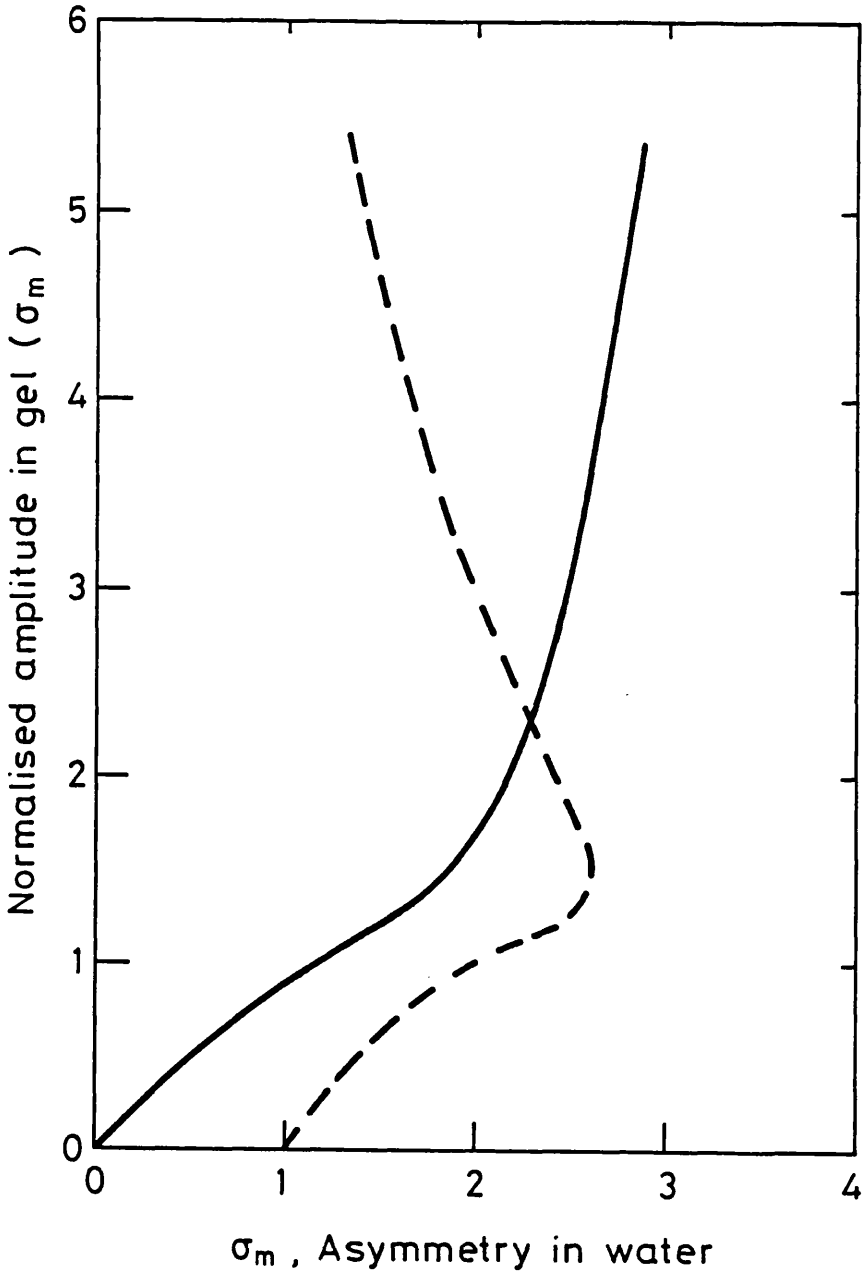

Figure 53 Calculated variation of the peak-to-peak amplitude in gel as a function of the corresponding amplitude in water (—), and as a function of the asymmetry of the waveform in water (- -). The peak-to-peak amplitudes are normalised so that they correspond to the parameter σ_m (Equation A.8).

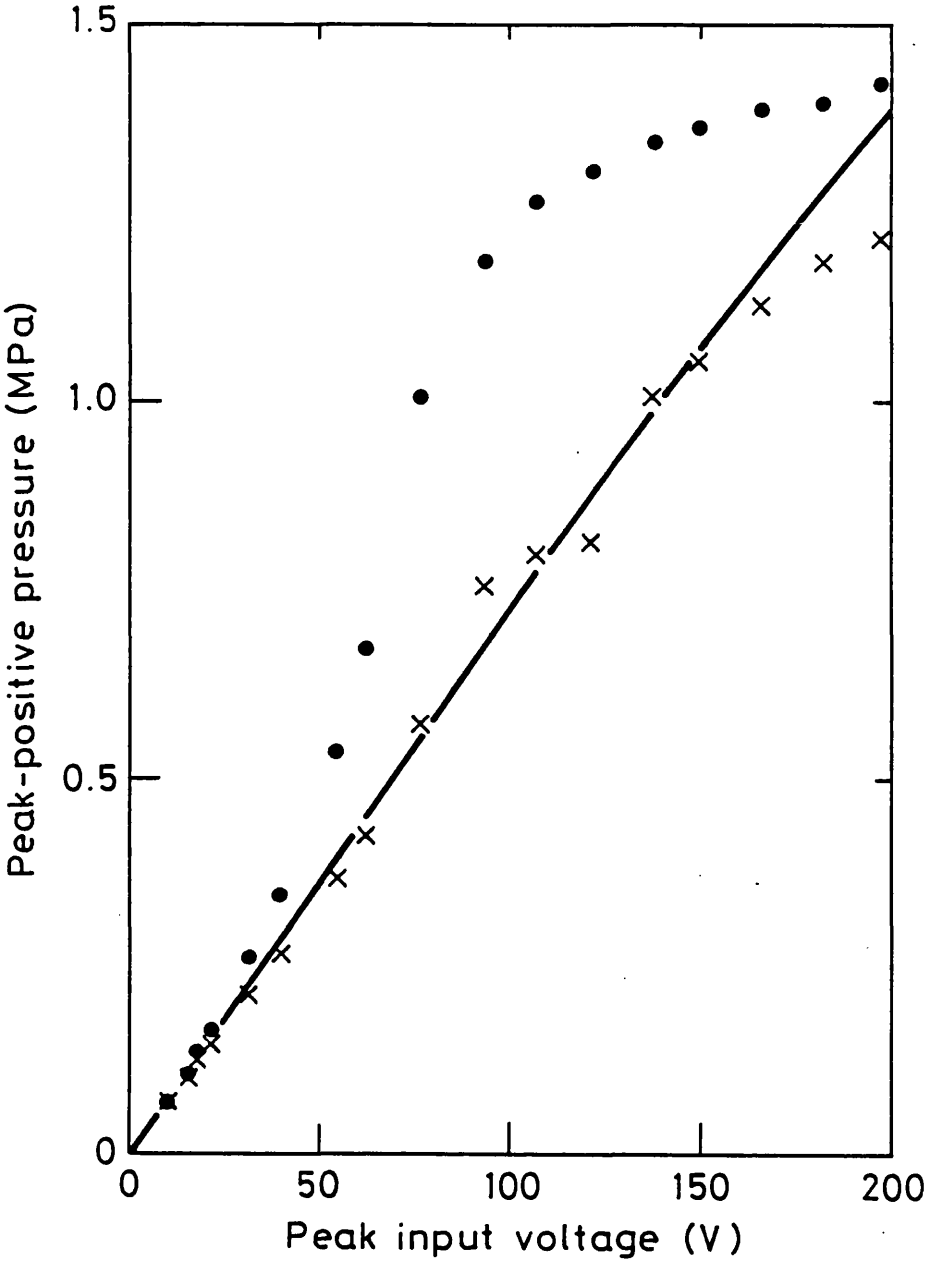

Figure 54 Variation of the peak-positive pressure in gel as a function of the input voltage to the transducer. - measured amplitude, • amplitude predicted by linear theory, based on measurements of the field in water, x amplitude predicted from measurements in water using the procedure described in section 4.6.

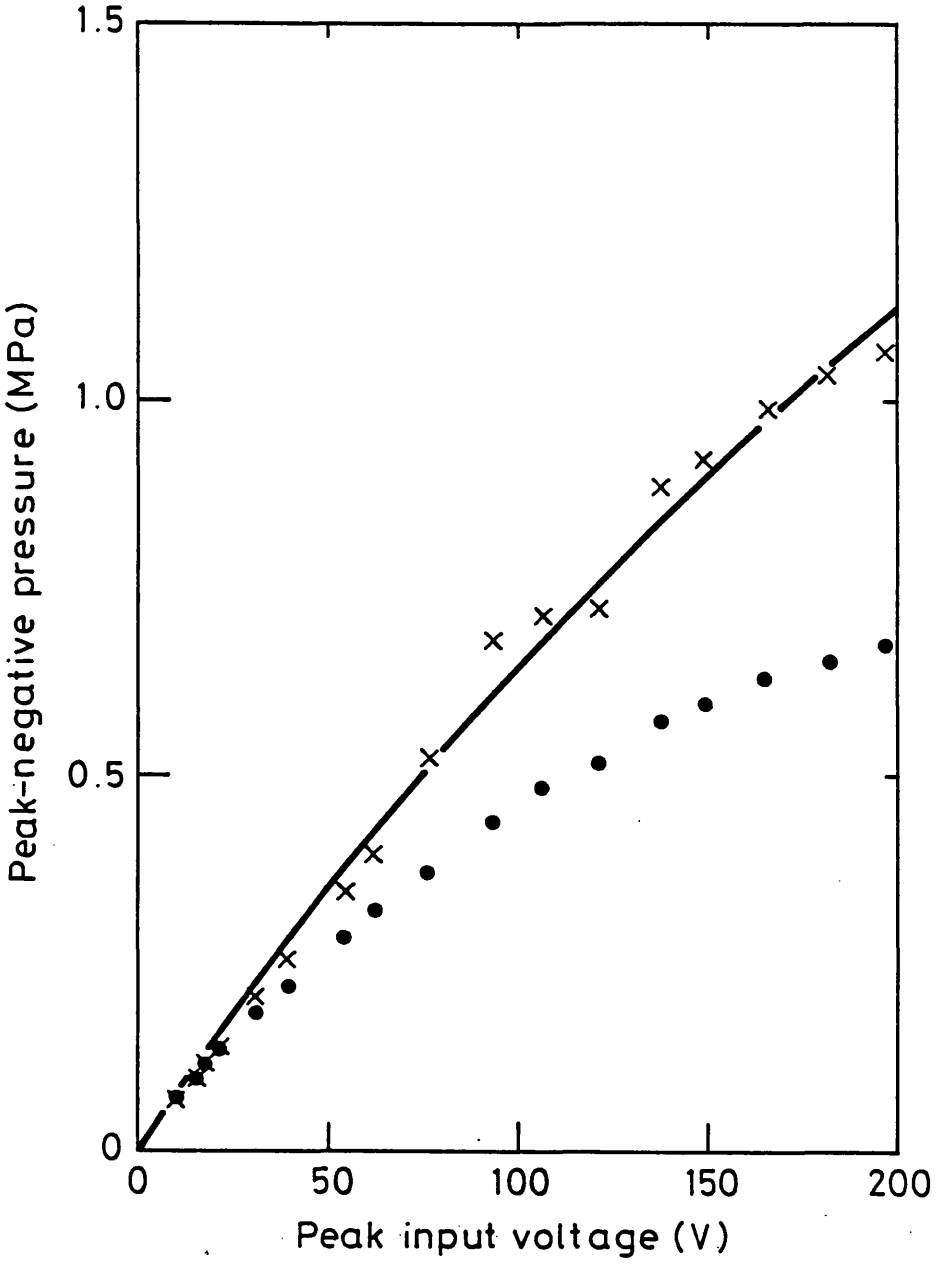

Figure 55 Variation of the peak-negative pressure in gel as a function of the input voltage to the transducer. The curve and symbols are derived in the same way as for Figure 54.

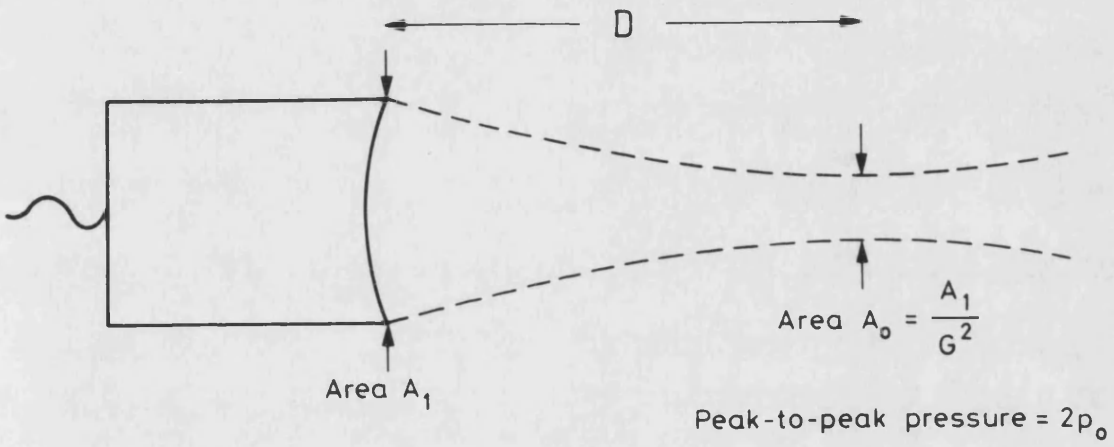

Figure A1 Diagram of a transducer field to illustrate some of the parameters required in Equation A.8.

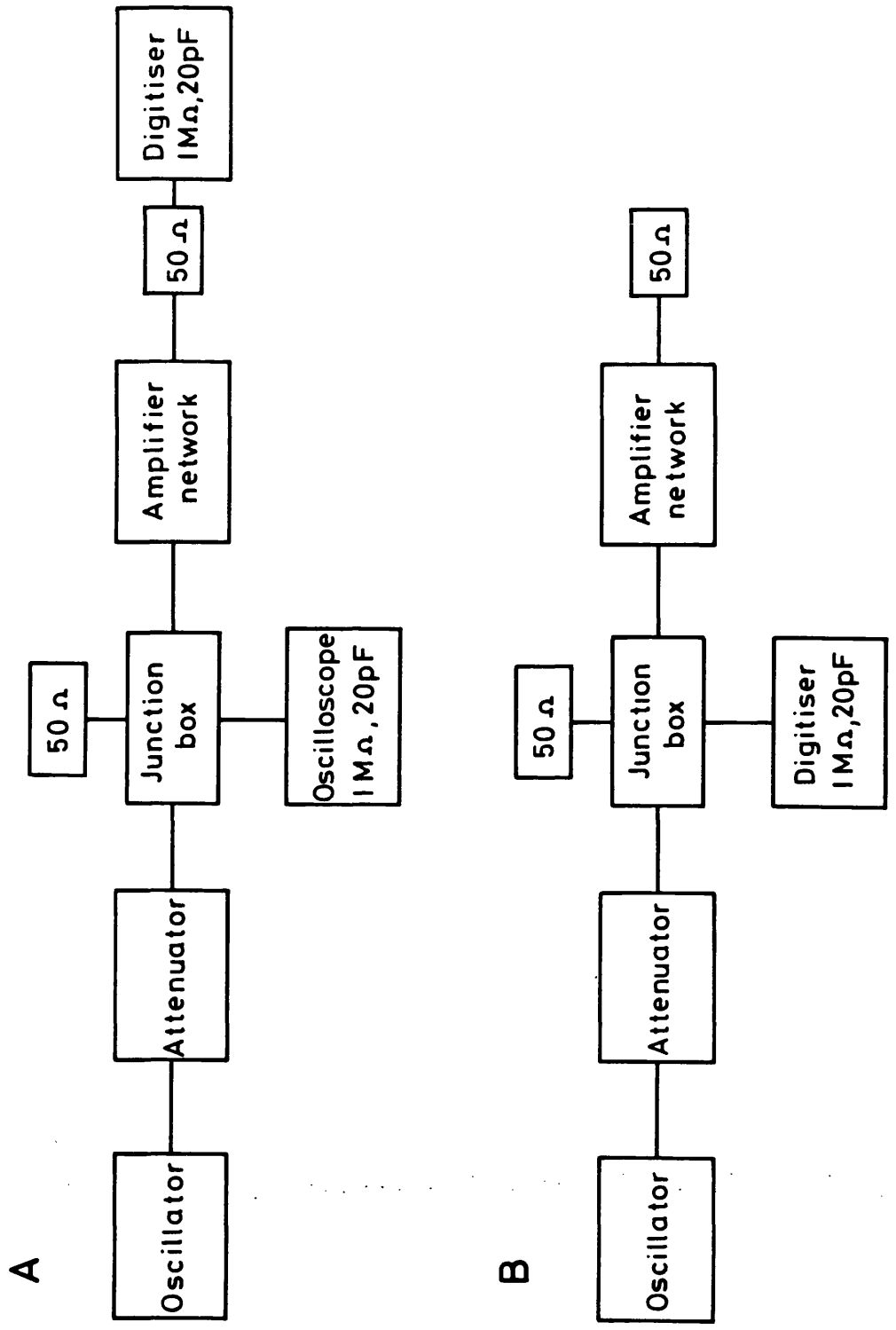

Figure A2 Block diagram of the arrangement used for measuring the gains of the amplifiers.